UNIVERSITY OF OKLAHOMA

GRADUATE COLLEGE

CHARACTERIZATION OF THE MECHANICAL PROPERTIES OF MICROSCALE CARBON FIBER AND CARBON-NANOTUBES GRAFTED FIBER WITH THE AID OF DYNAMIC MECHANICAL ANALYZER

A DISSERTATION

SUBMITTED TO THE GRADUATE FACULTY

in partial fulfillment of the requirements for the

Degree of

DOCTOR OF PHILOSOPHY

By

SAMUEL G. ADEOYE
Norman, Oklahoma
2012

CHARACTERIZATION OF THE MECHANICAL PROPERTIES OF MICROSCALE CARBON FIBER AND CARBON-NANOTUBES GRAFTED FIBER WITH THE AID OF DYNAMIC MECHANICAL ANALYZER

A DISSERTATION APPROVED FOR THE
SCHOOLOF AEROSPACE AND MECHANICAL ENGINEERING

BY

Dr. Mrinal C. Saha, Chair

Dr. M. Cengiz Altan (Co-Chair)

Dr. Zahed Siddique

Dr. James D. Baldwin

Dr. Dimitrios V. Papavassiliou

For…… David Adeoye

ACKNOWLEDGEMENTS

All glory must first be to the almighty God for giving me the knowledge and the potential to deliver that knowledge in the appropriate path towards this great outcome. Without Him nothing would be possible. Words could not actually convey my appreciation to my family for their great inspiration throughout this journey. My wife, Temitope, has been a helping hand through her encouragement and motivation in every step. The little and gentle smiles I always received from my daughter, Faith, when I got back from the laboratory also served as a source of strength. It always reminded me of the reason why I was carrying out this research. I will thank my parents for their prayers and their relentless calls from Nigeria. You are the best parents I have ever known. Thank you for your support right from my elementary schooling up until this stage. This section would not be complete without thanking my uncle, Elijah, and his family for all of the efforts they contributed towards making my program possible without a hitch. Thank you Dad, Mum, Honey and uncle!

Of course, without both financial (under AFOSR contract # FA 9550-10-1-0031) and moral support from my advisers I would not have been able to even start this work. I would like to thank Drs. M. Saha and M.C. Altan for their great mentorship, and all of the advice they provided throughout this period. Thank you for guiding me to the right path in every step of the way. I appreciate you for giving me freedom to make the "invisible" the great opportunities. My appreciations are also going to Dr. Z. Siddique, Dr. J. Baldwin and Dr. D. Papavassiliou for their untimely supports and encouragement. Special thanks go to D. Smith, F. Afzal, and Drs. L. Aktas, P. Larson and A. Balakrishnan.

TABLE OF CONTENTS

LIST OF TABLES

LIST OF FIGURES

ABSTRACT

Effects of surface modification on tensile and interfacial properties of PAN-based carbon fibers have been investigated. Four different types of commercially available PAN-based carbon fibers namely AS4, AS7, IM10 and T650 were chosen. Both sized and un-sized fibers were investigated. In order to de-size the sized fibers, the fibers were subjected to heat treatment at 435^{o}C in inert atmosphere with 20 minutes and 60 minutes hold time. Moreover, the surface of the fibers was modified using thermal treatment, POSS coating, and carbon nanotubes (CNTs) growth. Thermal treatment was performed inside the chemical vapor deposition (CVD) chamber without the presence of hydrocarbon substance, while CNT growth on the fiber surface was done in the presence of hydrocarbon substance inside the same CVD chamber under controlled temperature and gas environment. Catalyst was distributed on carbon fiber using dip- and spray-methods. The surface morphology was analyzed using high-resolution scanning electron microscope (HR-SEM) and atomic force microscope (AFM), while the mechanical testing was performed using a dynamic mechanical analyzer (DMA). The percent of catalyst particles that were deposited on the fiber were estimated using the thermogravimetric analyzer (TGA).

SEM images showed fewer surface flaws on the carbon fiber with sizing compared to un-sized and de-sized fiber, whereas de-sized fiber showed more surface flaws compared to un-sized fiber which is an indicative of significant thermal degradation of the fiber microstructure. Longer duration of thermal exposure resulted in more surface defects because some parts of the fiber surface layer had been damaged by the heat treatment. The POSS coating seemed to result in less surface defects due to coverage of the carbon fiber with the POSS molecules. It also showed that the catalyst deposition method has a significant effect on the CNT growth rate and their distribution of the carbon fiber during the CVD process. The dip-coating method resulted in more CNT growth than the spray-coating method. This can be attributed to the amount of catalyst particles that were able to be deposited on the respective fiber type as observed using the thermogravimetric analysis. AFM results indicated that the surface roughness is about 64% higher for the sized fiber compared to un-sized fiber. Similar trend is also found true with the de-sized fibers.

Sizing is believed to be chemo-mechanical bonded to fiber surface and thus alleviates the adverse effects of its surface flaws. Consequently, the sizing on the fiber resulted in about 7-12% increase in tensile strength and 8-17% increase in tensile failure strain. Two-parameter Weibull statistical model agrees with this finding as the higher Weibull modulus for the sized fibers is an indicative of the evenly distributed surface flaws. Thermal treatment of the fiber resulted in significant reduction in the tensile strength and failure strain of about 54% and 32%, respectively as a result of thermo-oxidative degradation. Although POSS coating resulted in a small improvement in the tensile strength (about 8%) a significant improvement in the interfacial shear strength (about 39%) was observed. It is believed that POSS molecules act as chemo-mechanical interlock created within the fiber-matrix interface. The poor interfacial performance exhibited by the CNT grafted carbon fiber (about 7% improvement) is possibly due to poor bonding strength of CNT on carbon fiber which possibly caused the CNT to pull-out at the fiber-matrix interface as evidence from the SEM images. It is believed that the CNT-carbon fiber bonding plays important role in the interfacial shear strength of fiber-matrix with CNT growth. The thermally-treated fiber showed about 31% improvement in the interfacial shear strength when compared to as-received un-treated fiber. It is believed that higher surface roughness due to heat treatment provided better anchoring sites on the fiber surface.

CHAPTER 1

INTRODUCTION

1.1 Carbon Fiber

1.1.1 Introduction

The word carbon comes from the Latin word ‘Carbo’, and it can refer both to the carbon element or coal [1]. Carbon, C, is a chemical element with an atomic number of 6, and it belongs to the member of group 14 in the periodic table; this makes it a non-metallic material. All allotropes of carbon (i.e, diamond, graphite, fullerene, and carbon nanotubes) are highly stable because they are formed by tetravalent bonding; thus, any reaction with these materials can only be possible at extremely high temperatures. The common source of inorganic carbon is from dolomite, limestone, and carbon dioxide, but carbon exists in large quantities as an organic deposit that can be found in petroleum, coal tar, and methane clathrates [2].

Carbon fibers (CFs) can be matched with a class of carbon materials consisting of finely thin fibers, in which carbon atoms are bonded together in microscopic crystals that are somewhat aligned parallel to the longitudinal axis of the fiber. The alignment of these crystals makes the fiber very strong for its size, compared to other traditional materials made for reinforcement. More than a thousand single carbon fibers can be bundled together to form a carbon tow, which may be used by itself or woven together to form a fabric. The diameters of single carbon fibers are between 4 - 10μm. They are smaller than glass or boron fibers, which have diameters ranging from 13 - 181μm. With a high content of carbon (92 - 95%), carbon fibers are one of the strongest materials available, when corrected for density. The high strength and stiffness, combined with their light

weight, makes these fibers the most attractive for high-volume applications in the medical, transportation, aerospace, offshore oil, and sporting goods industries.

In 1958, a high-performance carbon fiber was produced by Roger Bacon at Union Carbide Parma technical center [3] by heating strands of rayon until they carbonized. The carbon content in the resulting fibers was only about 20%, and as a result the fiber had lower strength and stiffness properties. In the early 1960s, a process was developed in Japan to produce carbon fibers using polyacrylonitrile (PAN) as a raw material, which contains about 55% carbon and has much better properties. In 1963, this process was fully patented and licensed in the UK for industrial production of high strength carbon fiber. A new breakthrough in the production of CFs, having excellent flexural strength and containing almost 85% carbon, using petroleum pitch derived from oil processing, was made known in 1970. However, PAN based carbon fiber is recognized as the most important and promising precursor for the manufacturing of high-strength carbon fibers. PAN based carbon fibers have excellent physical and mechanical properties as compared to rayon based carbon fibers [3]. Pitch-based carbon fibers' properties are generally inferior to PAN carbon fibers. This is because pitches are more isotropic before pyrolysis; as a result, the isotropy is maintained in the fibers, except if the orientation of the larger planes is carried out under tension during heat treatment at ~ 2000 to 3000^{o}C. Although this process is quite expensive, it gives the pitch carbon fibers excellent mechanical performance [4].

1.1.2 Processing and Applications of PAN-Based Carbon Fiber

PAN precursor has a glass transition temperature of ~ 120^{o}C (due to its highly polar nature), and hence it tends to decompose before melting. Therefore, PAN precursor fibers must be produced by either wet or dry-spinning processes. The solution in a wet-spinning process normally contains 10-30% by weight of PAN copolymer dissolved in sodium thiocyanate, nitric acid, or dimethylacetamide. The solution is first filtered and then extruded through a spinneret into a coagulation bath that contains a solution like dimethylacetamide, ethylene glycol, or dimethylformamide [5]. As the PAN solution is forced through the spinneret, the solidifying polymeric structure tends to re-orient parallel to the flow direction. After being spun into fibers, the axial orientation within the PAN fibrils is then enhanced through stretching during the heat-drawing process (as illustrated in Figure 1.1). The production of PAN-based CF involves applying tension on the precursor while still undergoing the stabilization process at ~ 200-300^{o}C for 2 hours. This aids in limiting the relaxation of the polymer structure.

PAN-based fiber is stabilized under considerable stress at a temperature range of 200^{o}C-300^{o}C in an oxidizing atmosphere. During this stage, the fiber undergoes chemical changes that normally lead to an increase in density,and evolution of hydrogen (dehydrogenation) and oxygen gas [6]. Having stabilized the stretched structure of the molecular chains, the tows of PAN fibers is subjected to thermal pyrolysis in an inert atmosphere. The non-carbon elements are removed as volatiles, such as HCN, H_2O, NH_3, CO, CO_2, and N_2 [7-9]. The rate of heating in the early stages of the carbonization process is generally low so that the release of volatile gases does not damage the fiber.

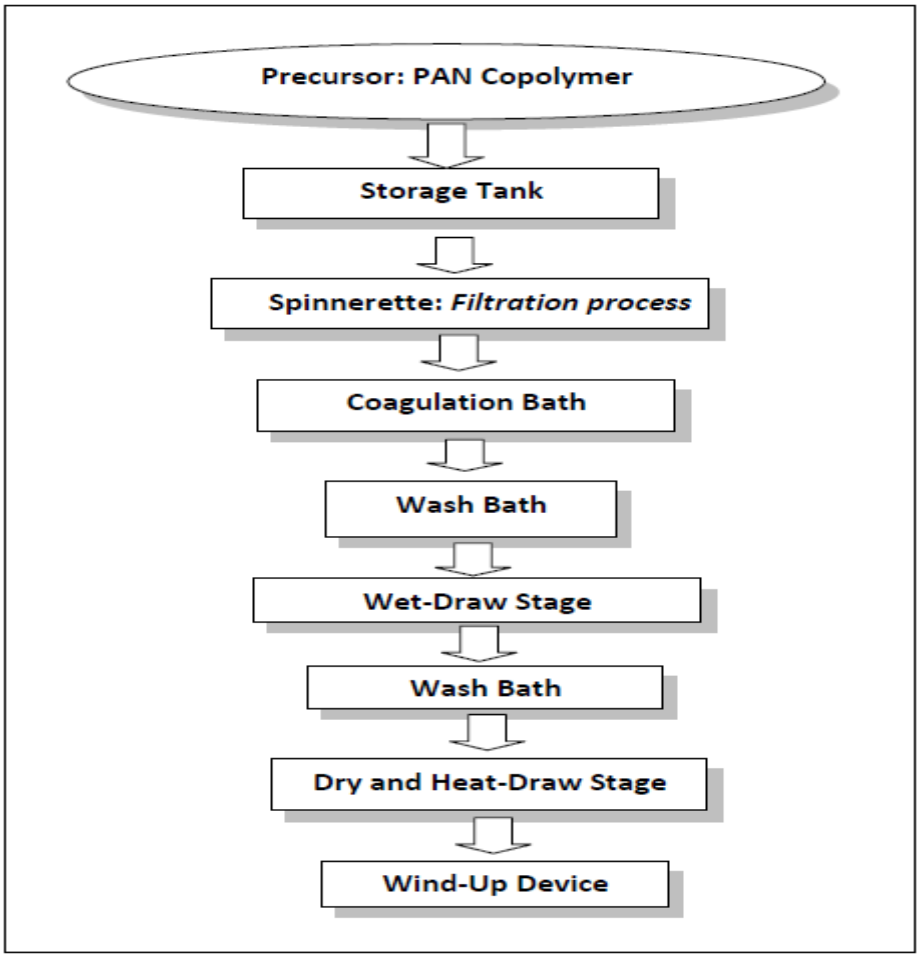

Figure 1.1. Wet-spinning process for PAN copolymer fibers' production

Most of the volatile gases are evolved at a temperature below 1000^{o}C,and only carbon and nitrogen (~6%) are left. The stabilized fibers are carbonized in an inert atmosphere at a temperature range of 1000 - 1700^{o}C. The carbon content increases to 90% during the carbonization process, and a three-dimensional carbon structure is formed. However, during the early stage of carbonization, the hydroxyl groups present in the oxidized PAN fibers start cross-linking in order to reorganize and coalescence the cyclized sections. The cyclized structures undergo dehydrogenation and begin to link up in a lateral direction producing a graphite-like structure consisting of three hexagons bonded together by nitrogen atoms [10,11]. Graphitization treatment can be done on the

carbonized fibers by further heat treatment at 2000^{o}C - 3000^{o}C in an inert atmosphere (non-nitrogen gas).

The main characteristics of an ideal engineering material are its high strength, high toughness, low density, and creep resistance. Metals and their alloys, the conventional engineering materials, possess the first two characteristics but have high density. High performances CFs have improved strength, stiffness, and very low density,and they are the recent engineering materials that have found a place of replacement for the conventional materials.

The use of carbon fibers in various fields is driven mainly by the expected mechanical performance, cost, matrix compatibility and the specific area of application. Its physical strength, specific toughness and light weight make it suitable for use in the high technology sector. Some parts of missiles, aircraft brakes, and aerospace antenna are also manufactured from carbon fiber. Chemical and nuclear fields make use of carbon fiber in manufacturing valves and pump components because of its chemical inertness and high corrosion resistance. Most recently it was used to fabricate the Maxillo-facial surgery board, and this helped to minimize the electromagnetic interferences during the medical operations [12].

1.1.3 SurfaceTreatment and Sizing of Carbon Fibers

Carbon fibers are mainly produced for composite reinforcement due to their exceptional characteristics such as high strength and modulus. Whenever a load is applied to the carbon fiber composite, the stress is shared among the filaments via the matrix material. If there is an existence of a weak fiber-resin bond, then this will result in a poor mechanical performance of the composite. This is majorly attributed to lack of proper

bonding between the fiber surface and the resin matrix. In order to overcome this issue, the surface of the fiber is specially treated by various methods including the deposition of an active form of carbon or by grafting a polymer onto the fiber surface through gas-phase oxidation [13-15], liquid-phase oxidation [16-18] or anodic oxidation processes [19-21]. Wright [22] mentioned that the possible effects of surface treatment include the removal of a weak fiber surface layer, and a possible formation of a chemically modified surface that has yielded in producing active functional groups such as carbonyl, carboxyl and hydroxyl.

The application of a coating (usually a polymeric materials) is normally termed a size or finish which is typically done after the fiber surface has been surface-treated. Sizing has been reported to improve the inter-filamentary adhesion, aid in wetting out the fiber in the resin matrices, acts as a lubricant to prevent fiber damage during handling and processing, and it helps to effectively reduce the stress concentration at the fiber surface flaws by blunting the crack tips [23]. Sizing could be achieved by deposition of polymer onto the fiber surface by electrodeposition or electropolymerization process, or simply through direct deposition from solution of a polymer [24-27]. The latter method has been the typical approach normally adopted for the coating process in most fiber producing industries. Figure 1.2 shows the schematic illustration of the direct deposition of polymer onto the fiber surface from the sizing bath before being air-dried and packaged.

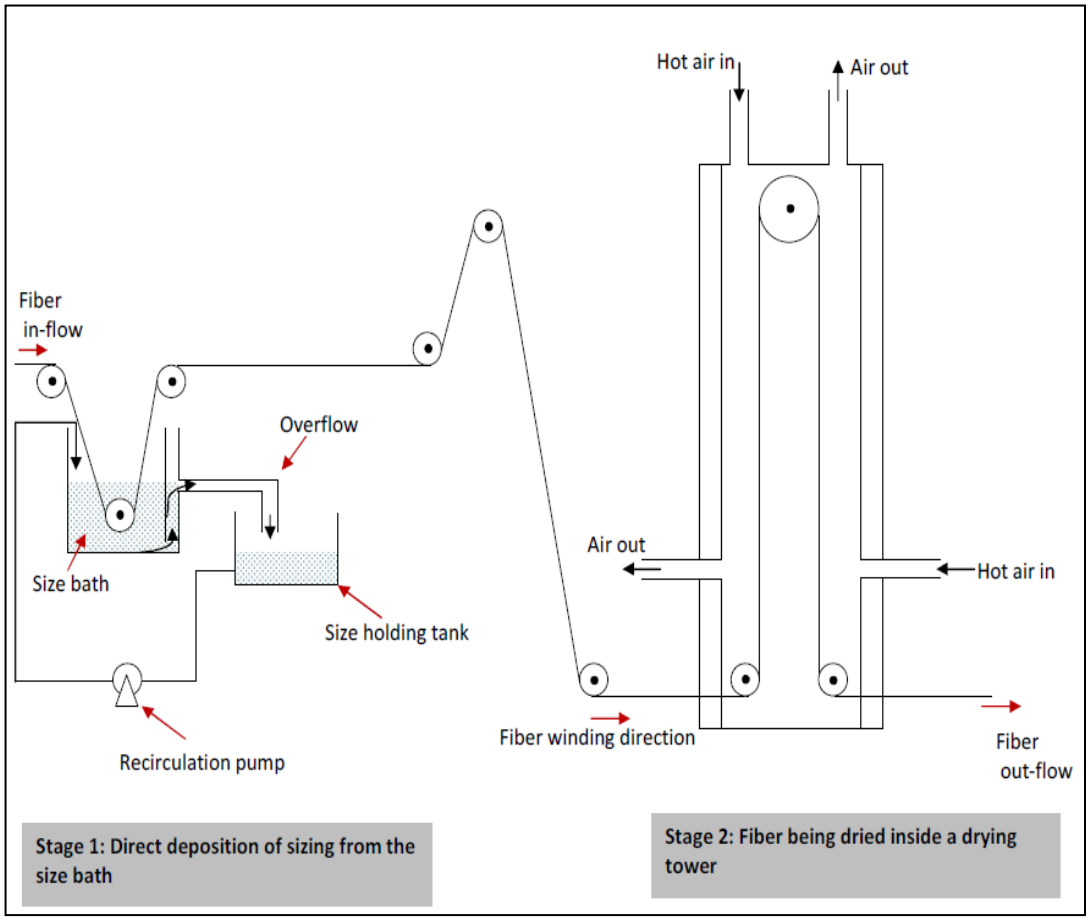

Figure 1.2. Schematic showing typical fiber sizing and drying procedures

1.2 Carbon Nanotubes (CNTs)

1.2.1 Introduction

The decomposition of hydrocarbon substance at a very high temperature in the presence of metal catalyst particles was reported to produce a very thin filament in 1980's [28-31]. However, no detailed investigation of such very thin filaments was launched until the observation of carbon nanotubes in 1991 by Iijima (an electron microscopist) by the use of a high resolution transmission electron microscope (HRTEM) [32]. At the same time, Russian researchers also reported the discovery of CNTs and nanotube bundles [33]. It was Iijima's observation of the multi-walled carbon nanotubes'

(MWCNTs) electronic properties that launched the full research in the field of CNTs. Less than two years after the MWCNTs' discovery in 1991, single wall carbon nanotubes (SWNTs) were discovered by Iijima and his group at the NEC laboratory, and Bethune and coworkers at the IBM Almaden research center, independently [34,35]. The discovery of SWNTs was especially important because SWNTs were fundamental for all of the theoretical studies and predictions that preceded the experimental findings.

Smalley and his workers at Rice University were able to synthesize bundles of aligned SWNTs (with a small diameter distribution) in 1996, which brought about a remarkable breakthrough to many sensitive experiments [36]. With this breakthrough in science, the issue of structural defects found in carbon nanotubes because of its finite length and larger diameter distribution that always lead to premature bending of the nanotubes was addressed.

1.2.2 Synthesis

1.2.2.1 Laser Ablation Method

The growth of high quality SWNTs using a laser oven approach was first reported by Smalley et al. [36] and Smalley and Yakobson [37]. The approach involved using intense laser pulses to ablate a graphite target containing 0.5 atomic percent of nickel and cobalt inside a furnace that is maintained at ~ 1200^{o}C in the presence of argon gas flowing through the 5cm diameter tube at a constant pressure of 500 Torr. A laser is aimed at a block of graphite in order to vaporize it. The inert gas carries the grown nanotubes downstream and deposits them on a water-cooled copper collector. Contact

with a cooled collector causes the carbon atoms to be deposited as nanotubes. The nanotube 'felt' or forest can then be collected at the copper tip.

It is interesting to note that Pennycook et al. [38] used laser-induced imaging and spectroscopy diagnostic methods, along with transmission electron microscope, to study the dynamics of the SWNTs' growth process. It was concluded that SWNTs of about 10 μm in length can be produced from the small amount of Graphite/(Ni-Co) material set to vaporize at 1000^{o}C in a single Nd: YAG laser shot. The result also proved that just after the ablation, the plumes produced at room temperature and 1000^{o}C settings exhibited oscillations in both axial and radial directions inside a tubular reactor.

1.2.2.2 Arc-Discharge Method

A breakthrough in growing high-quality multi-walled nanotubes (MWNTs) by arc-discharge was first made possible by Ebbesen and Ajayan [39] in 1992. The nanotubes growth conditions,such as inert gas pressure and the arcing current, were set as the controlling parameters. The grown MWNTs have a typical length of about 10μm, and their diameters are usually within the range of 5-30nm. Purification of the MWNTs was carried out in an oxygen environment in order to oxidize the graphite particles. However, this method of purification has been reported to remove an appreciable amount of nanotubes during the process [39,40]. After the chamber is thoroughly evacuated by a vacuum pump, a predetermined ambient gas is introduced at the desired pressure and a dc arc voltage is supplied between the two separated graphite rods. The anode graphite rod gets excited and evaporated to form fullerenes, which are deposited as carbon soot inside the chamber. Moreover, a significant part of the evaporated anode is also deposited on the cathode rod. This includes co-axial graphene sheets called MWNTs.

SWNTs have also been produced by an arc-discharge method, simply by doping the anode graphite rod with metal catalyst and by the use of a pure graphite cathode. The produced SWNTs are collected as soot [41,42]. Arc-discharge evaporation of pure graphite rods can be done in the presence of He, Ar, or CH_4. However, Ando [43] reported that CH_4 gas favors the growth of highly crystalized MWNTs with a few coexisting carbon nanoparticles. Mass production of SWNTs in a He environment by the arc-discharge method was achieved by Journet et al. [44] with the use of a bimetallic Ni-Y catalyst.

1.2.2.3 Chemical Vapor Deposition (CVD) Method

Catalytic CVD is another method widely used for producing CNTs. In this method, a hydrocarbon vapor thermally decomposes in the presence of a metal catalyst. SWNTs were first synthesized by Dai et al. [45] using this method through the disproportionation of CO at 1200^{o}C in the presence of Mo catalyst particles. As a result of his contributions, SWNTs can now be produced from benzene, ethylene, methane, and acetylene using different catalysts [46-49]. Growth of MWNTs from ethylene and methane had also been reported [50,51]. The schematic representation of the CVD setup is shown in Figure 1.3.

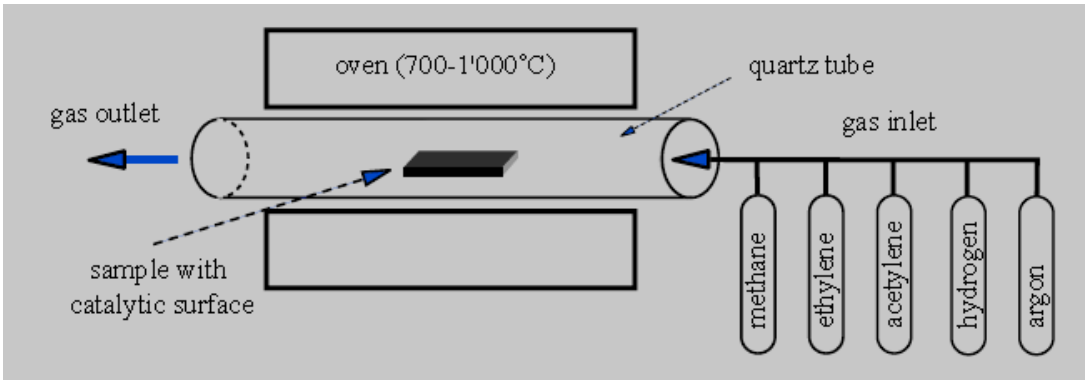

Figure 1.3. Schematic of the experimental setup for CVD technique

The process involves passing a hydrocarbon vapor through a tube furnace set at ~ 600-1200^{o}C for 15-60 minutes in the presence of a catalyst in order to decompose the hydrocarbon. CNTs are made to grow upon the catalyst, and they are harvested when the system cools to room temperature. This is a versatile method used in growing CNTs on many substrates, including the carbon fiber, and this also allows for the growing of a desired architecture of nanotubes at predefined locations on the substrate.

1.3 Carbon Hierarchical Structure

1.3.1 Introduction

The incorporation of carbon nanotubes into conventional fiber-reinforced polymer composites produces a hierarchical reinforcement composite that can significantly improve the composite mechanical performance. Excellent in-plane tensile properties of fiber-reinforced composites have been achieved by the use of various fiber architectural configurations, including one-dimensional unidirectional roving or two-dimensional woven fabrics. However, the weak compression and interlaminar properties of these composites remain very critical issues and limitation of the use of these fibers [52]. Most of these limitations can be eliminated by the use of hierarchical (multiscale) composites, in which a conventional microscale reinforcing fiber is utilized alongside a nanoscale CNTs. CNTs could offer both intralaminar and interlaminar reinforcement which could, thus, contribute to improving delamination resistance and through-thickness properties of the composite, without compromising in-plane performance.

The combination of CNTs with conventional fiber-reinforcements in polymer composites have been achieved predominantly through two different methods: dispersing CNTs completely throughout the composite matrix or grafting CNTs directly onto

reinforcing fibers [53]. Grafting CNTs onto fiber surfaces is an effective method to improve the fiber surface area, creating mechanical interlocking, and local stiffening at the fiber/matrix interface, all of which may improve stress transfer and interfacial properties [54]. The radial placement of the nano-reinforcement to the fiber axis, extending into the surrounding matrix, is likely to stiffen the matrix and provide increased lateral support for the load-bearing microscale fibers. These effects could basically reduce the microbuckling failure as normally observed in composite under longitudinal compression loading.

1.3.2 Synthesis and Properties

Electrophoretic deposition (EPD) is an industrial scalable process for the deposition of nanomaterials with good homogeneity. This method was adopted by Schaefer et al. [55] to deposit carbon nanofibers (CNFs) on single carbon fibers. They first dispersed 6.5mg of acid-functionalized CNFs (O-CNF) in 300 mL of ultrapure water, using the sonication process. The mixture was further diluted with an additional 800 mL of ultrapure water in a clean electrophoretic tank. Single fibers were separated from the bundle and mounted on the metal frame holder, and then placed inside the prepared solution inside the tank (Figure 1.4). Once lowered inside the tank, a 30 V field was applied and left for a complete deposition time of 1 min. After the treatment, the fibers were removed from the tank and placed inside an oven to dry at 100^{o}C for 1 hr. The interfacial shear stress (IFSS) between the sized fabric grafted with CNF and epoxy matrix was reported to improve by 79%, as compared to the unsized fibers that had undergone the same procedure.

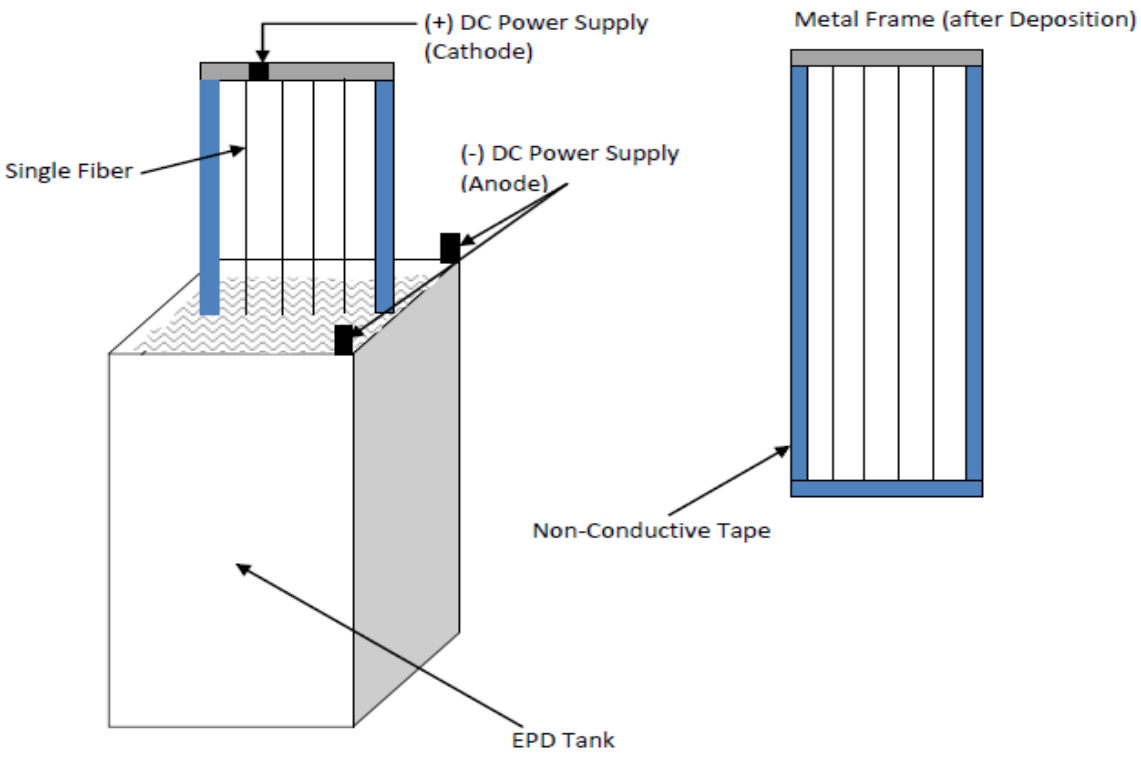

Figure 1.4. Electrophoretic deposition setup

The process was carried out under a constant voltage of 30V for 5 minutes. The composite fabricated from fabric grafted with MWCNTs through cathodic EPD was reported to possess 15 times higher electrical conductivity than the plain-woven composites. The short beam strength of the hybrid composite had also increased by 13%as compared to that of the composite without nanotubes. The same report and enhancement have been reported by other authors [56-58].

Recently, similar work using the EPD method was done by Lee et al. [59]. MWCNTs and CNFs were deposited onto carbon woven fabric (Mitsubishi TR30) by anodic and cathodic EPD processes. In the anodic EPD process, a carbon woven fabric was used as the anode, and a copper plate with a thickness of 0.3 mm was used as the

cathode. In the cathodic EPD process, they connected the carbon fabric and copper plate to the opposite electrodes of the anodic process.

High density MWCNTs were grown directly on the PAN-based T650 and IM-7 carbon fibers using the thermal CVD technique by Zhang et al. [60]. The CVD procedure adopted made it possible to vary the growth temperature (800^{o}C, 750^{o}C, and 700^{o}C) and also to control the flow rate of carbon source/catalyst (xylene/ferrocene) mixture (5sccm and 10sccm). A vapor mixture made from a 0.01 g/ml mixture of ferrocene in xylene was made to flow within the heated quartz chamber by the aid of argon and hydrogen (serving as carrier gases). They showed that the tensile strength of the sized T650 CF was reduced by almost 40% compared to the pure fiber, due to its exposure to the higher temperature growth environment. This degradation was attributed to the decomposition of the organic material on the fiber at a particular growth temperature. However, the unsized T650 fibers with CNTs grafted maintain their tensile strength up to 750^{o}C and then start to degrade at about 800^{o}C by almost 46%. It is worth mentioning that it was not stated where the grafted fibers have been extracted from within the CNT-CF tows.

Dey et al. [61] showed that population density of CNTs grafted on CF could be varied by adjusting the concentration of Ni plating solution; in this way the thickness and particle size of Ni catalyst would also be varied. Similar works have been reported by Sager et al. [62], Yang et al. [63] and Down and Baker [64].

Recently, the growth of CNTs on CF using the CVD technique has been an element of debate due to the thermal degradation effect on the carbon fabric during the fabrication process. However, the CVD method still remains a very versatile approach of

grafting CNTs on CF because of its easy scale-up, limited equipment required, and greater success in producing uniform CNT growth on complex surfaces.

1.3.3 Application

CNTs being grafted on carbon fibers offer the benefits of introducing the remarkable nanoscale reinforcement to well-known fibrous composites in order to form multiscale hybrid micro-nanocomposites. Bekyarova et al. [65] grafted CNTs on Magnamite IM7 carbon fiber by using the electrophoresis technique, and it was reported that the interlaminar shear stress of CNT/CF/epoxy was enhanced by 30% compared to that of traditional CF/epoxy composite. The improvement was attributed to the strong reinforcement made by CNTs in the matrix-rich regions found between the interlaced fiber bundles. In the same trend, Naito et al. [66] also reported 15% and 9% enhancements in the tensile strength and failure strain for CNTs grafted T1000GB PAN-based CF respectively as compared to the ungrafted fibers (single fiber tensile report). They also reported similar results for grafted K13D pitch-based CF in the amount of 22% and 6% for tensile strength and failure strain, respectively. The nanotubes were grafted on the fibers at 700^{o}C (K13D) and 750^{o}C (T1000GB) for 900 seconds with the use of the thermal CVD method. In general, the growth of CNTs on CF has been demonstrated possible using techniques like CVD [67-69] and electrodeposition [33,65]. Sager et al. [70] showed that CNTs grafted on CF by the CVD method could be aligned properly with the use of different type of carbon source. However, it was highlighted that random CNT-CF improved the interfacial shear strength of a fiber embedded within a polymer matrix by ~ 35%, as compared to the aligned CNT-CF.

1.4 Polyhedral Oligomeric Silsequioxane (POSS)

POSS refers to one kind of compound that contains a silicon-oxygen nanostructural units with intermittent siloxane chains of the general formula $RSiO_{1.5}$, R can be hydrogen, alkyl, alkaline, aryl, aromatic alkylene, or their derivative groups [71]. The possibility of varying these R groups makes POSS versatile nano-particles. Incorporating POSS molecules into polymer matrices have shown many property improvements, such as mechanical and thermal properties. It also provided both oxidation and chemical resistance [72]. Zhao and Hunag [73] reported that POSS is an effective coupling agent used to functionalize convectional carbon fiber surface in order to increase its polarity, surface energy and roughness and also to improve the interfacial strength of the composites through improved chemical bonding and mechanical interlock.

For efficient load transfer from the matrix to fiber, there is a need for an improved fiber surface.Numerous methods have been employed as dicussed earlier to improve the fiber surface wettability and to increase the fiber surface functional groups by performing fiber surface modification process [74-76]. For instance, in an attempt to improve the interfacial properties between fiber and epoxy matrix, Zhao and Huang [77] coated the carbon fiber uniformly with octaglycidyldimethylsilyl POSS. After the mechanical test the composite impact toughness increased from 2.62 to 3.59 J and the interlaminar shear strength increased from 68.8 to 90.5 MPa when compared to the control samples. Also reported on their work was the improvement observed in the fiber surface roughness as a result of the coating. A similar work was also performed by Mahfuz et al. [78] by the use of two different POSS systems (Octaisobutyl and trisilanolphenyl) to modify the fiber surface in order to promote the fiber/matrix interface. Composites were fabricated from

the surface modified fibers using vinyl ester resin. It was reported that the composite mechanical properties determined through short beam shear test, transverse tension test, and low velocity impact test improved by 10-38%. In the same trends, the carbon fiber/vinyl ester resin interface was improved by using two different POSS systems having different functional groups by Mahfuz et al. [79] in order to study the hydrophobic characteristics of POSS particles. Octaisobutyl and trisilanophenyl POSS systems were selected to modify the fiber surface in order to improve the durability of the fiber/matrix interface exposed to three different environmental situations. The composite samples were soaked in seawater at room temperature, seawater at 40^{o}C, and in 85% relative humidity at 50^{o}C over a period of six weeks. They reported that POSS coated samples reduced water absorption by 20-32% when compared to the control samples and the short beam shear test reported about 7-32% improvement in the interlaminar shear strength.

Zhao et al. [80] prepared a carbon fiber/POSS/carbon nanotubes (CNTs) hybrid reinforced composites by grafting CNTs onto the carbon fiber surface using octaglycidyldimethylsilyl POSS as the linkage in order to improve the interfacial properties between carbon fibers and an epoxy matrix. It was reported that POSS and CNTs effectively improve the interfacial adhesion of the composites by enhancing resin wettability, increasing chemical bonding and mechanical interlocking. Multiscale hybrid composites were fabricated by Bekyarova et al. [81] in which the nanotubes were completely integrated into the fiber bundles by the electrophoresis technique. The CNT/carbon fiber/epoxy composites showed 30% improvement in the interlaminar shear strength as compared to that of traditional carbon fiber/epoxy composites.

1.5 Literature Review

1.5.1 Single Fiber Characterization

Characterization of tensile properties such as strength, elastic modulus, and failure strain of carbon fiber (CF) are important for the accurate design and analysis of a reinforced fibrous composite. Various methods have been devised to characterize these properties. Some of the most commonly used methods are: bundle fiber tensile test (BFTT), single fiber tensile test (SFTT) and single-fiber composite test. Typical values using these methods as gathered from the literatures are presented in Table 1.1 [82-86].

The BFTT is the most common approach usually adopted to characterize the tensile properties of carbon fiber because it is less laborious and time consuming. However, the result obtained using this test is less accurate compared to the other methods. BFTT includes the unknown variable of friction between fibers which account for the low value of the tensile properties as obtained using this approach. Friction also accounts for almost 30% apparent strength loss in BFTT results [87]. It has also been reported that the computation of the single fiber strength from the BFTT is possible by adopting an existing numerical model [88-90]. SFTT, on the other hand, is time consuming and it involves testing a large number of samples for the statistical data treatment. Although the results obtained using this method is more reliable than the one got from BFTT.

Table 1.1. Tensile properties of different carbon fibers

Fiber Type (manuf.) [Fiber type]	Gauge length (mm)	Method/Description	Conditioning	Modulus (GPa)	Tensile Strength (GPa)	Reference
AS-1(HexCel)	24.89	Hand-driven tensile testing machine (MTS)	Single fiber composite test	228	3.10	[82]
AS-6G (HexCel)				243	4.17	
IM-6G(HexCel)				278	4.38	
IM7-GP (Tex. Prod)	25.40	Sintech 3365 MTS	As-received single fiber	200	3.80	[83]
AS-1 (Hexcel)	25.40	Tabletop Instron MTS	As-received single fiber	195	2.67	[84]
	0.30				4.47	
AS-6 (HexCel)	25.40			220	3.34	
	0.30				5.94	
IM6 (HexCel)	25.40			276	4.13	
	0.30				6.03	
T650-35 [sized]	25.40	Sintech 3365 MTS (ASTM D3379)	As-received single fiber	217	4.02	[85]
T650-35 [unsized]				200	2.86	
AS4 (HexCel)	5.08	Instron 5566 MTS	As-received single fiber	200	4.00	[86]
	9.91			230	3.60	
	20.07			250	3.40	

Due to the micro-size and fragility of the carbon fibers, close attention should be exercised when the test is being carried out on the tensile testing machine. Yao and Yu [91] mentioned that there are five major error sources that can be introduced into the test data whenever the single fiber tensile test is done without the proper procedures.

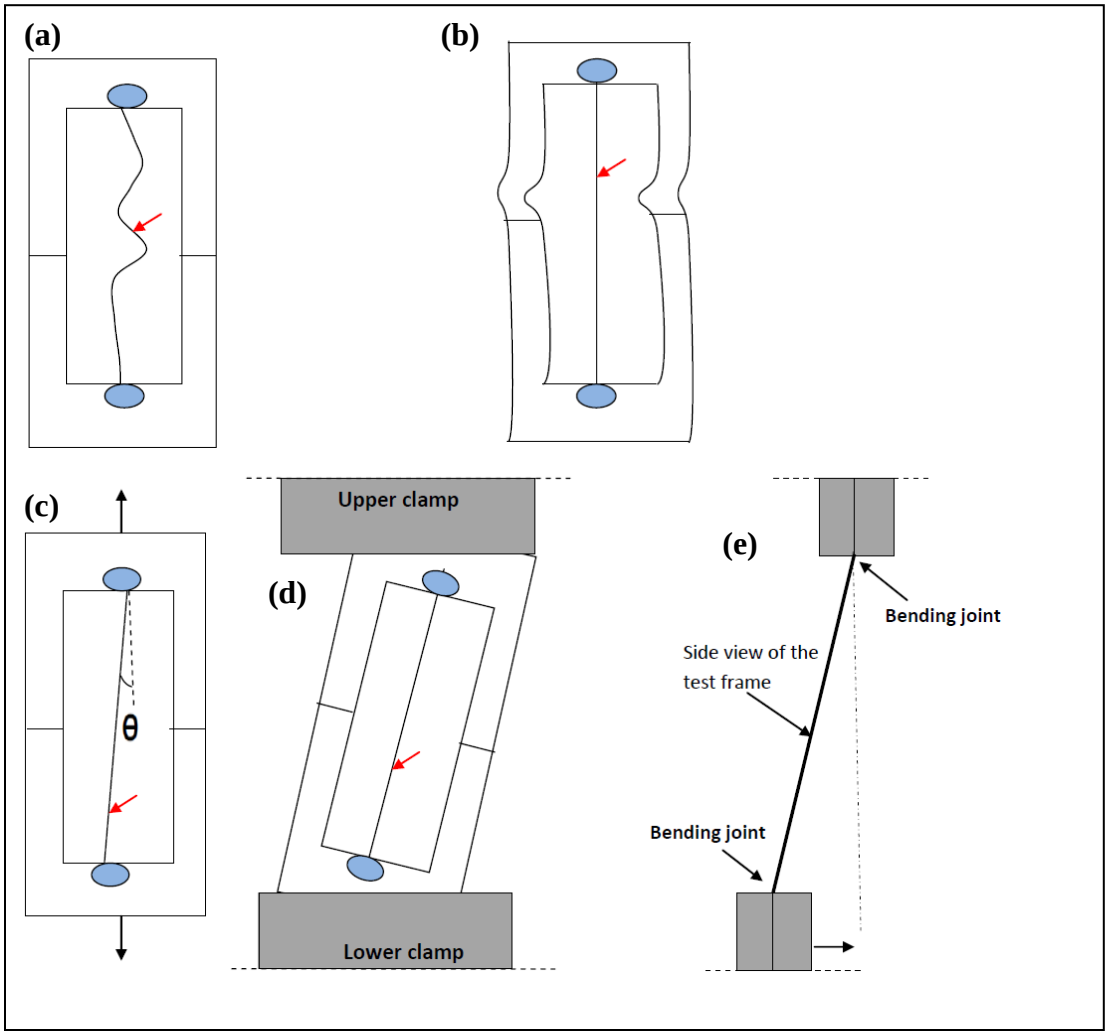

Figure 1.5. Possible sources of error: (a) negative pretensioning, (b) positive pretensioning, (c) fiber misalignment, (d) frame misalignment on the clamps, and (e) clamp misalignment [red arrows pointing to the single fiber]

These errors are schematically shown in Figure 1.5. Under pretension, the fiber should be straight but not stretched. Stretching the fiber can introduce premature cracks and bending. If the pretension is negative (Figure 1.5-a), the fiber between the glued ends

is bent and therefore the tested strain will be greater than the actual fiber failure strain. This is because the fiber length is longer than the nominal length. Positive pretensioning occurs if the window frame is bent instead of the fiber (Figure 1.5 -b) and as a result, the tested strain will be smaller than the actual fiber failure strain because the gauge length is shorter than nominal length. Fiber and frame misalignments (Figure 1.5 -c and -d) are the most common errors experienced while mounting the fiber on the testing frame. When the fiber or the frame is not aligned and parallel to the direction of stretching, both recorded strength and failure strain values become inaccurate due the presence of bending and shearing stresses at the glued ends because of an inclined angle, Θ. However, if the inclined angle is less than 4^{o}, the error due to misalignment can be ignored. Clamp misalignment (Figure 1.5 –e) can be corrected through careful experimental procedure and machine calibration.

Many authors have investigated the effect of the gauge length of PAN-based carbon fibers on their tensile properties, owing to the varying severity of flaws along the fiber length. Heil et al. [92] reported the tensile behavior of AS4 PAN-based carbon fibers of 7.07μm diameter in an ambient environment at three different gauge lengths. It was deduced that samples with a 5.08 mm gauge length exhibited about 10% higher tensile strength compared to samples with a 9.91 mm gauge length, and about 15% higher when compared to samples with a 20.07 mm gauge length. The tensile properties of high performance XA-S carbon fibers were reported by Stevanovic and Pesikan [93]. According to their report, the decrease in fiber strength and failure strain was related to size effect behavior. It was assumed that the strength of the fiber was mainly controlled by the critical stability of the graphene crystals, which were statistically distributed in the

fiber volume. Paiva et al. [94] considered Sigrafil C320PAN-basedCFs to examine the effect of gauge length on the overall fiber tensile properties at the ambient temperature. The gauge lengths considered were 20 mm and 40 mm. They determined that the average tensile strength for about 94 single filaments dropped by only 1%.

Recently, Sager et al. [70] indicated in their data that sized T650 carbon fibers have consistent improvement in the tensile properties, as compared to the unsized (without sizing application) fiber. A single fiber test was carried out on 25 mm window size and the data showed that tensile strength, modulus, and failure strain for sized fiber increased by 29%, 8%, and 23%, respectively as compared to the unsized fiber. A similar result was also reported by Deng et al. [95] for G34-700 (Grafil) carbon fibers using a 20mm gage length. The as-received fibers were surface-treated by electrochemical oxidation, followed by applying a thin layer of epoxy sizing (about 0.4% by mass). It was reported that the surface treatment increased the tensile strength of the sized fiber by about 8% when compared to the untreated fibers; however, the modulus was reported to be constant. It was also deduced that the tensile strength for both fiber types greatly depends on the fiber gage length.

Naito et al. [66] were able to grow CNTs on the PAN-based carbon fiber bundles using the thermal CVD method at 750^{o}C for 15min. It was reported that at this growth temperature the CNTs grew uniformly into a three-dimensional network on the bundles. The strength, ductility, and Weibull modulus were also reported to be improved. In contrast, Sager et al. [70] also reported a dramatic decrease in the tensile properties of the CNTs' grafted single fibers prepared at 800^{o}C for 30min in an Ar/H_2 environment. The

observed decrease of about 30% in tensile strength value was attributed to the location of extracting single fibers in the bundles after the growth and the reaction temperature.

Downs and Baker [96] performed similar work using a Cu-Ni catalyst at the loading rate of 1:9 in the presence of a H_2/He mixture at 600^{o}C for 5min, followed by a 15min heat soak at 350^{o}C to ensure the complete reduction of the catalyst before the system reached a situation where this conversion could induce PAN-based carbon fiber degradation. After the single fiber testing was performed on the CNFs grafted carbon fibers, they reported an improvement of about 3% in the tensile strength value when compared to as-received samples. The improvement was attributed to the method adopted as mentioned.

Many studies have been done on desizing (removing sizing content) fibers through solvent extraction or thermal treatment at different temperatures and hold-times in order to improve the fiber/matrix interfacial properties [97,98]. Lee and Kang [99] performed an experiment on desizing T300 carbon fiber by heat-treating the fibers at 300^{o}C for 4 hours in an inert environment. They concluded that the heat treatment increased the fiber surface area, thereby transforming the surface micropores into macropores for matrix molecules' better penetration. This, however, was shown to be the reason for the improved fiber/matrix interfacial properties.

Weitzsacker et al. [100] also carried out the heat extraction of sizing materials from T40R (PAN-based) and P75 (Pitch-based) carbon fibers by passing a current through the fibers in a specially modified vacuum chamber, and then monitoring the temperature with an aid of an optical pyrometer. The samples were held at 870, 1250, and 1650^{o}C for about an hour. The same experiment was repeated using the solvent extraction

method by making use of Dimethylformamide (DMF) and Methylene Chloride ($MeCl_2$). The reaction was carried out under reflux by putting the samples in the solvent for about 30 minutes and then, after the treatment, the samples were rinsed in acetone and dried in an oven set at 60^{o}C for 30 minutes. Their findings showed that fiber sizing can be partially removed through the use of the solvent extraction method, and complete extraction can be achieved by heating the fiber at a high temperature in order to decompose the sizing content. However, once the sizing is removed, there is an indication of critical fiber surface damage.

Recently, Zhishuang et al. [101] reported that the strength of the T300B carbon fiber/matrix interface reduced drastically after the fiber had been subjected to a series of heat treatments. The change was described to be as a result of a reduction in their surface energies. The fiber was heat treated from room temperature to 150^{o}C for 2 hours; held at this temperature for another 2 hours; then heated from 150 to 180^{o}C at 2^{o}C/min; held at this temperature for 2 hours; heated again from 180to 200^{o}C at 2^{o}C/min; and held at this temperature for another 4 hours. Similarly, the graphitization degree of T300 carbon fiber, when subjected to heat treatment between 400 - 1400^{o}C inside the vacuum for an hour, had been found to improve. This was attributed to a reduction in their interlayer spacing and an increase in their crystalline dimensions [102].

1.5.2 Characterization of Fiber-Matrix Interfacial Properties

The interface between two materials determines, to a great extent, the optimum mechanical performance of the heterogeneous systems, such as composite materials. Most of the composites are made of the matrix and other inclusions that are distributed within it in the form of fibers, nanoparticles, or other fillers. The interfacial adhesion

between the surface of the fibers (for instance) and the matrix need to be characterized in order to understand the failure mechanism of the composite at the fiber/matrix interface. Several characterization techniques have been developed in order to determine fiber/matrix interfacial properties. These techniques are usually based on single fiber tests, although there have been some reports that adopted the same technique for semi-bundle tests. The single fiber-matrix interface is loaded uniaxially until failure, and the experimental data are reduced based on certain theories to calculate for the interfacial shear strength (IFSS).

Micromechanical tests can be categorized into two groups, based on the method of load application on the fiber [103-111]. The first group involves the direct loading of the fiber, and this includes techniques such as the fiber pull-out test, microbond test, three-fiber test, and push-out test. The second group involves direct loading on only the matrix, and this includes the Broutman test, fragmentation test in tension mode, and fragmentation test in bending mode. Figure 1.6illustrates the different micromechanical tests as mentioned above. Single fiber pullout and fragmentation tests have remained a dominant approach to characterize the interfacial properties of fiber-matrix.

Hung et al. [112] carried out single-bundle pull-out tests on the CNT grafted carbon fibers using a room temperature cured resin. The bundle was selected because the fiber proved to be very brittle after the CNTs' growth. After a close examination of the pullout holes, they discovered that the pullout of fibers leaves micro-scale holes on the resin wall, while pullout of nanotubes leaves nano-scale holes. Three major types of CNT fractures were reported during the pullout, and this was attributed to the nature of growth and the population density of the CNTs. Polacek and Josef [113] also investigated the

effect of the composition of the particulate filled esthetic composite veneer (PFC) on the shear strength of adhesion between the fiber reinforced composite framework and the PFC. The nominal shear adhesion strength was measured to be dependent on the filler content and the embedded length of the FRP rod in the PFC cylinder.

Mooney and McGarry [114] developed a single fiber compression test method based on microcomposites in order to measure the bond strength of glass fibers with transparent polymer matrices. Two different types of specimen geometry were adopted depending on the modes of failure that occur at the fiber-matrix interface: one has along the hexagonal shape with a uniform cross-section and the other has a curved neck in the middle (Figure 1.6 (f)). When the parallel-sided specimen is loaded in a longitudinal compression, shear stresses are generated near the fiber ends as a result of the difference in elastic properties between the fiber and the matrix. Further loading eventually causes the debond crack to start from these areas due to the interfacial shear stress concentration. When the curved-neck specimen was loaded under longitudinal compression, the interface debonding occurred in the transverse direction (tension debonding) due to the transverse expansion of the matrix when its Poisson ratio is higher than that of the fiber.

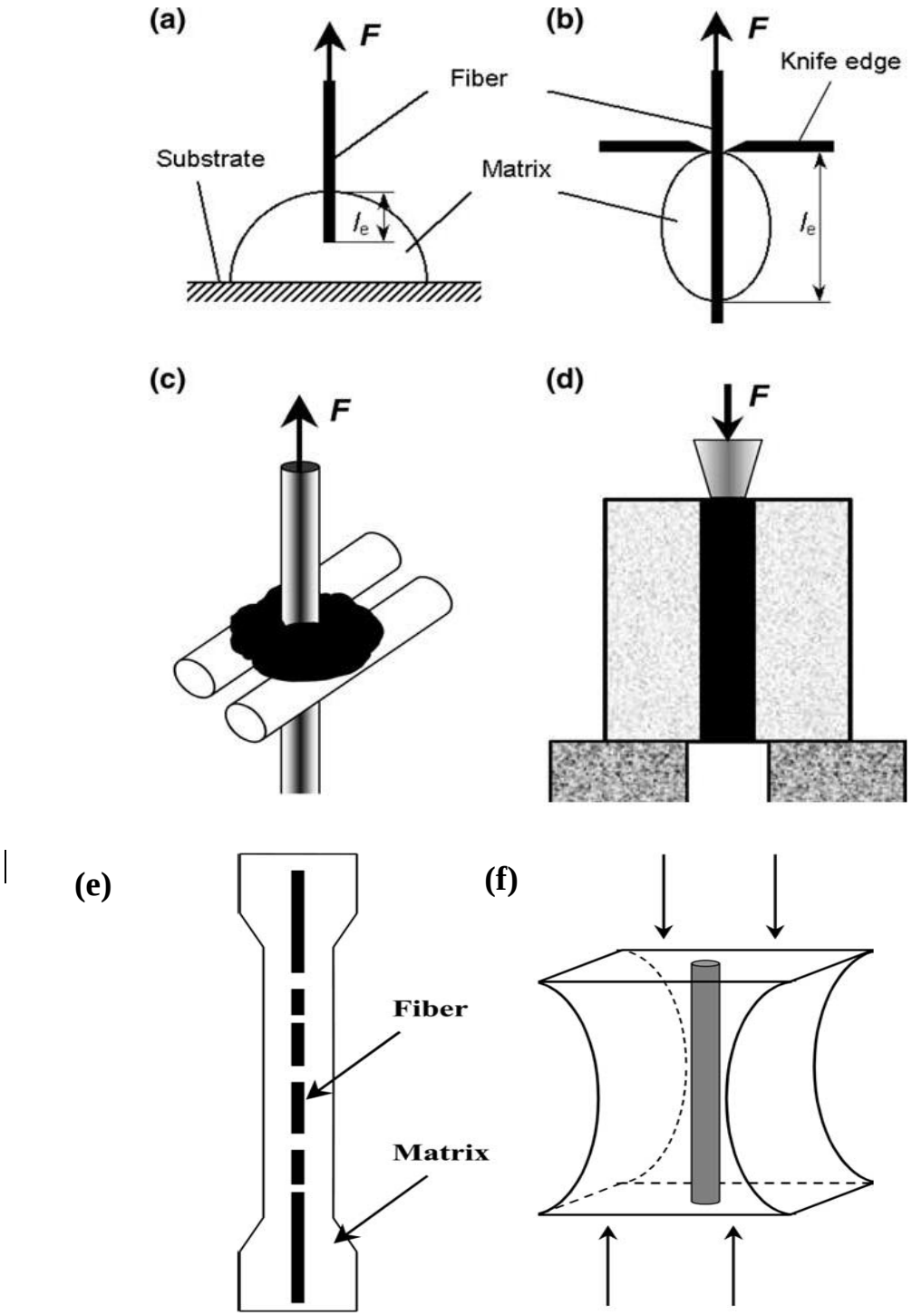

Figure 1.6. Different micromechanical tests: (a) pull-out test, (b) microbond test, (c) three-fiber test, (d) push-out test, (e) fragmentation test, and (f) Broutman test

The fiber push-out test is also commonly known as microindentation test. This is a single fiber test technique capable of examining fibers embedded in the actual composite system. In this test a microhardness indenter with various tip shapes and sizes is normally used to push against a fiber end into the matrix block. Mandell et al. [115], performed this test with the use of a spherical indenters in steps of increasing force and the interface bonding is monitored between each step until total debonding is observed.

In the fiber pull-out test, a fiber is partially embedded in a matrix of various sizes and shapes. The matrix is fixed in place and the fiber is loaded in tension. The external force applied to the fiber is recorded as a function of time and displacement during the whole pull-out process.

1.5.3 Dynamic Mechanical Analyzer (DMA)

There are many micromechanical devices designed basically to determine the tensile performance of micron-sized materials. Paiva et al. [116] characterized the tensile properties of ultra-high and high modulus pitch-based circular (P120J and P75S) and ribbon-shaped fibers, and high-strength PAN-based fibers using an Instron 1122 universal testing machine equipped with a load beam of 5 N at a crosshead speed of 0.5 mm/min. The typical crosshead speed range of this machine is between 0.002 to 50 in/min, and it has a load range 0.1N – 5kN. A 6-41 mm gauge length was selected for their work. It was concluded, after the single fiber test, that for some of the samples and for the 6, 10, and 15 mm gauge lengths, an inconsistency of the strength was observed. This was attributed to the degree of end-effect introduced into the test data from the hydraulic grips.

Axial tension and transverse compression tests were also performed on hydraulically driven MTS-180 by Lim et al. [117] on single fibers in order to investigate the mechanical behavior of three high-performance fibers (Kevlar, Kevlar 129, and Twaron) with diameters in the order of 9-12 μm. The effect of gauge length on the tensile properties was investigated on 2.5mm, 5.5mm, 10mm, 50mm, 100mm, and 250mm fiber lengths, and it was concluded that the gauge length variation did not have any significant effect on these properties. However, close observation of the data acquired at strain rate 0.001/s for all the fiber quasi-statically tested indicated a nonlinear stress-strain behavior. This might be a result of error introduced as a result of the machine's non-capability to resolve the strain accurately.

Drzal and Rich [118] carried out a similar micro-tensile test on the PAN-based carbon fibers using a Tecam microtensile tester. It was reported that the tensile strength of all the fibers tested (AS-1, AS4, AS6, and IM6) at 0.012-inch was more than 25% higher than the manufacturers specification. This machine has the capability to handle a specimen with dimensions as small as 0.5mm, however, it was reported that its normal electronic system stability is insufficiently drift-free as the sample length decreases. The machine employs a torsion balance to apply the loads, and a mirror autocollimating telescope system to detect the extensions. Since it depends wholly on mechanical and optical principles, it is practically not a drift-free system at a constant temperature. As a result, the source of the huge variation between the experimental and manufacturer report might be from the error generated when the torque was transmitted through the torsion wire to the specimen ends and the over-pressurization of the frame-gripped ends.

Dynamic mechanical analyzer (DMA-Q800 by TA Instruments) is the world's best-selling DMA because it utilizes state-of-art, non-contact, linear drive technology to give an accurate and precise control of stress, and it also uses an air bearing for low friction support. Strain is measured using optical encoder technology that provides unmatched sensitivity and resolution (1nm). Figure 1.7 shows the major components of the Q800 [119]. The drive motor is constructed of high performance composites that ensure low compliance, and is thermostated to eliminate heat build-up even when using large deformation amplitudes and high deformation forces. Sophisticated electronics enable the motor current to be rapidly regulated in small increments, thereby enabling the reproducibility of forces over a wide range. The force is transmitted directly to a rectangular air bearing slide from the non-contact drive motor that provides the oscillatory or static force during the test. The rectangular slide is guided by eight porous carbon air bearings. The pressurized air is made to flow into the bearings forming a frictionless surface, which permits the slide to float vertically within a 25mm distance. The rectangular shape of the slide prevents any testing error that might be generated from twisting the gripped sample frame. The optical encoders provide a better resolution as compared to the conventional linear variable differential transformer (LVDT) used on most of the MTS tensile testers.

The high-resolution linear optical encoder is therefore used for precise measurement of the sample displacement. The principle is based on the light diffraction patterns created through moveable and stationary gratings on the encoders. The encoder has a high resolution of about 1nm, and this typically provides the precise measurement of very small amplitude. With this high strain resolution, combined with the non-contact

drive motor and air bearing system, the Q800 is able to provide excellent modulus precision and high tan δ sensitivity for a broad range of materials, including carbon fiber. The Q800 is equipped with a variety of sample clamps that have been optimized using finite element analysis.

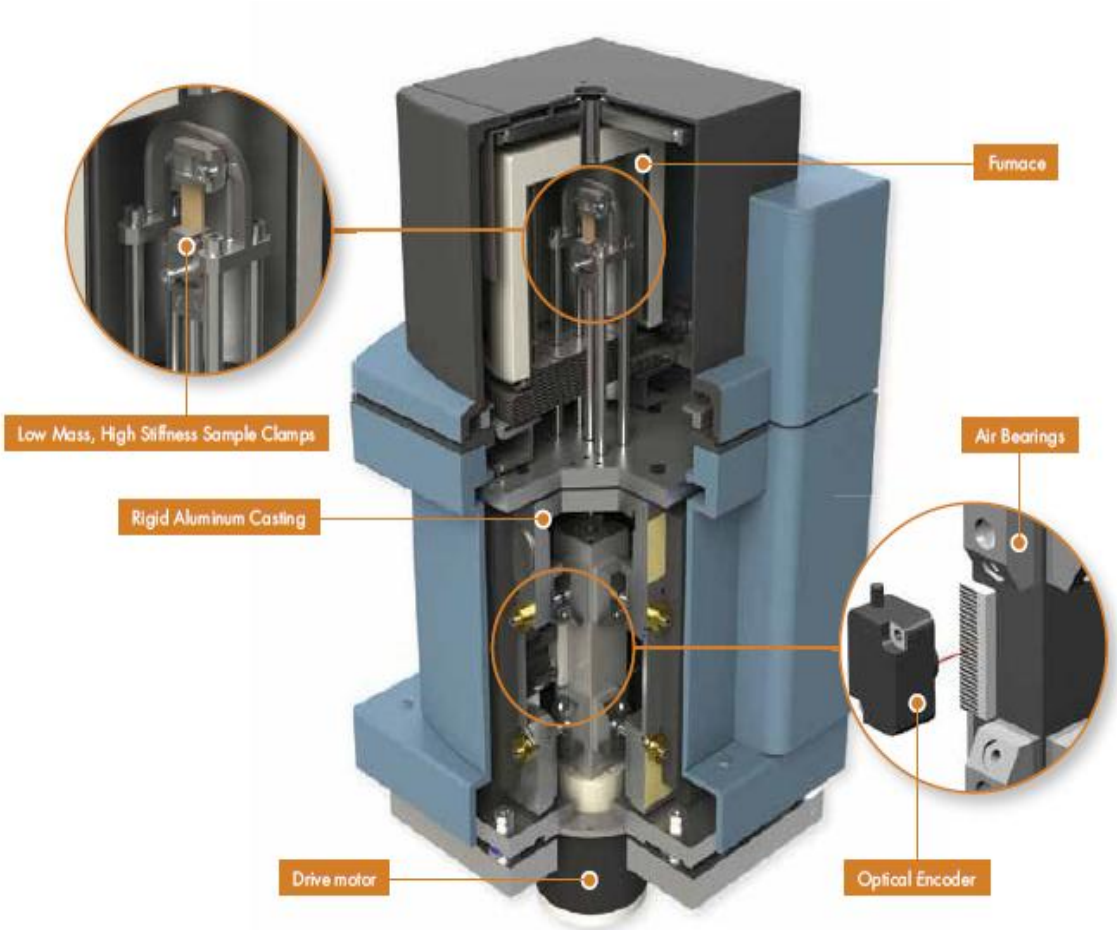

Figure 1.7. Major features of the DMA Q-800 [121] -***Copyright 2012, TA Instruments. Used with permission***

The clamps provide multiple modes of deformation based on the sample preparation, clamp selection, and calibration. High stiffness property of the clamp enables minimum compliance requirement, whereas the clamp low mass ensures faster

temperature equilibration. The available clamps include dual/single cantilever, 3-point bend, shear sandwich, compression, submersible, and tension clamps. The tension clamps are suitable for micron-sized materials.

1.6 Research Questions and Objectives

Some of the fundamental research questions to be addressed in this work will include:

- How different surface modification methods could affect the tensile properties of single fiber, and
- How different surface modification methods could also affect the interfacial performance of fiber-reinforced composite

The research tasks would, therefore, involve carrying out the aforementioned research questions in the following approaches:

- Determine the feasibility of using DMA-Q800 to carry out both tensile and pullout tests on different types of (treated and untreated) PAN-based fibers
- Develop a test method to improve the accuracy and testing of single fiber
- Examine the effect of sizing and heat treatment on the tensile properties of AS4, AS7, and IM10 PAN-based CFs
- Examine the effect of sizing on the interfacial performance of AS4 PAN-based CFs in an epoxy matrix
- Examine the effect of sizing and other surface modification treatments including the CNTs grafted fiber on the surface roughness of treated and untreated micron-sized PAN-based CFs

CHAPTER 2

SURFACE MODIFICATION AND CHARACTERIZATION

2.1 Removing Sizing by Thermal Process

2.1.1 Selecting the Fibers

The fibers were chosen based on the areas of application, year of existence, epoxy compatibility, and the type of sizing. Commercially available sized PAN-based AS4, AS7, and IM10 carbon fibers were supplied by Hexcel Corporation. The sized fibers were supplied with proprietary surface treatments and a protective sizing (epoxy compatible sizing). The AS4 sized fiber was available in woven fabric form, and the other fibers were supplied in continuous roving form. All of the sized fibers were coated with the same sizing ingredients [120]. The physical and mechanical properties of the sized fibers are listed in Table 2.1. Each of the fiber bundles contains 12,000 filaments, and has approximately the same density (1.8 g/cm^3).

Table 2.1. Physical and Mechanical Properties of As-received Sized Fibers (manufacturer's specifications except the diameter values)

Fiber Type	Precursor	Diameter (μm)	Filaments (counts)	Yield (m/g)	Density (g/cm^3)	Tensile Strength (MPa)	Tensile Modulus (GPa)	Failure strain (%)
AS4	PAN	7.1 ± 0.16	12k	1.17	1.79	4475	231	1.8
AS7	PAN	6.9 ± 0.12	12k	1.25	1.80	4889	246	1.8
IM10	PAN	4.4 ± 0.09	12k	3.09	1.79	6964	303	2.1

2.1.2 Experimental Method

The fibers were desized using a TA Instruments Q50 thermogravimetric analyzer. A single tow from each of the fiber types was separated from the bundles, curled, and inserted inside the TGA ceramic pan (500 μL). The analyzer was programmed to ramp from 35^{o}C to 435^{o}C at 2^{o}C/min. The first set of samples was heat treated by subjecting them to the prescribed procedure and cooling to the room temperature without being held at this set point. The other sets of samples were held at 435^{o}C for 20 and 60 minutes, respectively. The samples are designated as D-M1 (for samples without hold-time), D-M2 (for samples with 20 minutes hold-time) and D-M3 (for samples with 60 minutes hold-time).

2.1.3 Thermogravimetric Analysis (TGA)

Carbon fiber weight loss as a result of heat exposure in a nitrogen atmosphere was determined using TGA as mentioned above, and the results are displayed in Figure 2.1. The set point temperature (435^{o}C) was chosen based on the formal conversion with the fiber manufacturer and data verification [121]. The heat treatment caused a small weight loss in sized AS4, AS7, and IM10 carbon fibers as shown in Figure 2.1A(ii), B(ii) and C(ii). Figure 2.1A(i), B(i) and C(i) show the derivative weight change with respect to temperature. The weight loss was due to decomposition of the organic-based sizing and some of the fiber burn-off. There were two significant weight drops noticed in AS4 and AS7 fibers, but no noticeable second weight drop was observed in the IM10 carbon fiber.

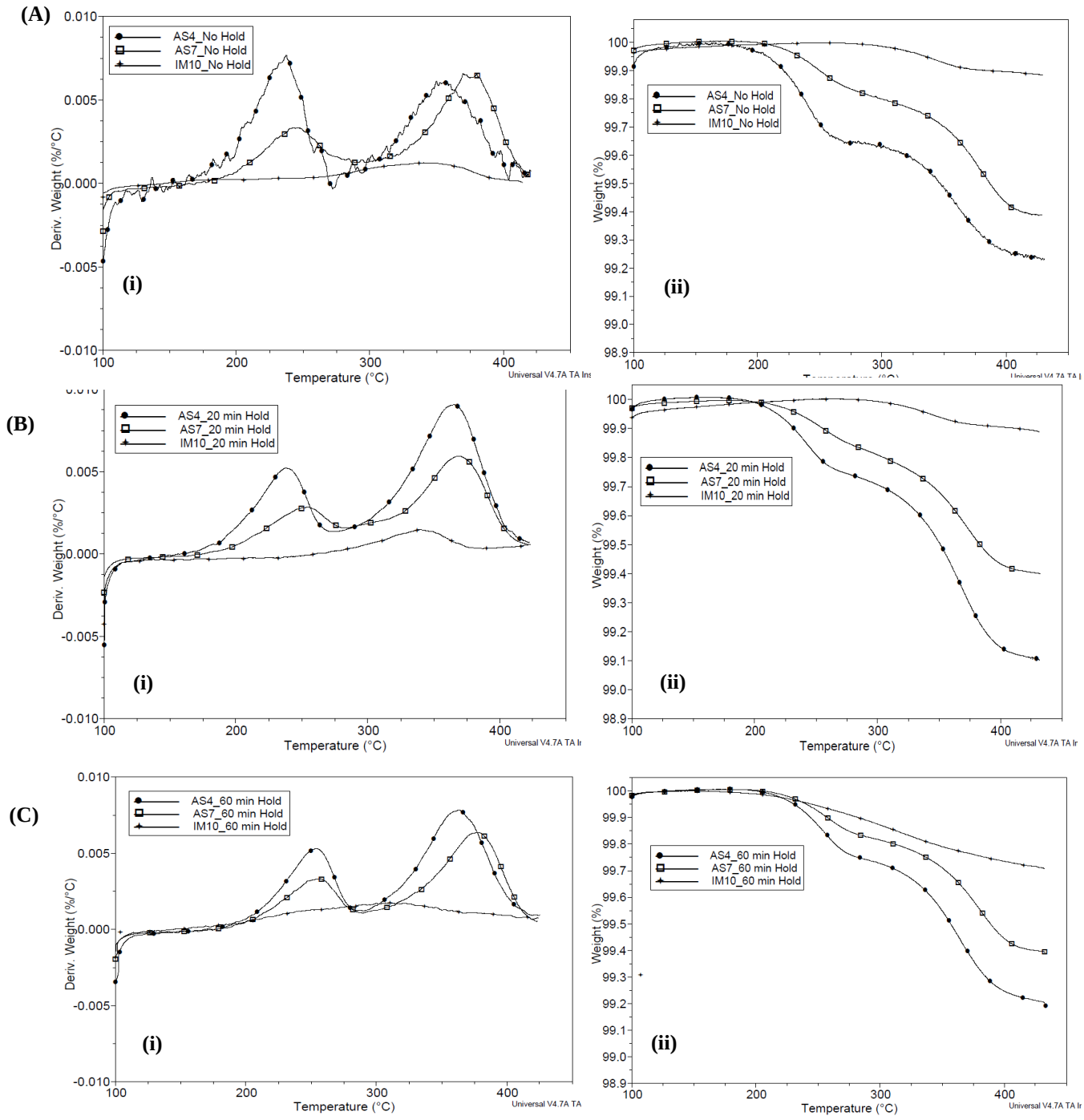

Figure 2.1. Thermogravimetric analysis (TGA) for the thermal stability study of: (A) AS4 fiber (B) AS7 fiber (C) IM10 fiber [(i) Derivative weight change with respect to temperature variation; (ii) Change in weight with respect to the temperature variation]

The first drop in mass might be from the remaining spinning oil that stayed on the fiber, as explained earlier, and the second drop could be from the organic sizing. Note that sized IM10 showed a significant shift in mass.

This could be as a result of a gas flow drag and velocity effects. The gas flow over the hang-down system, such as TGA Q50- used for this work, has been reported to have a dragging effect in the direction of the gas flow. The dragging effect also depends on the type of atmosphere used and the length of the hang-down system [122]. There is evidence from the thermogravimetric analysis that the IM10 fiber is the best thermally stable fiber, followed by AS7 fiber, within the temperature range considered for this work. This might be a result of well-aligned graphene crystals within the fiber due to a higher heat treatment process and stretching during the production procedures, as required for an intermediate modulus fiber.

2.1.4 X-Ray Photoelectron Spectroscopic Analysis (XPS)

XPS is a surface sensitive analysis technique used to obtain chemical compositional and structural information. It identifies all elements (except hydrogen and helium) that are present in the outer 10nm of the skin surface of the fiber (with a detection limit of ca. 0.1 atomic percent). Sized and unsized type of AS4, AS7, and IM10 carbon fiber surfaces were analyzed using the XPS (Physical electronic PHI 5800 ESCA) with standard non-monochromatic Al X-rays (1486.6 eV) operated at 250 W and 15 KV. About 93.9 eV pass energy was used for analysis, and the electron takeoff angle was set at 45^{o} with respect to the sample surface. Figure 2.2 shows the basic illustration on how the electrons are emitted from the fiber surface (typical depth is about 0.01μm) on XPS.

The displaced electrons are collected by the energy analyzer and the detector. The electron kinetic energy and CPS (count per seconds) are measured and recorded for further analysis. Because the energy of an X-ray with particular wavelength is known, the electron binding energy of each of the emitted electrons can be determined using an equation that is based on the work of Ernest Rutherford [123].

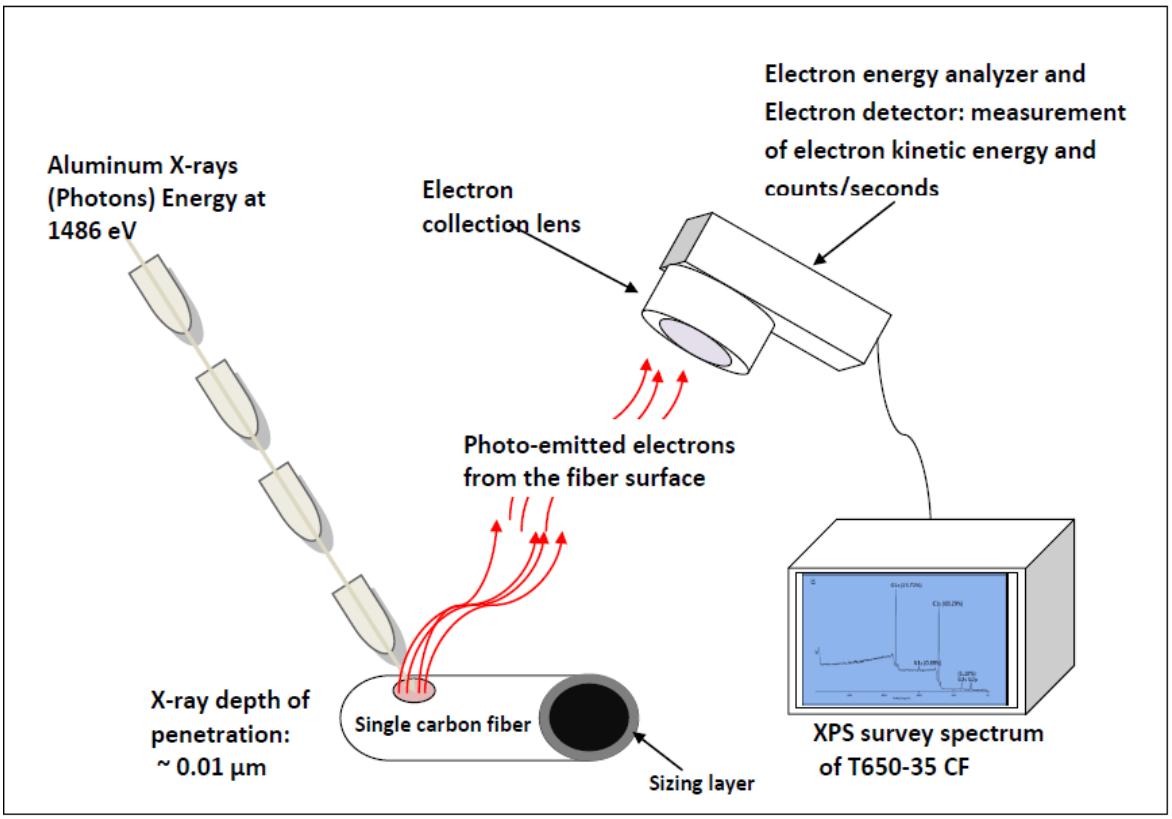

Figure 2.2. Schematic of XPS photo-electric effect on carbon fiber surface

As displayed in Figure 2.3, the main elements on the surface of the sized and unsized AS4, AS7, and IM10 carbon fibers are oxygen and carbon. The concentration of nitrogen for the unsized fibers is higher than that of the sized fibers in all of the fiber types. However, a lower concentration of nitrogen was observed in AS4_UnS. The nitrogen on the sized fibers has been reported to be attributed to the nitric functional

groups in sizing, while the nitrogen on the unsized fibers might have come from the incomplete carbonization of a PAN-based precursor [97]. Therefore, it seems that AS4_UnS underwent the same thorough carbonization process as AS4_S. The surface chemical compositions of the sized and unsized fibers are shown in Table 2.2. It was found that the surface carbon element concentrations are 75.71%, 88.14%, and 85.9% for AS4_UnS, AS7_UnS, and IM10_UnS fibers, respectively. Moreover, surface carbon element concentrations are 78.13%, 82.94%, and 80.80 % for AS4_S, AS7_S, and IM10_S carbon fibers, respectively. When considering the increase in oxygen atomic concentrations in the sized fibers as compared to unsized, there are oxygen content increments of 7.3%, 37%, and 37% for AS4_S, AS7_S, and IM10_S fibers, respectively. This indicates that the sizing has introduced a large amount of oxygen present on the fiber surface due to the presence of carboxyl, hydroxyl, and carbonyl functional groups.

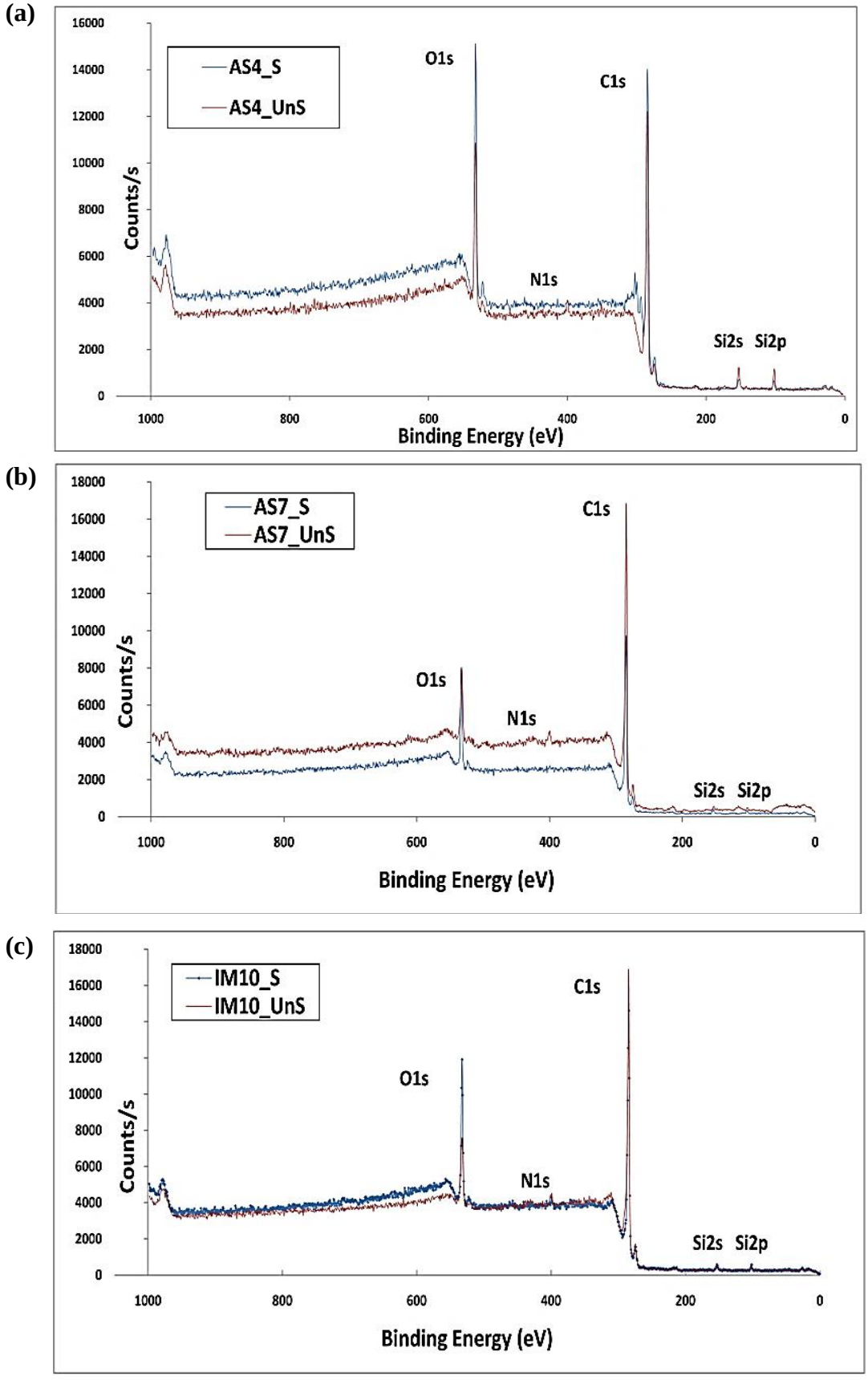

Figure 2.3. Overall spectra of sized and unsized carbon fibers: (a) AS4, (b) AS7 and (c) IM10

Table 2.2. XPS surface element analysis

	Chemical Composition [at %]				Atom Ratio	
Fiber Type	C	N	O	Si	O/C	N/C
AS4_UnS	75.71	1.88	18.29	4.12	0.2416	0.0248
AS4_S	78.13	0.98	19.72	1.16	0.2524	0.0125
AS7_UnS	88.14	2.07	9.79	0.00	0.1111	0.0235
AS7_S	82.94	0.02	15.65	1.39	0.1887	0.0002
IM10_UnS	85.90	2.12	10.55	1.43	0.1228	0.0247
IM10_S	80.80	1.51	16.62	1.07	0.2057	0.0187

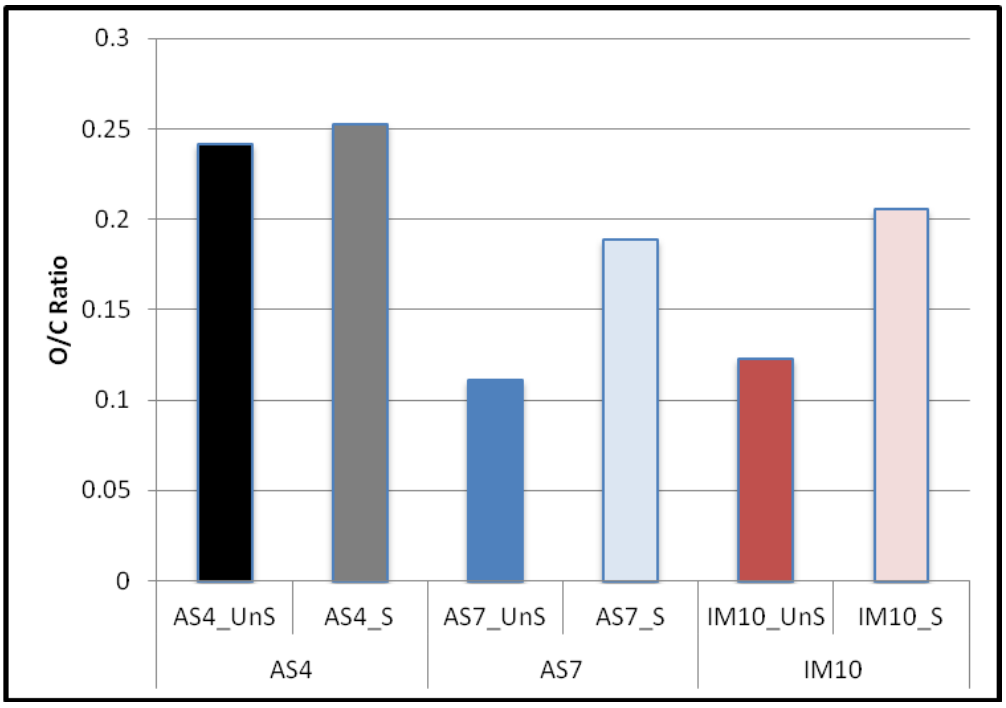

Figure 2.4. The oxygen contents on both unsized and sized CFs: AS4, AS7 and IM10

As shown in Figure 2.4, the ratio of oxygen to carbon atomic concentration in the unsized and sized fibers are 0.24:0.25, 0.11:0.19, and 0.12:0.21 for AS4, AS7, and IM10 carbon fibers, respectively. The increase as observed in these ratios might be attributed to the fiber surface active species. A peak was observed at 289.1 eV binding energy in all the sized fibers, corresponding to carboxyl group (O=C-O), suggesting that the active

species are from the sizing [124,125]. The increase in the amount of surface active functional groups normally provides a good tendency for improved adhesion on carbon fiber/matrix interface.

2.1.5 Electron Microscopic Analysis

Figure 2.5(a,c, and e) presents SEM images of AS4_S, AS7_S, and IM10_S all in as-received nature. This is the truest representation of about fifteen images taken on each fiber type. The relative smoothness of these fibers was attributed to the wet spinning process employed to produce the PAN filaments used as raw material in the carbon fiber processing and sizing application. The striated pattern was noticed along the fiber's axis. The striation depth was found slightly deeper in AS4_UnS, AS7_UnS, and IM10_UnS (as shown in Figure 2.5 b, d, and f, respectively) as compared to the sized fibers. This is attributed to the uncovered surface grooves, since the fibers are not coated with any sizing material. However, the striation depth for IM10_UnS was clearly displayed compared to AS4_UnS and IM10_UnS.

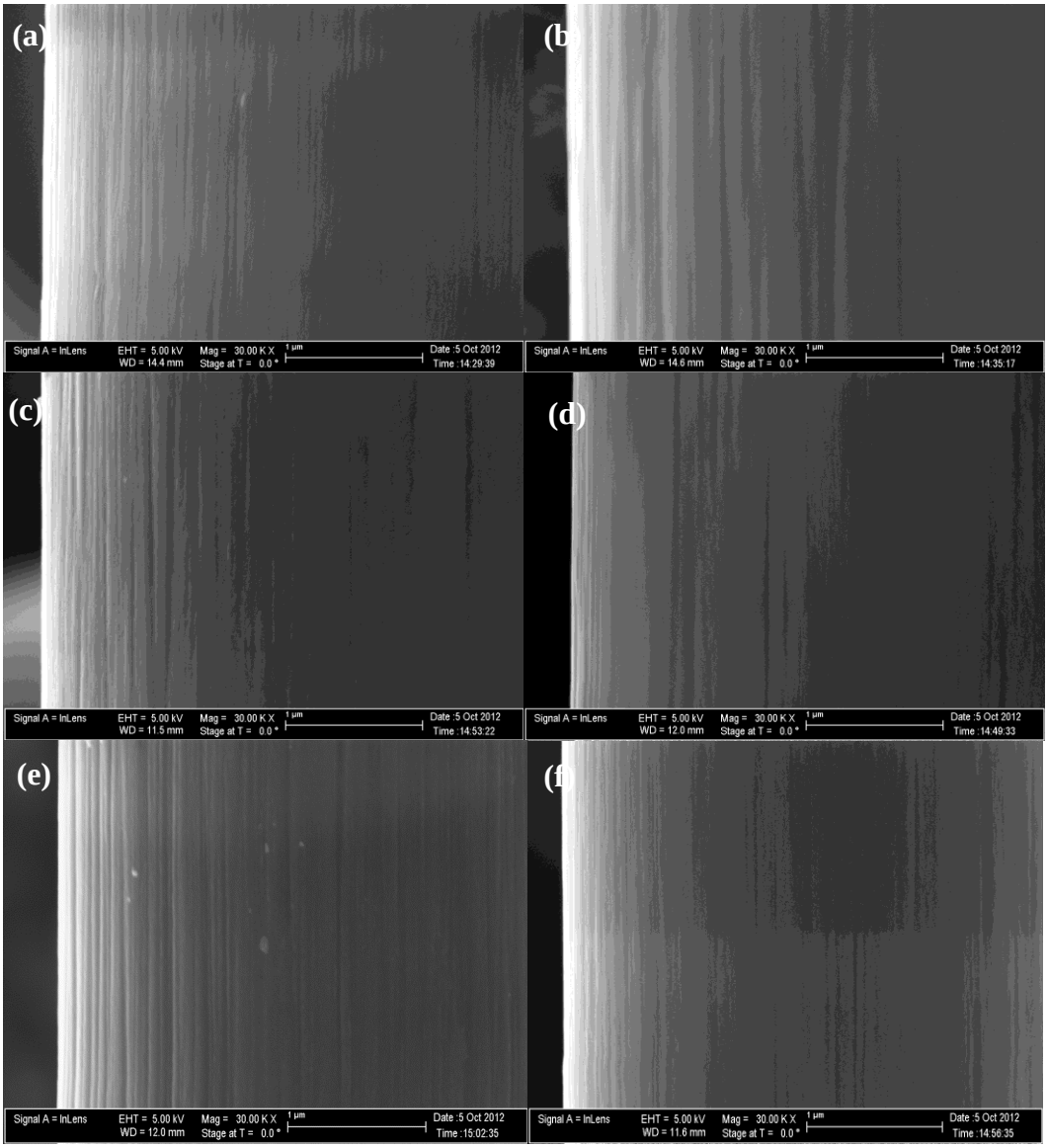

Figure 2.5. SEM images of carbon fibers: (a) AS4_UnS, (b) AS4_S, (c) AS7_UnS, (d) AS7_S, (e) IM10_UnS, and (f) IM10_S

Figure 2.6 (A, B and C) also presents SEM images of AS4, AS7, and IM10 carbon fibers at their respective heat treatment hold-time. This is the truest representation of about eight images taken on each fiber type. There is an indication of well-pronounced surface striations along the fiber axis in D-M1 and D-M2 samples in all the fiber types.

The striation depth and defects were found well defined in D-M3 in all the fiber types, with more defects shown clearly in IM10_D-M3 than the others.

Interesting features on the decomposition of sizing is shown in Figure 2.7. The high-resolution micrographs were also taken with a Zeiss NEON 40-EsB. As shown, there was an indication that as these fibers were held at the set point, the sizing layer began to melt and the level of decomposition depended more on the hold-time. Complete removal of the sizing layer from all three fibers seemed to occur when the fibers were held for 60 minutes at 435^{o}C. The micrographs taken on these samples (D-M3) gave clearer skin surfaces. The remains of the polymer coating were analyzed for oxygen content using the energy dispersive spectroscopy (EDS) at the specified locations as shown in Figure 2.8. The oxygen to carbon ratio for location 1,2, and 3 is 6.2%, 5.5%, and 1.9%, respectively. The melted sizing content in location 3 is lower than the other locations.

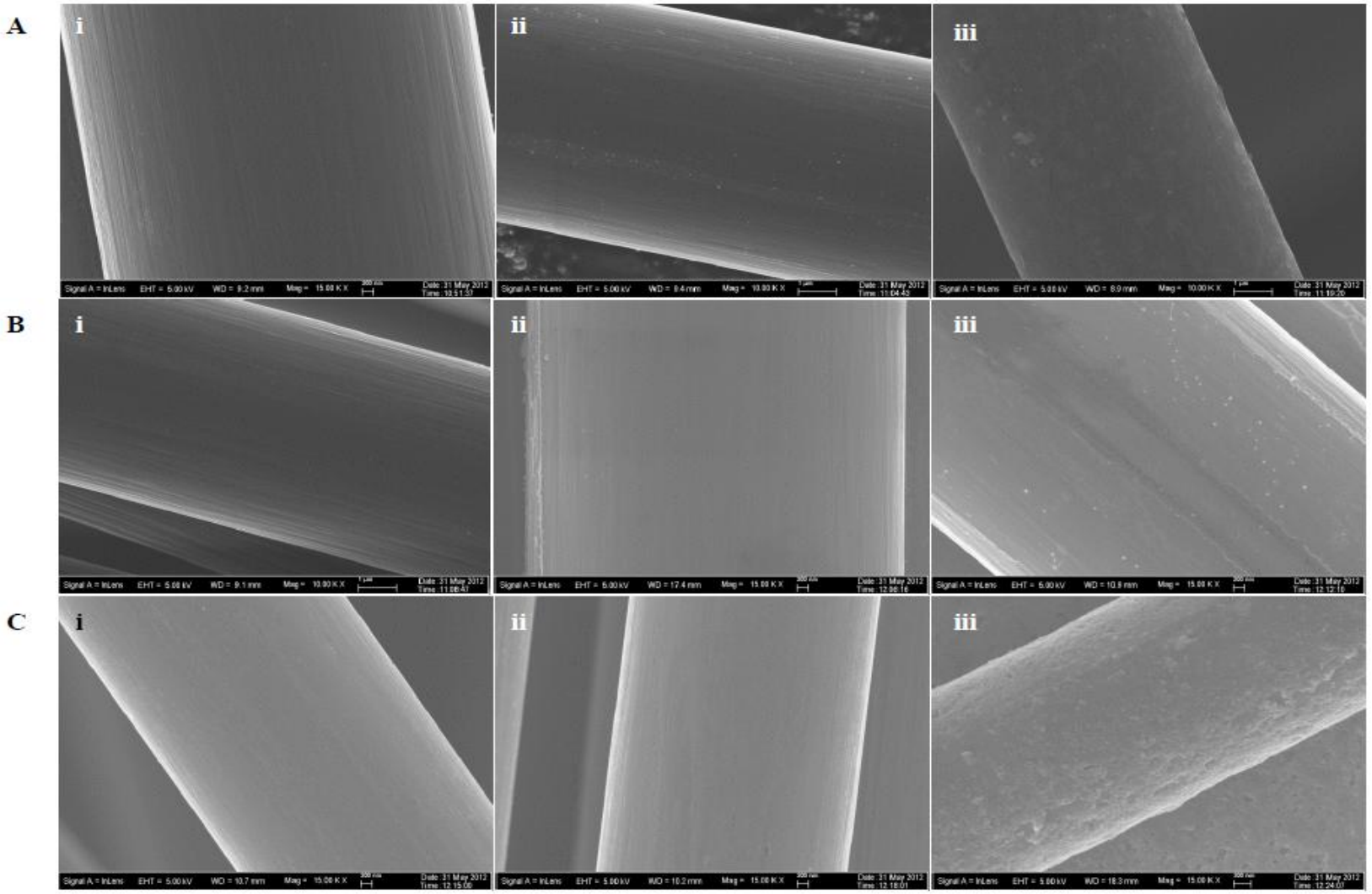

Figure 2.6. SEM micrographs showing the individual fiber skin morphologies: (i) D-M1, (ii) D-M2, and (iii) D-M3 [A- AS4 CF, B- AS7 CF, and C- IM10 CF]

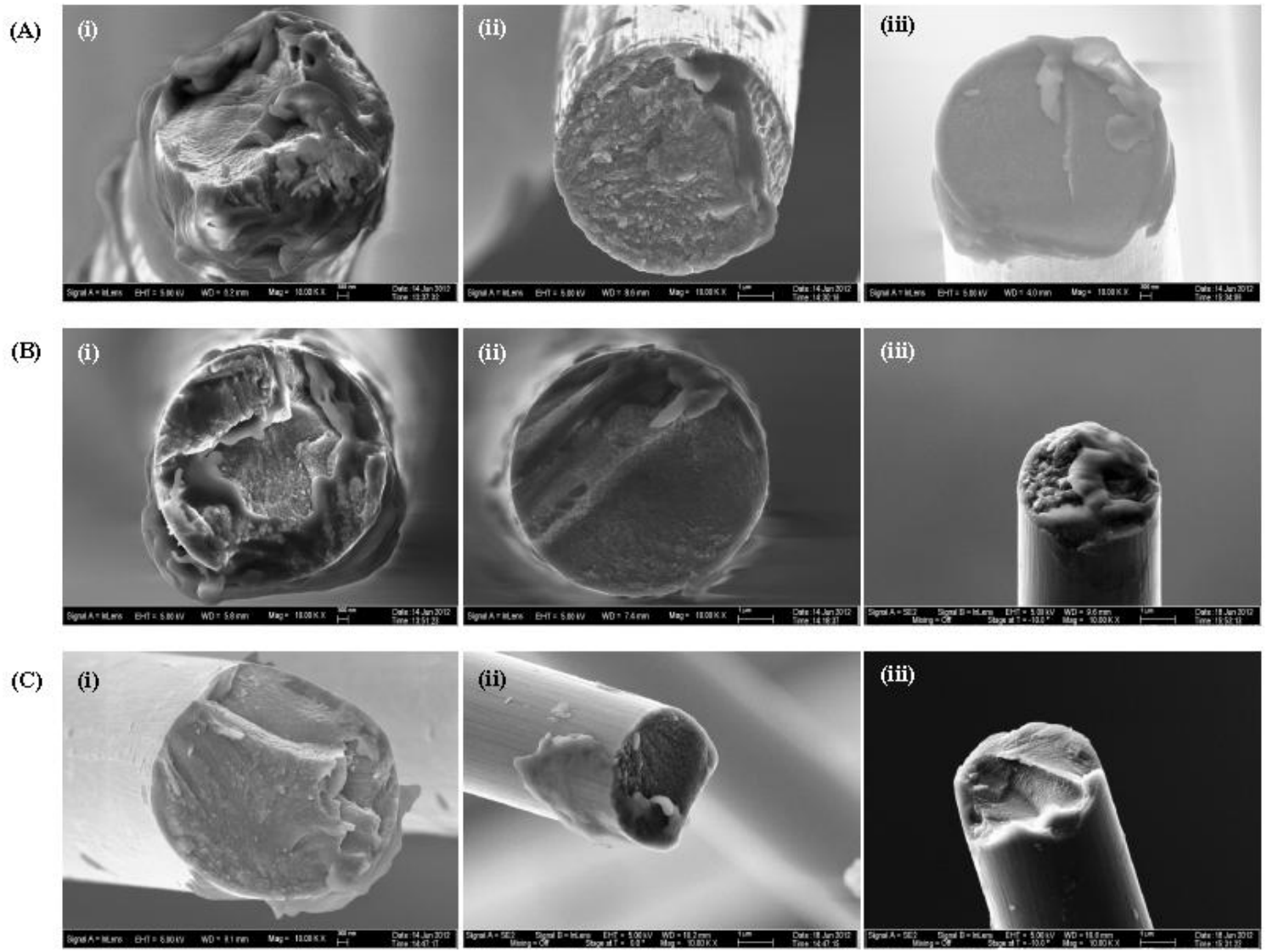

Figure 2.7. SEM micrographs of the desized fiber surface treated at respective hold-time: (A) D-M1 (B) D-M2, and (C) D-M3 [(i) AS4 fiber; (ii) AS7 fiber, and (iii) IM10 fiber]

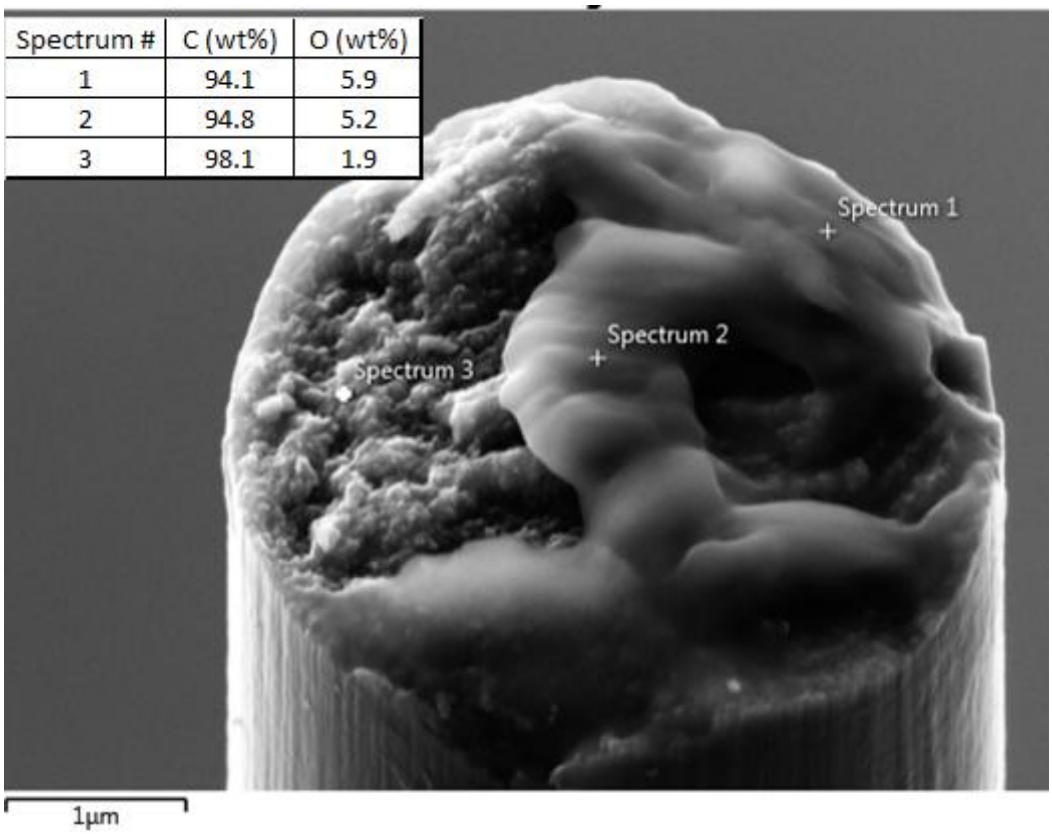

Figure 2.8. EDS spectrum of the sizing remains after the heat treatment on IM10_D-M2

2.1.6 Topography Analysis of Fiber Surface using Atomic Force Microscope (AFM)

The fibers' surface roughness was examined with the use of an atomic force microscopy (AFM) named Pacific Nano-R Nanotechnology. A mounted nano-close-contact silicon probe with a tip radius of 10nm was considered for this measurement. The V-shaped microlever (where the probe is mounted) was designed with a spring constant and resonance frequency of 40 N/m and 300 kHz, respectively. A single carbon fiber from each fiber type was fixed to a microscope slide with dimensions of 22 x 22 x 0.17 mm at two points using super glue® with special care taken so that the top surface of the

fiber was not covered with the glue. All images were collected in air in the close contact mode within 1 µm x 1 µm image area as shown in Figure 2.9.

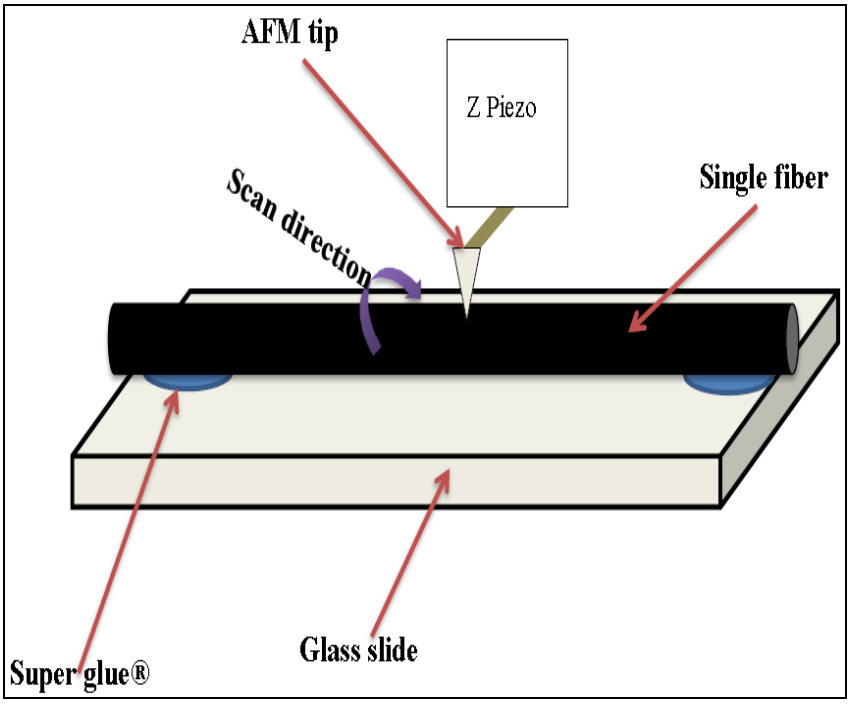

Figure 2.9. Sample preparation approach for AFM

Figure 2.10 (a) and (b) shows the three-dimensional AFM images for unsized and sized AS4 fiber surfaces, respectively. Figure 2.10 (c) and (d), and Figure 2.10 (e) and (f) also show the images for unsized and sized AS7 and IM10 fibers, respectively. Surface roughness parameters including root mean square (R_q), arithmetic mean roughness (R_a) and the profile maximum height (R_t) were calculated using Equation (1), (2), and (3).

$$R_q = \sqrt{\frac{1}{N^2}\sum_{i=1}^{N}\sum_{j=1}^{N}(Z_{ij} - \hat{z})^2} \quad (1)$$

$$R_a = \frac{1}{N}\sum_{i=1}^{N}\sum_{j=1}^{N}|Z_{ij} - \underline{z}| \quad (2)$$

$$R_t = |Z_{ij}|_{max} - |Z_{ij}|_{min} \quad (3)$$

Where *N* is the number of data points in the image,*i* and *j* is the location of the pixel on the AFM image, z_{ij} is the height at i and j locations, $\hat{z}$ is the average height value within the given area, and $\underline{z}$ is the height value from the center plane [126,127].

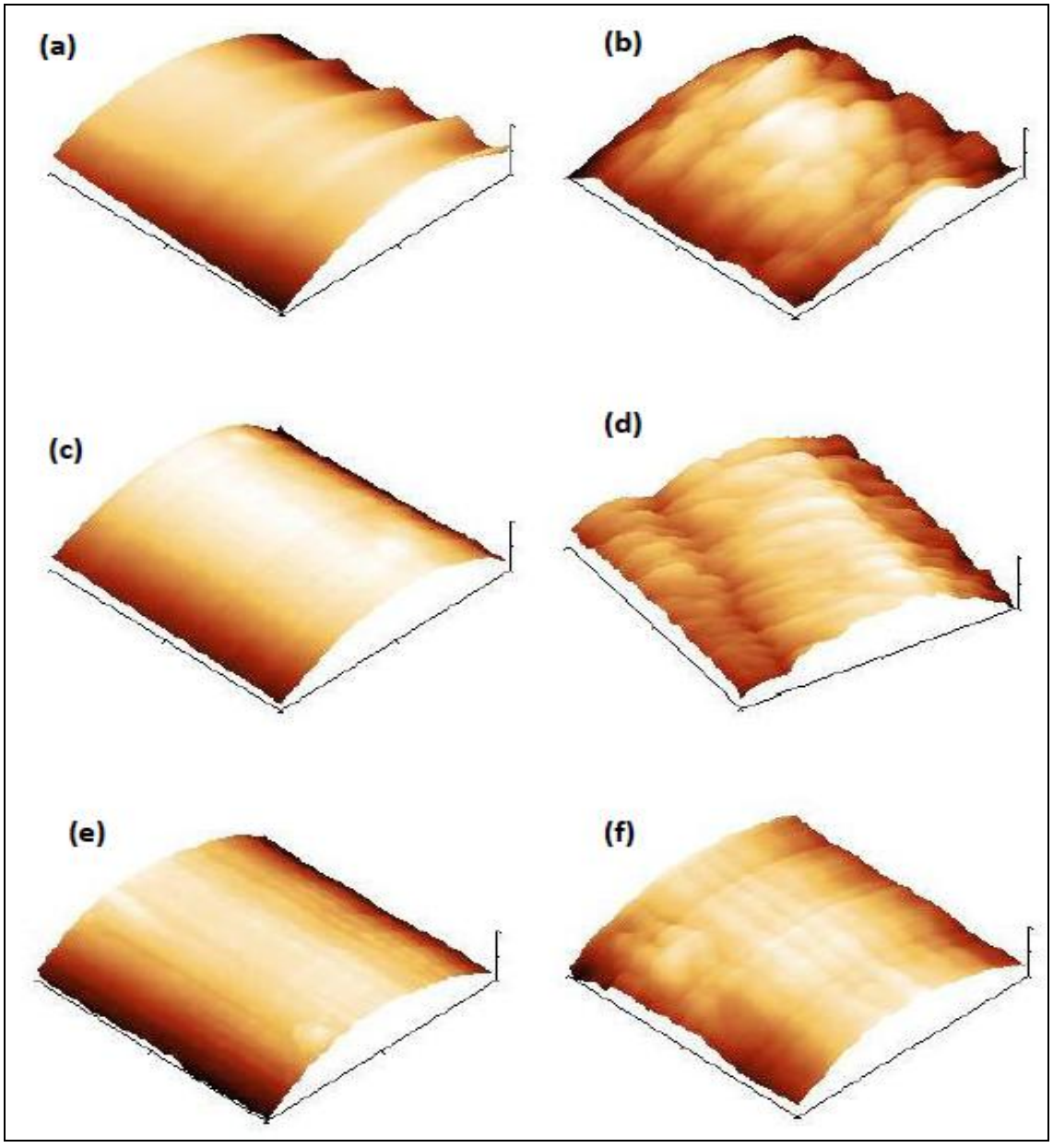

Figure 2.10. AFM fiber surface topographic images of (a) AS4_UnS, (b) AS4_S, (c) AS7_UnS, (d) AS7_S, (e) IM10_UnS, and (f) IM10_S

The images obtained from the AFM were further analyzed for quantitative measurement of the fiber surface roughness using Gwyddion software. The scan direction was made perpendicular to the fiber longitudinal axis. Table 2.3 summarizes the results obtained for the surface roughness of respective unsized and sized fibers, as obtained from the AFM images. A comparison of the three-dimensional AFM topographic images of the carbon fibers, irrespective of the fiber type, shows that the sized fiber had the highest roughness parameters. The R_q, R_a and R_t values for AS4_S (and AS4_UnS) are 42.10 (12.74), 35.10 (9.88), and 127.4 (34.76) nm, respectively. AS7_S (and AS7_UnS) fibers had R_q, R_a and R_t of 44.40 (15.80), 37.70 (13.39), and 166.00 (56.56) nm, respectively. The R_q, R_a, and R_t parameters for IM10_S (and IM10_UnS) are 86.2 (25.7), 74.10 (21.40), and 300.50 (96.34) nm, respectively.

Table 2.3. AFM roughness parameters for unsized and sized AS4, AS7 and IM10 carbon fibers

Parameters	AS4		AS7		IM10	
	UnS	S	UnS	S	UnS	S
Root mean square, Rq (nm)	12.74	42.10	15.80	44.40	25.70	86.20
Mean Roughness, Ra (nm)	9.88	35.10	13.39	37.70	21.40	74.10
Max Height, Rt (nm)	34.76	127.40	56.56	166.00	96.34	300.50

It can be inferred from the results that sizing actually created pronounced cleavages on the fiber surface, and thus increase the surface roughness. The higher surface roughness might improve the fiber-matrix interfacial strength properties. The higher surface roughness found in the sized fibers should be considered beneficial in the composite reinforcement system, since the level of surface roughness dictates to a great extent the mechanical interlock between the fiber surface and matrix [128,129]. The

sizing creates an interface (chemisorbed) region on the fiber skin, which promotes the chemical and mechanical bonding between the sizing and the fiber skin [130].

The desized fiber surface roughness measurement was also made from the images taken using the aforementioned AFM's mode. Figure 2.11A (i), (ii), and (iii) shows the three-dimensional morphology AFM images of AS4 carbon fiber surfaces desized at 435^{o}C without hold-time, with 20 minutes hold-time, and 60 minutes hold-time, respectively. Figure 2.11 B (i), (ii), and (iii) and Figure 2.11 C (i), (ii) and (iii) represent the same desizing procedures for AS7 and IM10 carbon fibers, respectively.

Table 2.4 summarizes the results obtained for the surface roughness of the desized fibers at different hold-times, as obtained from the AFM images shown in Figure 2.11. Comparison of the three-dimensional AFM topographic images of the carbon fibers, irrespective of the fiber type, show that heat treatment of the fibers could change its surface topography. As shown in Figure 2.11 A (i), (ii), 2.11 B (i), (ii), and 2.11 C (i), (ii), the surface roughness of the desized fibers (if observed visually) are rougher and full of cleavages compared to Figure 2.11A (iii), B (iii), and C (iii). The detailed roughness parameter estimation shows that there are more nano-cleavages presence in D-M3 than in both D-M1 and D-M2 samples.

The R_q, R_a, and R_t for AS4_D-M1 are 14.39, 11.77, and 45.38 nm, respectively. After heat treatment for 20 minutes at 435^{o}C, the fiber surface morphology changed. The number of grooves increased nanoscopically, which is reflected in their roughness parameters.

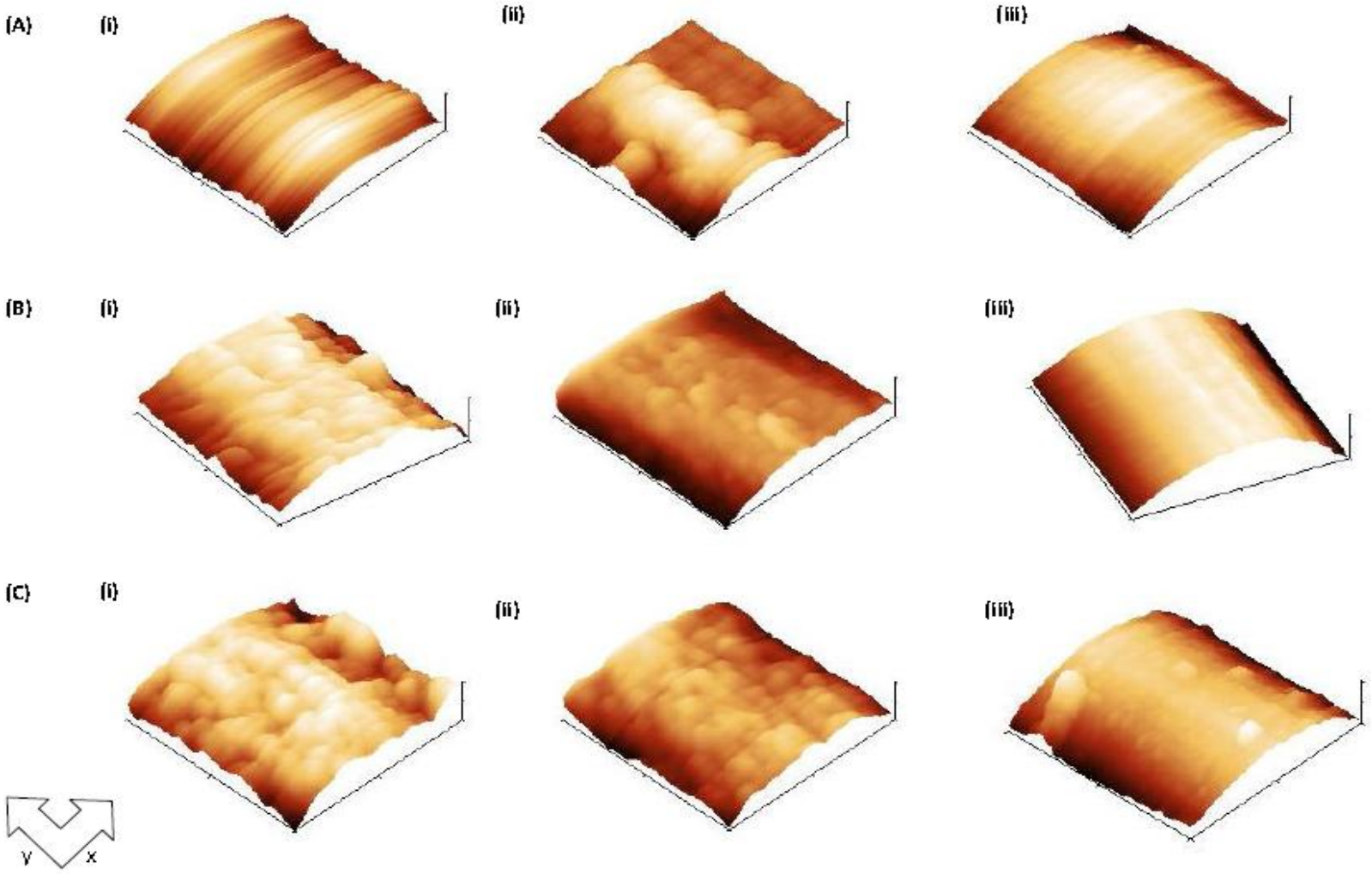

Figure 2.11. AFM images of carbon fiber surface (A) AS4, (B) AS7, and (C) IM10 [(i) D-M1 (ii) D-M2, and (iii) D-M3]

The R_q, R_a and R_t parameters for AS4_D-M2 are 28.90, 24.20, and 99.18 nm, respectively. Holding the fiber at 435^{o}C for 60 minutes caused the fiber surface to become rougher, and more grooves developed nanoscopically. This caused the RMS roughness parameters to increase accordingly. The R_q, R_a, and R_t parameters, as estimated from the surface profile, for AS4_D-M3 are 59.00, 49.50, and 194.20 nm, respectively. Similar trends were also observed in AS7_D-M1, AS7_D-M2, and AS7_D-M3. Moreover, a close examination of the roughness parameters for IM10_D-M1, IM10_D-M2, and IM10_D-M3 samples also depicts the same trends as observed in AS4 and AS7desized fibers.

Table 2.4. Desized carbon fiber surface roughness parameters

Fiber Type	AS4			AS7			IM10		
	D-M1	D-M2	D-M3	D-M1	D-M2	D-M3	D-M1	D-M2	D-M3
RMS, Rq (nm)	14.39	28.90	59.00	14.06	21.00	71.80	14.58	23.50	66.80
Mean Roughness, Ra (nm)	11.77	24.20	49.50	12.05	17.70	61.70	11.90	19.30	56.30
Max Height, Rt (nm)	45.38	99.18	194.2	51.96	77.54	247.5	52.34	83.24	237.4

The increase in the surface roughness after 60 minutes hold (D-M3 samples) should be considered beneficial in the composite reinforcement system, since a higher surface roughness provide higher mechanical interlock between the fiber surface and the matrix.

2.1.7 Quantifying the Sizing Content

A tow of fiber from each sized fiber type was curled inside the pan before being transferred to the TGA hanger. The measurements were done in a nitrogen atmosphere (sample space flow rate ~40mL/min). The amount of sizing content, spinning oil, and additive content on sized and unsized AS4, AS7, and IM10 carbon fibers was investigated at a 10^{o}C/min to 600^{o}C. Although little information on the fiber production was given by the manufacturer, it was believed that in a typical production line anti-static lubricating oil that is made from water soluble mineral oil is normally used to lubricate and smoothen the tow for greater loom efficiency and fiber-to-metal lubrication.

TGA thermograms for sized and unsized AS4, AS7, and IM10 carbon fibers are shown in Figure 2.12 (a), (b), and (c), respectively. The results indicate that at approximately 200^{o}C, the first weight loss was observed in almost all of the fibers, and it was well pronounced in AS4_S and AS7_S samples. The initial weight loss might be attributed to the burn out of the anti-static and lubricant agents used on the production-line during fiber processing. This weight change was not clearly noticed on the IM10_S carbon fibers, and this is probably due to the diameter and lighter weight of the fiber sample. Therefore, fiber with a larger diameter would have more contact points and surface reactivity with anti-static agents and sizing materials than the fiber with a smaller diameter.

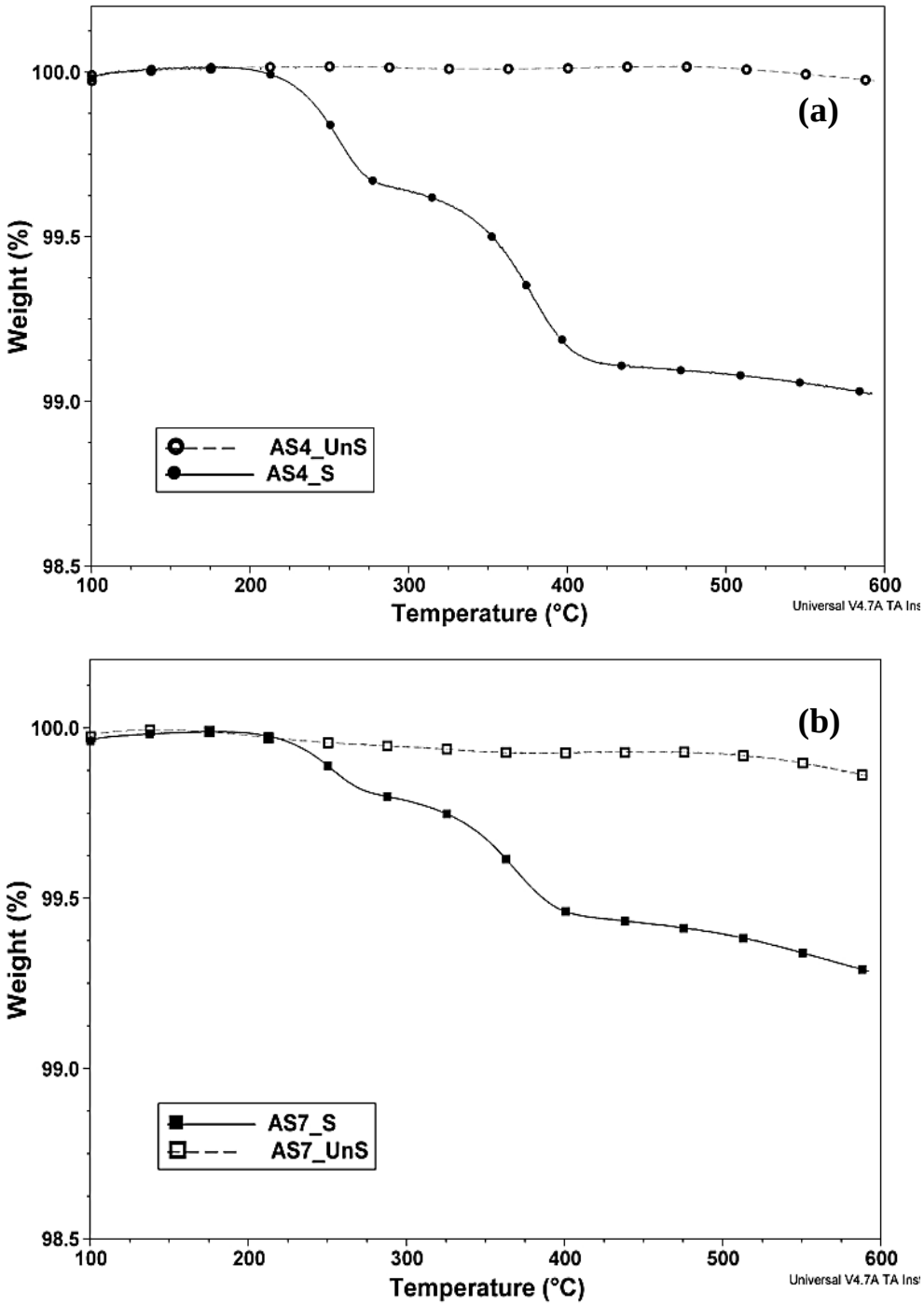

Figure 2.12. Thermograms showing the decomposition of spinning oil and sizing for sized and unsized CFs: (a) AS4, (b) AS7, (c) IM10, and (d) the derivative weight change for the sized fibers

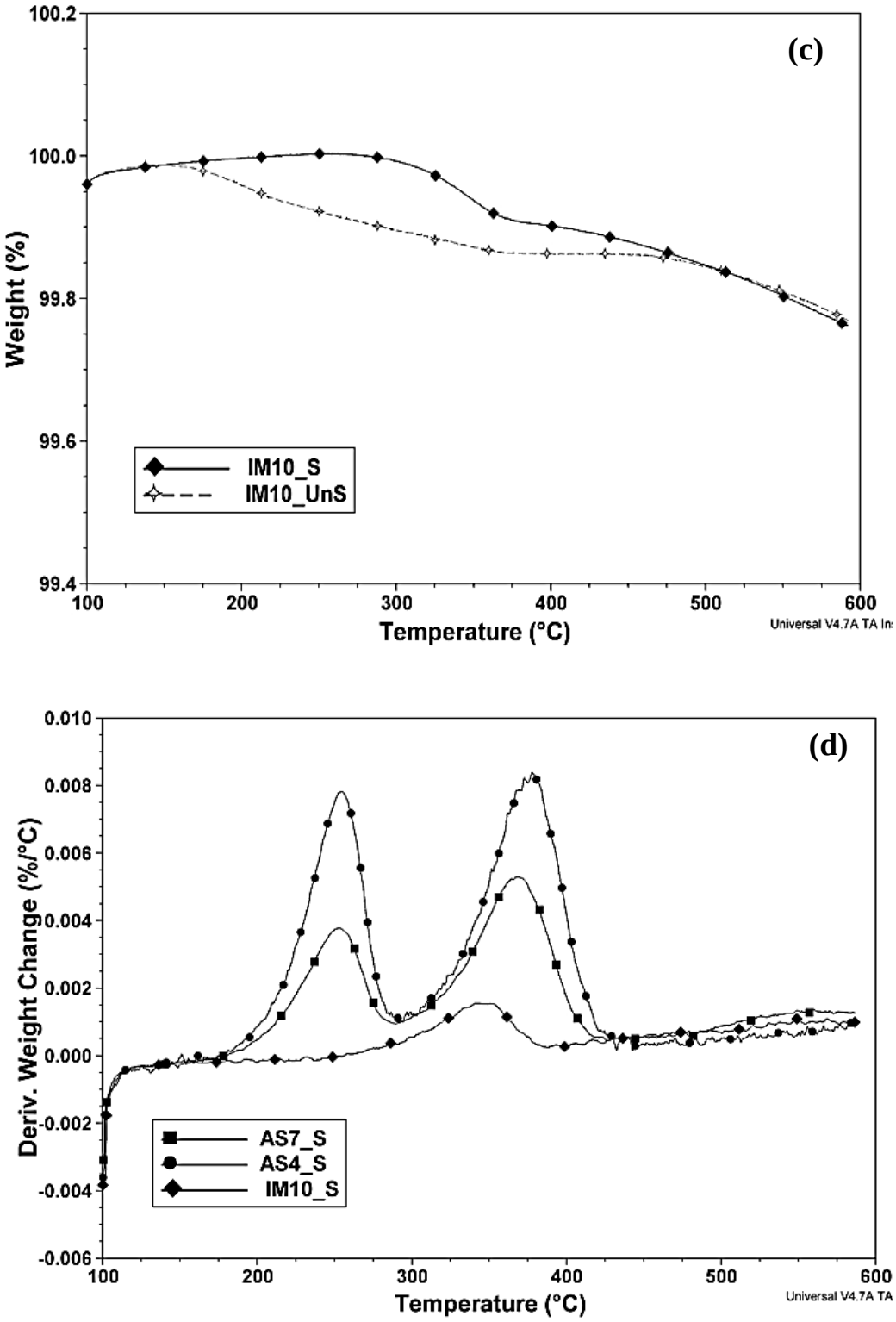

Figure 2.12. ***(Continues)*** **Thermograms showing the decomposition of spinning oil and sizing for sized and unsized CFs: (a) AS4, (b) AS7, (c) IM10, and (d) the derivative weight change for the sized fibers**

Approximately 0.5353%, 0.3590%, and 0.1129% weight loss was noticed between 300^{o}C and 450^{o}C for AS4_S, AS7_S, and IM10_S fibers, respectively. This temperature range was chosen based on the information provided by the fiber manufacturer as the range when the sizing would be removed under thermal treatment. For the unsized samples AS4_UnS, AS7_UnS, and IM10_UnS, the total weight losses were 0.05%, 0.14%, and 0.22%, respectively. The weight change was attributed to the thermal degradation of the fiber. The higher weight loss observed in the sized fibers was due to the thermal degradation of the organic sizing layer [131]. The derivative weight change for all the sized fibers is shown in Figure 2.12 (d). The most apparent weight loss regions can be seen clearly in this figure, and this gives more insight on the actual temperature at which the sizing removal began and ended. Table 2.5 and Figure 2.13 give the details on the weight change, with regards to the spinning oil and sizing.

Table 2.5. Weight change percent for spinning oil and sizing

Fiber type	Spinning oil (%) [Temperature range(^{o}C)]	Sizing (%) [Temperature range (^{o}C)]
AS4_S	0.3750 [162-300]	0.5353 [300-450]
AS7_S	0.2026 [175-300]	0.3590 [300-450]
IM10_S	0.0024 [188-300]	0.1129 [300-450]

The buoyancy effect was well observed in IM10 fibers. The overall results indicate that sized fibers underwent a larger weight loss than the unsized fibers. Above 450^{o}C, all of the fibers (sized and unsized) underwent a continuous weight loss up to 600^{o}C, and this might be associated with the fiber thermal degradation. This can only suggest that the fibers had been exposed to over-heating; this could lead to poor tensile properties.

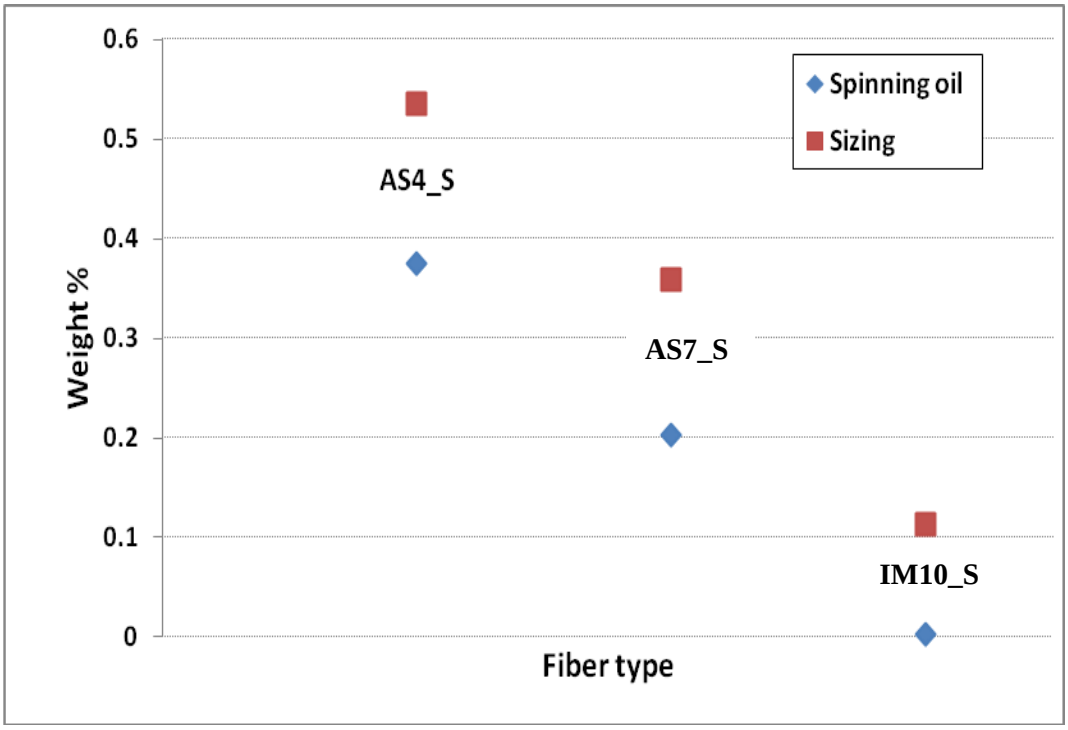

Figure 2.13. Weight change percent for spinning oil and sizing within the specified temperature range

AS4_UnS and AS7_UnS CFs are more thermally stable when compared to IM10_UnS fibers. Since the chemical nomenclature of the sizing and the fiber processing parameters are highly confidential, it is difficult to further deduce the origin of these differences.

2.2 Surface Modification of Carbon Fiber using POSS

2.2.1 Experimental Method

At first the fibers were chemical vapor deposition (CVD)-thermally treated by adopting the procedure used in grafting CNTs on the fiber surface. As-received sized fabric fibers were cut to a size of 114mm x 64mm and inserted into the CVD chamber for the calcination process. The calcination was done at 300^{o}C for one hour in the presence

of air. After the calcination process, the fiber was then subjected to the hydrogenation process by allowing hydrogen gas to flow at 250 sccm through the chamber at 500^{o}C for 30 minutes. Hydrogenation was followed by a reaction process at 750^{o}C for 20 minutes in the presence of ethylene and hydrogen flowing at 1000 sccm and 250 sccm, respectively. The main reason of following this procedure was to simulate the process of grafting CNTs on fiber during the CVD thermal exposure without actually growing the nanotubes, and also to investigate the thermal degradation effect on the fiber during the CVD process. It has been reported that the mechanical properties of single carbon fibers were reduced dramatically after being exposed to CVD thermal treatment; although, the reduction in the mechanical properties could be controlled by lowering the treatment temperature and eliminating oxygen within the processing chamber [66,70,88]. Thermally treated fibers are believed to have carboxyl, carbonyl, and hydroxyl functional groups that chemically bond effectively with the epoxy matrix.

Based on the report provided by Mahfuz et al. [132], trisilanolphenyl POSS-1458 was used to perform this experimental work. The POSS was purchased from Hybrid Plastics, Inc. Trisilanolphenyl POSS possesses silanol functional groups that have silicon atoms at the core, which interact with the carbon fiber surface to form Si-O-C chemical bonding. Similarly, the hydroxyl groups from the silanol can also form chemical bonds with the epoxy molecules. This normally contributed to the improved fiber/matrix interfacial strength. Figure 2.14 shows the structure of trisilanolphenyl POSS-1458.

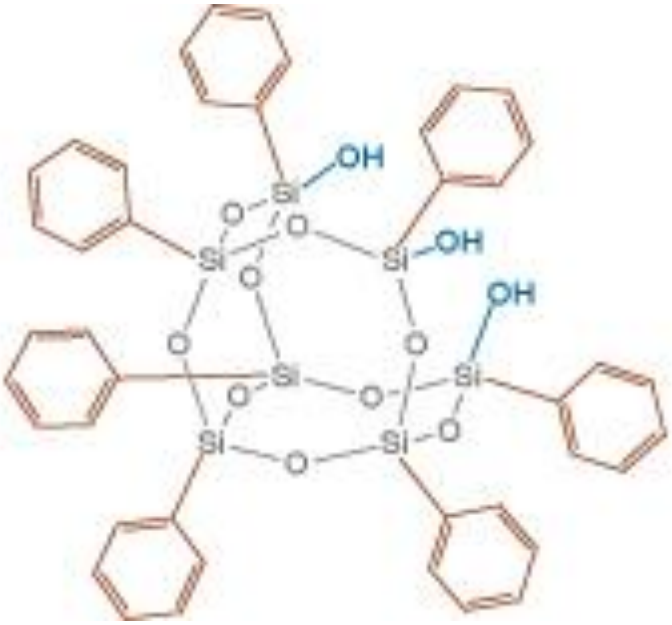

Figure 2.14. Trisilanolphenyl POSS-1458 structure

POSS-1458 can actually be dissolved in any solvent, provided there is a match between the polarity of the POSS and the medium. POSS has been reported to dissolve completely in a medium like acetone, methanol, chloroform, and others by many researchers [72]. Therefore, three different solvents, namely acetone (99.5% purity), methanol (99% purity), and isopropanol (99% purity) were selected to dissolve the POSS particles in order to better understand the effect of the selected medium on the de-agglomeration of the POSS particles and the overall tensile properties of the fibers. Methanol and isopropanol were purchased from PTI process chemicals, while acetone was obtained from the Sunnyside Corporation.

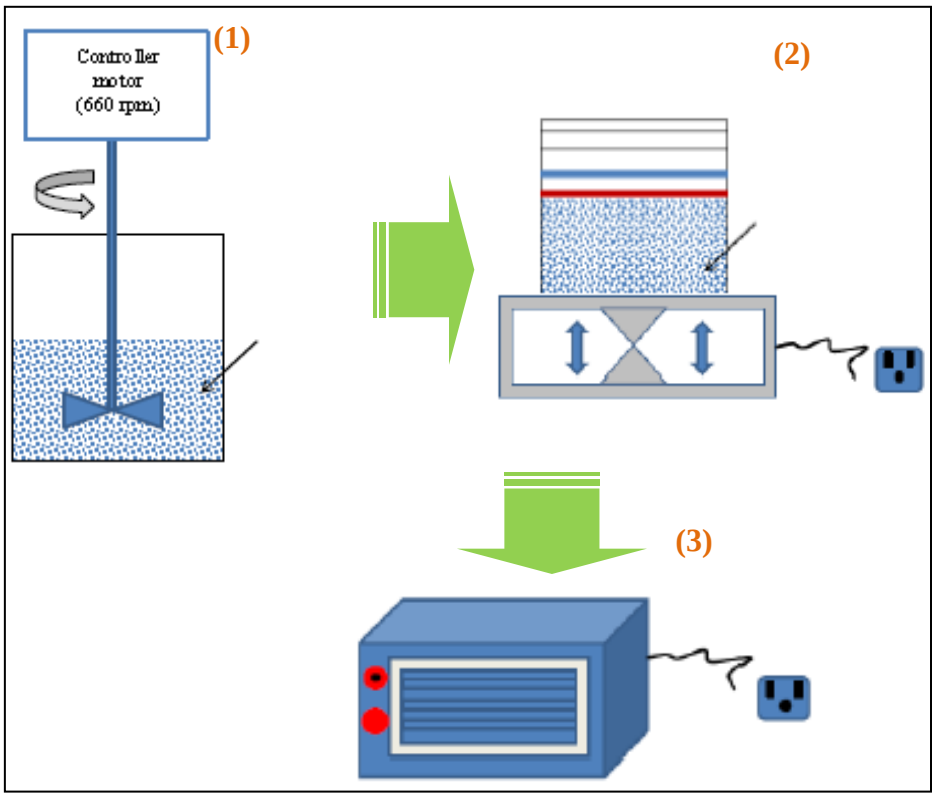

Figure 2.15. Schematic of the procedure for coating fiber with POSS: (1) POSS particles and solvent were mixed by mechanical stirrer, (2) the fiber fabric was put inside the POSS solution in a ziplock bag and put on the mechanical agitator, and (3) the fabric was dried in an oven [black arrows indicating POSS solution]

About 250mL of acetone, methanol, and isopropanol were measured separately and poured inside beakers that contained 2g of trisilanolphenyl-POSS particles. The POSS product and respective solvent were thoroughly mixed by a mechanical stirrer at 660 rev/min for 30 minutes, as shown in Figure 2.15. After the de-agglomeration process, the resulting solution was examined to be homogeneous by visual observation.

Three pieces fabric sized 114mm x 64mm were selected from the thermally treated fibers and then placed inside Ziploc bags®. The admixture was then poured into the respective bags, and the bags were placed on the mechanical agitator regulated at 20 rev/min for 3 hours. The amount of solvent in each bag was sufficient enough to soak the

fiber completely. After the three-hour treatment, the fabrics were removed from the bags and dried in an oven at 100^{o}C for 30 minutes.

Figure 2.16 (a and b) shows the initial and the final volume change in the respective solvent used for the evaporation rate study of the three different solvent used for this study. 14mL of the solvent was measured and 0.11g of POSS was thoroughly dispersed inside the respective solvent. There was also a control experiment prepared in the same way. The exposed area of the container was measured to be about 181.48mm^2 and the room condition was maintained at 20.9 ± 0.1^{o}C and 56 ± 1.24% RH.

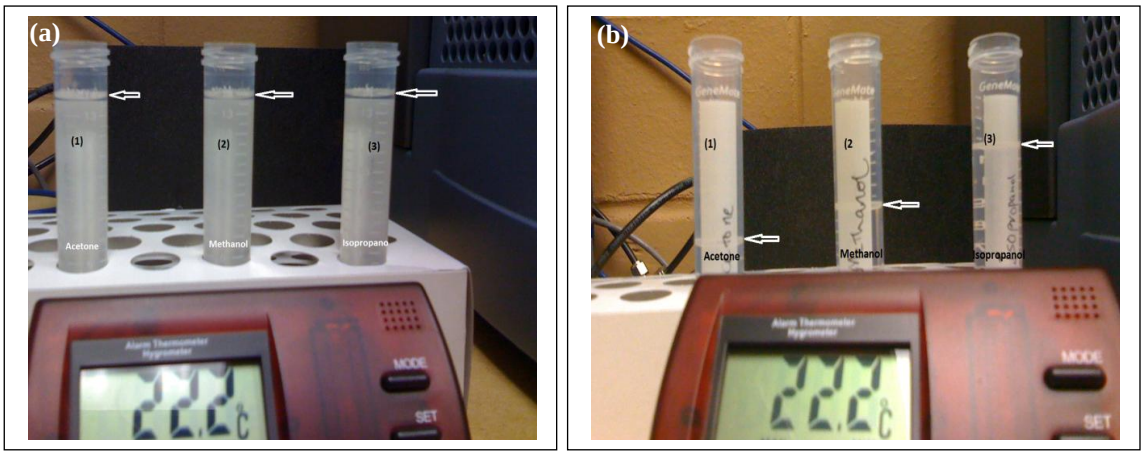

Figure 2.16. Evaporation rate experimental setups (a) initial volume at 0hr, and (b) final volume after 52hrs [(1) Acetone, (2) Methanol, (3) Isopropanol] ***white arrows pointing to the level of solvent at the respective time***

After 52 hrs of the same environmental exposure, the evaporation rate was measured as displayed in Figure 2.17. The solvent volume of the control samples after 52hrs was measured to be 4.2mL, 6.6mL and 10mL for acetone, methanol and isopropanol, respectively. The measurement is done on the POSS solution samples of acetone, methanol and isopropanol after the 52hrs was 4.4ml, 6.9ml and 10.2ml, respectively. The evaporation rate was dropped by almost 5% as a result of the POSS dissolution.

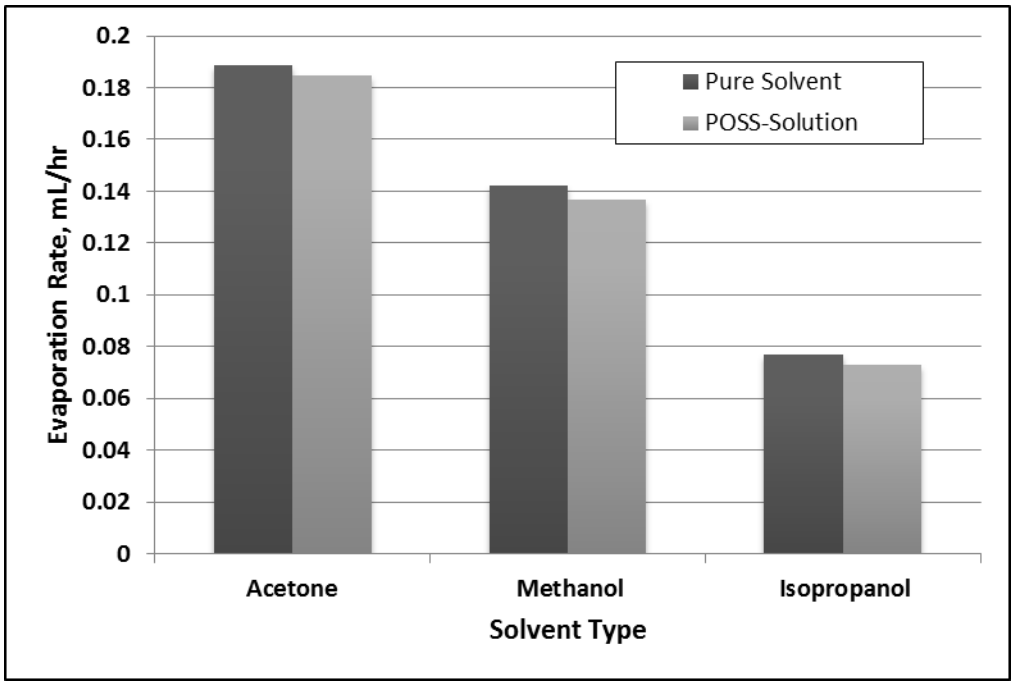

Figure 2.17. Evaporation rate of POSS solution with the respective solvent

The presence of POSS in the solvent did seem to reduce the evaporation rate of the POSS solution and the isopropanol solution gave the lowest evaporation rate when compared to others. This can explain why the deposition of POSS on the fiber using isopropanol seems to be higher than the others. This might be attributed to the rate of evaporation of the solvent from the coated fiber surface inside the oven; since micro- and nanoparticles presence in a solution affect the rate of its evaporation and the thickness of the coating on the substrate [133].

2.2.2 Analysis of the POSS Coated Fiber using SEM

POSS-coated fiber skin morphologies were examined with the aid of a Zeiss NEON 40-EsB high resolution SEM. Figure 2.18 (A, B, C, and D) presents SEM images of thermally treated fiber (T650-TT), POSS-coated fabric using acetone (POSS-Acetone),

POSS-coated fabric using methanol (POSS-Methanol), and POSS-coated fabric using isopropanol (POSS-Isopropanol), respectively. The assessment of the TT-fiber surface shows well-pronounced striations along the fiber axis, which indicates that the fiber surface has more flaws than before the treatment. Also revealed in the micrographs is the presence of POSS coating on all the coated fibers, with a high indication of more deposition on POSS-Isopropanol samples. The coating is smooth and uniform on all the fiber samples. The smoothness may be because of the silanol functional groups forming chemical bonds with the hydroxyl groups on the fiber surface.

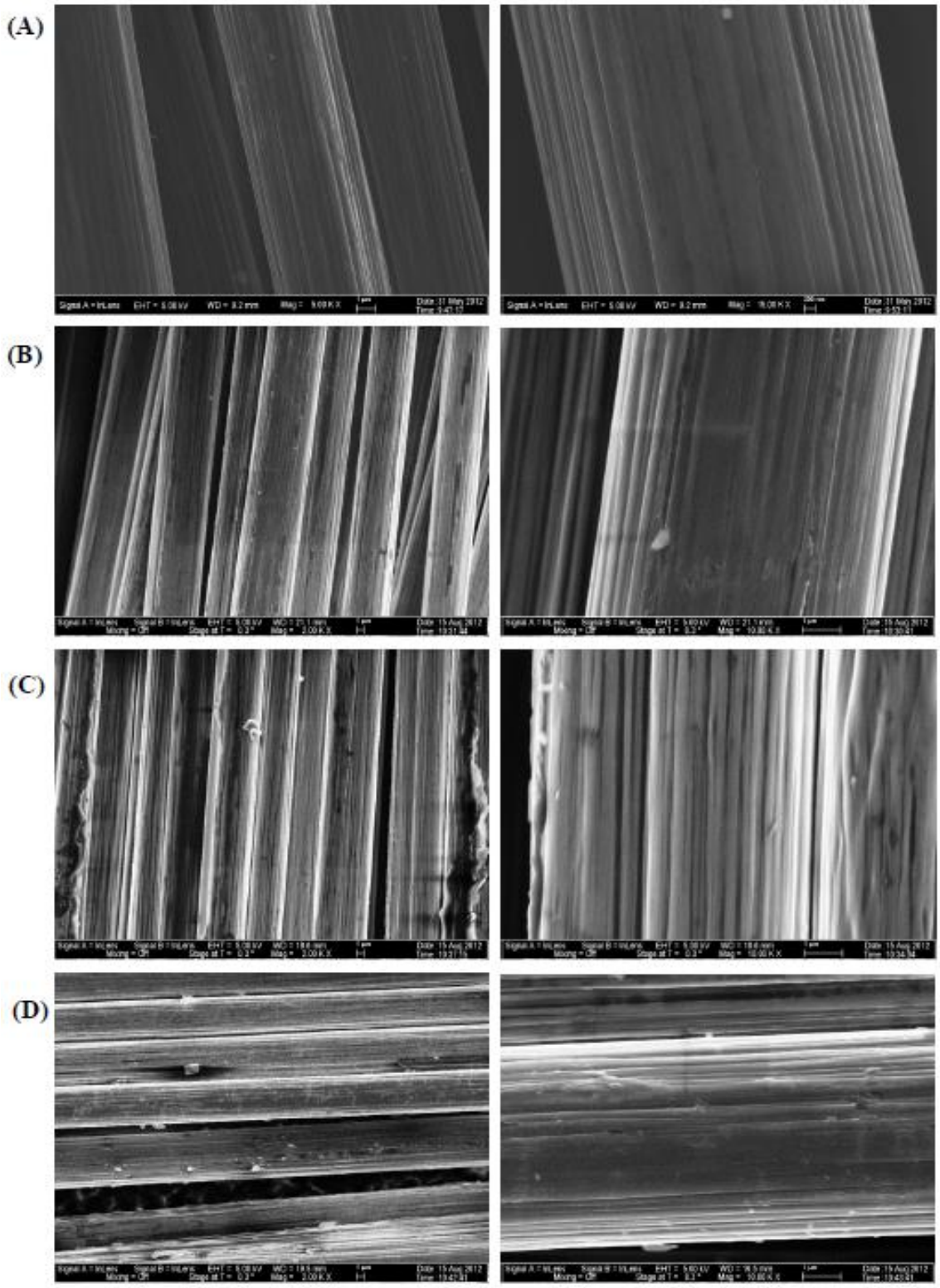

Figure 2.18. Surface morphologies of: (A) T650-TT (B) POSS_Acetone (C) POSS-Methanol, and (D) POSS_Isopropanol [taken at lower and their respective higher magnification]

2.2.3 Thermal Stability of the POSS Coated Carbon Fiber

The samples used for the thermal stability and quantification studies were as-received T650-35 CF (T650-AR), thermally treated T650-35 CF (T650-TT), as-received Panex-35 CF (PX-35) obtained from Zoltek Inc. in sized form, POSS coated thermally treated T650-35 CF (POSS-T650), and POSS coated PX-35 (POSS-PX35).

T650-TT were obtained from the same treated batch as described in section 2.2.1. Panex-35 CF was used for validation purposes because of: (1) the different number of filaments per bundle (50K), and (2) different sizing material. POSS was then dissolved in acetone and then deposited on T650-TT and PX-35 and they are designated as POSS-T650 and POSS-PX35, respectively.

Thermal stability study was done with the aid of a TA Instruments Q50 thermogravimetric analyzer (TGA). One tow (~76mm long) from each sample was chopped into several pieces and carefully arranged in a 500-µL ceramic pan. The analyzer was programmed according to the thermal profile cycle shown in Figure 2.19. In order to remove the moisture and impurities that might be on the samples, the analyzer was set to 100^{o}C for 30min in the presence of nitrogen flowing at 60mL/min. It was then set to switch the gas selection to air (30mL/min) and ramp to 800^{o}C at 2^{o}C/min. Switching to air was necessary in order to understand the oxidation behavior of each sample between the temperature range of 100-800^{o}C. The system was set to remain at 800^{o}C for 30min in order to obtain complete oxidation of the samples.

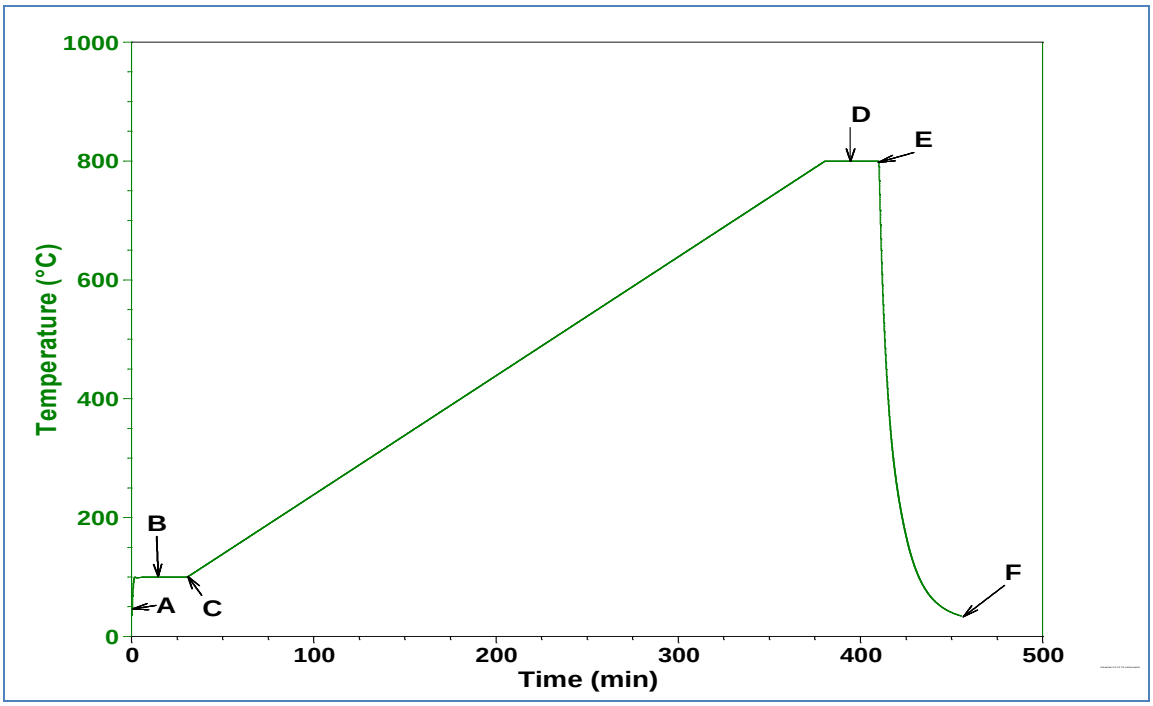

Figure 2.19. Thermal profile cycle used for the thermogravimetric analysis [A: equilibration at 35°C and jump to 100°C in nitrogen atm flow rate 60mL/min, B: isothermal at 100°C for 30min in N_2 atm flow rate 60mL/min, C: gas switched to air flow rate 30mL/min then ramp to 800°C at 2°C/min, D: isothermal at 800°C for 30min in air flow rate 30mL/min, and E to F: cool to 35°C in air]

After the complete oxidation, the system was programmed to cool to 35°C in the presence of air. During the sample run, air was introduced to the samples and maintained at the rate of 30mL/min (unless otherwise stated) to maintain an oxidizing environment around the sample. Air flow of 30mL/min was found to be sufficient to remove oxidation products without introducing buoyancy effects into the system. It is well known that amorphous carbon decomposes at the lowest temperature, followed by CNTs (~600°C), and then graphite materials (700-800°C) [134-143]. Therefore, the thermal profile cycle used for this study was based on these deductions.

TGA can be used to evaluate the thermal stability of a material and characterize the purity of the sample. Figure 2.20 (a) shows the derivative weight curve with respect

to temperature for T650-AR samples. The experiment was carried out in the presence of air and nitrogen gas in order to critically analyze the decomposition temperature of the ingredients present on and in the carbon fiber. The nitrogen atmosphere is particularly compulsory in limiting the oxidation of the fiber and complete removal of polymer sizing. The derivative curve can be used to determine the oxidation temperature of the material, as well as define the mass-loss condition as a single peak. Figure 2.20 (b) clearly shows the respective decomposition temperature of the sized T650-35 carbon fiber in both air and nitrogen atmospheres. As shown, the decomposition of the anti-static spinning oil occurred at approximately 198^{o}C, and the sizing decomposed completely at 250^{o}C in the presence of either air or nitrogen gas. As stated by Galasso et al. [144] and Brown et al. [145] and demonstrated here in this work, the oxidation of amorphous carbon occurred at approximately 575^{o}C and the complete oxidation of carbon fiber occurred at about 720^{o}C only in the presence of air.

This has demonstrated that the complete oxidation of carbon fiber is possible in the presence of air. As a result, the thermal analysis was carried out only in the presence of air following the aforementioned thermal cycle.

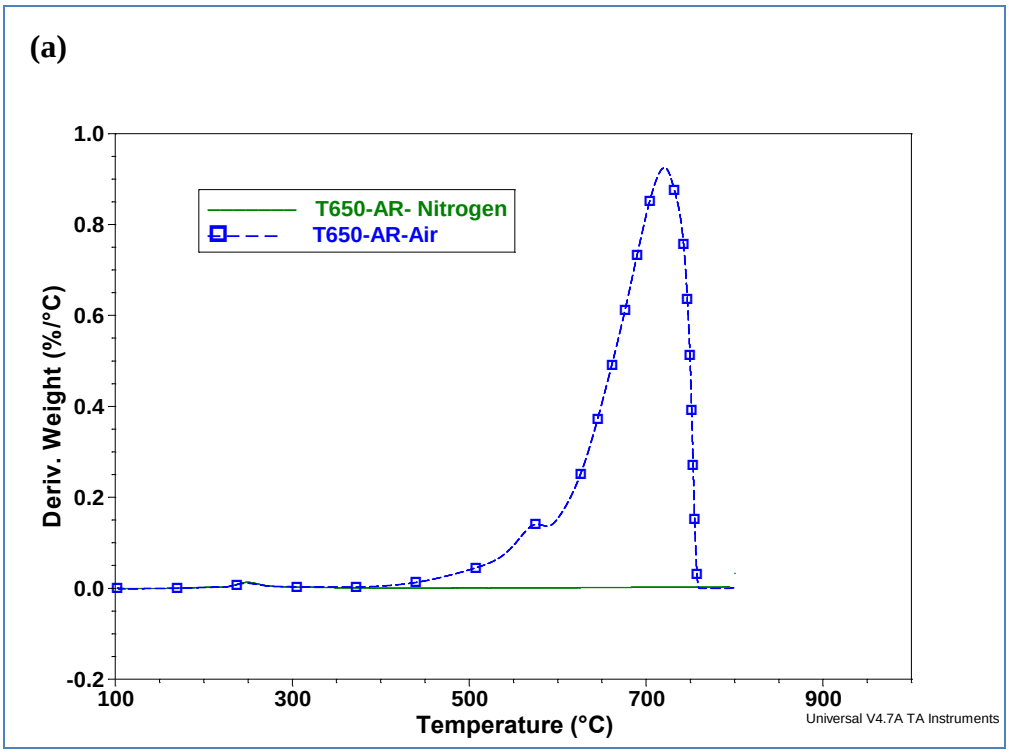

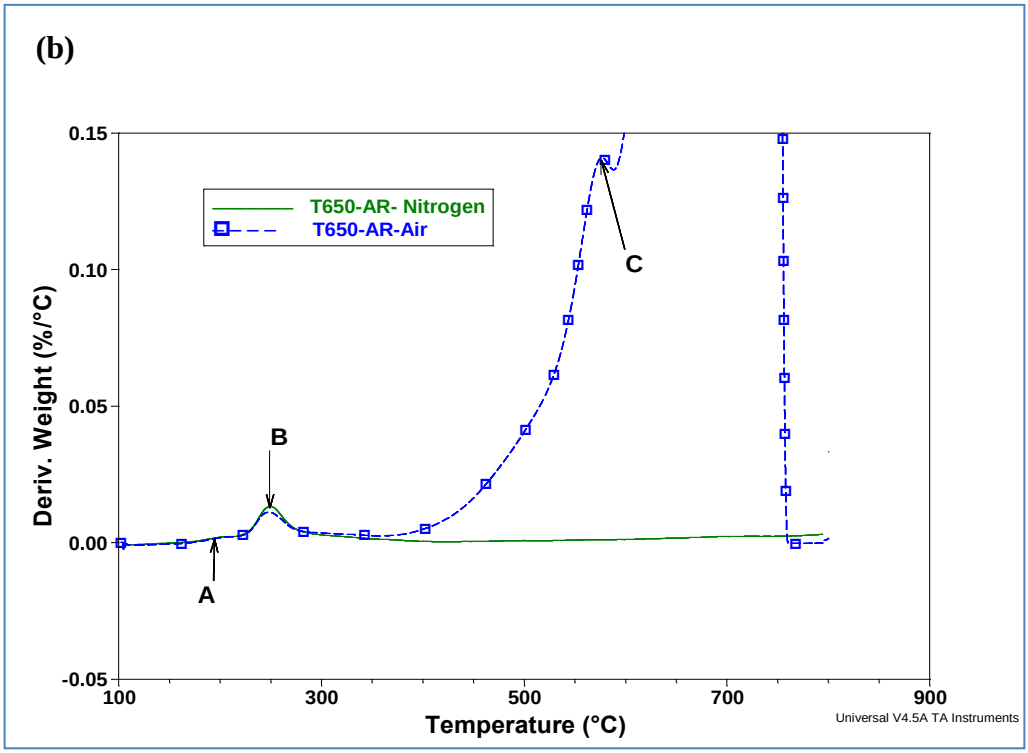

Figure 2.20. TGA for thermal stability of sized T650-35 in the presence of air and nitrogen: (a) complete analysis, and (b) enlargement of the critical regions [A: anti-static oil decomposition point, B: sizing decomposition point, and C: amorphous carbon oxidation point]

Figure 2.21 (a) shows a typical plot of the derivative weight curve with respect to temperature for at least three samples weighing ~15mg considered for each case. The primary oxidation temperature is defined as the temperature at the highest peak for each sample on the derivative weight curve, and can actually represent the thermal stability of the sample. It is evident that T650-AR was more thermally stable than T650-TT. This might be attributed to the thermal degradation effect caused on the latter as a result of the CVD heat treatment. The wider oxidation temperature range observed in both T650-AR and PX-35 was due to the higher filament diameter and the larger microstructures compared to T650-TT. T650-AR and PX-35 had a larger filament diameter (6.9µm and 7.2µm, respectively) than T650-TT (6.8µm). Therefore, with T650-TT fiber, the space between the filaments was larger, and the accessibility of air to the internal surface and diffusion of gasification products away from the surface, was higher than in the T650-AR and PX-35 fibers. This was probably the reason for the sharper and higher peak seen in T650-TT samples [140,146]. The restriction of air flow and the gasification product's diffusion rate within the filaments of PX-35 was obviously lower than other fibers due to the larger filament diameter.

There was also a shift in the oxidation temperature for T650-TT when coated with POSS (~2%), and a smaller change was noticed in PX-35 when coated with POSS (~1%) as shown in Figure 2.21 (b). It is evident that the POSS coating was able to improve the thermal stability of the thermally treated fibers that had more carboxyl and hydroxyl functional groups than the sized fibers. Lower diffusion of gasification products was observed in POSS-T650 due to a larger filament diameter, as compared to T650-TT.The same trends were not noticed in POSS-PX35.

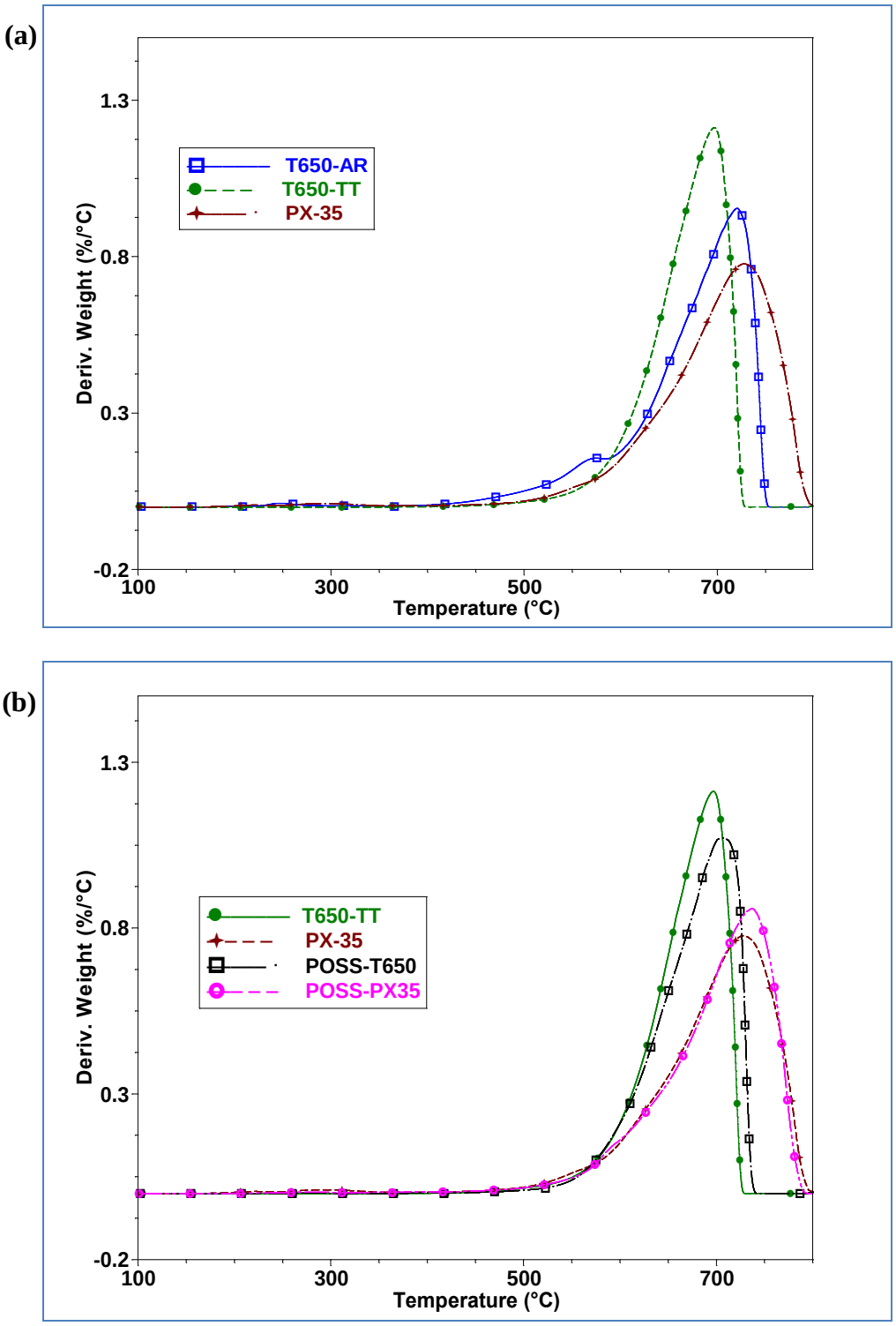

Figure 2.21. Derivative weight percent versus temperature curve for: (a) untreated fibers, (b) POSS treated fibers and untreated PX-35

The lower diffusion rate of the gasification products observed in PX-35 might be associated with the mode of surface treatment, since the sizing on the fiber was not thermally removed before the POSS coating. There is a high tendency that the POSS coating created more spacing between the filaments.

2.3 Grafting Carbon Nanotubes on T650-35 Carbon Fiber

2.3.1 In-Situ Grafting of CNTs on Single Fiber

Due to variations in coverage of CNTs' growth that exist between fibers, which are positioned near the outer surface of the fiber bundle as opposed the fibers which are positioned near the middle [70,83], an attempt was made to grow CNTs on single fibers using the thermal CVD approach in this work.

In an attempt to uniformly grow the CNFs on carbon fiber fabric using the thermal CVD method, a catalyst solution was prepared by dissolving 0.0080g CuN and 0.0854g NiN in 30mL of isopropanol. The catalyst was applied on single as-received T650-35 fibers mounted on the picture frame. The single fibers were mounted on the frames with the aid of high temperature ceramic paste (Sauereisen: Insa-Lute Hi Temp Cement No. 7) and left to cure at room temperature for at least 48 hours. The paste was selected because it can withstand high temperature between 700 - 1371^{o}C inside the CVD chamber.

The catalyst was applied to the prepared mounted single fibers in three different ways, as listed: (A) mounted fibers were vertically positioned and soaked inside the catalyst solution for about 5 minutes, (B) mounted fibers were horizontally positioned and dipped inside the catalyst solution for about 5 minutes, and (C) the catalyst solution was sprayed on the prepared mounted fibers by droplet sprayer. The aforementioned

methods were chosen in order to verify the catalyst deposition amount and 3-dimensional uniform CNTs' growth on carbon fiber. Figure 2.22 shows the illustration of the three methods used to deposit the catalyst on the fiber. The same thermal cycle as stated in section 2.2.1 was adopted for this procedure.

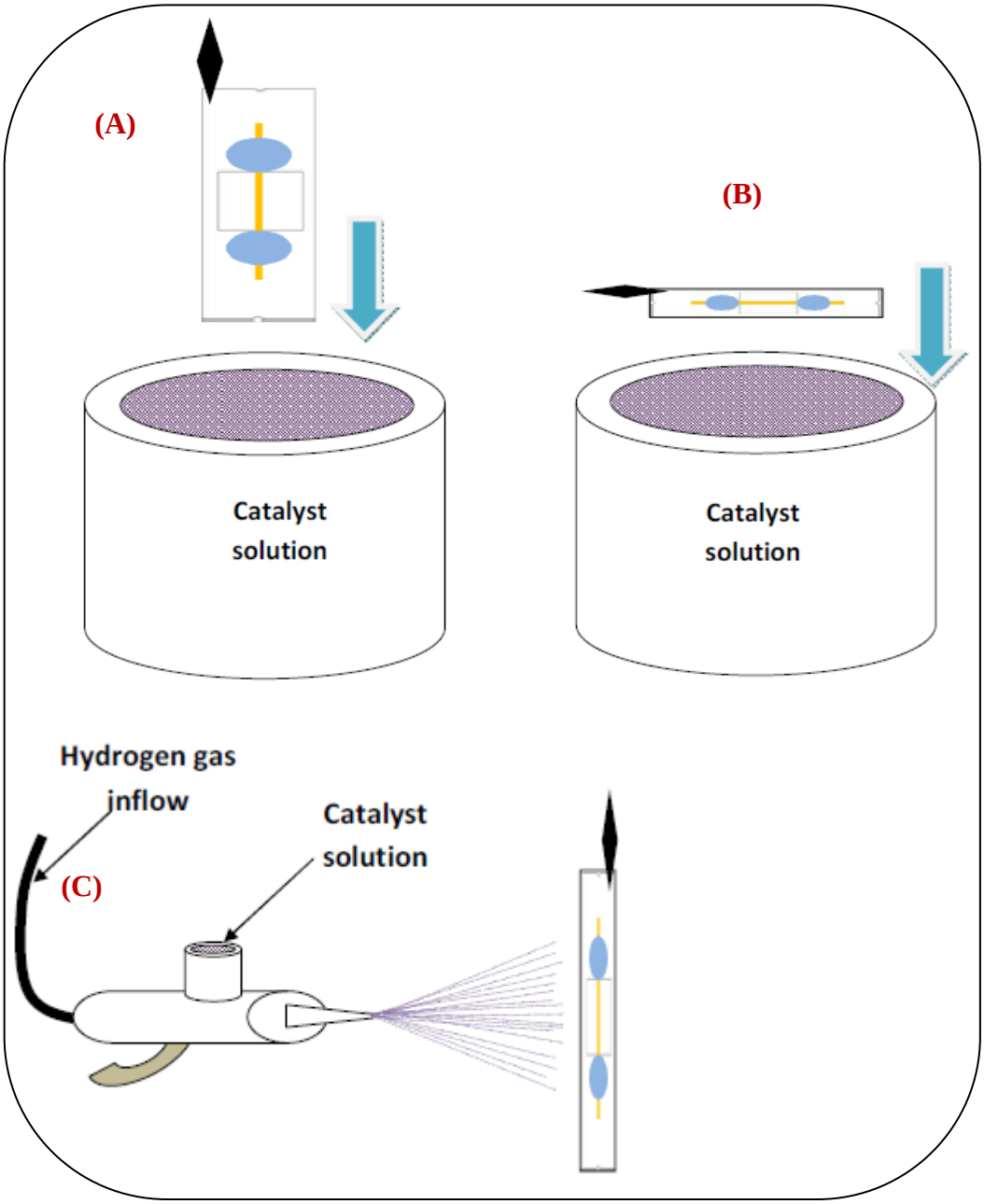

Figure 2.22. Schematic of the methods adopted for catalyst deposition: (A) vertical dip, (B) horizontal dip, and (C) spray method [black pointer showing the frame grip end and green arrow indicates the direction of dipping]

About ten to twelve samples were clipped on the flat steel bar that had been cleaned thoroughly with acetone. The samples clipped on the bar were then placed in the CVD chamber for the grafting process. The growth temperature and time for CNTs grafting were selected as 750^{o}C for 20 minutes in the presence of ethylene and hydrogen flowing at 1000 sccm and 250 sccm, respectively.

The CNTs grown on carbon fibers were examined using a scanning electron microscope (JEOL JSM-840A lithography (3nm resolution and operated at 15kV)). Figure 2.23 shows the SEM micrographs of the nanotubes growth using the aforementioned procedures. The presented micrographs represent at least ten samples prepared from each batch. There was an indication of more CNTs growth on the fiber when method- A was adopted for the procedure, as compared to method-B and C. Also displayed in the micrographs are the bottom and top portions of the mounted fiber after the growth. As shown in (A), the CNTs growth at the bottom and top section of the fiber is lower when compared to the middle section of the fiber. This might be a result of the direction of gas flow and the blockage caused by the ceramic paste during the growth process.

However, when method-B was adopted, the CNTs' growth of the middle section of the fiber became fewer, non-uniform, and sparsely distributed along the fiber length, although, the growth at the bottom section seems to be higher, compared to other parts of the fiber. The CNTs grafted on the fiber using the method-C seem to be fewer and not a 3-dimensional growth if compared to other methods. The bottom and top sections also show little growth.

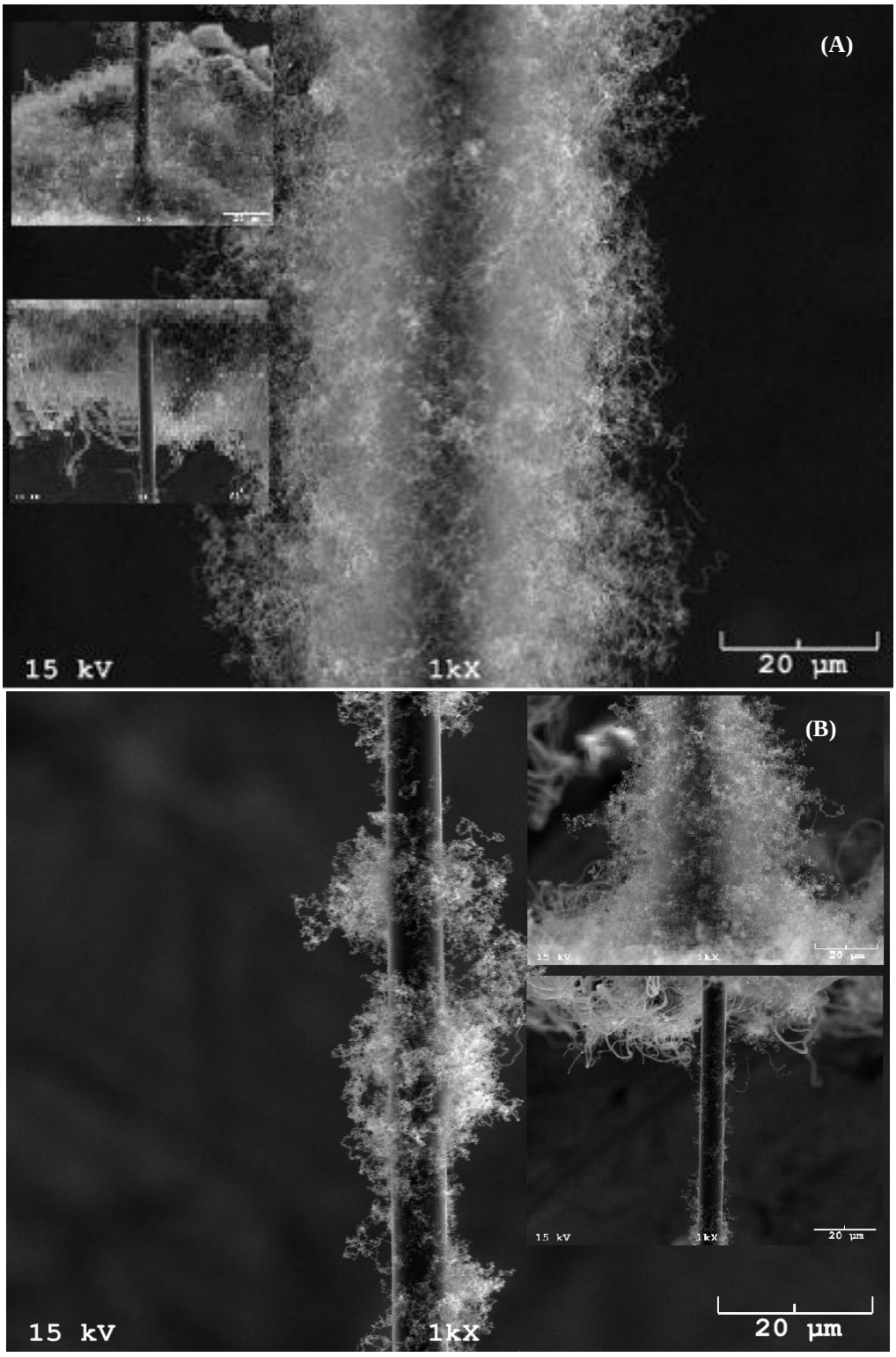

Figure 2.23. SEM micrographs showing different methods of catalyst deposition on single fiber: (A) dipped vertically, (B) dipped horizontally, and (C) spraying method [inset: bottom section (up) and top section (down) of the fiber]

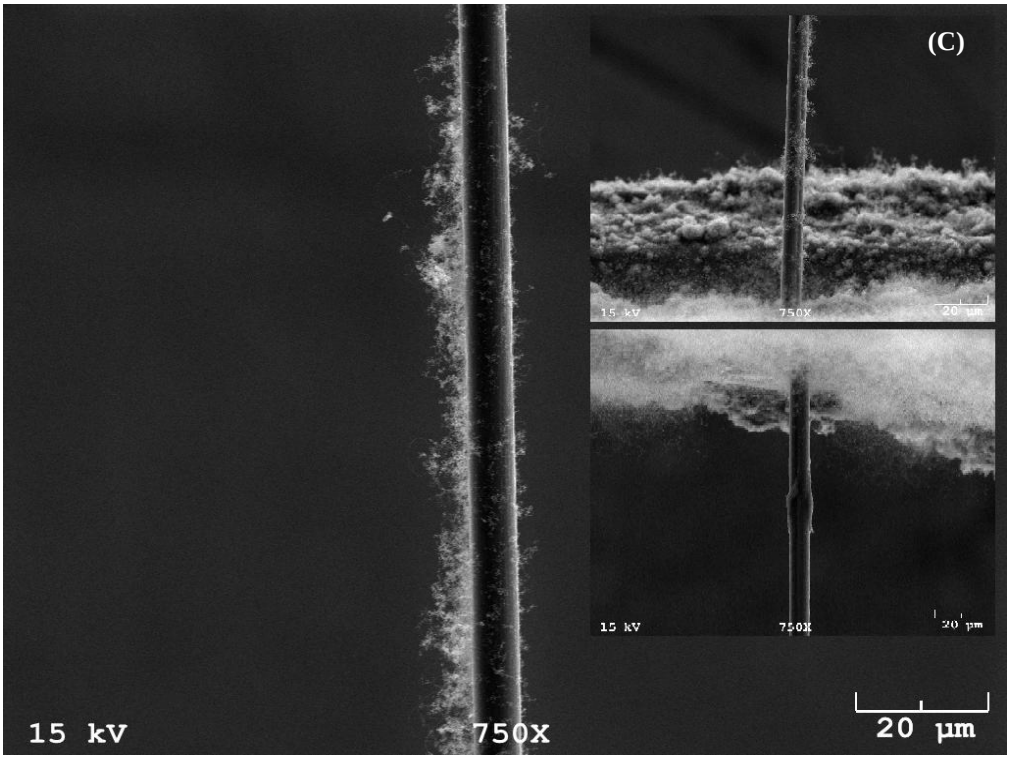

Figure 2.23. ***(Continues)*** **SEM micrographs showing different methods of catalyst deposition on single fiber: (A) dipped vertically, (B) dipped horizontally, and (C) spraying method [inset: bottom section (up) and top section (down) of the fiber]**

There is a high tendency to believe that the catalyst particles did not stay in most parts of the fiber while spraying, and this might be the main reason for non-uniform and fewest growth as observed.

Limitations of the Approach:

As a result of variation in growth patterns as observed in each method, and shown in the electron micrographs, the following observations were made: (1) the fibers did not remain perfectly aligned after the growth, (2) the steel picture frames used for mounting the fibers were twisted as a result of the heat generated during the reaction, (3) the bottom or top portions of the fibers hardly had uniform CNF growth, (4) there was an un-

controlled deposition of catalyst on the fiber, frame, and ceramic paste; as a result, CNFs grew on the paste and the frame as well, (5) the paste could not remain perfectly adhered to the frame after the growth; as a result the success rate for the procedures was about 30%, (6) the clips used to attacked the frame to the steel bar were thermally damage, and as a result they lost their grip and the samples fell on each other.

Based on the aforementioned observations, the following limitations have been deducted: (1) uncontrolled catalyst deposition on the fiber; (2) non-uniform 3-dimensional growth; (3) unaligned CNF grafted fiber after the growth; (4) a success rate of about 30%; (4) non-adherence of the paste to the frame after the growth; (5) for better output only, one sample is recommended per CVD run; (5) the tensile test could not be carried out.

2.3.2 Chemical Vapor Deposition (CVD) Growth of CNTs on Carbon Fabric

CNTs were grown on the carbon fabric using the same thermal CVD approach as mentioned earlier. The fabric was cut into six plies of 114mm x 64mm size, and the Fe-Mo catalyst was then added to the fabric. The catalyst was deposited on the fabric by: (1) spraying the catalyst solution on the T650-AR using the droplet sprayer (CNTB1), (2) dipping the T650-AR CF inside the catalyst solution for 24 hours, (3) spraying the catalyst solution on T650-TT CF (CNTB3), and (4) dipping the T650-TT CF inside the catalyst solution for 24 hours (CNTB4). Different approaches of catalyst deposition were chosen in order to study the deposition method versus the CNTs' population density using the thermal CVD procedure as described in section 2.2.1. The fiber was then allowed to dry at room temperature (RH: 70%), and then the final weight of the fabric

was determined from which the final catalyst loading was found to be 0.2% by weight. Henceforth, 0.2% by weight of Fe-Mo catalyst was applied to the fabric for this work.

The catalyst coated fabric was then placed in the CVD chamber, and the following procedures were followed for the CNTs' growth on the fabric: First, the calcination process was done on the impregnated fabric at 300^{o}C for one hour in the presence of air in order to transform the metal nitrates into the respective oxides. Conversion of the metal oxides to the alloy state was performed in a 250 sccm hydrogen environment at 500^{o}C for 30 minutes. The reduction was followed by a reaction process at 750^{o}C for 20 minutes in the presence of ethylene and hydrogen gas flowing at 1000 sccm and 250 sccm, respectively. These conditions favored the creation of a uniform coverage of CNTs on the parent structures. All gases used have a stated purity of >99.99% and were used without further purification.

2.3.3 Thermal Stability and Quantification of CNTs using TGA

The samples used for the thermal stability and quantification studies were carbon fibers grafted with CNTs prepared using the aforementioned four different methods of catalyst deposition (CNTB's). POSS was also used to coat the CF-CNTs (POSS-CNTB's). POSS was dissolved in acetone and deposited on each batch of CNT grafted fibers using the method described in section 2.2.1, and they are designated as POSS-CNTB1, POSS-CNTB2, POSS-CNTB3, and POSS-CNTB4, respectively.

The thermal stability study was done with the aid of a TA Instruments Q50 thermogravimetric analyzer (TGA). One tow (~76mm long) from each sample was chopped into several pieces and carefully arranged in a 500-µL ceramic pan following the same procedure as described for the section 2.2.3 . The analyzer was programmed,

likewise, according to the thermal profile cycle shown in Figure 2.19. The analyzer was set to 100^{o}C for 30min in the presence of nitrogen flowing at 60mL/min. It was then set to switch the gas selection to air (30mL/min) and ramp to 800^{o}C at 2^{o}C/min. The system was set to remain at 800^{o}C for 30min in order to obtain complete oxidation of the fiber, CNTs and POSS particles. After the complete oxidation on the sample, the system was programmed to cool to 35^{o}C in the presence of air. Air was introduced to the samples during the run and it was maintained at the rate of 30mL/min in order to maintain an oxidizing environment around the sample. It is well known that amorphous carbon decomposes at the lowest temperature, followed by CNTs (~600^{o}C), and then graphite materials (700-800^{o}C).

As stated by Galasso et al. [144] and Brown et al. [145] and demonstrated here in this work, the oxidation of amorphous carbon occurred at approximately 575^{o}C and the complete oxidation of carbon fiber occurred at about 720^{o}C only in the presence of air. This has demonstrated that the complete oxidation of carbon fiber is possible in the presence of air. As a result, the thermal analysis was carried out only in the presence of air following the thermal cycle as described above. The primary oxidation temperature is defined as the temperature at the highest peak for each batch on the derivative weight curve, and can actually represent the thermal stability of that batch.

Mansfield et al. [137] examined the effect of carbon nanotubes' length and diameter on their TGA measurements, and it was discovered that the oxidation temperature for shorter CNTs was higher than that of the longer CNTs. The early decomposition (lower oxidation temperature) of the long nanotubes was associated with the increased probability of defect sites along the length of the nanotubes. In order to

carry out the quantification of CNTs grafted on carbon fiber in this study, it was necessary to program the TGA using the thermal cycle profile described above to ensure a complete oxidation of the fiber and nanotubes. A sample weighing about 15mg was cut from the extreme tow of each batch of CNT grafted fabric. At least three separate TGA runs were done on each batch, and this was chosen based on the NIST recommendation [147]. Figure 2.24 (a) shows the typical derivative weight percent versus temperature for the CNT grafted fibers of different batches. It was clearly shown that CNTB1 and CNTB3 had the highest oxidation temperature (657^{o}C and 661^{o}C, respectively) when compared to CNTB2 and CNTB4. A higher oxidation temperature indicates the presence of uneven, shorter, and poor CNT population density on the fiber. Lower oxidation temperature as observed in CNTB4 (~626^{o}C) and CNTB2 (~573^{o}C) was an indication of higher and uniformly grafted CNTs on the fibers. CNTB2 seems to possess a higher population of CNTs when compared to other batches.

It has been reported that after the CNTs are heated to a temperature at or above 500^{o}C, all carbon-containing components are gasified, and the remaining residual mass is comprised mainly of catalytic metals and their oxidation products [148]. Therefore, it is possible to actually quantify the amount of CNTs grafted on the carbon fiber based on the mass of the remaining residues after the oxidation process. As shown in the zoomed region (inset) displayed in Figure 2.24 (b), it is evident that CNTB2 had the highest residual mass as compared to other batches.

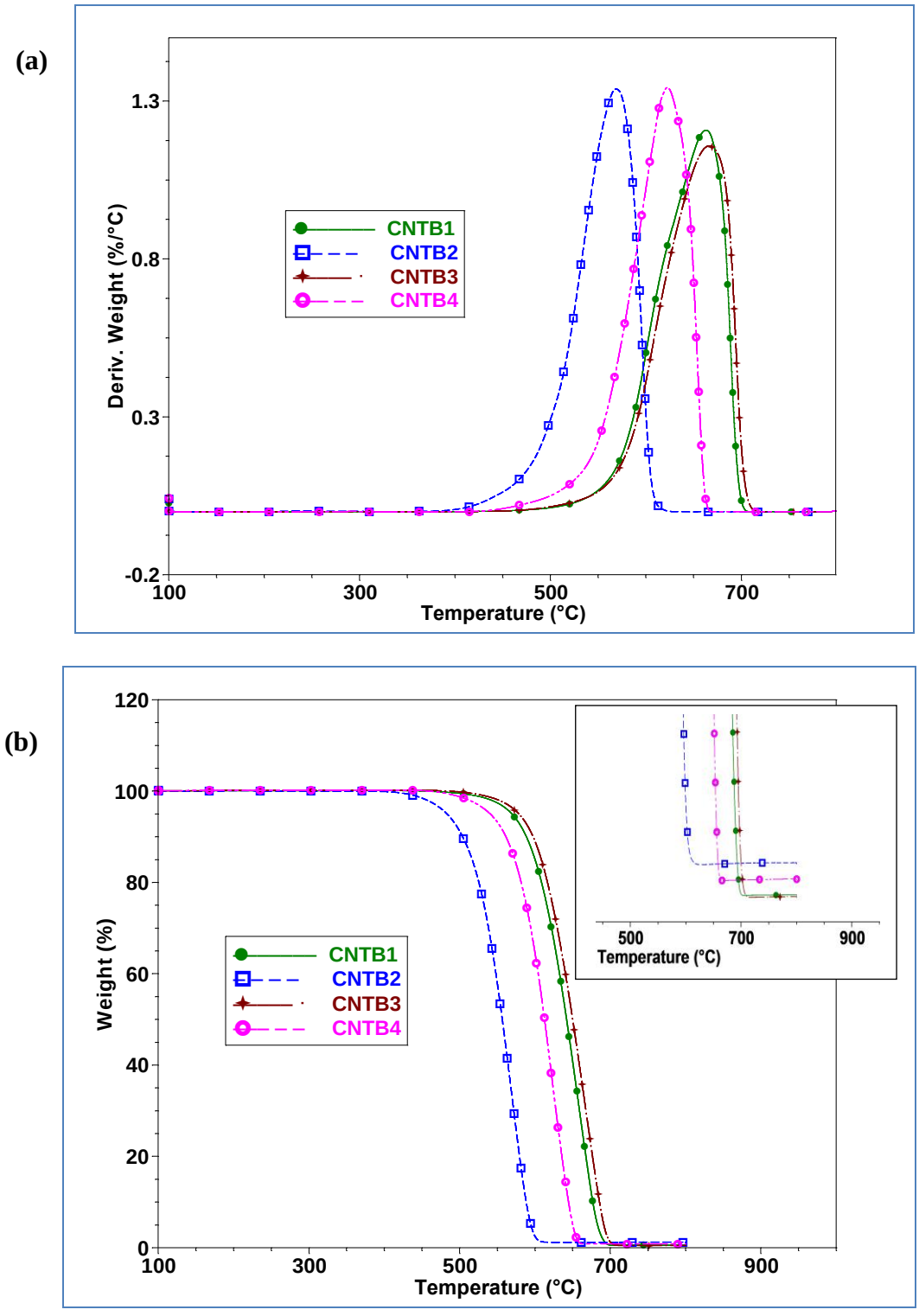

Figure 2.24. TGA plots for the four different batches of CNTs growth (a) Derivative weight percent versus temperature curve for the respective batches, and (b) weight percent versus temperature curve for the respective batches [inset: enlargement of the residue weight percent from (b)]

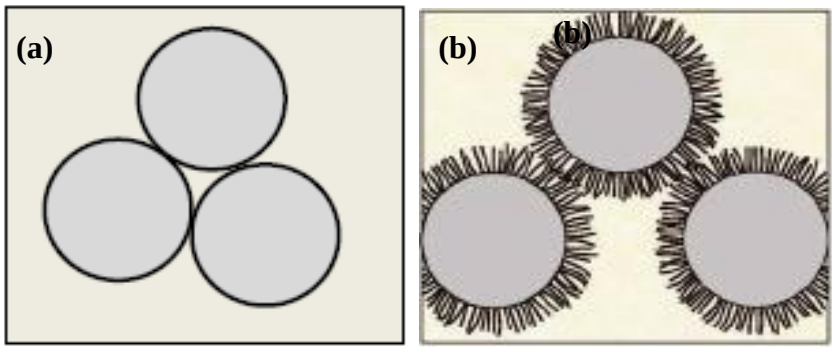

Figure 2.25. Illustration of the population density of CNTs on the fiber: (a) without any CNTs growth, and (b) highly populated CNTs on the fibers

The sharp peaks, seen in CNTB2 and CNTB4 (Figure 2.24 (a)), were due to the faster diffusion of gasification products as a result of wider spacing between the filaments created by the highly populated nanotubes on the fiber (Figure 2.25). Figure 2.26 shows the variability of CNTs' percent presence in each batch. The CNTB1, CNTB2, CNTB3, and CNTB4 have a residual mass of 0.70%, 1.06%, 0.71%, and 0.82%, respectively. Although these numbers clearly show that the CNTs' growth rate in each batch was lower than expected, the fibers catalyzed through the dipping method (CNTB2 and CNTB4) seemed to yield better growth. Also deducted from Figure 2.27 is that the oxidation time remained relatively consistent irrespective of the batch, and the onset temperature for CNTB2 still remains the lowest.

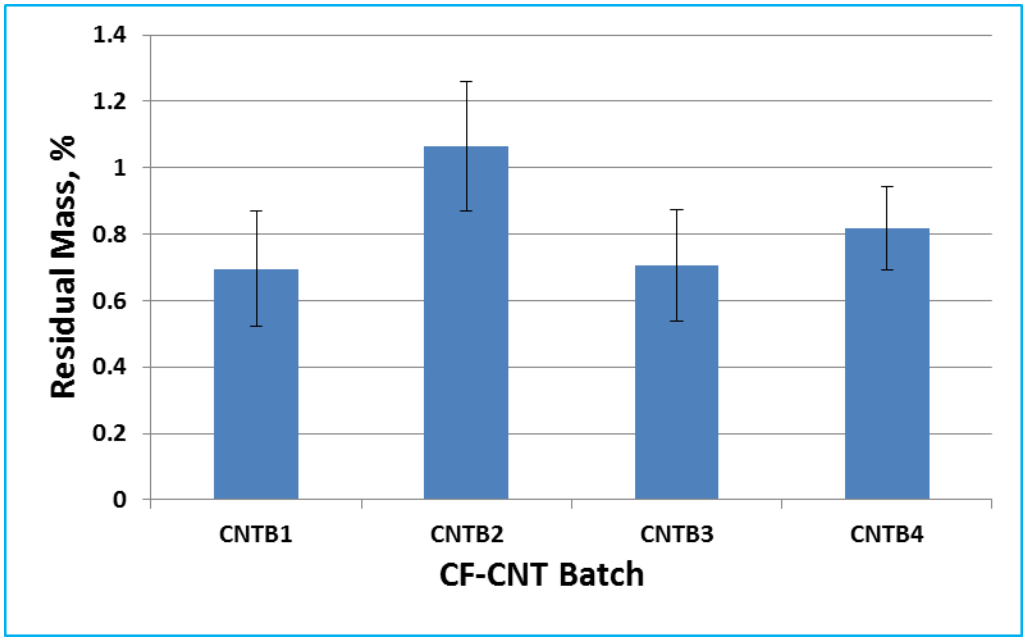

Figure 2.26. Variability of CNTs percent in each batch

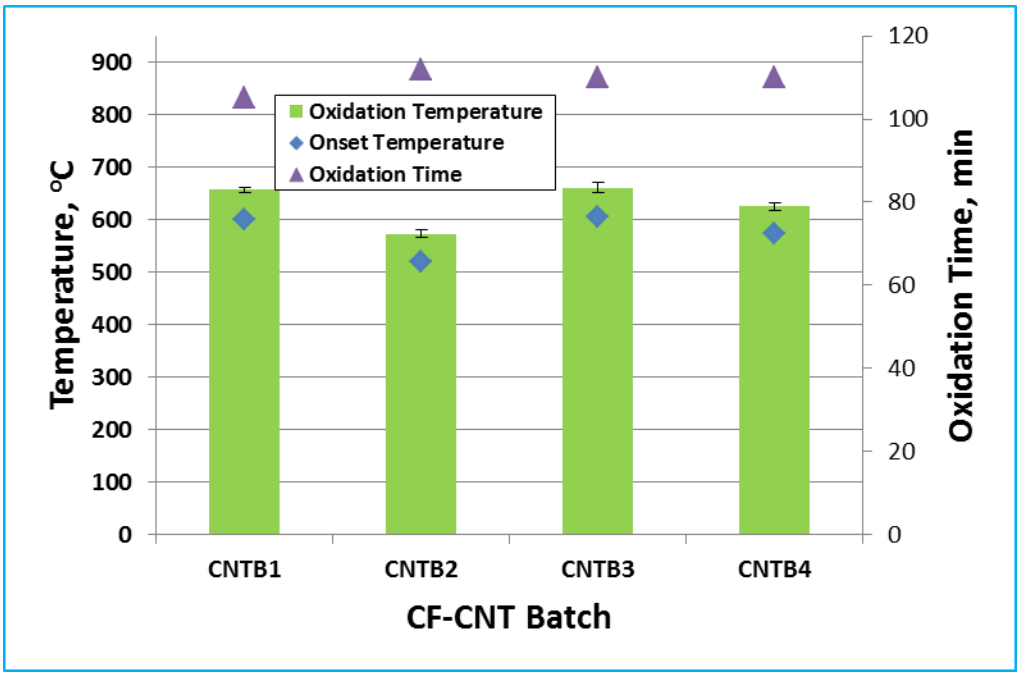

Figure 2.27. Effect of growth method on the thermo-gravimetric analysis

In understanding the effect of POSS coating on the thermal stability of CNT grafted fibers, the grafted fabric was coated with POSS and one tow was separated from each batch, chopped, and set to undergo the thermal cycle. Figure 2.28 (a) shows the derivative weight percent against the temperature for the uncoated and POSS coated batches. As shown, the effect of the POSS coating on the catalyst sprayed samples (CNTB1 and CNTB3) was not well-pronounced compared to POSS coated CNTB2 and CNTB4. This is shown clearly in their respective weight percent change versus temperature in Figure 2.28 (b). The shift in the oxidation temperature for POSS-CNTB1, POSS-CNTB2, POSS-CNTB3, and POSS-CNTB4 was estimated to be 0.2%, 1.4%, 0.4%, and 3.4% higher than their respective uncoated samples as shown in Figure 2.29. Also shown in the figure is an indication of an increase in the relative oxidation time for POSS coated samples in the amount of ~ 6% when compared to uncoated batches.

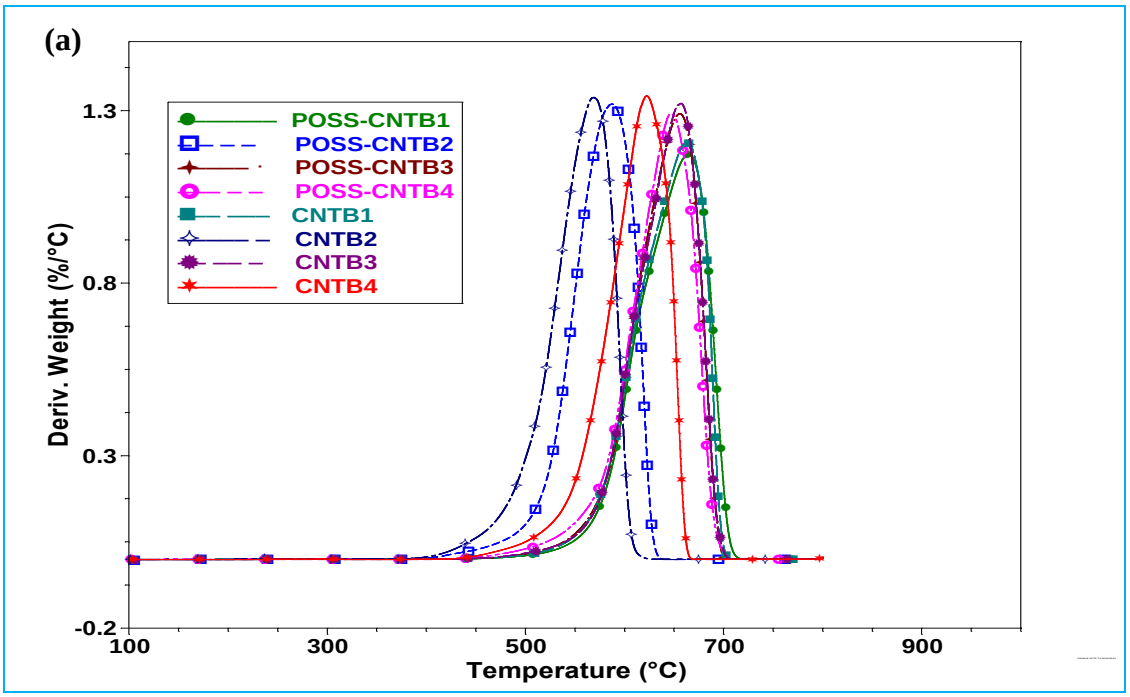

Figure 2.28. TGA plots for the four different batches of POSS coated CF-CNTs samples (a) Derivative weight percent versus temperature curve for the respective batches, and (b) weight percent versus temperature curve for the respective batches

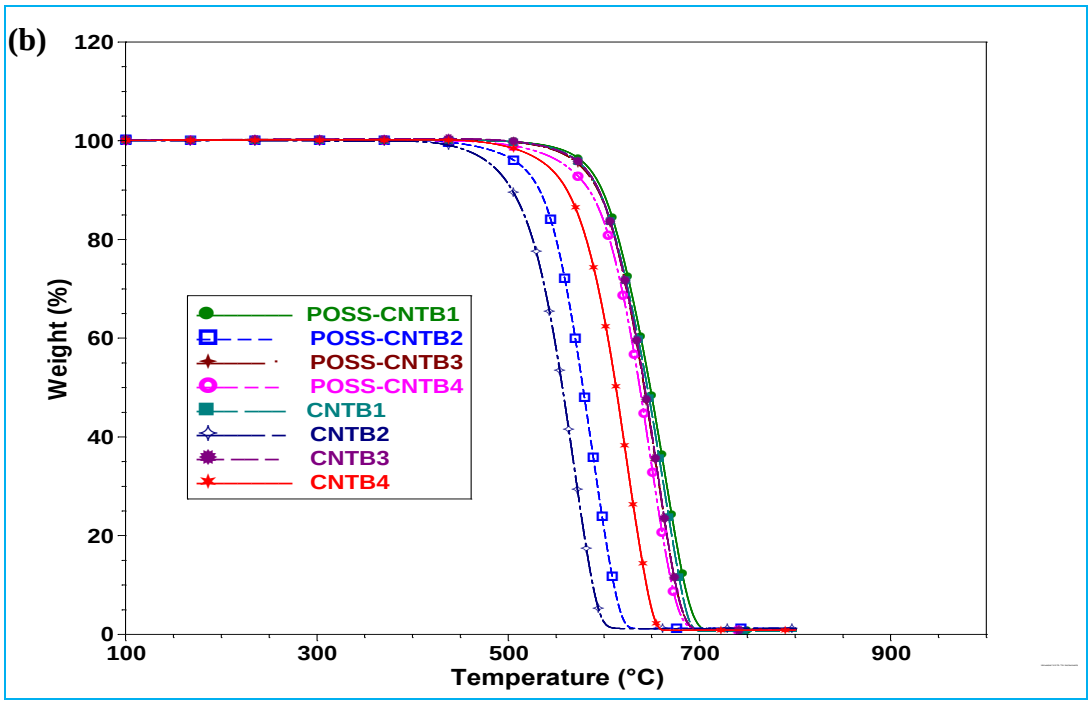

Figure 2.28. ***(Continues)*** **Four different batches of POSS coated CF-CNTs samples (a) Derivative weight percent versus temperature curve for the respective batches, and (b) weight percent versus temperature curve for the respective batches**

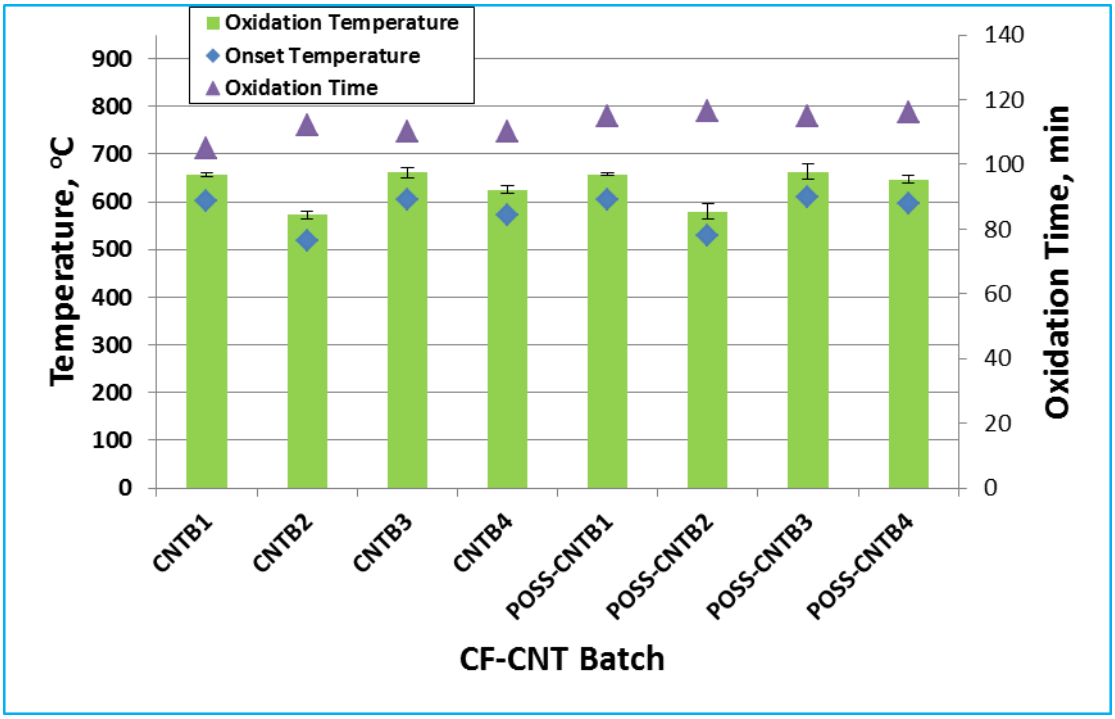

Figure 2.29. Thermo-gravimetric behavior of POSS coated CF-CNTs

2.3.4 Characterization of CNTs using SEM

CNTs grafted fiber surface morphologies were examined again with the aid of a high resolution SEM Zeiss NEON 40-EsB. The images of CNTB1, POSS-CNTB1, CNTB2, POSS-CNTB2, CNTB3, POSS-CNTB3, CNTB4, and POSS-CNTB4 are shown in Figure 2.30 (a-h), respectively. The presence of a high density of CNTs was shown distinctively in CNTB2 and CNTB4 samples. The growth on CNTB3 also seems to be higher than on CNTB1. This might be attributed to the method of catalyst deposition on the fiber with more growth well-pronounced on the thermally treated fibers. T650-TT samples have more hydroxyl and carboxyl groups on the surface of the fiber; as a result, the catalyst particles were able to adhere to this fiber surface better than the untreated fiber. There is an indication that CNTB1 possesses the least growth when compared to the others. Catalyst deposition using the dipped method seems to have more CNTs growth. These micrographs have shown clearly and demonstrated the validity of CNTs' quantification previously discussed in the last section. As discussed earlier and shown in the micrographs, the nanotubes' population density was low in all of the batches.

After the moderate POSS coating, the nanotubes' roots on the fiber surface were completely covered with the POSS. The inset image on the coated fibers shows the higher magnification of the treated samples. POSS-CNTB3 shows a complete coating of both the nanotubes and fiber surface better. The striations noticed on the other CNTs grafted batches after the coating were covered with the POSS completely in POSS-CNTB3 samples.

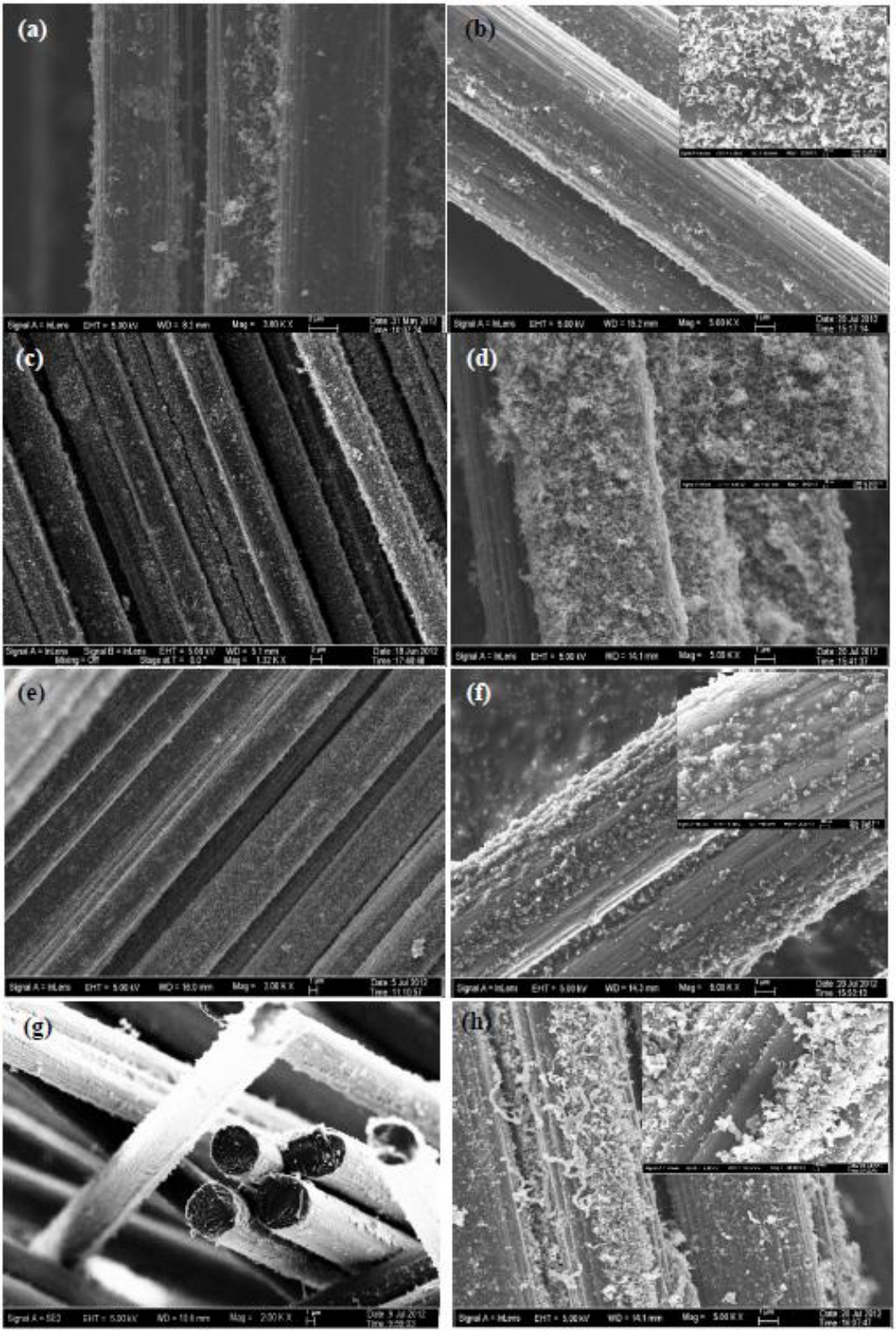

Figure 2.30. SEM images of (a) CNTB1, (b) POSS-CNTB1, (c) CNTB2, (d) POSS-CNTB2, (e) CNTB3, (f) POSS-CNTB3, (g) CNTB4, and (h) POSS-CNTB4

Figure 2.31 shows the EDS analysis images of the residues obtained (after the run) from the TGA runs of T650-AR, CNTB1, CNTB2, CNTB3 and CNTB4, respectively.

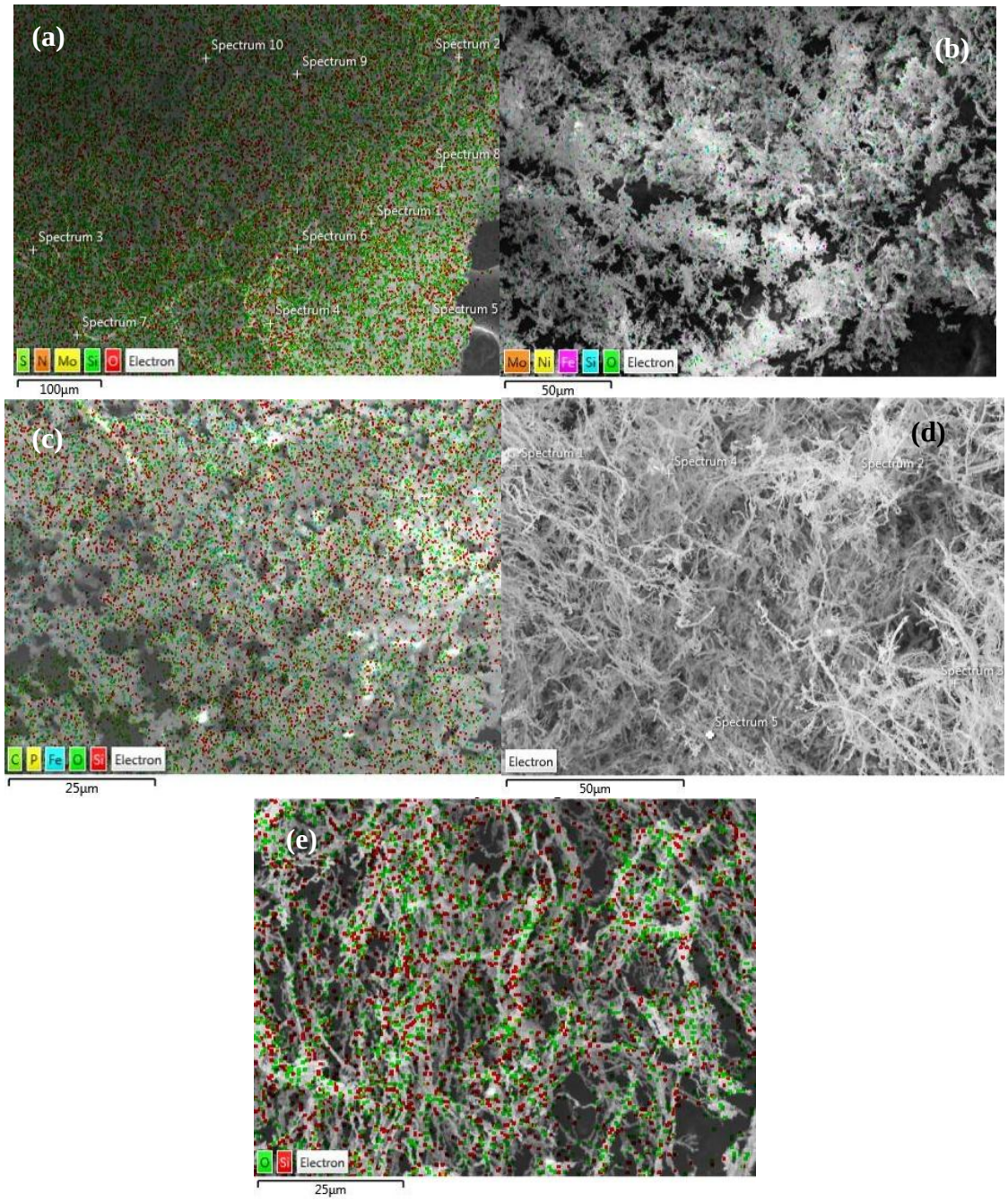

Figure 2.31. SEM-EDS images of the burn-off residue of (a) T650-AR, (b) CNTB1, (c) CNTB2, (d) CNTB3, and (e) CNTB4

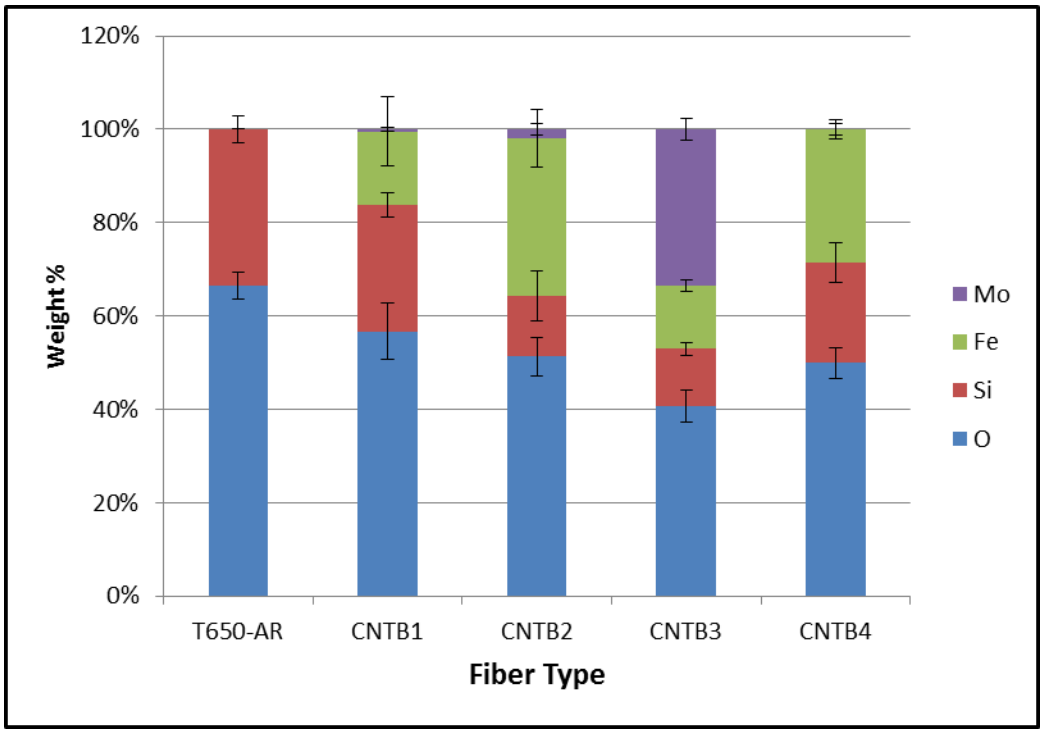

Figure 2.32. EDS analysis of the burn-off residue

The T650-AR residue was not as fibrous-like as others. The result of the EDS analysis done on the individual residues shown in Figure 2.32 only reveals the presence of catalytic metals. The presence of iron metal particles was detected by the EDS only in the CNTs grafted fibers. Molybdenum elements were also detected by the EDS in CNTB1, CNTB2, and CNTB3 samples, but not in T650-AR samples. The percentage of catalytic metals can only be determined quantitatively by using the adopted TGA techniques. The presence of Silicon particles might have come from the silicone oil and/or granuated silica gel used with the antistatic lubricating oil applied to the spinneret holes and the conveying systems during the fiber production process.

CHAPTER 3

TENSILE PROPERTIES CHARACTERIZATION

3.1 Sample Preparation

3.1.1 Design of Test Frame

To measure a single fiber tensile properties, it is quite necessary to mount the fiber on a thin sheet of cardboard [149,70] or metallic frame [116]. The use of cardboard for this kind of test is examined to cause a fiber twist during the test. For this work, therefore, the picture frames are made out of a steel shim flat sheet of 0.10mm thickness and 152mm x 457mm dimensions with different window sizes to accommodate single fibers with different gauge lengths. The fiber length between the fixing points is called the gauge length, which was 6.35 ± 0.02 mm and 12.7± 0.02 mm in this study. The frames are made based on the maximum spacing allowed between Q800 tension clamp grippers. The frame's inner window width and outer width are 0.38 ± 0.02 –in and 0.50 ± 0.02 –in, respectively for both gauge lengths. For the 0.25-in (6.35 mm) gauge length frame, the frame height was kept at 1.00 ± 0.01-in and for the 0.5-in (12.70 mm) gauge length frame the frame height was 1.25 ± 0.01- in (Figure 3.1). Due to the high precision and accuracy required for consistent window size, a 2D Mazak laser cutting machine operated at 1000 Watt was used to cut the frames according to the test specification. Engraved marks were created by laser-cutting at the center ends of all the frames to ensure the proper alignment of the fiber on the frame.

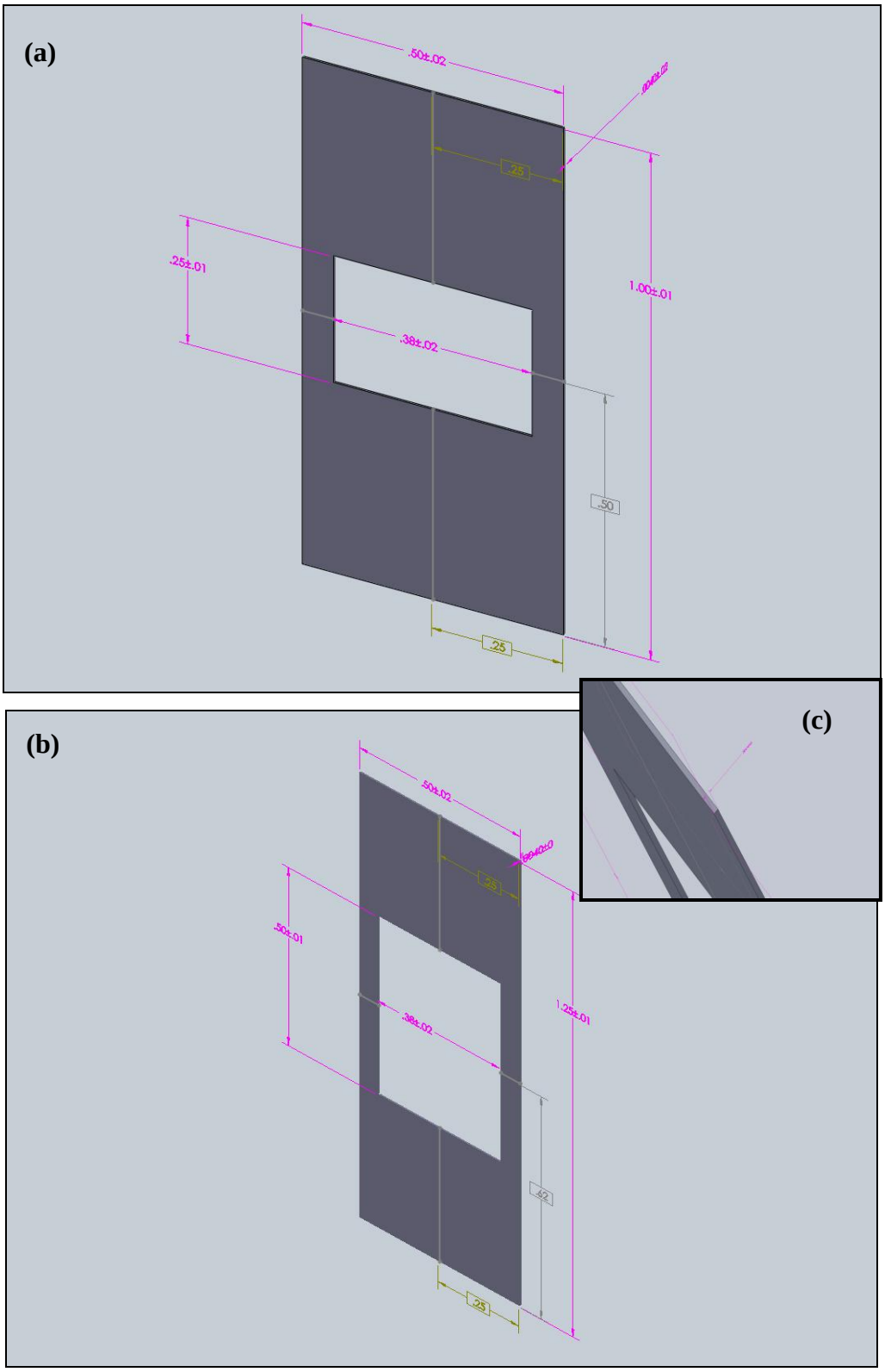

Figure 3.1. Testing frames design for gauge length effect study: (a) 6.35mm window size, (b) 12.70 mm window size, and (c) the thickness of the frame [all dimensions in inches]

3.1.2 Testing Procedure

The fibers were aligned straight along the central axis of the frame to ensure that the axis of the filament was parallel to the direction of the stretching. Two engraved alignment marks on the steel frame made it possible to align the test fibers during mounting as shown in Figure 3.2 (a). Figure 3.2 (b) shows the actual picture of the frames used for the test.

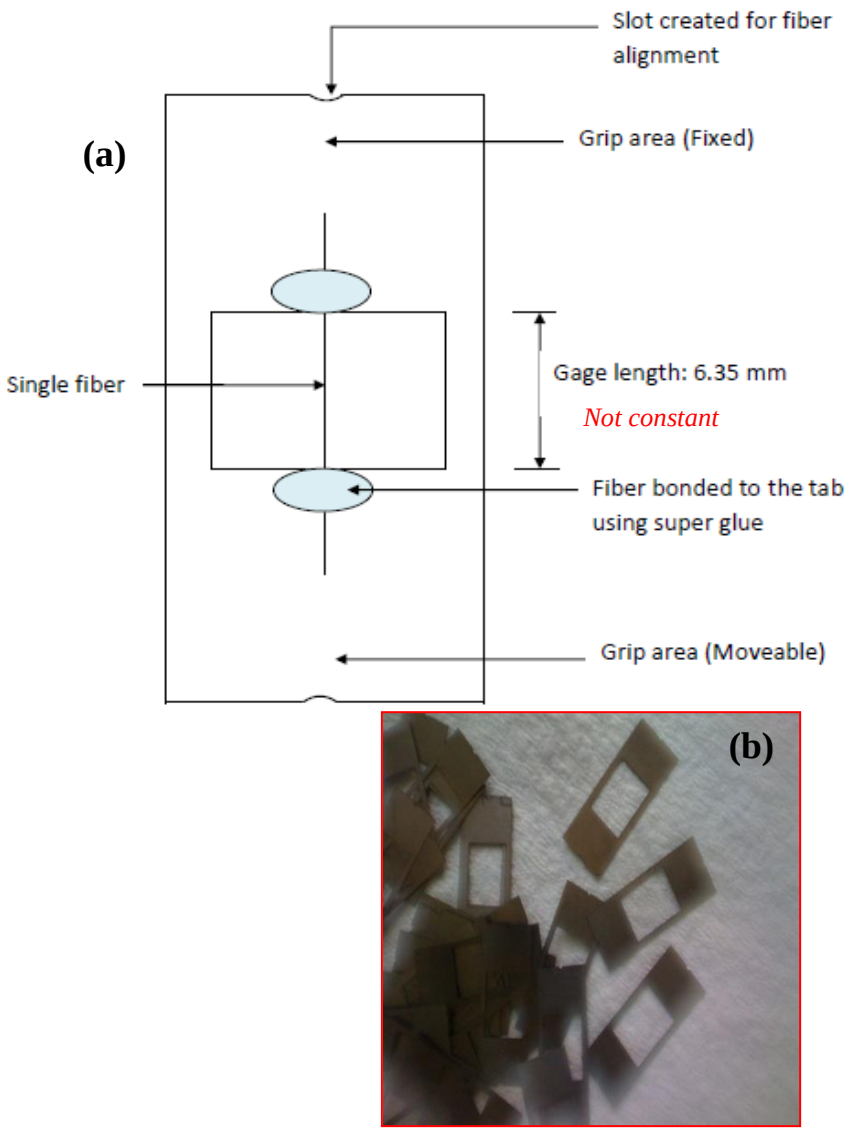

Figure 3.2. Single fiber test frame (a) Schematic of single fiber mounted on a steel frame *(Sketch drawn not to scale)*, (b) Picture of the testing frames

One of the necessary measures to note during the tensile tests of a single fiber is to ensure that the interfacial shearing force between the fiber and adhesive material is higher than the tensile force needed to break the fiber. Otherwise, the fiber would be pulled out from the adhesive, and thus, accurate measurements of the fiber's tensile properties might not be possible. It is necessary to have the major portion of the fiber ends covered with the adhesive material (such as super glue), as illustrated in Figure 3.3. The glued ends of the fibers had to be adhered strongly to the frame to ensure that the filament would not be pulled out during the tensile loading. As a result, the interfacial bond strength between the fiber and glue must be sufficient to cause fiber fracture rather than pullout.

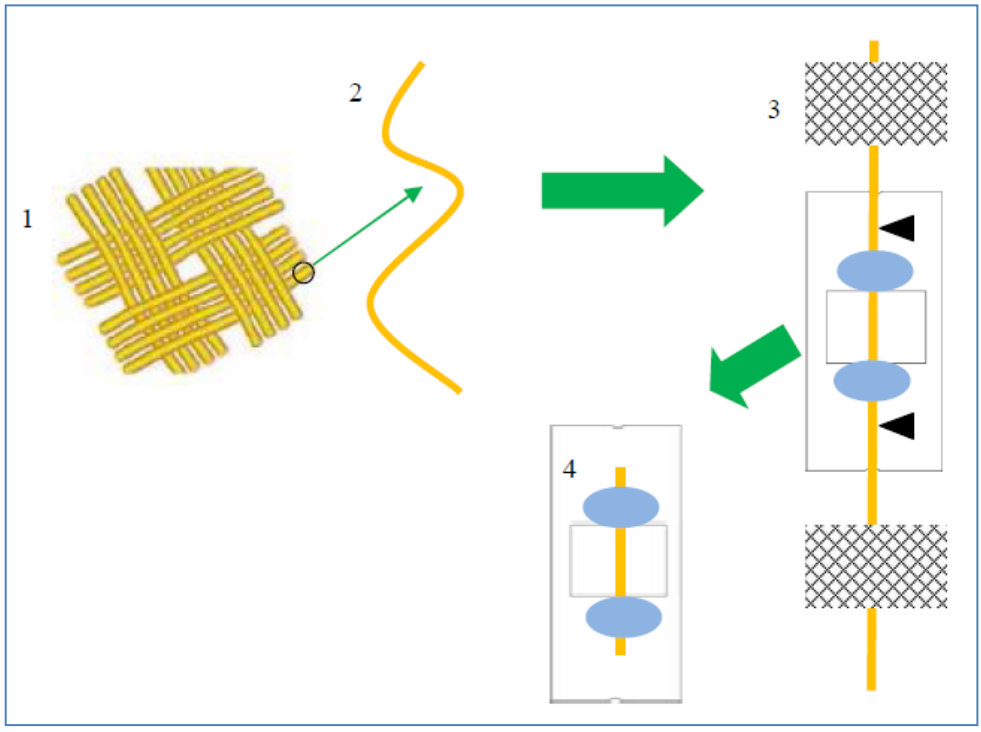

Figure 3.3. Single fiber mounting process: (1) carbon fabric; (2) single fiber extracted from the fiber tow; (3) adhesive tape used to affix both ends of the fiber to the mounting board, then a drop of super glue (marked blue circle) was poured on both fiber ends and the ends were later cut with a razor blade (marked black triangles); (4) a finished sample ready to be cured

Before the use of super glue for this study, a high-temperature ceramic cement paste (Insa-Lute P-1) was used to bond sized AS4 carbon fibers to the steel frames.

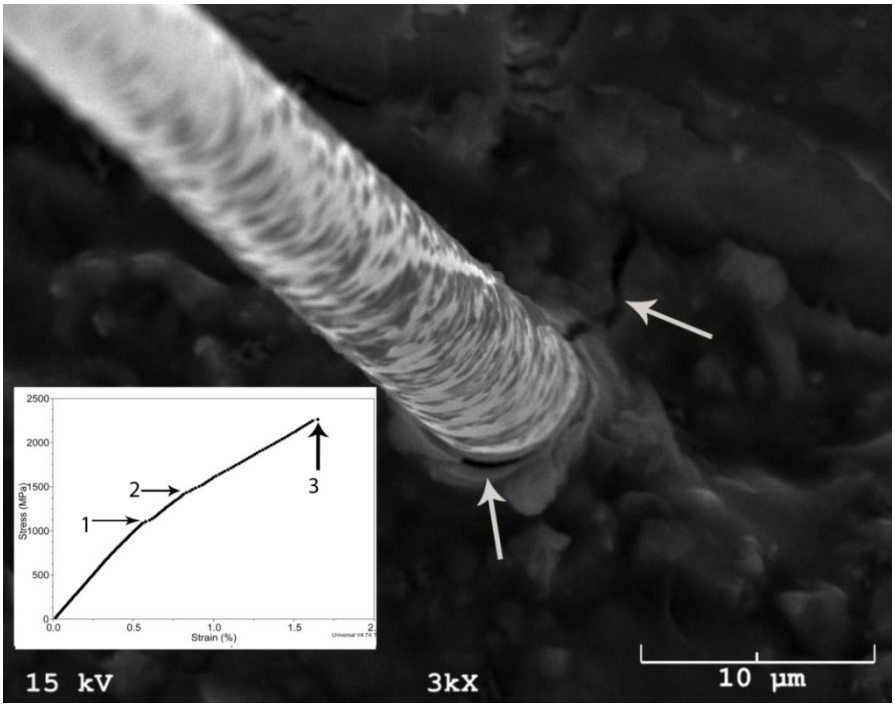

Figure 3.4. AS4 carbon fiber pulling out from the cement paste used to bond the fiber to the tab: White arrows pointing to the cement cracking areas at the base of the fiber; [Inset showing a stress - strain plot of the sample after the tensile test: (1) the initial fiber pull-out point, (2) the second point of pull-out, (3) fiber failure point]

The cement is air-setting and cures within 18-24 hours at room temperature. A micrograph of the fiber pulling out of the cement paste is shown in Figure 3.4. The stress-strain curve for the specimen is inserted in the image. It can be inferred from the curve that the interfacial shear force was higher than the tensile fracture force of the fiber up to point 1. The fiber experienced an initial pullout from the paste immediately at point 1, and this changed the slope abruptly up to point 2. However, there was still a frictional force between the fiber surface and the cement paste. The second fiber pullout from the paste occurred at point 2, and this also led to slope change. The change in the curve slope

would give an error in fiber modulus estimation at that point. Due to the existence of frictional force between the two surfaces, the interfacial shearing force increased, and eventually the fiber broke at point 3 [91]. As a result of the pullout, the cement paste was not used to bond the fiber to the frame for this work.

Efforts to incorporate a fully integrated random selection procedure have not been completely successful to date; however, it has been shown that significantly improved sampling methods which employ random numbers and counting procedures have reduced the degree of nonuniformity [150]. To ensure the consistency of the measurements, all of the fibers were taken from the same tow. The tensile specimen was prepared by fixing both ends of the filament onto a picture frame with an instant cyanoacrylate adhesive (Loctite gel-type super glue). The diameter of the single filament from the different type of fibers used under this test approach was measured using a digital-scanning microscope (ZEISS DSM-960A). The resolution of the digital microscope is 0.007 μm, with a useful magnification range of X10 to X30,000. At least three locations along the length of each filament were examined for diameter measurement [151]. The fibers were aligned and glued to the picture frames carefully, as mentioned above, and then allowed to cure at 22 ± 0.5^{o}C. The cured samples were then stored in a Gel-Pak (MB-150T/100) transparent membrane box at the same room temperature in order to prevent fiber damage.

Tensile tests of a single carbon fiber were done on a DMA-Q800 at room temperature (22 ± 0.5^{o}C) using 0.02 N/min force ramp. The machine has a force resolution of 0.00001 N, with a minimum and maximum force of 0.0001 N and 18 N, respectively.

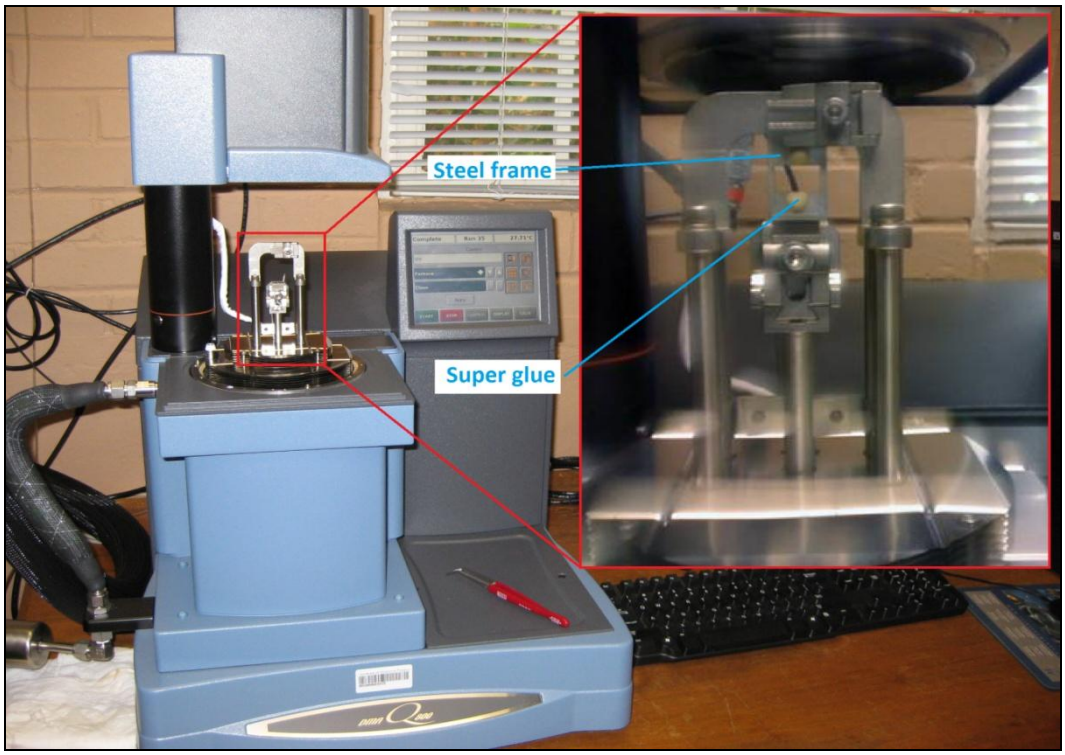

Figure 3.5. Tension clamp installed on DMA-Q800 [Inset showing showing the sample frame inserted between the moveable and the fixed ends of the clamp]

A picture frame with a single fiber is secured in the test apparatus and subjected to quasi-static uniaxial tensile load as shown in Figure 3.5. A series of tests is done in which a single fiber is subjected to tensile loading in accordance with American standard (ASTM D 3379). A preload (0.0001N) is applied to make the fiber filament straight on the testing frame before the final testing. Two legs of the picture frame are cut immediately before testing begins so that the applied tensile load is completely taken by the single fiber during the testing.

3.2 Gauge Length Effect on the Tensile Properties of T650-35 CFs

The filament diameter, tensile strength, tensile modulus, failure strain, and filament counts per tow, as given by the manufacturer, are 6.8 μm, 4.28 GPa, 255 GPa, 1.7%, and 3K, respectively. The fibers were obtained in woven fabric form and the average diameter as measured was 6.8 ± 0.11μm.Single filament fiber specimens were prepared under a stereoscopic microscope and the procedure as illustrated in Figure 3.3 was followed to align and mount the filament on the frame. All of the sources of experimental error as shown in Figure 1.5 were taken into account when preparing the samples and at the time of testing them in this study. For instance, the fiber and frame alignment issues were taken care of by the use of center-marked frames that were well fitted and positioned axially on the clamps, making sure the frames were well-aligned along the line of action of the machine. The clamp-mass calibration and testing procedures were done as specified by TA Instruments, ASTM C-1557-03, and ASTM D-76M.

The stress-strain behavior of the specimens showed a brittle failure and a linear stress-strain curve, as illustrated in Figure 3.6. As shown, the samples tested at 6.35mm gauge had the highest tensile strength, modulus, and failure strain. This behavior is expected, as fiber with smaller gauge length would have few surface flaws compared to the fiber with larger gauge length. As shown, the stress applied to the specimen was almost linearly proportional to the strain until failure. This is common in high strength PAN-based carbon fibers. Figure 3.7 shows the properties of the fibers at the two gauge lengths. As seen in Figure 3.7, the fibers tested at 6.35mm gauge show 14% and 13%

higher tensile strength and failure strain respectively, as compared to 12.70mm gauge samples.

According to the Chain of Link model [152], each fiber can be divided into links, each containing flaws of varying severity. Thus, the fiber would fail if one of the links fails. Thus, the strength of this fiber is found to be statistically distributed due to the presence of these varying flaw severities. The severity of flaws varies with the sample length, and hence, the longest fiber possesses the highest flaw density. This is also observed in the results presented here, as the 6.35mm gauge length samples have the fewest flaw distributions. This is reflected in the average tensile strength of 3,830MPa and 3,2942MPa measured for the 6.35 mm and 12.7 mm samples, respectively.

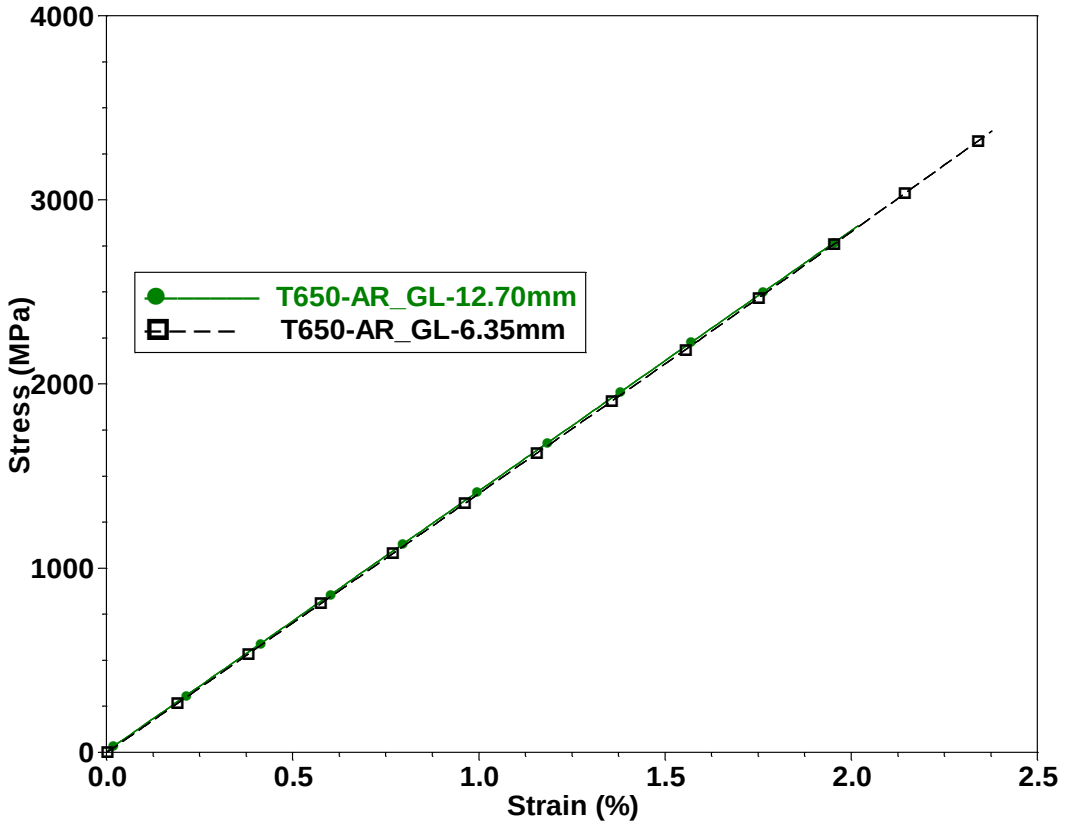

Figure 3.6. Representative tensile curves for gauge length effect on T650-35 CF

The toughness of T650-35 fibers, which represents the energy absorbed by the fiber before failure as calculated based on the area under the stress-strain curve of individual fibers, is shown in Figure 3.8. The toughness is considered the average of an integrated area underneath the stress-strain curves for an individual fiber.

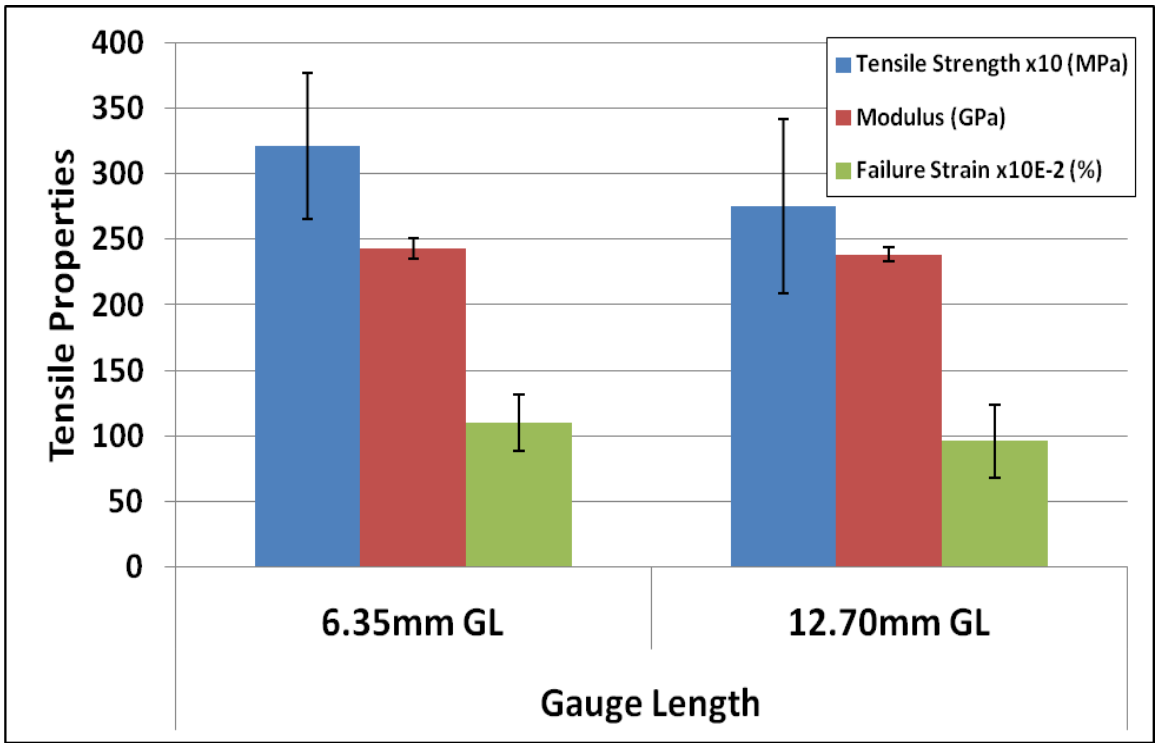

Figure 3.7. Histogram showing the effect of gauge length on the tensile properties of T650-35 CF

As shown in the plot, 6.35mm gauge length samples are about 11% tougher when compared to 12.70mm gauge length samples. This is also a reflection of both the surface and internal flaw densities associated with individual samples. The work of fracture, as obtained from the stress-strain curves, is also depicted in Figure 3.8. Work of fracture (WoF) for 6.35mm gauge length fibers is about 14% higher as compared to 12.70mm

gauge length samples. The WoF is calculated from the individual filament strength, and the average is reported. This represents the work done to propagate the crack from one end of the fiber to the other across the cross-sectional area.

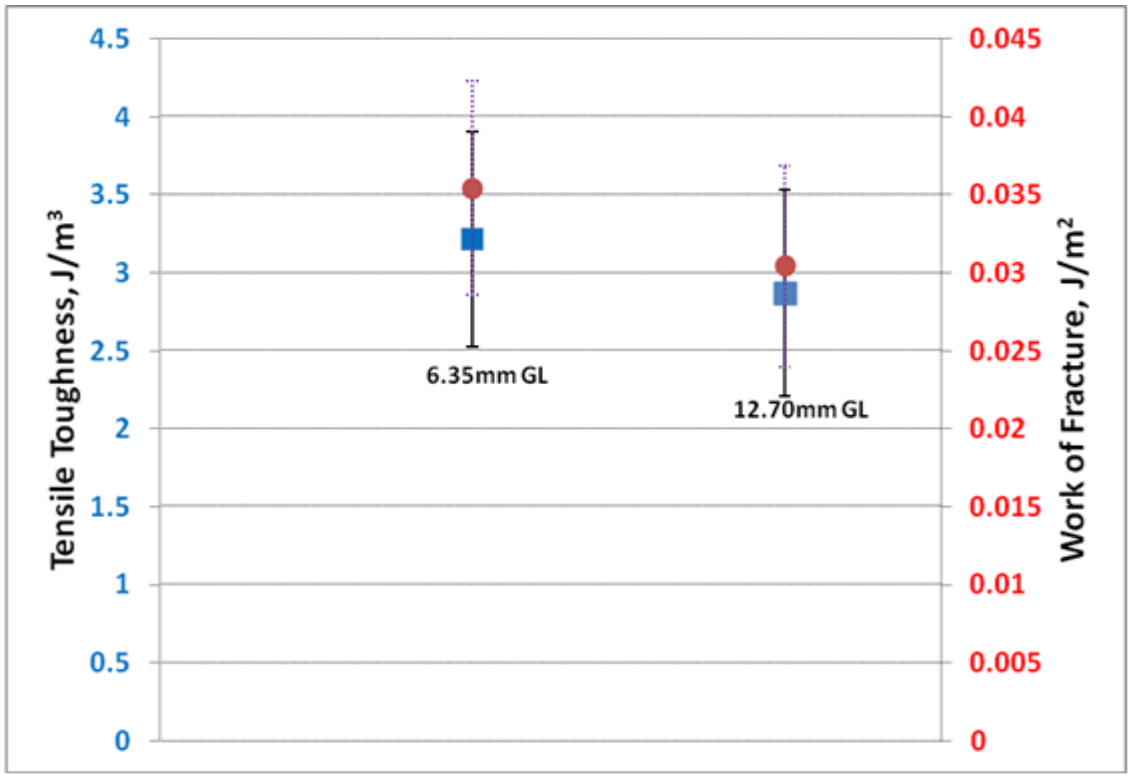

Figure 3.8. Examining the tensile toughness and WoF for both gauge lengths

3.2.1 Electron Microscopy Examination of the Fracture Surface

The transverse cross-sectional views of the fractured surfaces for both gauge lengths were observed under SEM, and are displayed in Figure 3.9 (a). The cross-section of the fiber shows intrinsic fracture initiation points near the edge of the fiber, as shown in Figure 3.9 (b). It is believed that fracture is propagated from these points towards the second edge,where there is a pulling effect between the sizing and fiber due to the chemo-mechanical bonding that existed between the two surfaces. To complete the fracture, the separation of the two surfaces required higher tensile force, and hence, this contributed to the higher values noted in the fiber tensile strength. The initiation of failure from surface defects for the PAN-based carbon fibers was also reported by Naito et al. [66]. The fracture surface shows a planar mirror region, a misty region, and a hackle region where the crack initiated. The initiating flaw may be an impurity, a surface nick due to handling, or even a very minor chemical heterogeneity. Fracture of this kind occurs in three-dimensionally bonded materials with no yield mechanisms.

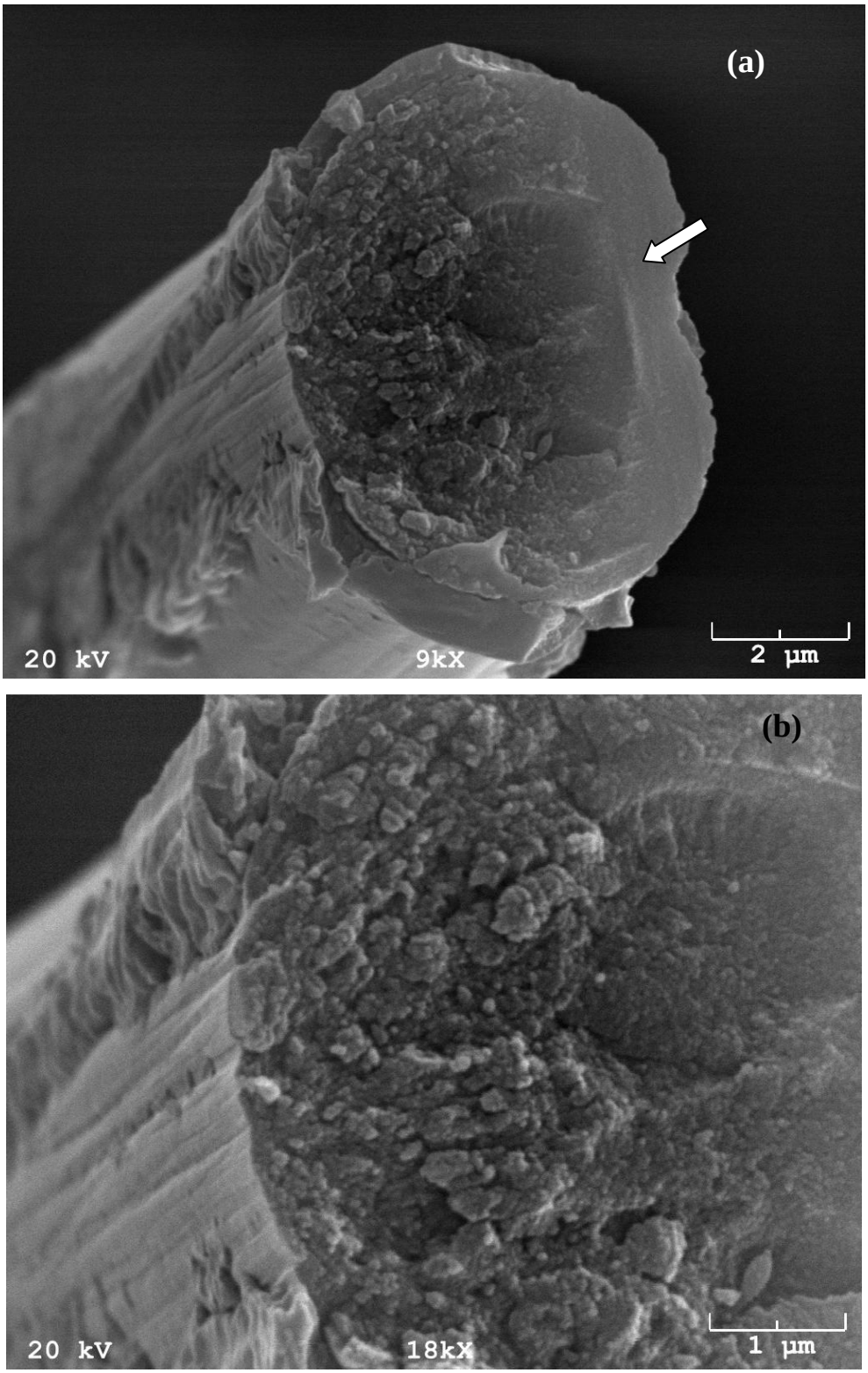

Figure 3.9. Fracture surface of T650-35 CF tested in tension at room temperature: (a) at low magnification- white arrow indicating the start of the crack, (b) hackle region at high magnification

3.2.2 Weibull Modeling of the Tensile Strength for Gauge Length Effect

The failure stress distribution of the carbon fibers can be analyzed using a two-parameter Weibull distribution function [153,154]. This is based on the assumption that all of the samples have the same volume and take the form:

$$P = 1 - exp\left[-\left(\frac{\sigma}{\sigma_o}\right)^m\right] \quad (1)$$

In Eq. (1), P is the cumulative failure probability of a fiber at a stress less than or equal to stress σ. σ_o is the scale parameter that gives the variability of the failure stress and represents the strength at which 63.2% of the fibers would fail. There are two major approaches in estimating the parameters of the Weibull distribution: the linear regression (LR) method (or graphical method), and the maximum likelihood estimate (MLE) method. This work concentrates on using the linear regression method. The linear regression method may be derived from re-arranging Eq. (1), which will yield the following equation:

$$ln\left(ln\left(\frac{1}{1-P}\right)\right) = mln\sigma - mln\sigma_o \quad (2)$$

Hence, the scale and the shape parameters can be obtained from the linear fitting of lnln [1/(1-P)] and ln σ, whose slope is the Weibull modulus, *m*, and from the intercept the characteristic strength, σ_o, may be obtained. The main problem of the method is how to estimate the P values in such a way that the calculated *m* and $\sigma_o$values are unbiased estimators of the real values. Normally, the P value is estimated by a function commonly known as the probability index. There are four different probability indices commonly used by various authors, and it has been shown that they all give conservative estimations of the Weibull modulus and the same coefficient of variation [155]. The probability of

failure, P_i, at the i-th ranked specimen from a total of N specimens is estimated from Eq. (3)

$$P_i = \frac{i-0.3}{N+0.4} \quad (3)$$

The LR unbiased strengths reported in Table 4.1 are calculated in accordance with ASTM C 1239-07 from the respective Weibull plots.

The differences in Weibull modulus can be attributed to the nature and distribution of the flaws that are present in the fibers. As a result, the Weibull modulus can be regarded as a defect frequency distribution identifier. A high value of *m* was noticed for the 6.35 mm gauge length specimens, indicating that flaws are evenly distributed throughout the fiber, and hence there was a little variation on the measured strength. Low values of *m* indicate that defects are less evenly distributed, causing greater scatter in strength. As expected, the characteristic strength was found to decrease as the gauge length increases as a result of the increased likelihood of flaws in a longer length.

It can be inferred from the calculated values in Table 3.1 that the 6.35mm gauge length samples possessed higher characteristic strength and lower surface flaws than their longer counterpart. The coefficient of correlation for each group is higher than 90%, which is an indication of good linear fitting.

Table 3.1. Weibull parameters obtained for the fibers tested

Gauge Length	*m*	$\sigma_{o,}$ (MPa)
6.35 mm GL	7.38	3468
12.70 mm GL	2.03	3146

3.2.3 Conclusions on the Effect of Gauge Length

In this study, the effects of gauge length on tensile properties of T650-35 carbon fibers were investigated with the aid of a Weibull statistical model. It is found that fiber samples with smaller gauge length showed higher tensile properties. The Weibull moduli for 6.35mm and 12.7mm gauge length samples are 7.38 and 2.03, respectively. The characteristic strength tends to decrease as the gauge length increases. The tensile strength of the smaller (6.35mm) gauge length samples was noted to be higher compared to the larger (12.70mm) gauge length samples. Fracture surface showed an uneven ridge-like morphology that exists on the fiber as a result of sizing application and the manufacturing procedure. The SEM fractographic images of the fiber also showed that a peel off exists between the fiber surface and the sizing during the test; this actually contributed to higher tensile strength of the fiber. This work has shown that both gauge length and sizing content on a PAN-based T650-35 fiber actually played a critical role in its tensile property improvement. This study was also proved beyond any reasonable doubts that DMA-Q800 can be used to carry out the single fiber test without twisting the testing frame. The cut of the frame's legs with surgical scissors was easier with the use of 12.70mm gauge length. It was also demonstrated, for the first time, the use of a highly precise dynamic mechanical analyzer for the tensile test of single carbon fibers.

3.3 Effect of Sizing on the Tensile Properties of AS4, AS7 and IM10 CFs

Over the years, many authors have reported on how the tensile properties of single fibers could be affected by the fiber gauge length, as discussed in section 1.1. However, there are a few reports that typically investigates how the tensile properties of carbon fiber could be affected by the addition of sizing contents.

Tensile tests of sized and unsized single fibers extracted from three different commercially available PAN-based carbon fibers were performed in order to investigate the effect of sizing on their tensile properties. The fibers were chosen based on the areas of application, year of existence, epoxy compatibility, and the type of sizing. Commercially available sized and unsized PAN-based AS4, AS7, and IM10 carbon fibers were supplied by Hexcel Corporation. The sized AS4, AS7, and IM10 fibers are designated by AS4_S, AS7_S, and IM10_S (these are the fibers used for the desizing procedures as described in section 2.1.1) the unsized fibers are designated by AS4_UnS, AS7_UnS, and IM10_UnS, respectively. The sized fibers were supplied with proprietary surface treatments and a protective sizing (epoxy compatible sizing), while the unsized types were only surface treated without any protective sizing added. All physical and mechanical properties of these fibers are listed in the Table 2.1.

The samples for the tensile test were prepared based on the previously discussed procedures, and the test was carried out on a DMA-Q800 at 0.02N/min to 0.2N. Figure 3.10 shows typical tensile stress-strain curves for all sized and unsized carbon fibers considered for this work. As shown, the stress applied to the specimen was almost linearly proportional to the strain until failure. All the specimens tested showed a brittle failure; the linear stress-strain curves were obtained.

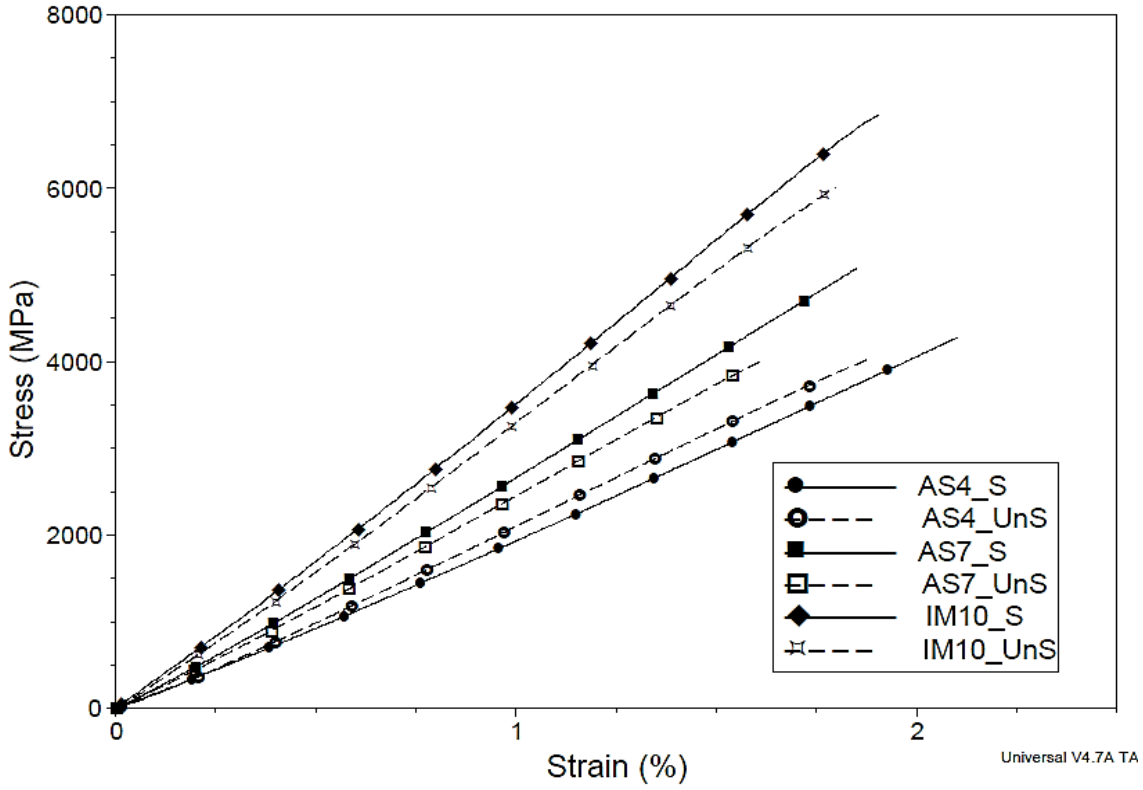

Figure 3.10. Typical tensile stress-strain curves for sized and unsized carbon fibers [Data point range per fiber type: ~150 -300 points; Data sampling interval: 2s/pt; Gauge length : 12.70mm]

As expected, the sized fibers are stiffer than the unsized fibers in all of the fiber types except for AS4_S fibers. There are two possible reasons for this reduction. The interwoven architectural fabric layout of AS4_S before the fiber separation might be the reason, as they were kept in this form over a long period of time. Chen and Diefendorf [156] reported that the modulus of high-modulus carbon fibers (Hercules HMS) reduced by approximately 40% when the fiber surface was etched for about twenty hours uniformly by electrochemical process. Another possible reason is related to the curvature made at the interlaced regions. Keeping filaments in bent form over a while might introduce internal microstructural disclination, as discussed by Guigon and Oberlin [157].

Since modulus is a function of the layer stacks diameter, it is possible to change the filament modulus by changing the stacking layer orientation. The persistence of bent layers is explained by the persistence of disclinations.

The tensile strength, modulus, and failure strain for samples under examination are shown in Figure 3.11. The results show that AS4_S has an average tensile strength and modulus of 4.45 ± 0.94 GPa and 221 ± 23 GPa, respectively, while AS4_UnS has an average tensile strength and modulus of 4.16 ± 0.64 GPa and 241 ± 18 GPa, respectively. Moreover, AS7_S has an average tensile strength and modulus of 4.82 ± 0.95 GPa and 255 ± 45 GPa, respectively, and AS7_UnS has an average tensile strength and modulus of 4.24 ± 0.74 GPa and 244 ± 25 GPa, respectively. The average tensile strength and modulus for IM10_S are 5.75 ± 0.99 GPa and 299 ± 75 GPa, respectively, while IM10_UnS possess an average tensile strength and modulus of 5.36 ± 1.44 GPa and 296 ± 23 GPa, respectively.

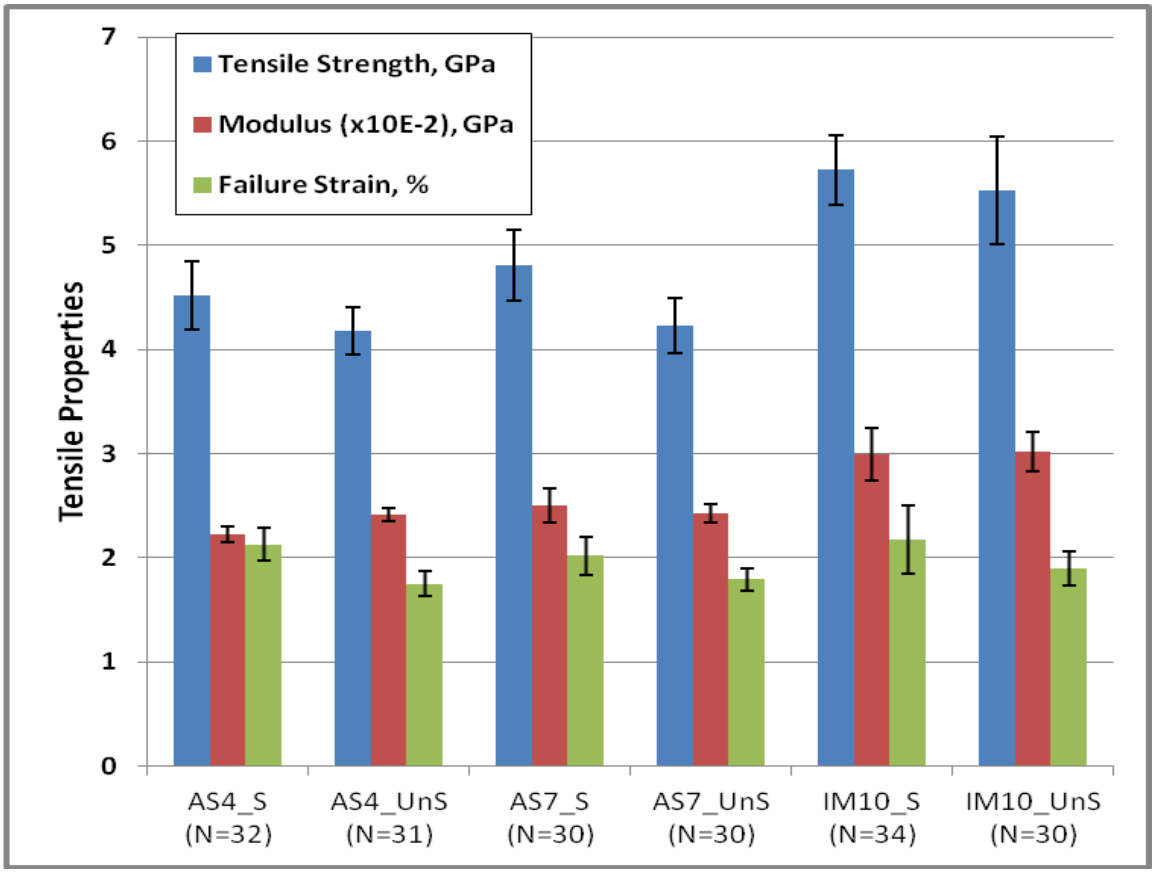

(N is the total number of tested fibers; Gauge length = 12.70mm)

Figure 3.11. Effect of sizing on the tensile properties of sized and unsized carbon fibers

The higher tensile strengths, as observed in sized fibers, are probably due to the effective reduction of stress concentration at the fiber surface flaws by sizing covering the crack tips. Whenever an epoxy-based sizing was used, the distribution of fiber surface defects became narrower than fiber without any sizing [158-160]. There was about 17% reduction in average failure strain by comparing AS4_S and AS4_UnS samples, and about 8% reduction in AS7_S and AS7_UnS samples. About 17% reduction in average failure strain was observed in IM10_S and IM10_UnS samples. The elongation to failure for the sized fiber was observed to be higher than that of unsized fiber.

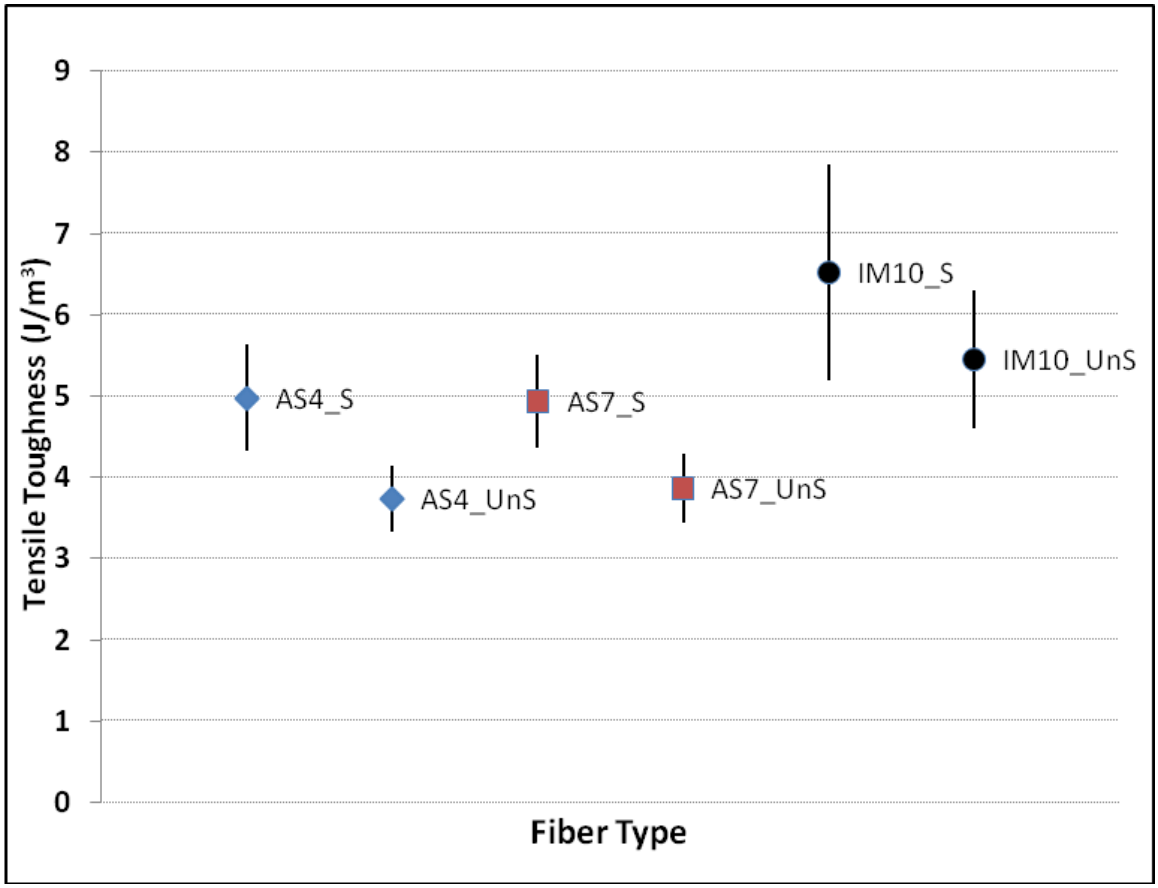

Figure 3.12. Tensile toughness of sized and unsized carbon fibers

The average toughness of a fiber, which represents the energy absorbed by the fiber before failure as calculated based on the area under the stress-strain curve of individual fibers, is shown in Figure 3.12. The toughness is considered the average of an integrated area underneath the stress-strain curves for individual fibers. As shown in the plot, AS4_S was about 25% tougher than AS4_UnS, and AS7_S was 20% tougher than AS7_UnS samples. It was also examined that IM10_S was 16% tougher than the IM10_UnS samples.

3.3.1 Electron Microscopy of the Fracture Surface

The SEM micrographs of single fiber fractured surfaces, which have been carefully selected from a very large number of micrographs, are displayed in Figure 3.13. They represent the most frequently occurring fracture types, as observed in the case of a single carbon fiber. The transverse cross-sectional views of the fractured surfaces for both sized and unsized fibers were taken. The first difference is that most of the fractured-ends of unsized fibers are plane, which means that once the crack is initiated the crack would propagate without any resistance until the fiber fractured (Figure 3.13 b, d, f). This actually contributed to the lower tensile properties observed in unsized fibers when compared to the sized. It is worth emphasizing that the epoxy sizing layer thickness can be somewhat identified in AS4_S and IM10_S samples, as shown in the micrographs(Figure 3.13a and c) and there is a presence of the granular morphology on their surfaces. The surfaces of the sized fibers showed rough, and rather poorly defined, granular texture with no presence of sheet-like structures.

It can be inferred from the images that there was a peel-off on the fiber skin at the failure point due to chemo-mechancial bonding between the fiber/sizing interface as the fracture propagated from the internal crack towards the fiber edge. This same peeling effect was not noticed in unsized fibers, as there was no sizing present on the surface. The irregular and uneven surface crack tips on the unsized fiber provided a means for smooth crack propagation, thereby causing the tensile strength to reduce.

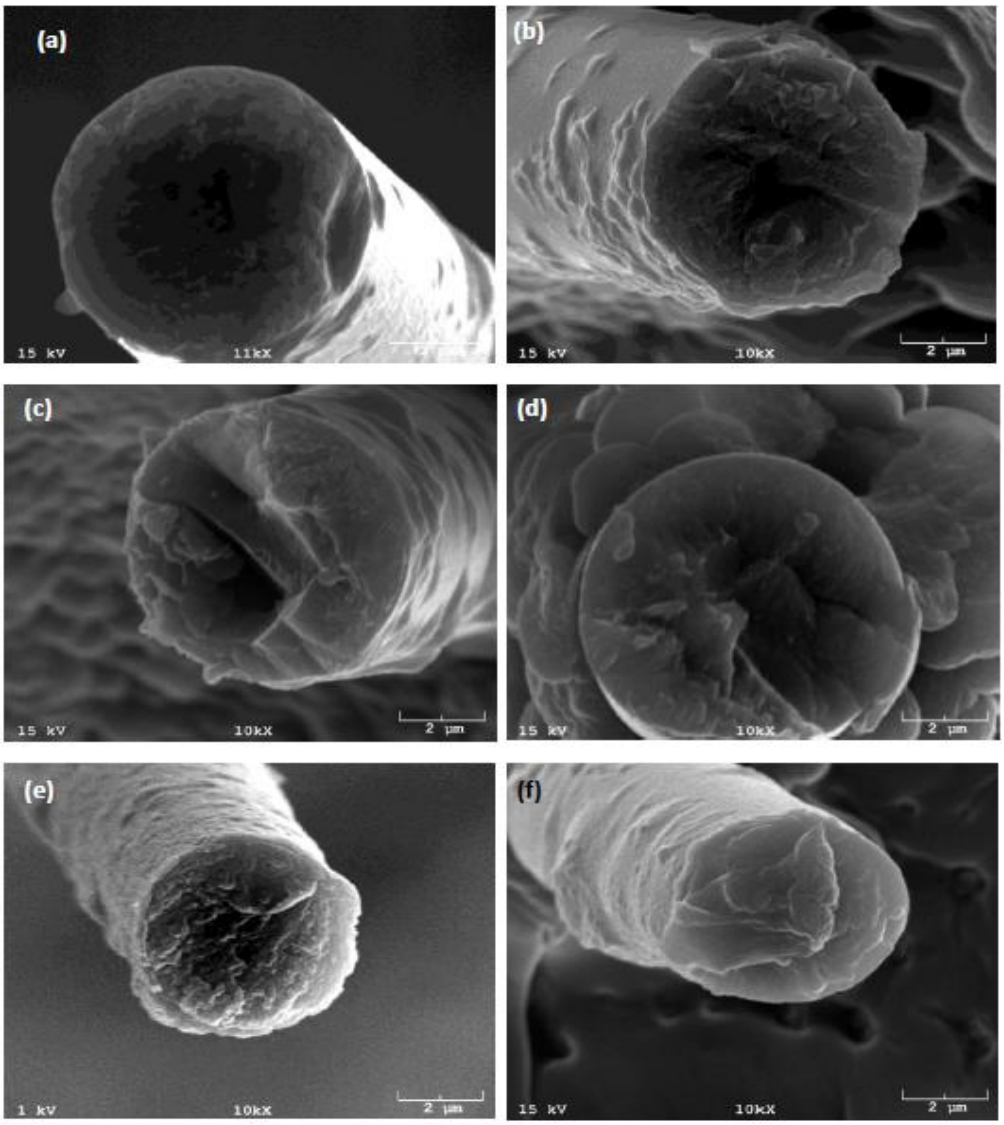

Figure 3.13. SEM micrographs of the tensile fractured surfaces showing the transverse cross section structure of (a) AS4_UnS, (b) AS4_S, (c) AS7_UnS, (d) AS7_S, (e) IM10_UnS, and (f) IM10_S

3.3.2 Weibull Analysis of the Tensile Strength for Sizing Effect

The results shown with 95% confidence interval error bar in Figure 3.11 clearly indicate that there is an appreciable scattering of tensile strength in all of the fiber types tested. It is well known that the variation of the strength of carbon fibers can be characterized by its distribution. From the pool of experimental data from carbon fiber tensile tests, there is an indication that if the volume of the entire sample is the same, the strength distributions of the carbon fibers can be fitted with a two-parameter Weibull distribution function, as discussed earlier.

The Weibull parameters for sized and unsized fibers (done with the commercial software Weibull++7) are displayed in Table 3.2, and the plots are shown in Figure 3.14. The differences in Weibull modulus can be attributed to the distribution and nature of the flaws, which are present in individual fibers, since the Weibull modulus is regarded as a defect frequency distribution indicator. The Weibull modulus of AS7_S and IM10_S fibers is higher than their respective unsized type. This suggests that the flaws are evenly distributed throughout the fiber, and hence there was a little scatter in the strength of sized fibers compared to the unsized counterparts. Low values of *m* indicate that defects are less evenly distributed, causing greater scatter in strength as noticed in the unsized fibers. As expected, as a result of the increased likelihood of flaws in the unsized fibers, the characteristic strength was found to be lower as compared to the sized fibers.

However, the Weibull modulus for AS4_S and AS4_UnS are almost the same. This can further explain the issue discussed in section 3.3 related to the surface defect created in the interlaced regions, and also the microstructural disclination.

Table 3.2. Weibull parameters for the unsized and sized fibers

Fiber type	Description	Weibull modulus, m	Characteristic strength, σ_o (GPa)
AS4	AS4_S	5.9513	4.7123
	AS4_UnS	5.9519	4.3580
AS7	AS7_S	5.4368	5.3535
	AS7_UnS	5.3899	4.5607
IM10	IM10_S	5.8360	6.2493
	IM10_UnS	5.3503	5.9576

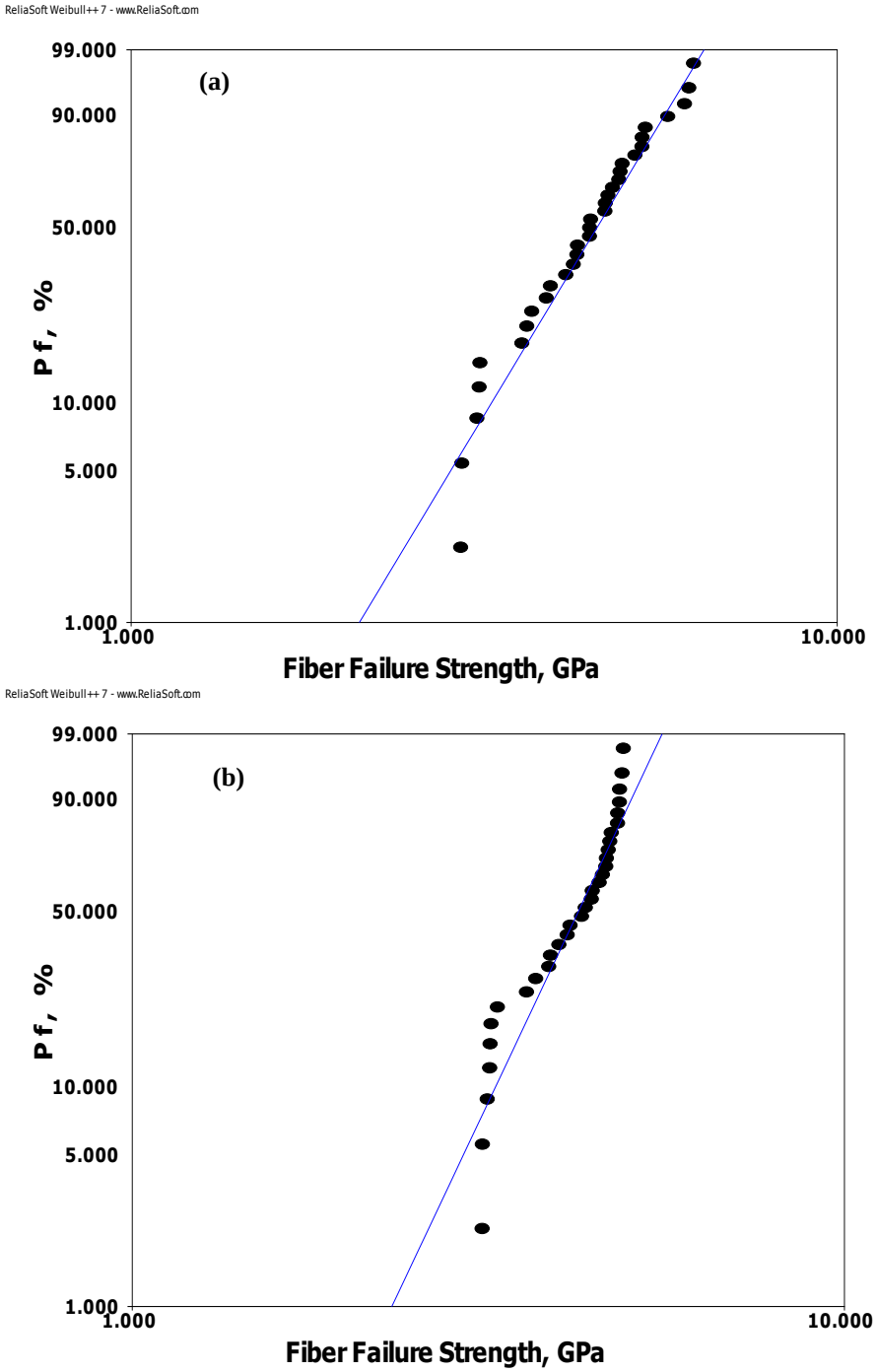

Figure 3.14. Weibull plots for the sized and unsized CFs: (a) AS4_S, (b) AS4_UnS, (c) AS7_S, (d) AS7_UnS, (e) IM10_S and (f) IM10_UnS

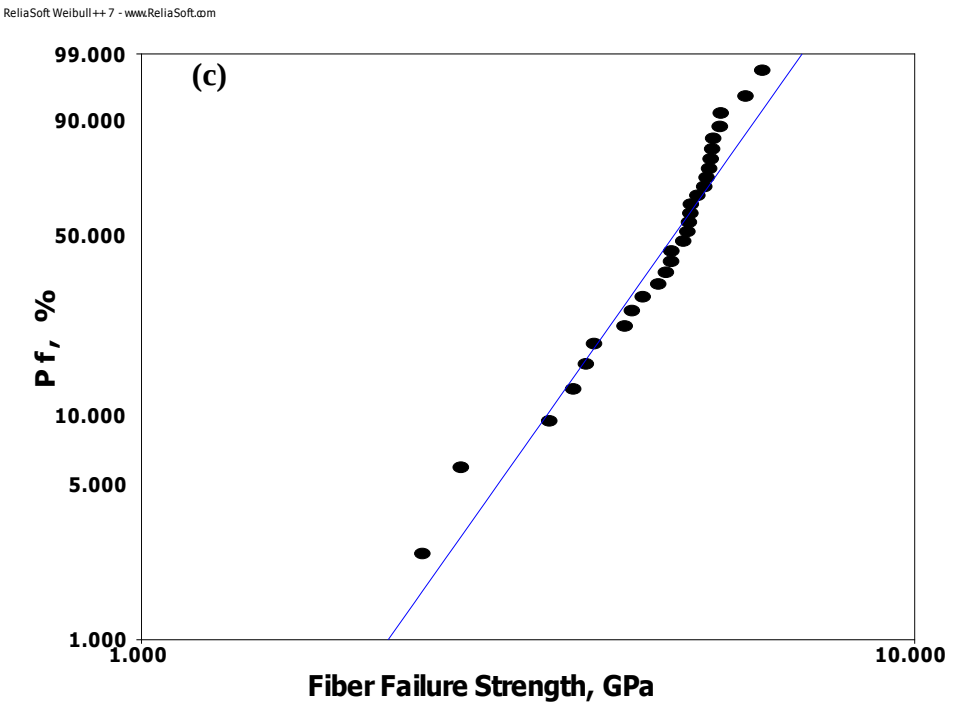

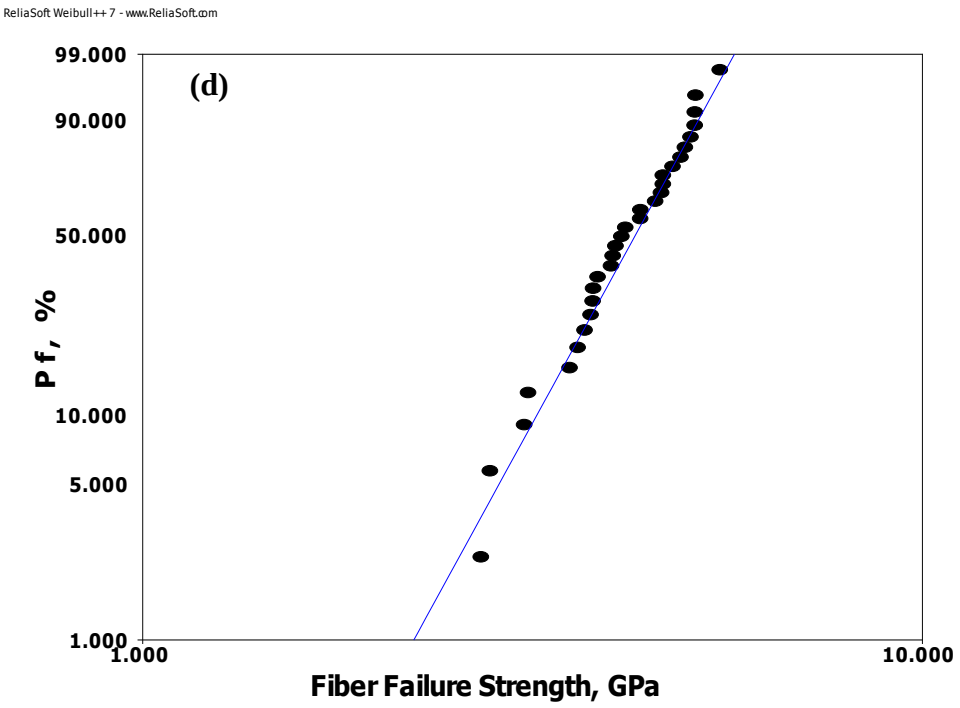

Figure 3.14.*(Continues)* Weibull plots for the sized and unsized CFs: (a) AS4_S, (b) AS4_UnS, (c) AS7_S, (d) AS7_UnS, (e) IM10_S and (f) IM10_UnS

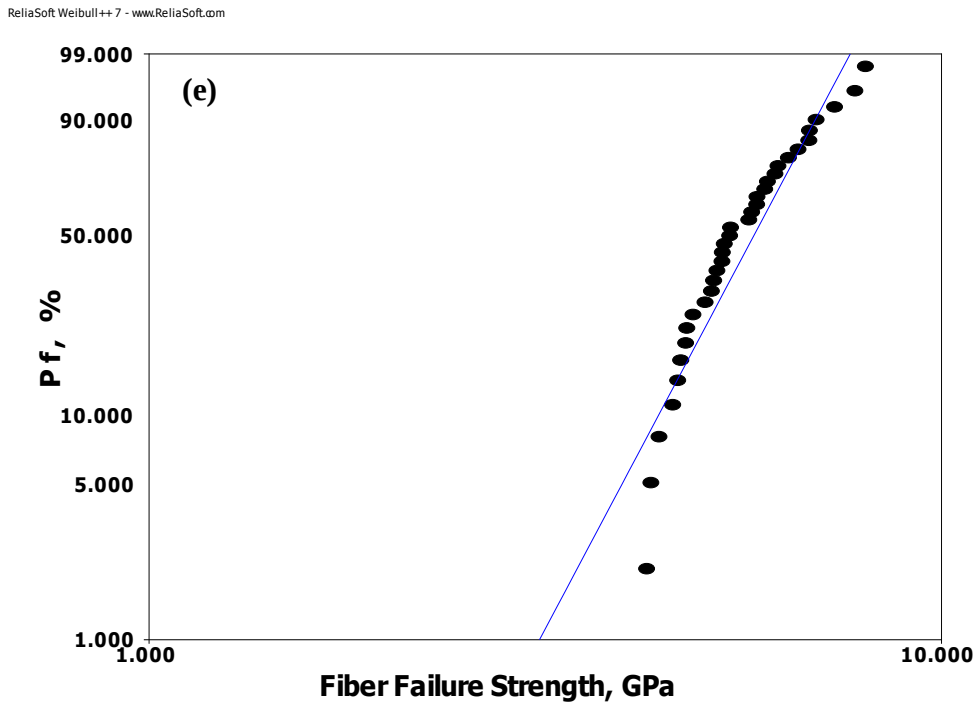

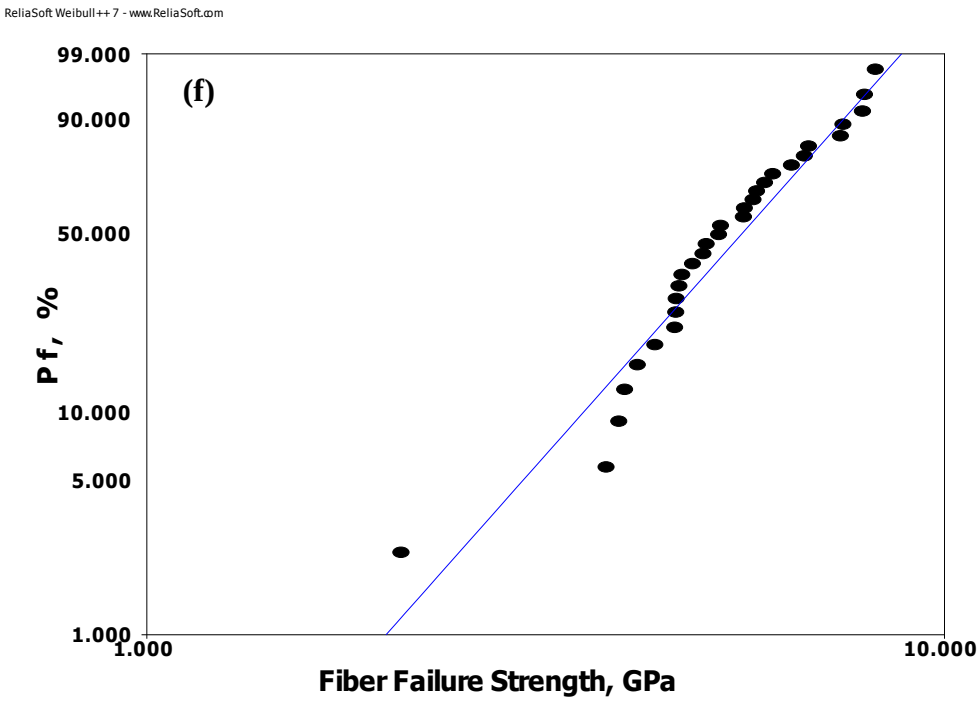

Figure 3.14.*(Continues)* Weibull plots for the sized and unsized CFs: (a) AS4_S, (b) AS4_UnS, (c) AS7_S, (d) AS7_UnS, (e) IM10_S and (f) IM10_UnS

3.3.3 Conclusions on the Effect of Sizing on the Tensile Properties

A surface topographic study done with the use of an atomic force microscope showed that the sized fibers possessed higher surface roughness because of epoxy-based sizing on the fiber. An increase in the surface roughness might help in improving the fiber-matrix interfacial properties in a fiber-reinforced composite. The striations on the unsized fibers, as shown in their respective SEM micrographs, are more pronounced than the ones observed on the sized fibers.The outputs of this work also showed that the tensile properties of PAN-based carbon fibers were, indeed, affected by sizing. There was an indication of a tensile strength increase of about 7%, 12%, and 7% in AS4_S, AS7_S, and IM10_S, respectively when compared to their unsized fiber type. This improvement was due to the chemo-mechanical bond between the fiber-sizing interface, which helped to reduce the fiber surface flaws. Regardless of fiber type, the Weibull modulus decreased with an increase in the characteristic strength for the sized fibers. This suggests that there is a small surface defect population on the sized fibers, compared to their unsized counterparts. For both unsized and sized fibers, the stress was almost linearly proportional to the strain until fiber failure.

Examination of the fiber toughness indicated that sized fibers were tougher than the unsized fibers in all of the fiber types considered. The fracture surface morphology also revealed that the unsized fibers possessed more smoothly fractured planes, which indicated that the fibers failed without any resistance. It was also demonstrated for the first time the use of a highly precise dynamic mechanical analyzer for the tensile test of single carbon fibers.

3.4 Effect of Thermal Treatment and Hold-Time

In order to investigate if the curling nature of the fiber tow inside the TGA pan can actually cause any positive or negative improvement of the fiber tensile properties, the fiber tows from the same batch were prepared in two different methods. The first set was prepared by curling the tow inside the TGA ceramic pan, and the second set by keeping the tow from the same batch straight on the Whipmix Pro-100 porcelain.The same TGA temperature profile was followed to desize the fibers as described in section 2.1.3. Only AS4_S was desized in this way at 435^{o}C for 20min (AS4_D-M2). Single fibers were separated from the tow and mounted on the picture frame for tensile testing. Figure 3.15 shows the tensile test results of the two methods. There is a negligible 0.96% difference in the tensile strength values between the two methods. From the result of this validation, it can be inferred that the tensile properties of AS4 fiber do not depend on whether the fiber is curled or kept straight while desizing. As a result, all the samples considered for the thermal treatment effect on the tensile properties of each fiber type were prepared by curling the fibers using the TGA pan and the results are presented here.

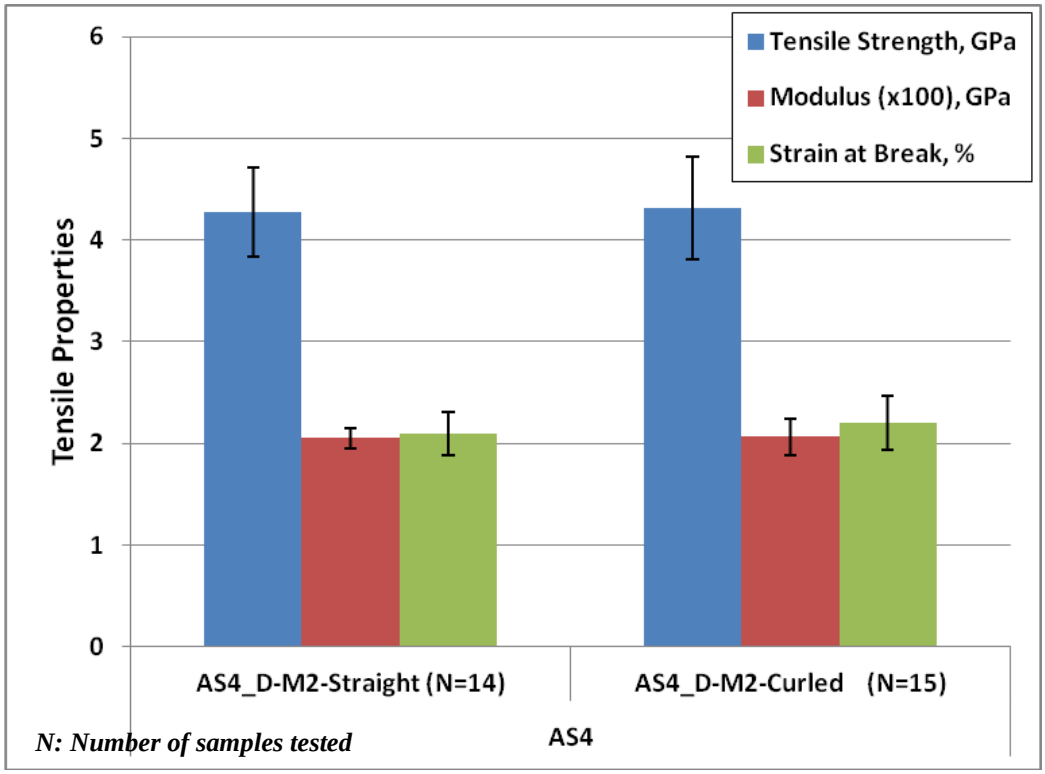

Figure 3.15. Tensile properties of curled and straight AS4 fiber

Similar trends of linear stress-strain relation until failure was also observed in this study, as observed and reported in the previous section. The average tensile strength, modulus, and failure strain are shown in Figure 3.16. The results show that the average tensile strength for AS4_D-M1, AS4_D-M2, and AS4_D-M3 is 4.65 ± 0.43 GPa, 4.40 ± 0.32 GPa, and 4.40 ± 0.36 GPa, respectively. The average tensile strength recorded for AS7_D-M1, AS7_D-M2, and AS7_D-M3 is 5.01 ± 0.38, 4.88 ± 0.30, and 4.64 ± 0.41, respectively. Finally, IM10_D-M1, IM10_D-M2, and IM10_D-M3 have an average tensile strength of 6.36 ± 0.49, 6.14 ± 0.43, and 5.69 ± 0.49, respectively.

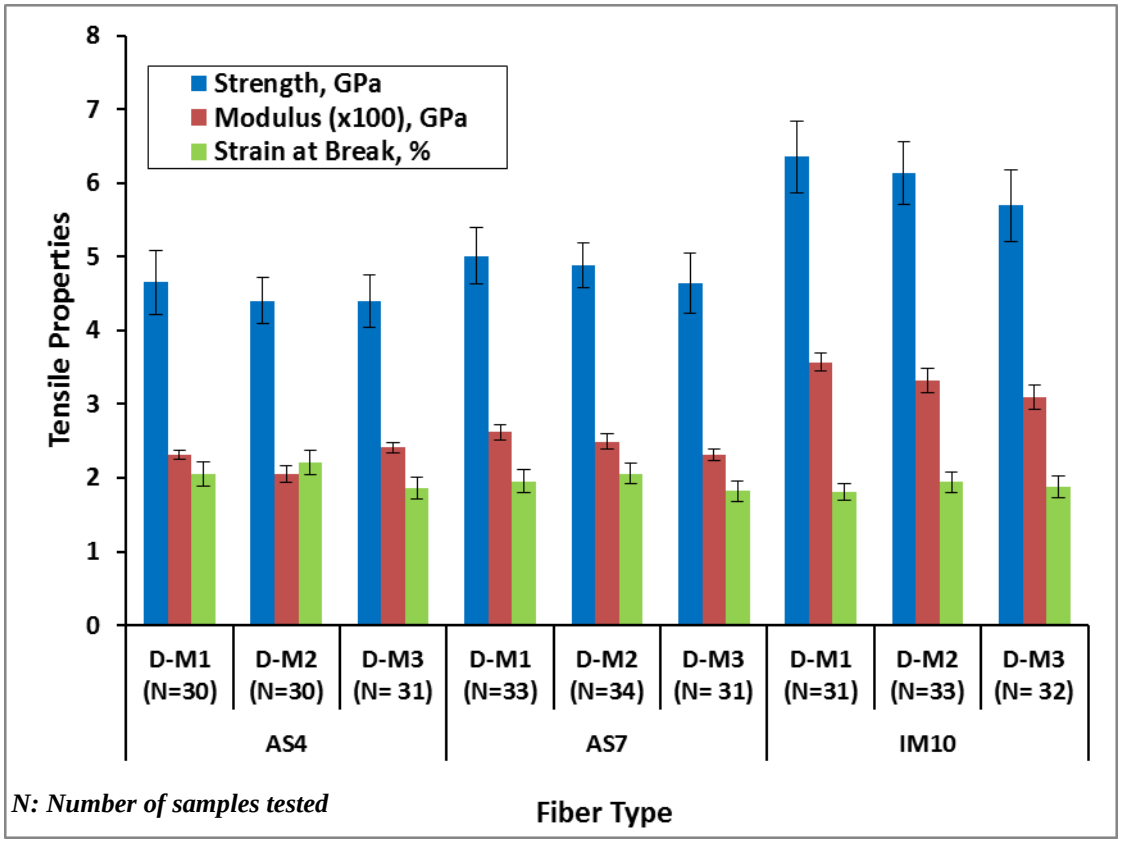

Figure 3.16. Tensile properties of the desized fibers

As shown, there is an approximately 5.6% drop in the strength of AS4 carbon fibers after being held for 20 minutes when compared to AS4_D-M1, and a reduction of 5.8% was observed when the fiber was held for 60 minutes at 435^{o}C when compared to AS4_D-M1. A different trend was noticed in their tensile modulus values. AS4_D-M2 has a reduction of about 12% in the tensile modulus when compared to AS4_D-M1; however, the modulus increased again by 4% when the fiber was held for 60 minutes at 435^{o}C, in comparison with AS4_D-M1. This unusual behavior might be a result of the fibers' architectural layout for AS4_S fiber, since AS4_S was obtained in the fabric form and others in the roving form. However, the failure strain of AS4 carbon fiber decreased accordingly. Moreover, there was a noticeable reduction in AS7 carbon fiber tensile

strength from 3% to about 8% when AS7_D-M2 was compared with AS7_D-M1, and AS7_D-M3 with AS7_D-M1, respectively. The same trend was also observed in their tensile modulus (from a 5% to 13% reduction). Similarly, by comparing the tensile strength value of IM10_D-M1 and IM10_D-M2, there was roughly a 4% reduction, and a higher reduction of about 12% was noticed when IM10_D-M3 was compared to IM10_D-M1. There was a significant reduction in the tensile modulus of IM10 carbon fiber from 7% to 15% when IM10_D-M2 was compared to IM10_D-M1 and IM10_D-M3 with IM10_D-M1, respectively. However, the failure strain of these fibers, irrespective of fiber type and desizing procedure, has a negligible 0.1% reduction when D-M2 is compared to D-M1 and D-M3 is compared to D-M1.

A further study on the fiber tensile toughness gives specific details in these reductions and changes, as shown in Figure 3.17. The toughness was determined by integrating the area underneath the stress-strain curve for individual fiber, and the average value was evaluated for at least thirty of the samples considered for the quasi-static uniaxial tensile tests [161]. The toughness values for AS4_D-M1 and AS4_D-M2 are relatively close to the toughness value of AS4_S fiber before the burn-off. AS4_D-M3 gave approximately a 14% drop in the toughness value when compared to others. Similar trends were found in the AS7 fibers, as toughness values for AS7_D-M1 and AS7_D-M2 samples are relatively close to the value obtained for AS7_S. The toughness value for AS7_D-M3 was about 10% lower, compared to others. Different toughness behavior was found in IM10_D-M1 and IM10_D-M2, as their values are lower than the values obtained for IM10_S for almost 9%. IM10_D-M3 still gave the lowest toughness value (about 6% less tough than IM10_D-M1 or IM10_D-M2). The same trends were

also noticed in their tensile strength percentage change. From this deduction, it seems the sizing on the fiber treated for 60 minutes at 435°C (D-M3) was completely removed from all the fibers considered for this work. The surface morphologies on each group can give more details on this inference.

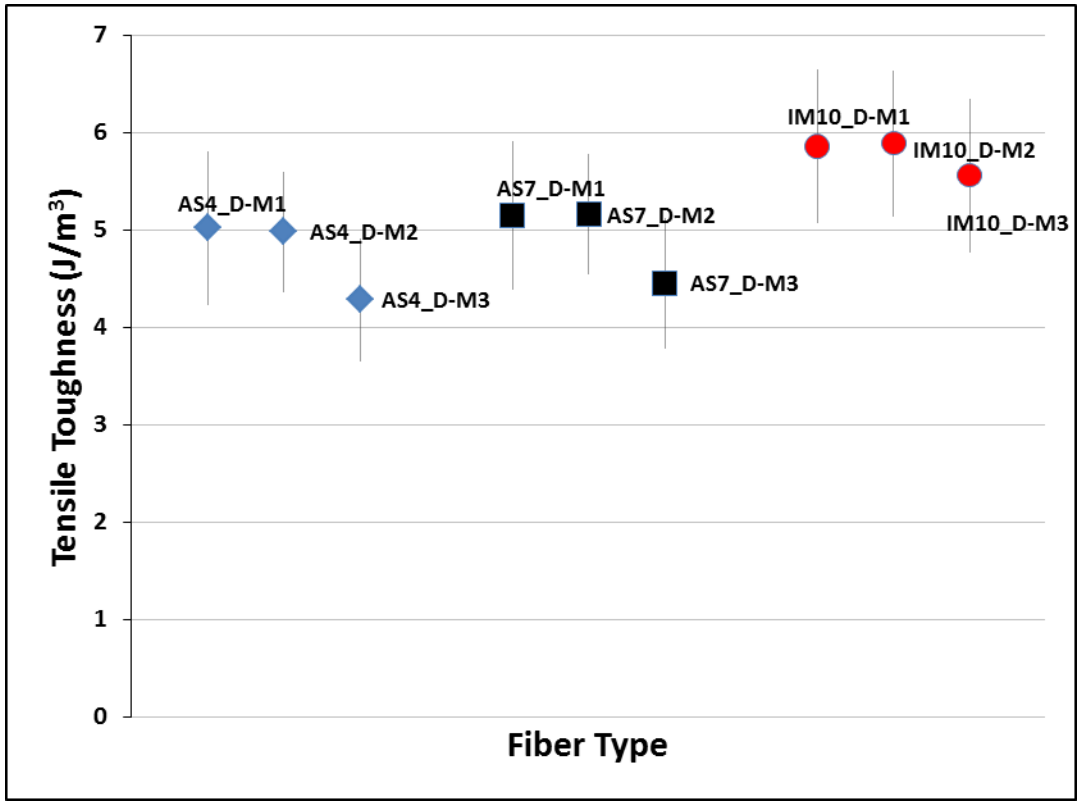

Figure 3.17. Tensile toughness of the desized fibers

3.4.1 Electron Microscopy of the Fracture Surfaces of the Desized Fibers

The SEM micrographs of the desized fiber fractured surfaces, which have been carefully selected from a very large number of micrographs, are shown in Figure 3.18. They represent the most frequently occurring fracture types as observed in the case of a single carbon fiber. Transverse cross-sectional views of the fractured surfaces for D-M1, D-M2, and D-M3 fiber samples were taken. There are no noticeable fracture initiation

points in the fractographic images for the desized fibers without hold-time (Figure 3.18A(i, ii, iii)). The fracture initiation site is obscured in all three types of the fiber desized without any hold-time, which is an indication of the presence of crystallites with increasing shapes and with well-pronounced orientation in the fiber axis direction [162].

As shown in Figure 3.18 A (iii), there is an indication of the internal pullout of the fiber micro-particles when the fiber is subjected to a tensile load. The fractured surface roughness and poorly defined granular textures are well pronounced in D-M1 and D-M2 fiber samples. The effect of heat treatment is noticed on the fiber microstructure as displayed in Figure 3.18 (B and C). The fiber microparticles seem to coagulate more in Figure 3.18 C (iii). Note that there is an obvious fracture mirror and mist hackle presence in the images taken from the D-M3 samples. Considering the location of fracture mirror, it can be inferred that the fracture originated from the fiber skin surface in D-M3 samples [163].

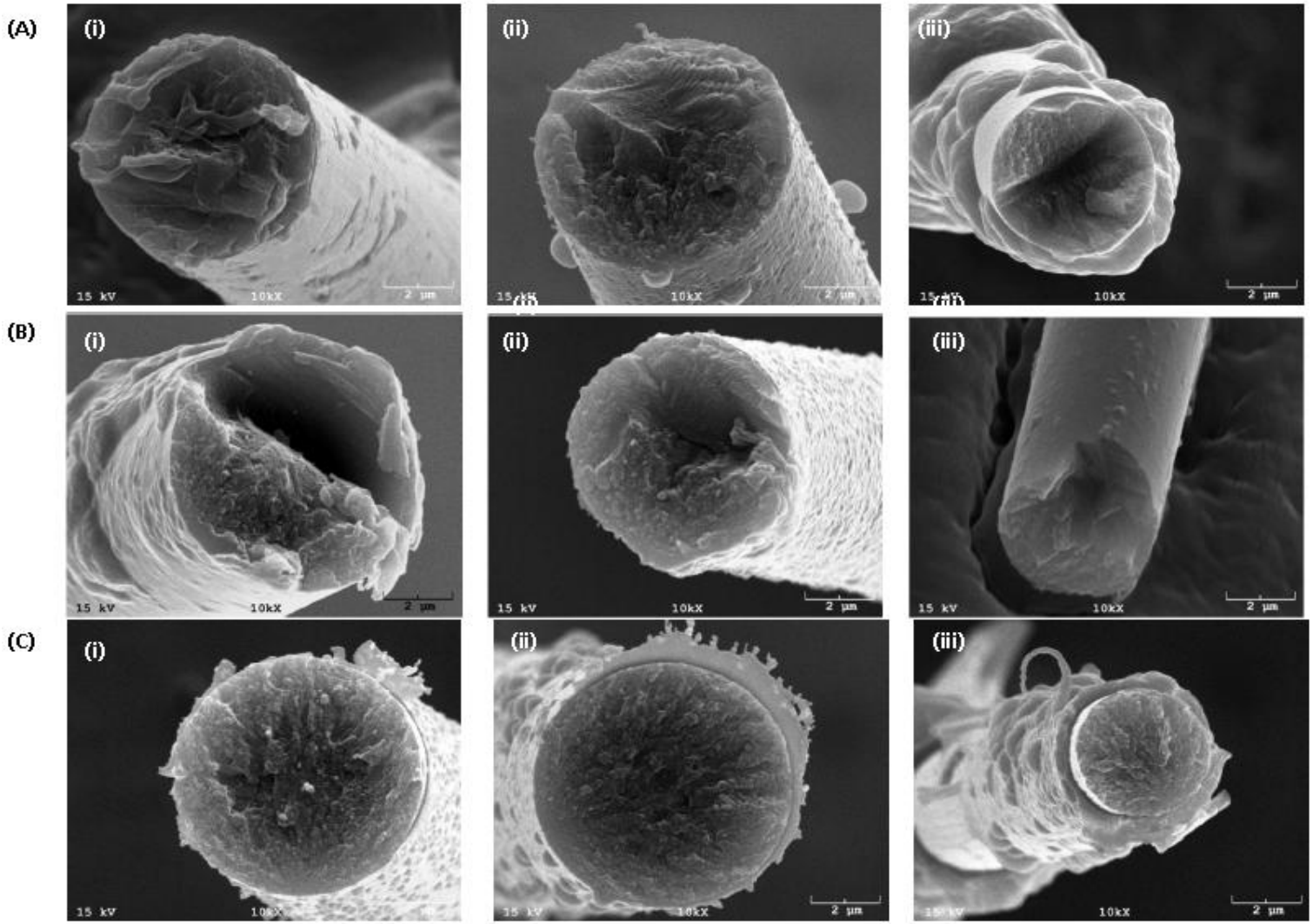

Figure 3.18. SEM micrographs of the tensile fractured surfaces showing the transverse cross section structure of: (A) D-M1 (B) D-M2, and (C) D-M3 [(i) AS4 fiber; (ii) AS7 fiber, and (iii) IM10 fiber]

3.4.2 Weibull Analysis of the Tensile Strength for the Thermal Treatment Effect

In order to reduce the potential variability in the tensile strengths arising from the irregularities on the fiber diameter, desized fibers from the same tow were carefully selected, with the aid of an optical microscope, for testing.However, after a close examination of the tensile strength results, there was a scattering in the values. Therefore, a two-parameter Weibull model, as described previously, was used to evaluate the strength distribution.

Figure 3.19 shows the Weibull plots of strength for D-M1, D-M2, and D-M3 samples. It is noted that IM10 carbon fibers possessed the highest characteristic strength, as expected, followed by AS7 and then AS4,as shown in the figure. There was a consistent decrease in the characteristic strength for AS7 and IM10 fibers, as shown in Table 3.3. A similar trend was not found in AS4 fibers, which might be a result of the fiber architecture. The Weibull modulus seems to remain higher on D-M2 samples in all the fiber types. There is a high tendency, as mentioned earlier and shown in Figure 2.7 (i,ii,iii), that the fibers desized at 435^{o}C without hold-time could still have some traces of sizing on their surface after the heat treatment, which could have contributed to a higher tensile strength. It is noted that the epoxy coating, such as sizing, covered the fiber surface cracks, and this positively increased the crack tip radius which contributed to the reduction of stress concentration in the defect areas. The effective crack length will be reduced, thus leading to reduction of fiber surface flaws, and indirectly increase the fiber tensile strength [158,159,164].

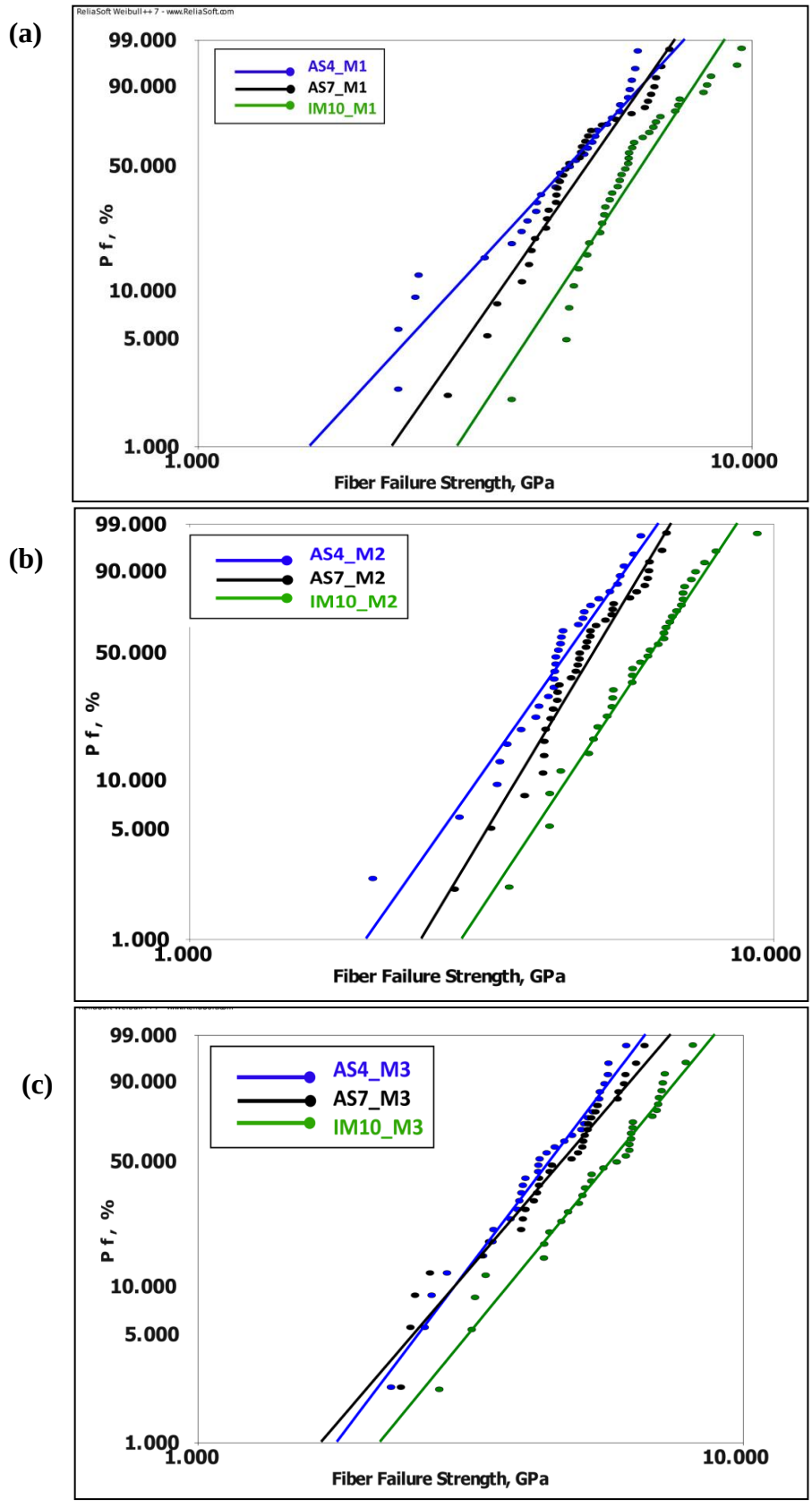

Figure 3.19. Weibull plots (a) D-M1 [no hold-time) (b) D-M2 [20 min hold-time], and (c) D-M3 [60 min hold-time]

Table 3.3. Weibull parameters for the desized fibers

Fiber type	Description	Designation	Weibull modulus, *m*	Characteristic strength, σ_o (GPa)
AS4	AS4_D-M1	AS4_M1	3.93	5.15
	AS4_D-M2	AS4_M2	5.32	4.78
	AS4_D-M3	AS4_M3	4.70	4.80
AS7	AS7_D-M1	AS7_M1	5.20	5.44
	AS7_D-M2	AS7_M2	6.22	5.24
	AS7_D-M3	AS7_M3	4.15	5.12
IM10	IM10_D-M1	IM10_M1	5.51	6.80
	IM10_D-M2	IM10_M2	5.64	6.63
	IM10_D-M3	IM10_M3	4.33	6.26

3.4.3 Conclusions on the Thermal Treatment Effect

Based on the tensile test results, it could be said that the tensile strength of carbon fiber depends on the desizing hold-time. The fibers desized at 435^{o}C for 60 minutes hold-time exhibited a higher reduction in their tensile properties. It is worth mentioning that the fiber architecture also plays a major role in the tensile properties of fibers, especially at the micro level. As observed in the current presentation, the tensile modulus values for the fibers obtained from a continuous roving are relatively consistent compared to the weave fabric AS4 carbon fibers.

Further investigations into fiber toughness clearly showed that heat treating the fiber for 60 minutes at 435^{o}C reduced the fiber toughness, irrespective of the fiber type. Moreover, there was a little drop in the fiber toughness between the fiber desized at 435^{o}C without any hold-time and the fiber desized for 20 minutes at the same set point. This might be an indication that the sizing was not removed completely when held for 20 minutes at 435^{o}C, and that the remaining sizing contents on the fiber after 20 minutes heat treatment time is close to the one desized without hold-time, as shown clearly in the

micrographs taken with an ultra-high resolution SEM. Examination of the fiber fractured surfaces across the transverse section indicated that after the fiber went through the 60 minutes hold-time, their microstructures became more coagulated. This negatively increased the effective crack lengths along the fiber length and, thus, increased the stress concentration at the crack tips.

3.5 Effect of POSS Coating on the Tensile Properties

The fiber used for the POSS coating are the CVD-thermally treated fibers as explained in section 2.2.1. Figure3.20 shows the typical stress-strain curves as obtained from the tested fibers. As shown, the as-received fiber (T650-AR) and CVD-thermaly treated (T650-TT) fibers demonstrated a very brittle failure and a linear stress-strain relation was observed. Tensile strength for each fiber was taken as the maximum stress that the fiber was able to withstand before the catastrophic failure from where the failure strain was also obtained. The least-square method was used to calculate the fiber stiffness from the stress-strain curve of each sample. The failure strain, tensile strength and the modulus of the T650-AR samples was higher than the T650-TT samples due to the thermal degradation effect on the latter.

The overall tensile properties of T650-AR fiber reduced dramatically after the thermal treatment as shown in Figure 3.21. A reduction of ~50% and ~32% in the tensile strength and failure strain in this sample was recorded respectively as a result of the thermal degradation effect on the fiber.

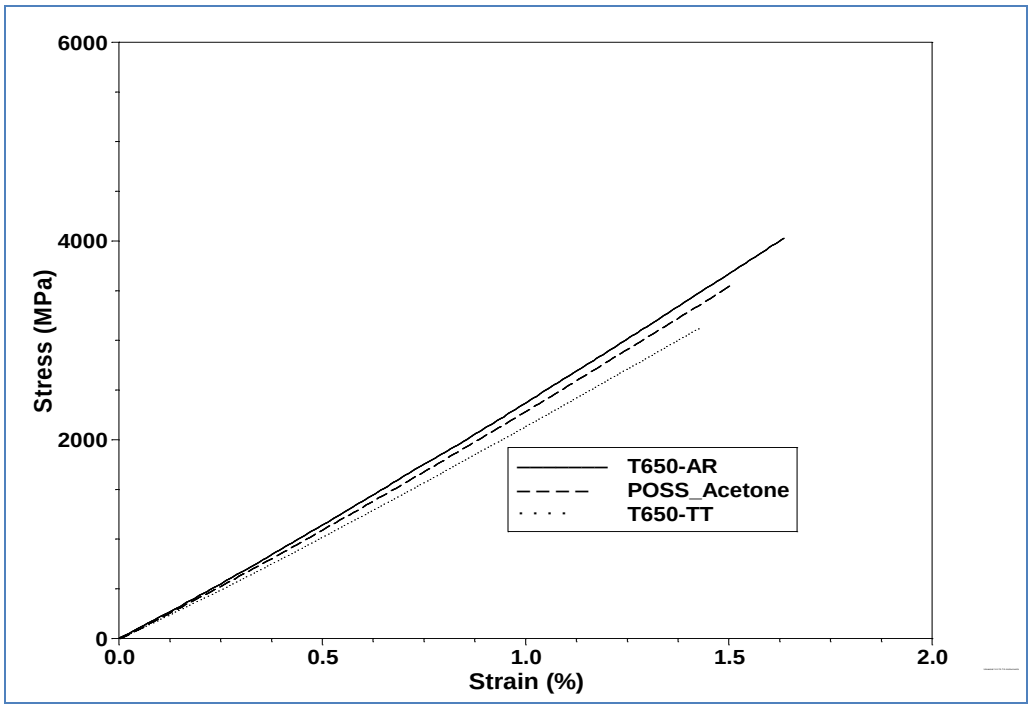

Figure 3.20. Typical stress-strain curves for the treated fibers

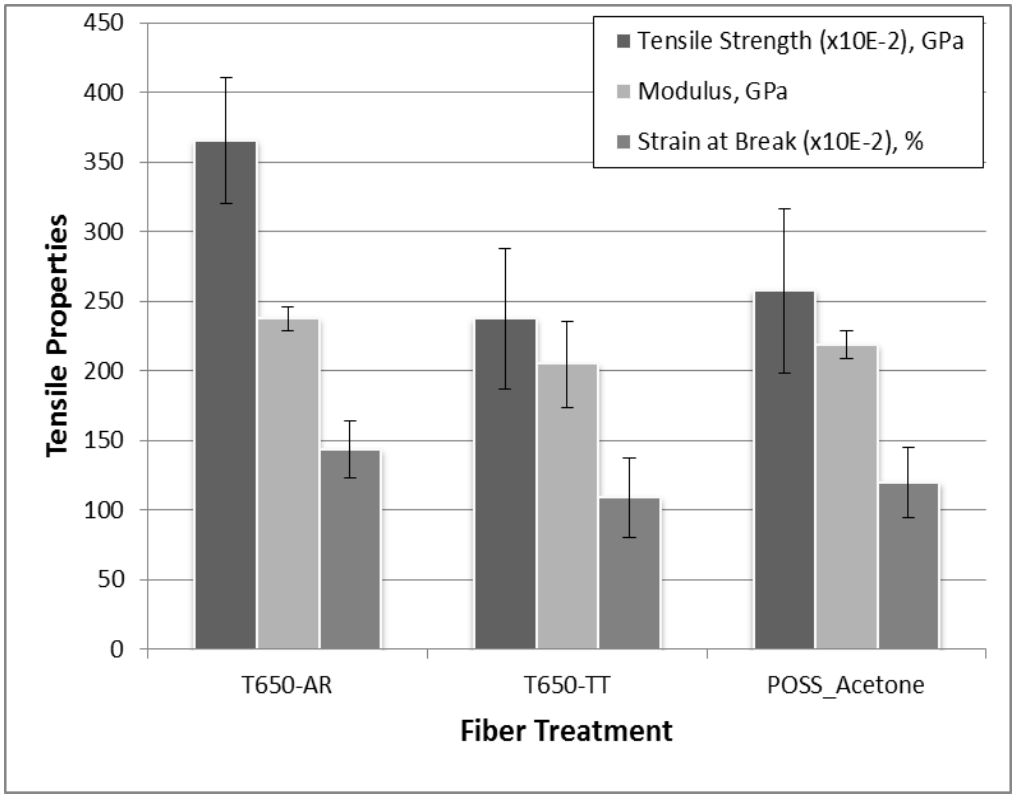

Figure 3.21. Tensile properties of surface modified fibers

The POSS coated fiber also failed in a very brittle manner. POSS_Acetone has a higher tensile properties as compared to T650-TT but lower properties when compared to the T650-AR samples. Figure 3.21 also shows the effect of the POSS grafting on the tensile properties of the T650-TT samples using the acetone dissolving solvent. When the T650-TT was coated with the POSS particles there was an improvement in the tensile strength and strain in the amount of 8% and 10%, respectively. This might be associated with the improved adherence of POSS to the surface of the thermally treated fiber which helped to block most part of the flaws on the fiber surface. There was still an appreciable degradation in the tensile strength, modulus and strain at failure of the POSS_Acetone samples in the amount of 42%, 8% and 19%, respectively when compared to T650-AR samples.

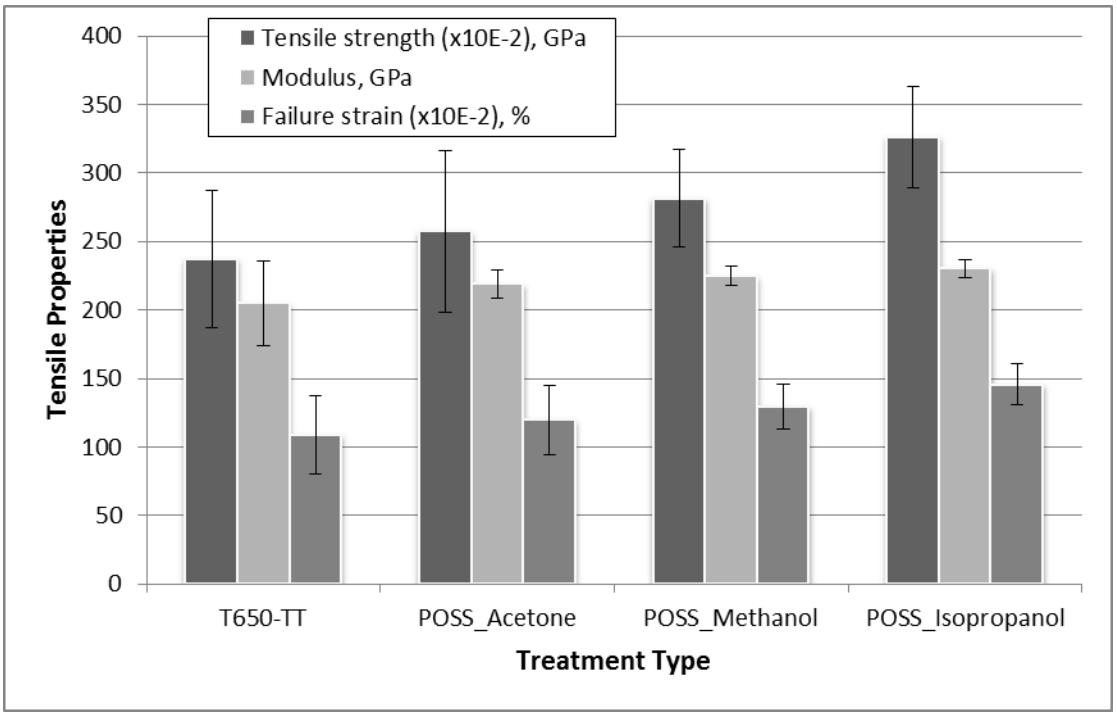

Figure 3.22. Tensile properties of POSS coated fibers using a different dispersion solvent

Figure 3.22 also shows the histogram plots for the tensile properties of the POSS coated fibers using the three types of solvent. As shown, the tensile strength, modulus and failure strain for POSS_Acetone samples improved by 8%, 7% and 10%, respectively when compared to T650-TT samples. When methanol was used (POSS_Methanol), higher improvement in the tensile strength, modulus and the failure strain was observed in the amount of 19%, 10% and 18%, respectively when compared to T650-TT samples. The highest improvement in these properties was observed when the T650-TT samples were coated using the solution of POSS_Isopropanol in the amount of 38%, 12% and 34%, respectively when compared to T650-TT tensile properties. As explained earlier that was due to the rate of evaporation of the respective solvent [133].

3.6 Effect of CNTs and POSS-CNTs Coating

Single fibers were separated from as-grown CNT grafted fabric using the previously mentioned approach. With all of the necessary measures taken to make sure that the variations in CNTs coverage between filaments, which were positioned near the outer surface of the fiber bundle, and filaments, which were positioned near the middle,were eliminated, there was an indication that the growth of the nanotubes in the middle of the fiber bundle was not as densely populated as the ones on the outer surface. As a result, single fibers were carefully separated from the outer layer of the bundle (as much as possible).

CNTs grafted on the T650-AR samples did not seem to improve its tensile properties as shown in Figure 3.23 probably because during the CVD’s calcination and reduction processes the iron particles was converted to its alloy forms and there might be a reaction between the decomposed sizing and these oxides on the fiber surface. This

process would cause further stickling of the interlaced regions of filament-to-filament and this would contribute to some part of the filament to be left empty without CNTs growth during the filament separation and mounting on the frame as elaborated in Figure 3.24. The tensile strength and the failure strain for the CNTB1 sample reduced by 16% and 13% respectively when compared to the T650-AR properties.

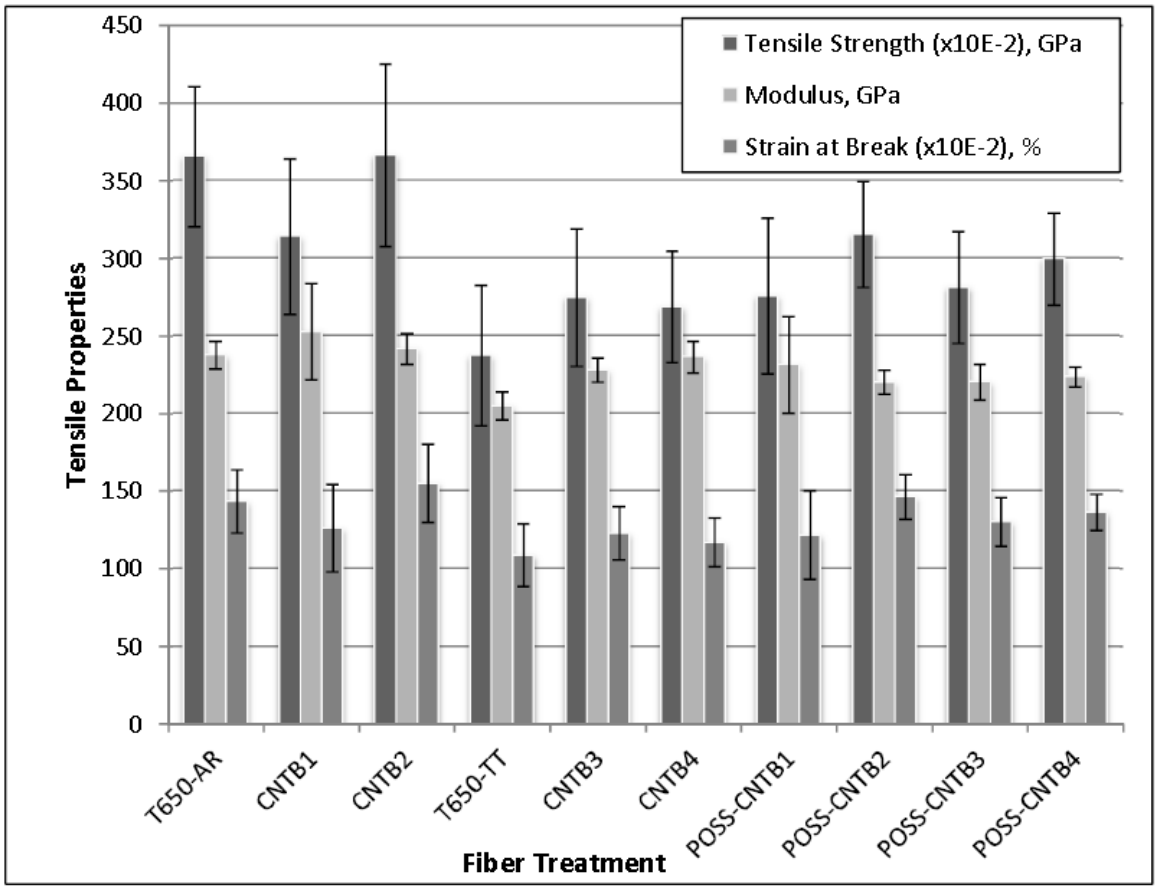

Figure 3.23. Overall tensile properties of untreated and treated fibers

There was a remarkable improvement in the tensile properties of the thermally treated fibers grafted with CNTs as shown in Figure 3.23. This significant change in the tensile properties could be explained in two ways: (1) the thermal treatment on the as-received fabric would create a gap between the filaments due to the removal of the sizing.

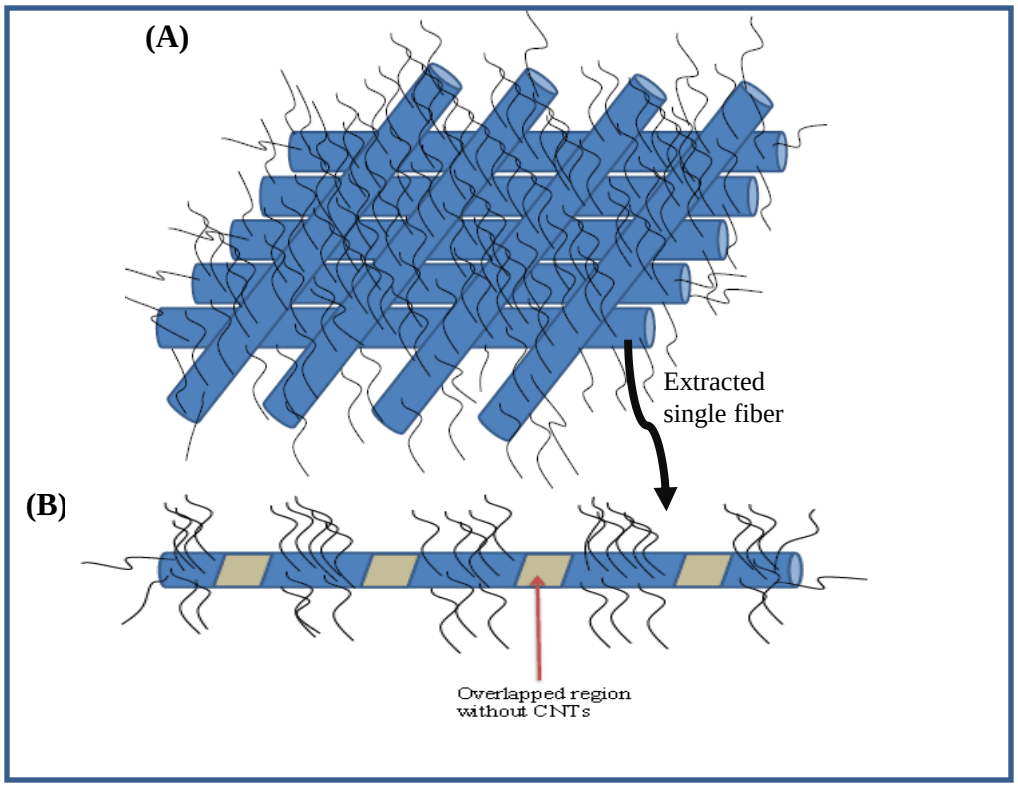

Figure 3.24. CNTs grafted carbon fabric: (A) as-grown CNTs on the fabric, and (B) extracted single filament from (A)

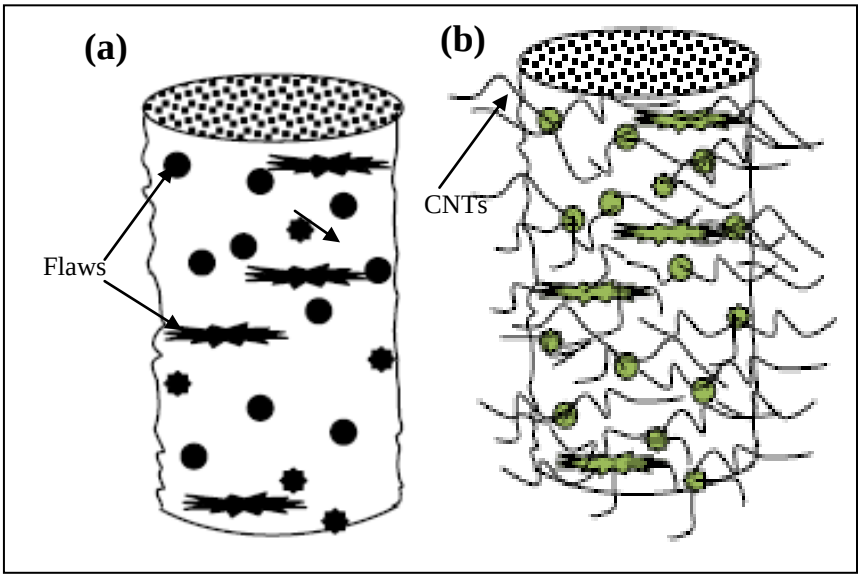

Figure 3.25. Hole-filling mechanism of CNTs: (a) thermally treated filament with many surface defects, and (b) CNTs grafted mostly on the defect sites of the filament

The gap would allow the catalyst to be deposited more uniformly all around the filament and as a result there would be complete 3-D CNTs growth on each filament, and (2) the hole-filling phenomenon might also play a critical role in this improvement. As the catalyst particles would be able to adhere and stay in the well-pronounced surface defects created on the T650-TT samples. This would lead to more CNTs growth in these areas compared to other areas on the fiber surface as also illustrated in Figure 3.25. The blockage created as a result of the nanotubes attachment to the defect sites would, in certain extent, help to prolong filament failure.

There was an indication of higher properties improvement in both CNTB1 and CNTB2 as compared to CNTB3 and CNTB4 due to the extensive thermal treatment of T650-TT used for CNTB3 and CNTB4 fabrication. The effect of POSS on the tensile properties of the CNTs grafted samples, as shown in Figure 3.23, was not well noticed probably due to the population density of CNTs on the respective fiber types.

3.6.1 Weibull Analysis of the Tensile Strength for the POSS Coating Effect

The lowest characteristic strength value was found in POSS-CNTB1, although its Weibull modulus value was higher. It should be noted that a higher Weibull shape parameter only indicated that the scatter degree of fiber tensile strength decreased as a result of coating. The Weibull modulus does not seem to follow similar characteristics as shown in the previous sections, probably because of the surface treatment. The grafting reactions introduced some defects on the fiber surface, although the fiber characteristic strength did not have a huge difference. The results of the single fiber tensile testing imply that the POSS coating would not lead to any major decrease in the in-plane properties of the resulting reinforced composites.

Table 3.4. Weibull parameters for the treated and untreated fibers

	m	σ_o(GPa)
T650-AR	2.4248	4.1343
T650-TT	3.5020	3.0537
POSS-T650	4.6606	3.7483
CNTB1	3.8275	3.4594
CNTB2	5.2034	3.9595
CNTB3	2.7882	3.1027
CNTB4	2.2035	3.0712
POSS-CNTB1	4.4417	3.0191
POSS-CNTB2	2.0711	3.6305
POSS-CNTB3	4.1646	3.0928
POSS-CNTB4	4.4476	3.2813

3.6.2 Conclusions on the Effect of POSS Coating

Based on the results obtained from the tensile properties characterization of the surface modified fibers, the following conclusions have been deducted:

- The choice of a highly polarized solvent (solubility compatibility) also plays major roles on the overall tensile properties of the POSS coated single filaments. Isopropanol has proved to yield improved results when used to dissolve POSS instead of acetone or methanol
- CNTs grafted on the thermally treated fibers seem to improve its tensile properties by providing a kind of hole-filling phenomenon on the treated fiber surface. However, the ones grafted on the sized fibers did not yield any better improvement. Although the dip method of catalyst deposition on the fiber proved to yield better results than the spray method probably due to the amount of the catalyst that was able to stay on the fiber surface before the CVD reaction

CHAPTER 4

CHARACTERIZATION OF FIBER-MATRIX INTERFACE USING FIBER PULLOUT METHOD

4.1 Sample Preparation

4.1.1 Materials

The resin system used for the pullout experiment was Araldite LY-1556 hardened by Aradur 2964 with the mix ratio of 100:50 parts-by-weight (pbw). They were supplied by Huntsman Corporation. Aradur® 2964 epoxy curing agent is a low viscosity modified cycloaliphatic amine hardener designed for solvent-free high performance coatings, and Araldite LY-1556 is a general purpose unmodified liquid epoxy resin based on bisphenol A and epichlorohydrin. The mixed system is cured within 7hrs at 25^{o}C, and the gel time specified by the manufacturer is within 30 minutes. Instant cyanoacrylate adhesive (Loctite gel-type super glue) was also used to provide stronger bonding strength at the non-pulling end of the sample.

Carbon fibers used for this work include AS4 (sized and unsized) supplied by Hexcel Corporation and T650-35 supplied by Cytec Industries, as described in section 2.1.1.

4.1.2 Testing Frame Design

The pullout test method has some limitations associated with the scale of the test. One of these limitations includes the maximum embedded length of the fiber inside the resin, *Lmax,* permitted for pullout without being broken. *Lmax* is usually very short and this usually caused experimental difficulties and large data scatter. As a result, careful design of the test frame should be put into consideration such that the target embedded

length of the fiber is far less than the *Lmax.* The *Lmax was* initially estimated from the relationship given in Eqn (1):

$$Lmax = \frac{F_{max}}{\pi D_f \tau_{app}} \quad (1)$$

Where *Fmax* is the maximum tensile load the fiber was able to withstand before fracture (as determined from section 3.2), D_f is the fiber diameter, and τ_{app} is the expected apparent shear strength of the fiber-matrix interface (10MPa) as obtained from literature.

The optimization of this procedure has shown that *Lmax* was about 1mm and therefore the critical fiber embedded length must be far less than this. After several trials the critical embedded length was determined to be ~ 0.3mm and at this length the fiber was able to be pulled out of the resin without fracture.

Steel picture frames used for the single fiber tensile test, as explained in section 3.1.2, were used in order to maintain the sample gauge length and keep to the testing procedure. Figure 4.1 shows the schematic diagram of the frame layout used for this work. A magnetic strip 0.57mm thick and 1.5mm wide was purchased and cut into two specified lengths of 6mm and 19.04mm. The longer length was stuck to the frame at both ends, making an opened cavity, while the shorter length was used to complete the square cavity. The adhesive side of the magnetic strip made it easier to precisely maintain the square cavity. Careful placement of the strips was enforced to ensure that the embedded lengths of the fiber were kept at ~0.3mm (at the resin end) and 6mm (at the glued end). The super-glued region was made larger so as to provide higher bond strength between the fiber and the glue which would not result in the fiber pullout. Placement of the strips on the frame was done under a stereoscopic microscope for a higher precision. All the necessary measures were applied to keep the embedded areas in square forms and make

sure the strips were not covering the engraved marks on the frame made for fiber alignment (as shown in Figure 4.1). Also shown in Figure 4.1 is the gripping sections of the frame by the DMA clamps. These regions were carefully selected, ensuring that both the glue and resin embedded region were totally excluded from the gripped area. Magnetic strips also helped with frame setting on the DMA metallic clamps.

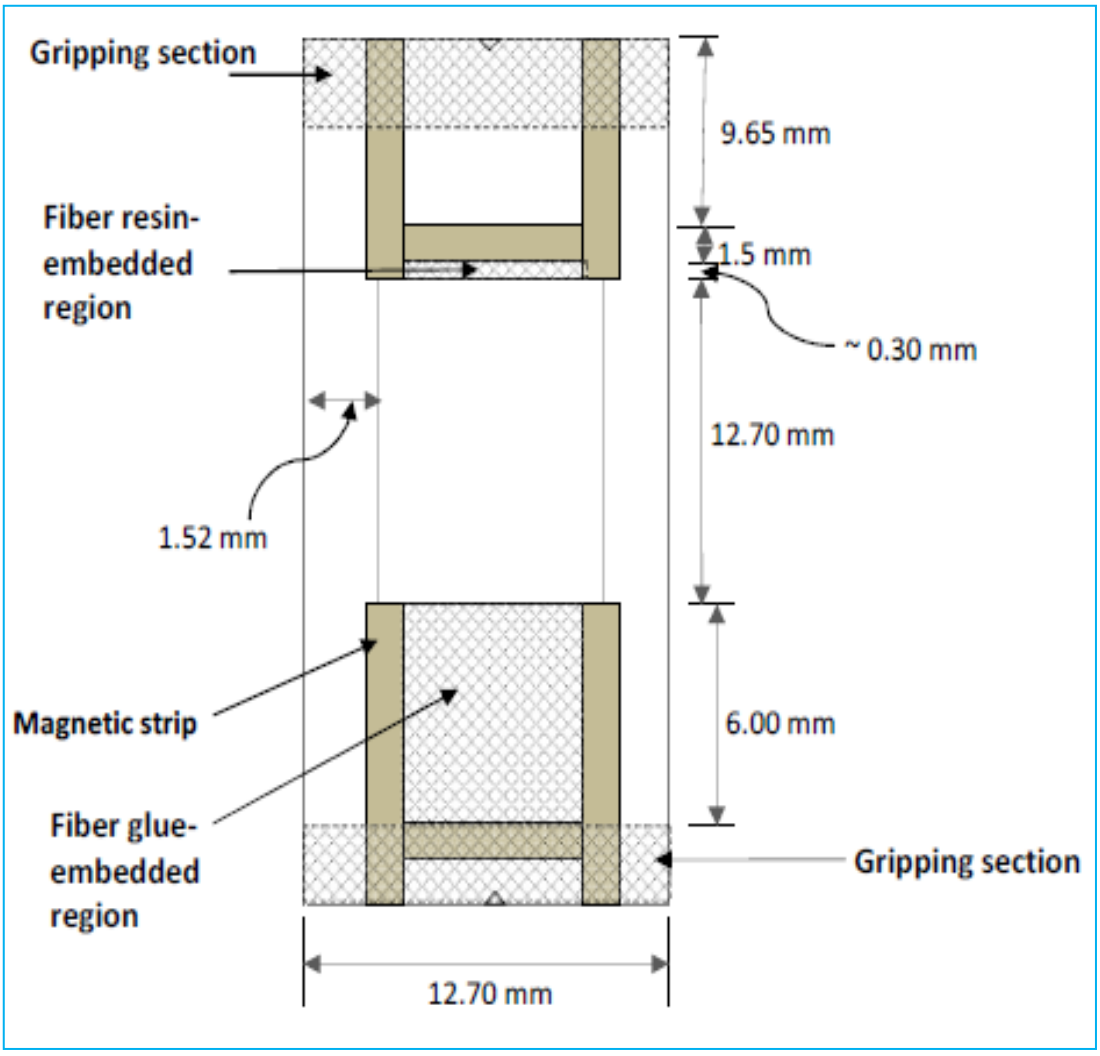

Figure 4.1. Schematic representation of the frame setup used for the pullout experiment

Any twist in the frame could also introduce an error of alignment into the test data. As a result, all the steel frames used for this work were carefully selected and washed with acetone to promote better adhesiveness of the strips. The frame width was kept at 12.70mm for easy gripping of the clamps at both ends and the frame legs was fixed at 1.52mm in order to have easy access when cutting the legs of the frames just before the test.

4.1.3 Sample Preparation Procedure

The listed careful procedures were followed for the sample preparation process: the chosen fibers were cut in ~70mm long fragments and attached to the test frame with the use of scotch tape under a stereoscopic microscope. The fibers were aligned along the frame slots. Super glue was then poured to the larger embedded end of the fiber (6mm) and the resin was applied carefully along the target embedded length (~0.3mm) by making sure that the fiber surface was well covered with the glue and the resin, respectively. The resin was applied with the aid of a narrow-shaped pipette tip. The thickness of the magnetic strip helped to leave the fiber up to a certain height (magnetic strip thickness) from the frame surface and this enabled complete coverage of the fiber by resin on all sides. The samples were left to cure at 24 ± 2^{o}C for about 48 hours to allow the resin and super glue to cure completely. After about 5 hours of the initial curing process of the resin the fiber end was cut with a razor blade along the magnetic strip (as indicated in Figure 4.2). This proceeding was necessary in order to have easy access to the fiber end. The cut was made under a light optical microscope ensuring that the cut was kept strict along the strip interface while maintaining the embedded length at about 0.3mm.

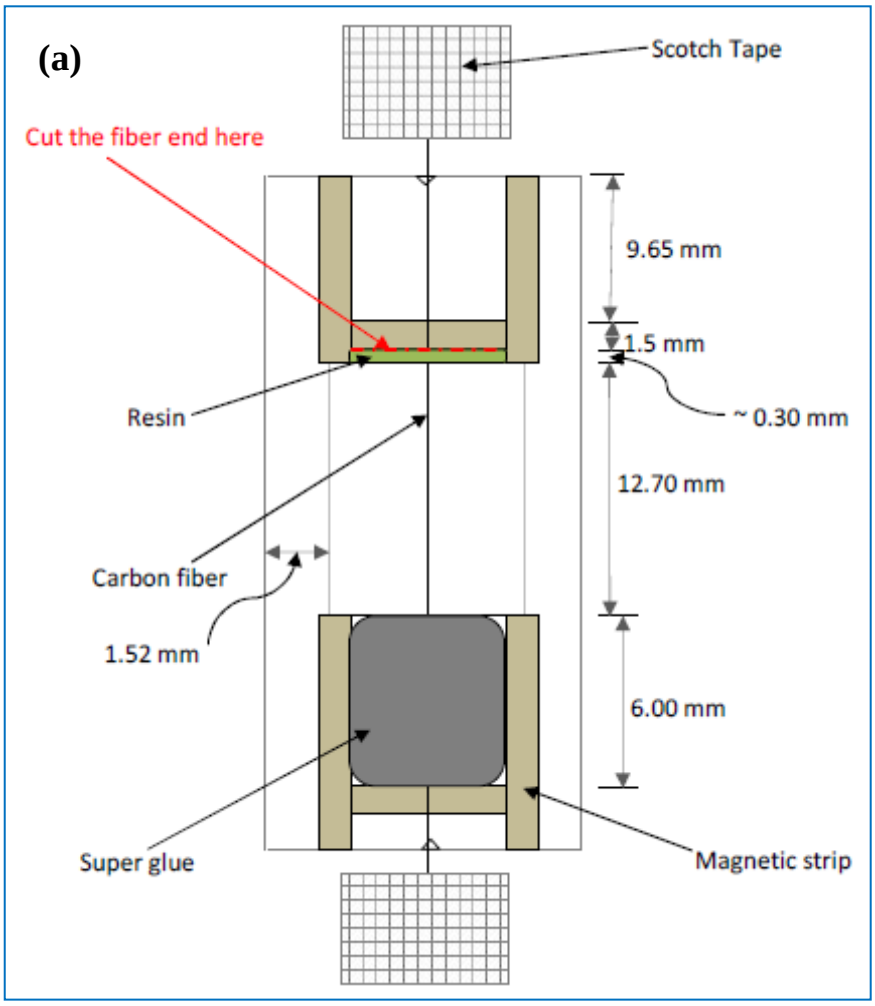

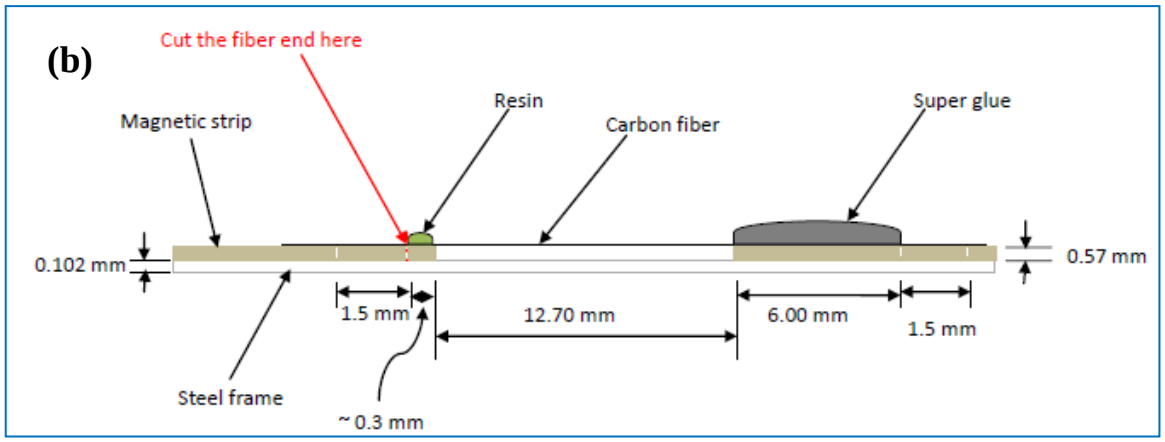

Figure 4.2. Schematic representation of the sample preparation approach used for the pullout experiment: (a) top view, and (b) side view

The main advantages of adopting this sample preparation method are that the embedded length could be controlled precisely and the resin capillary effect could be prevented by having a meniscus at the edge of the steel frame (as illustrated in Figure 4.3). Also shown in the figure is the point where the fiber end was cut with a razor blade before the test.

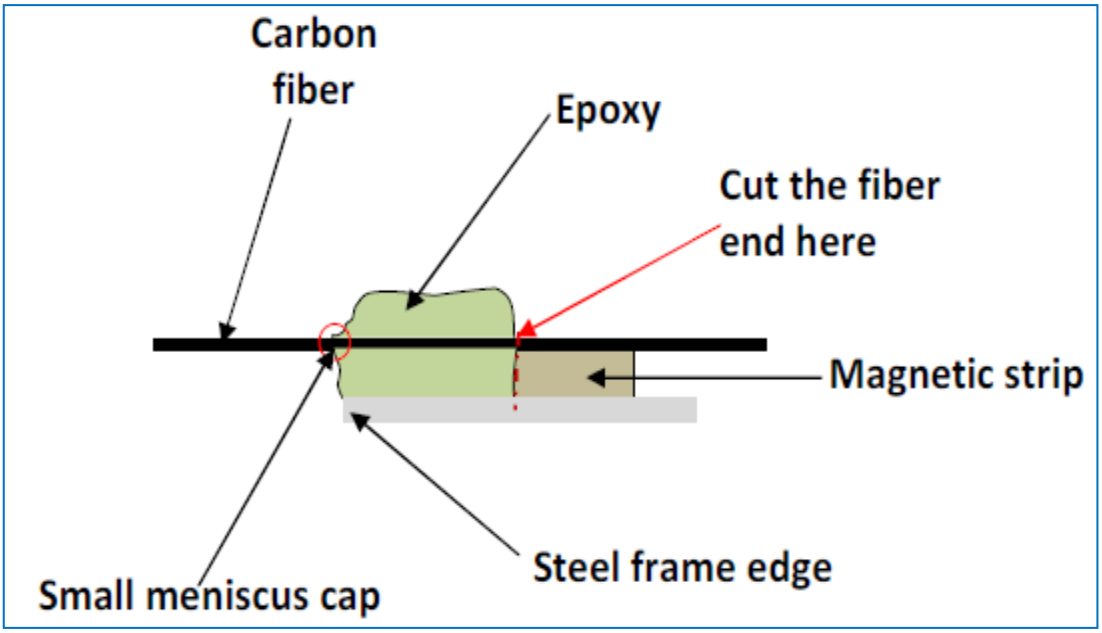

Figure 4.3. Schematic showing small meniscus cap of the resin on the fiber along the frame edge

4.1.4 Test Procedure

The prepared samples were fixed on the DMA clamps ensuring that the glued section and the resin embedded region were excluded from the gripping area and the legs of the frames were then cut with surgical scissors before the test was set to run. The specimen was subjected to tensile loading at the rate of 0.2N/min to 10N using the dynamic mechanical analyzer (DMA-Q800) and the load-displacement response was recorded, from which the peak load at pullout was obtained. The success rate of ~30%

was observed for about 50 samples considered in each case. After the test, the fiber embedded length was examined again with the aid of a scanning electron microscope (SEM-JEOL 840A) to make sure that the measured pullout length was the same as the length of the measured embedded region before the sample preparation (~0.3mm). The fiber entrance region to the resin was also examined critically to ensure that there was no form of meniscus built-up. The meniscus cap on the fiber ends has been reported to contribute a large error to the measured data [165-167]. The large amount of meniscus on the fiber can only indicate that the pullout process was not done under a pure debonding, meaning the fiber-resin interface was not completely debonded and the measured embedded length would not be correct. As a result, all the pullout fibers with a significant meniscus cap were excluded from the samples considered to evaluate the apparent interfacial strength of each sample.

4.2 Models for Evaluating the Fiber-Matrix Interfacial Shear Strength (IFSS)

The debonding and frictional shear stresses can be calculated using the relationship obtained between the pullout force and the embedded fiber length, if the distributions of the fiber stress in the embedded region are known. Unfortunately, the measurement of this distribution is normally impossible; therefore assumptions concerning the stress distribution have to be made based on theoretical analyses.

Kelly-Tyson Model: The simplest approach is to assume that the apparent shear stress, τ_a, along the entire interface is approximately constant and there is a perfect bond in the interface (107,168,169).

In this case,

$$F_{max} = \pi D_f L_e \tau_a \quad (2)$$

Where F_{max} is the maximum load, D_f is the carbon fiber diameter, and L_e is the embedded length.

Shear-Lag Model: Another approach to find the IFSS for a single fiber-matrix interface generally assumed an elastic strain distribution along the fiber in a pullout test using shear lag analysis [170] as:

$$\varepsilon_f = \varepsilon_{app} \frac{sinh\left[\frac{n(L_e - x)}{r}\right]}{sinh(ns)} \quad (3)$$

where ε_{app} is the strain in the fiber outside the matrix, ε_f the axial strain in the embedded region of the fiber at a distance 'x' from the matrix surface, r is the fiber radius, and

$$s = \frac{L_e}{r} \quad (4)$$

$$n^2 = \frac{E_m}{E_f ln(R/r)(1+\vartheta_m)} \quad (5)$$

E_m and E_f are the resin and fiber Young's modulus, respectively, ϑ_m is the Poisson's ratio of the matrix, R the effective radius of the fiber from the resin block surface.

When the stress is applied to the fiber in order to pull it out inside the resin, the fiber stress declines with distance x from the polymer surface.

The corresponding interfacial shear stress, τ, is obtained from the consideration of the equilibrium of forces exerted on a differential fiber element of length, dx:

$$\tau = E_f \frac{d\varepsilon_f}{dx} \frac{r}{2} \quad (6)$$

Differentiating Eqn (2) and substitute into Eqn (5) yields

$$\tau = \frac{n}{2} E_f \varepsilon_{app} \frac{cosh\left[\frac{n(L_e - x)}{r}\right]}{sinh(ns)} \quad (7)$$

This leads to an equation relating F_{max} to the interfacial shear strength τ_s, of the form:

$$F_{max} = \frac{2\pi r^2 \tau_s tanh(ns)}{n} \quad (8)$$

Eqn (8) can then be used to find the IFSS having obtained the maximum pullout force and the embedded fiber length experimentally.

4.3 Examining the Effect of Sizing on IFSS of AS4 PAN-Based CFs

The adhesion between sized and unsized AS4 fiber and matrix was characterized through measuring the interfacial shear strength. This was accomplished by embedding a small length of the fiber in resin as described in section 4.1.3. For this study, only single fibers were considered for examination. After the test frame was securely fixed on the DMA clamps its legs were cut and the fibers were subjected to tensile loading at 0.02N/min. Figure 4.4 shows the pullout embedded length of sized and unsized AS4 fibers and their respective glued ends as insets. The embedded length considered for this study was about 0.2mm. Also indicated in the figure is the maximum pullout force, as recorded after the test. The hole created inside the resin after the fiber pullout is also shown in Figure 4.5. A minimum of 15 samples was tested from each set of samples.

The interfacial shear strength for sized and unsized AS4 fiber were characterized with the use of both Kelly-Tyson and shear-lag models based on the aforementioned Eqn (2) and Eqn (8), respectively. The IFSS results of epoxy composites reinforced by AS4-S and AS4-UnS carbon fibers are shown in Figure 4.6.

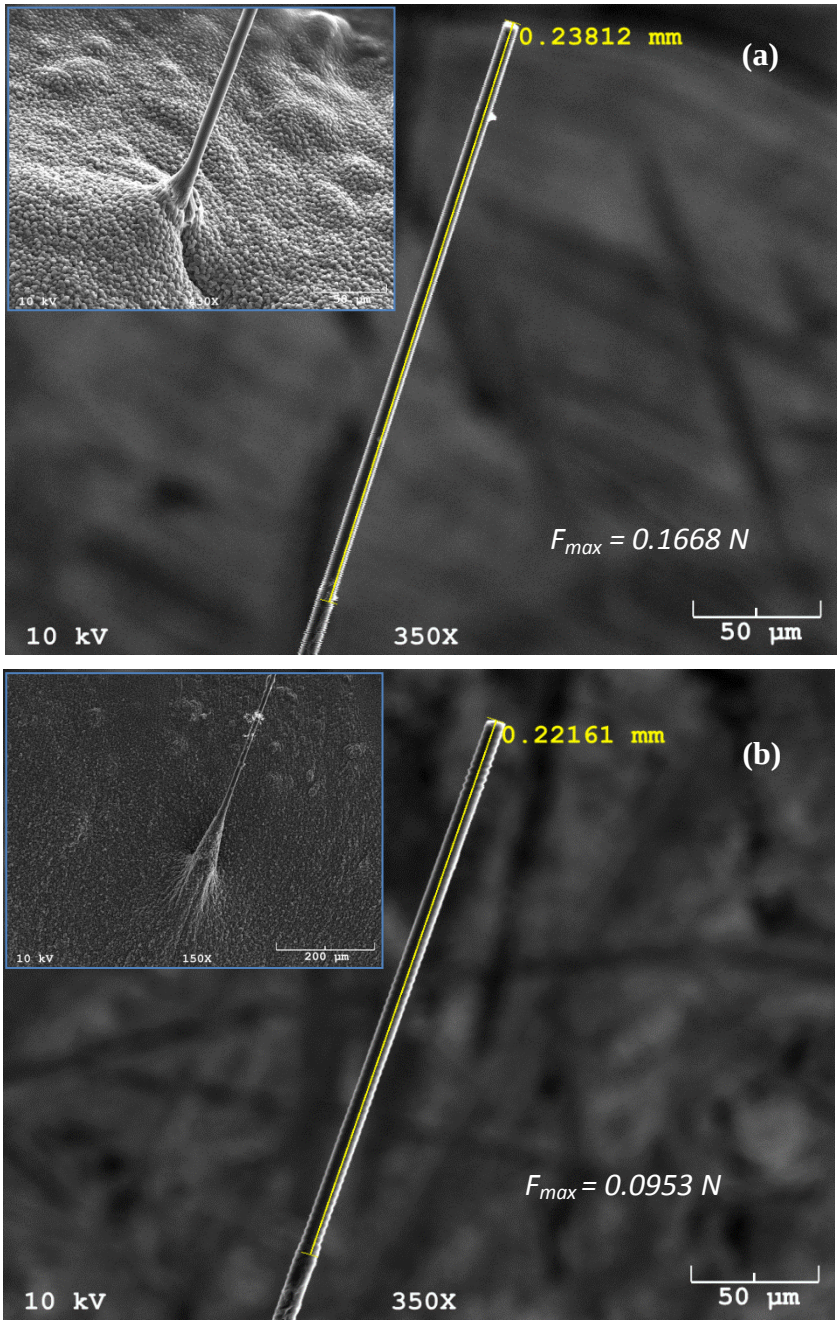

Figure 4.4. SEM micrographs of typical pullout length and glued ends (inset) for: (a) AS4-S, and (b) AS4-UnS

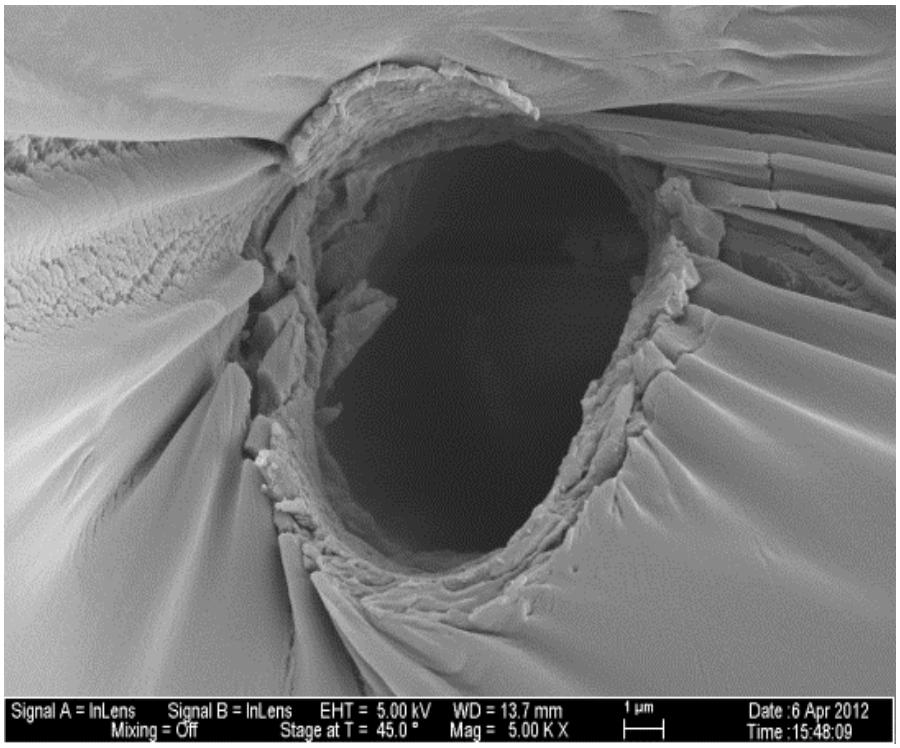

Figure 4.5. SEM micrograph of the typical pullout hole for the single fiber

The results showed that the IFSS increased from 12.43MPa for AS4-UnS fibers to 17.76MPa for the AS4-S fibers by ~ 30% using the Kelly-Tyson approach. The Shear-lag model, on the other hand, showed higher IFSS in AS4-UnS and AS4-S fibers in the values of 66MPa and 48MPa, respectively (~27% difference). The higher IFSS as observed using the shear-lag model might be as a result of over- or under-estimation of the effective resin block height as the height in each sample was differ by certain amounts. The improvement in IFSS as seen in the AS4-S sample might be attributed to the increase in the surface energy, the fiber surface structure and polarity match with the resin matrix [110].

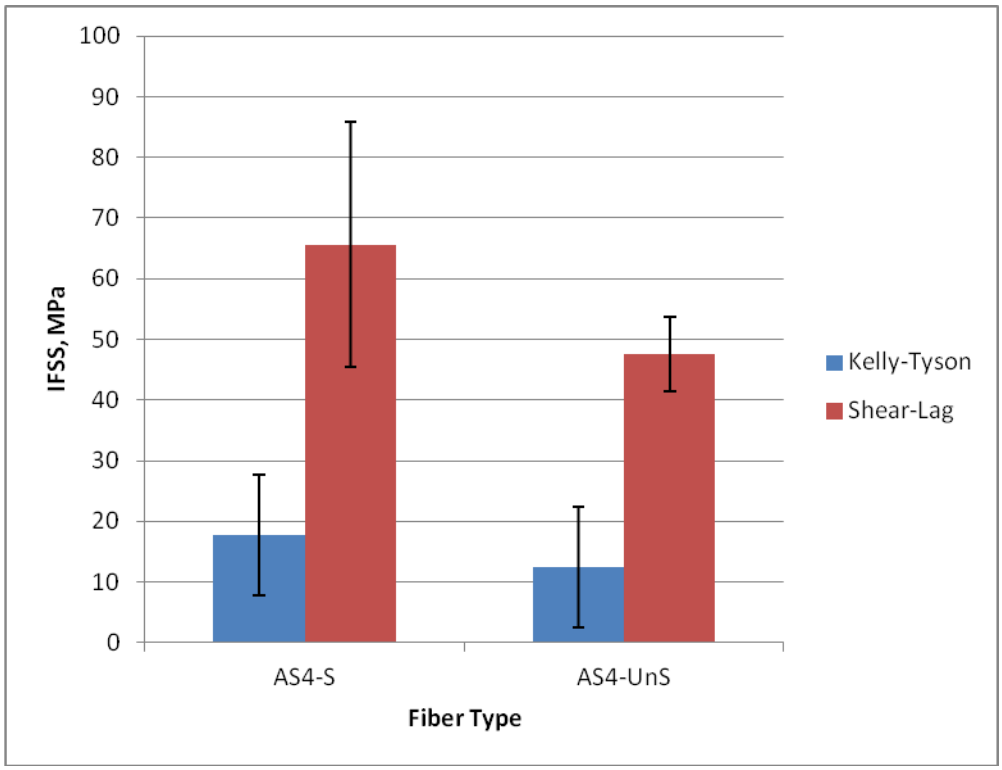

Figure 4.6. IFSS for AS4-S and AS4-UnS carbon fibers

4.4 Validation of IFSS using Fiber Bundle and Single Fiber Testing

4.4.1 Sample Preparation

Due to a lower tensile strength of the heat treated single fibers as discussed in section 3.6 when compared to the as-received fibers, it was absolutely impossible to pullout the fiber without fiber fracture. As a result, alternative method of characterizing the IFSS was considered by the use of fiber-bundle.

In order to validate the result of the pullout, both single and bundle fibers (in as-received forms) were separated from the fiber tow and mounted on the frame as discussed in section 4.1.3. Bundle fiber in this context refers to an assembly of twenty or more single fibers obtained from the same tow. Figure 4.7 shows the frame backview of the

single and bundle fiber pullout arrangement. As shown, two sets of magnetic strips were used for full support of the resin in the bundle fiber setup, unlike the single fiber setup. In this way, the resin was totally enclosed by the strips and, as a result, the fibers' surface was completely covered by the resin.

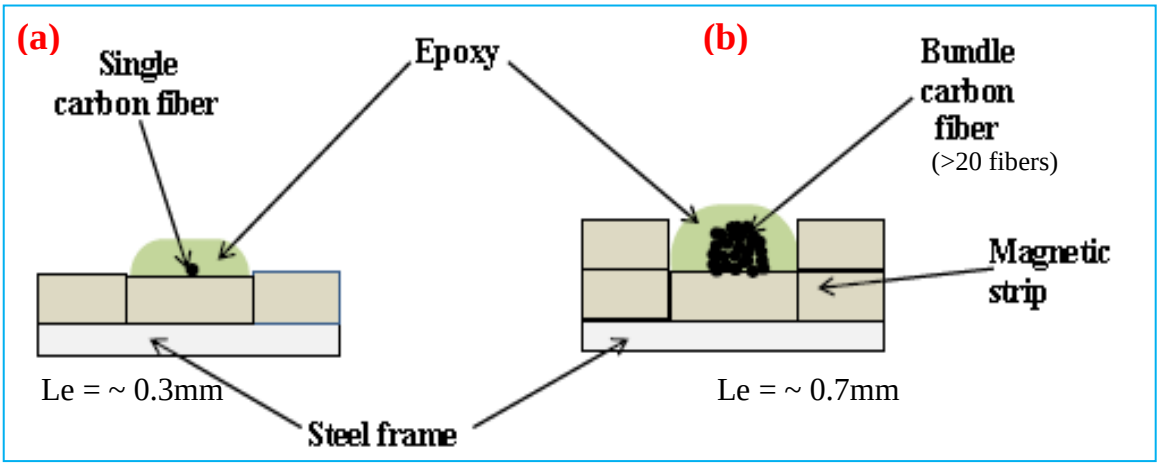

Figure 4.7. Schematic representation showing the back view arrangement of the frame setup for: (a) singe fiber composite, and (b) bundle fiber composite

In order to improve the coverage of the resin on the bundle fiber, the average embedded length considered was ~0.7mm.

4.4.2 Diameter Measurement of the Fiber Bundle

In order to estimate the value of the IFSS, there would be a need for accurate determination of the diameter of the fiber either in single or bundle form. The diameter of the single fibers was determined by the method adopted in section 3.1.2., by averaging the diameter measurements of ten sections in three regions of each fiber. However, the approach for diameter measurement of the bundle fiber is quite different from the single fiber diameter measurement. There are two different methods adopted for accurate

measurement. The first approach (Method-1) involved direct diagonal measurement through the bundle width as shown in Figure 4.8 (a). In the second approach (Method-2) the in-through diameter of the bundle was considered by averaging the diameter of the two circular rings used for fiber enclosure in the SEM micrographs as shown in Figure 4.8 (b).

Table 4.1 shows the measurement made for about ten samples using the two approaches. The standard deviation obtained from each method in each sample was less than 0.1, an indication of close agreements of the measurement between the two methods.

Table 4.1. Diameter measurement using the two methods (Units in mm)

Sample	Method-1	Method-2	Mean	Std	95% CI
1	0.0591	0.0467	0.0529	0.0088	0.0121
2	0.0567	0.0436	0.0502	0.0093	0.0128
3	0.0153	0.0132	0.0143	0.0015	0.0021
4	0.0183	0.0213	0.0198	0.0021	0.0029
5	0.1138	0.1233	0.1186	0.0067	0.0093
6	0.1166	0.0997	0.1082	0.0120	0.0166
7	0.0800	0.1057	0.0929	0.0182	0.0252
8	0.2100	0.1578	0.1839	0.0369	0.0512
9	0.2881	0.2933	0.2907	0.0037	0.0051
10	0.1445	0.1532	0.1489	0.0061	0.0085

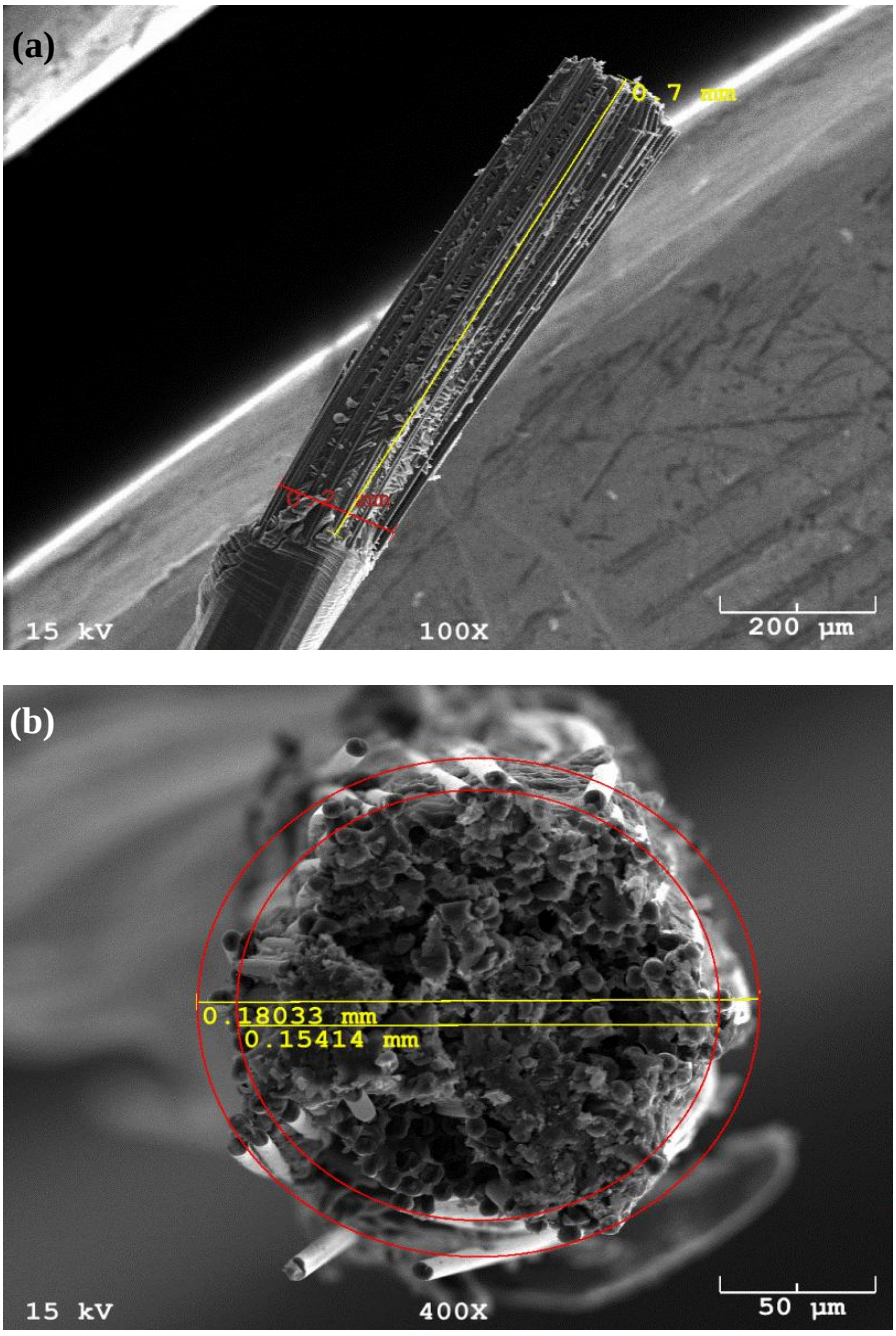

Figure 4.8. Diameter measurement using the two methods: (a) Method-1, and (b) Method-2

4.4.3 Results and Discussion

The typical pullout hole for the bundle samples is shown in Figure 4.9 (a) and the resin wall after the pullout is also shown in Figure 4.9 (b). As shown, the hole left after the pullout was not circular as expected, due to the asperities of the fiber bundles as compared to the single fibers. Close examination of the resin wall after the pullout also showed a great impression of the fiber surface striations. Due to the consistency in diameter measurement using the two methods, both methods were used to determine the diameter of each sample and the average was used for the analysis.

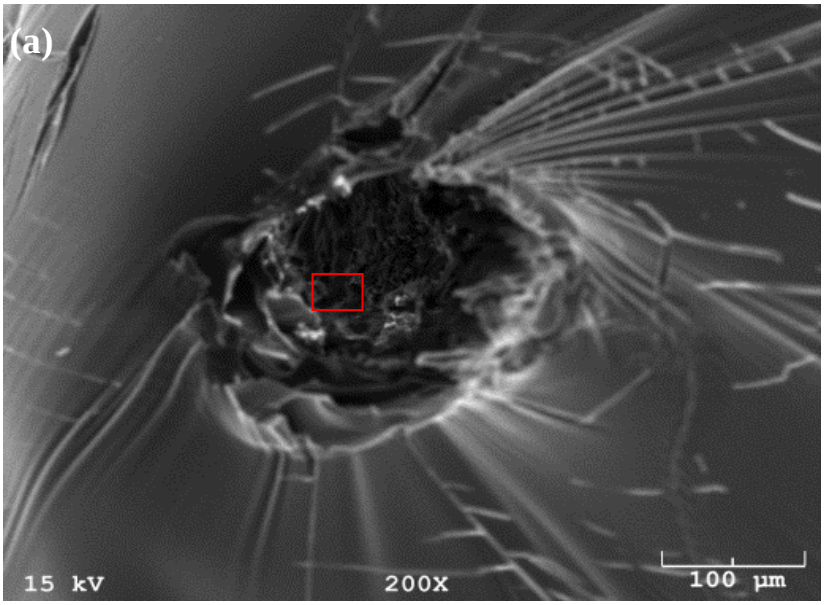

Figure 4.9. Bundle fiber pullout hole; (a) original hole, and (b) the resin wall after the pullout (higher magnification of the red rectangle)

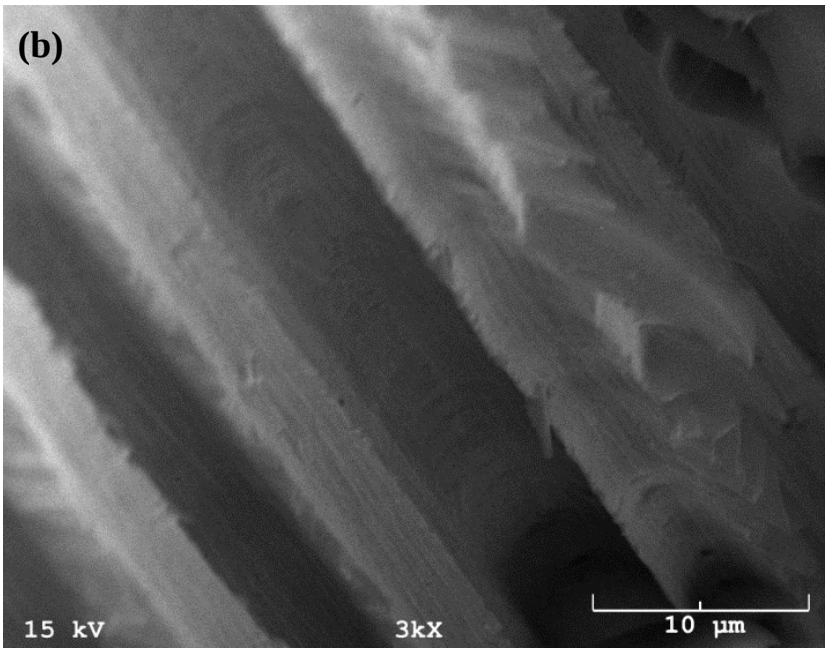

Figure 4.9. (*Continues)* Bundle fiber pullout hole; (a) original hole, and (b) the resin wall after the pullout (higher magnification of the red rectangle)

The IFSS calculated with the use of Kelly-Tyson approach for both single and bundle fibers after the pullout is shown in Figure 4.10. The results showed that the IFSS for single filaments obtained from T650-35 carbon fiber was 19.59 MPa, and for the bundle fiber it was 18.79 MPa; a difference of about 0.8 MPa was recorded. The result also showed that the debond force required in single fiber pullout was about 96% lower than that required for the bundle fibers. This might be as a result of difference in the load transfer mechanism in bundle fiber versus single fiber, since in bundle fibers if one fiber debonds from the resin the load would be transferred to another fiber within the system until all the fibers are completely debonded from the resin.

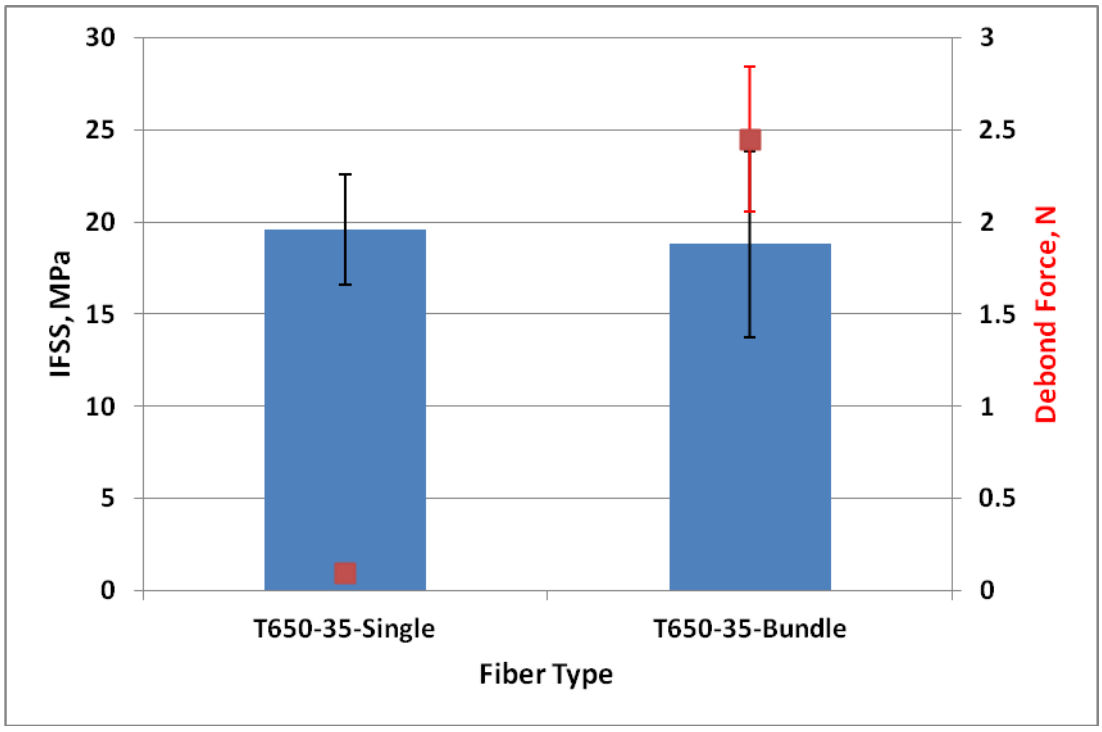

Figure 4.10. IFSS for the single and bundle fibers (T650-35 carbon fiber)

There was also a small meniscus cap observed in the bundle fibers as seen in single fibers after the pullout. This approach has successfully shown that the error introduced into the IFSS measurements as a result of the wrong measurement of the embedded length has been minimized due to the existence of a small (or no) meniscus cap, as shown in Figure 4.8(a) and Figure 4.11.

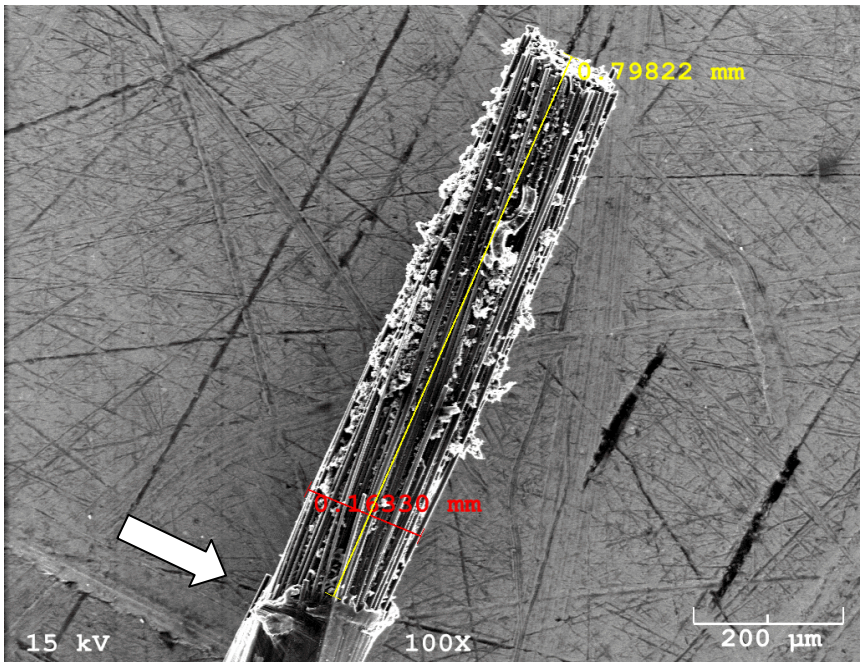

Figure 4.11. Pullout length of the bundle fiber showing small meniscus cap (arrow pointing to resin end on the fibers)

4.5 Surface Modification: Effect of Thermal Treatment, POSS Coating and CNTs Grafting on IFSS

The use of bundle fiber test to determine the fiber-matrix IFSS has proved to be accurate as discussed in section 4.4. As a result, the use of fiber bundle to evaluate the IFSS for the surface-modified fiber and resin interface was adopted in this section of the study due to the premature single fiber failure.

The IFSS of the fiber-matrix interface was calculated based on the Kelly-Tyson theory using Eqn. (2) and the diameters for the bundles were obtained based on the method described in section 4.4.2. T650-35 carbon fibers were considered for this work. The POSS coated samples, thermally treated, and CNT grafted samples were also extracted from the early prepared samples as described in section 2.2.1.

Figure 4.12 shows IFSS values for all the treated fibers including the CNTs grafted fibers. As shown, after thermal treatment of as-received fiber (T650-AR), the IFSS was improved for almost 32%. This can be attributed to the improvement in the mechanical interlocking created as a result of well-pronounced fiber surface flaws. When the thermally treated fibers were coated with POSS, the IFSS was further improved for about 6%. It has been reported in earlier works that POSS helped to improve the IFSS of fiber-matrix interface [78,79]. The contribution of nanotubes towards IFSS improvement was limited, due to its limited growth on the fiber surface. However, it should be noted that the samples with CNTs grown by dip CDT (Catalyst deposition technique) had better yield in IFSS when compared to spray CDT in each group. The debond force seemed to remain relatively the same in all CNT grafted samples and higher values were obtained for the POSS coated samples. After the pullout there were remains of CNTs on the fiber and there were more grooves (holes) on the resin wall as shown in Figure 4.13.

The poor interfacial performance exhibited by the CNT grafted carbon fiber is possibly due to poor bonding strength of CNT and carbon fiber which caused the CNT to pull-out at the fiber-matrix interface evidence from the SEM images. It is believed that the CNT-carbon fiber bonding plays important role in the interfacial shear strength of fiber-matrix with CNT growth. The thermally-treated fiber had almost 31% improvement in the interfacial shear strength when compared to as-received un-treated fiber due to the higher surface roughness possessed by the former which provided better anchorage within the resin matrix.

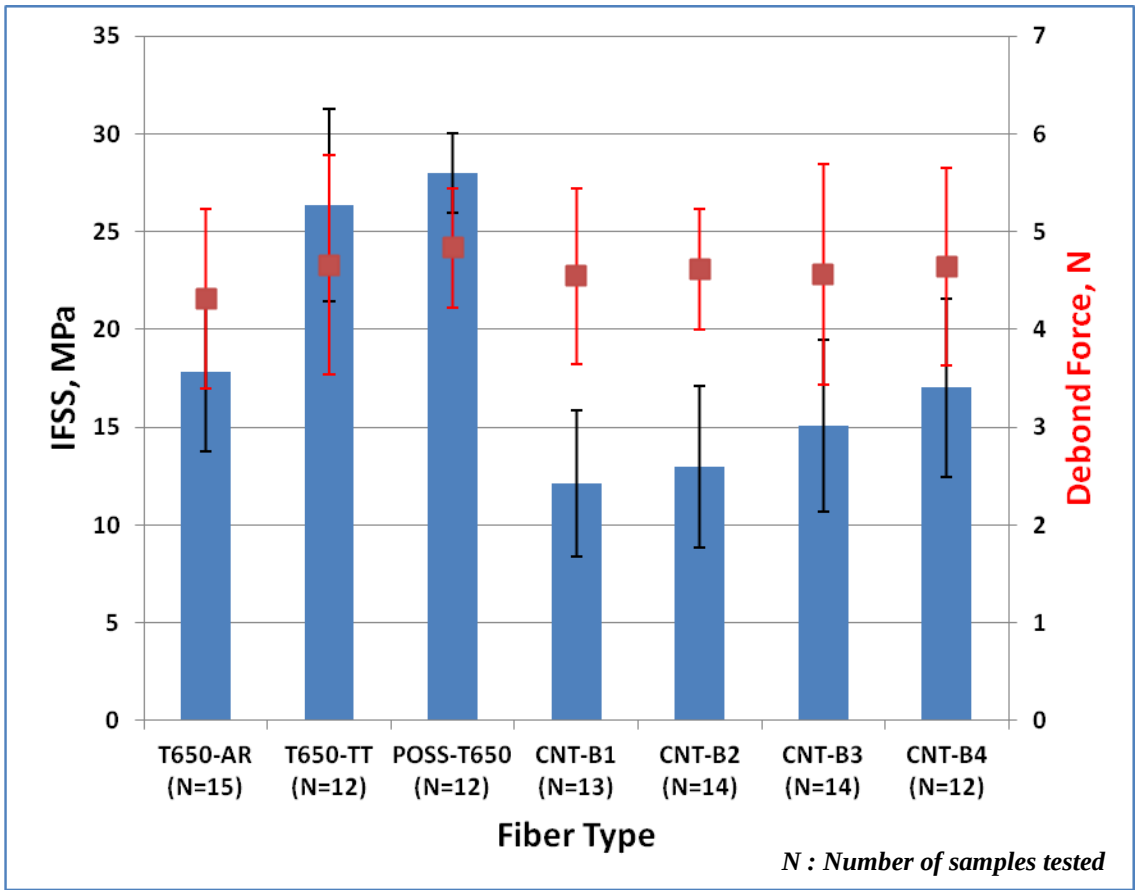

Figure 4.12. IFSS testing results of the composites reinforced by as-received and modified carbon fibers

From the results of the experiment, it can also be deducted that the percentage of CNTs grafted on the fiber plays a major role in the overall interfacial behavior of fiber-matrix. Figure 4.14 shows the treated fiber bundle and their respective pullout holes. It seems the POSS coated fiber were more bonded together as shown in their pullout hole when compared to others.

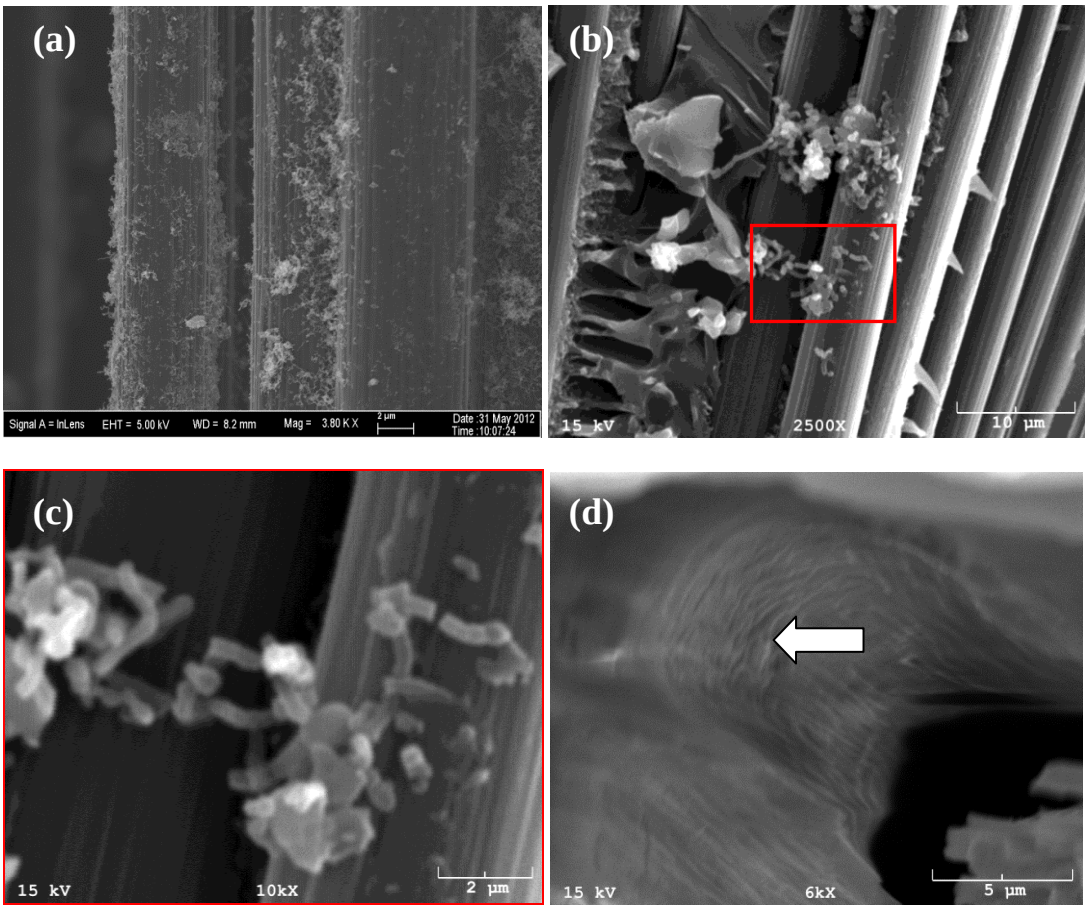

Figure 4.13. CNTs grafted bundle fiber after pullout: (a) the as-grown CNTs fiber before embedded inside resin, (b) indication of CNTs and resin attachment on the fiber, (c) higher magnification of the CNTs attached area (red square), and (d) part of the resin wall from the pullout hole showing the grooves created by the CNTs

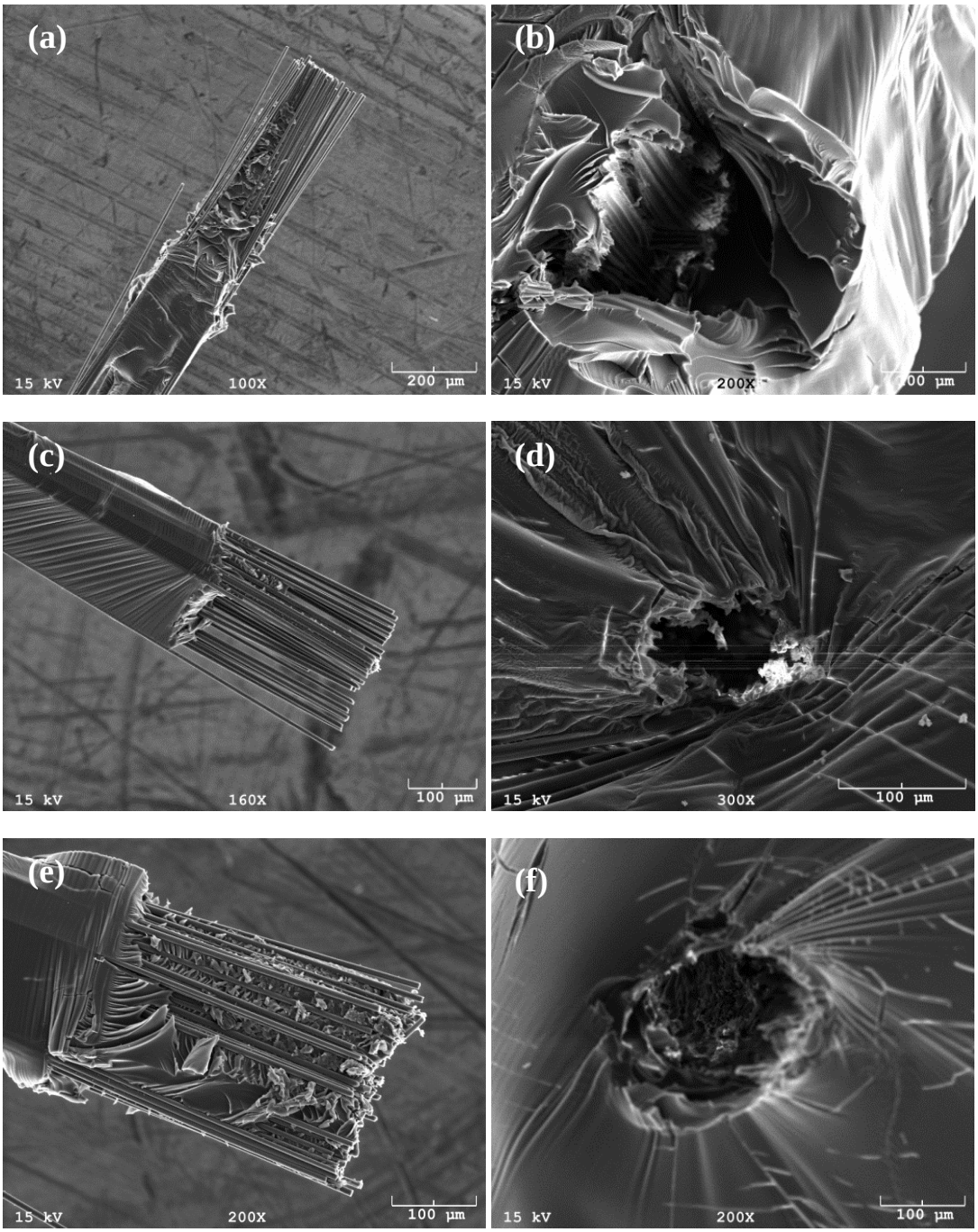

Figure 4.14. Bundle fiber after pullout: (a) as-received T650-35 CF, (b) the pullout hole for (a), (b) thermally-treated fiber, (c) the pullout hole for (b), (e) POSS-coated fiber, and (f) the pullout hole for (e)

CHAPTER 5

CONCLUSIONS AND RECOMMENDATION

5.1 Conclusions

Surface modification effect on the single fiber tensile properties and the fiber-matrix interfacial performance have been critically examined. Based on the main research questions about this work the respective contributions as related to the accurate measurement of the tensile properties and fiber-matrix interfacial strength are enlightened in this section.

Contributions towards the measurement of single fiber tensile properties:

- Development of a unique sample preparation procedure by the use of center-marked laser-cut frame in order to improve the filament handling and testing accuracy was successful. Test errors that could be introduced into the test data as a result of filament misalignment, pre- and post- tensioning effects has been minimized with this approach which was carried out under a stereo- microscope.
- Characterization of the tensile properties of a single carbon fiber with the aid of an air-bearing system (DMA-Q800) made it possible to resolve both strain and displacement adequately. The system is designed with optical encoder (that helps to have a high strain resolution of about 1nm) compared to the linear-variable differential transformer (LVDT) that can be found in the majority of MTS-Instron machine used for the similar microscale test. Moreover, the errors that could be introduced into the test data as a result of test frame misalignment and frame twisting on the clamps has been minimized by the use of a hand-controlled torque application instead of a hydraulically operated system. About 20% improvement

in the measurement accuracy was recorded as a result of the sample preparation techniques and the use of DMA to carry out the test within the same gauge length [86].

- Other than the typical reasons for applying sizing on the fiber, such reason as surface protection from being damaged during handling and processing, size application on the fiber has also proved to contribute significantly to the improvement of the fiber tensile properties. About 7%, 12% and 7% improvement in the tensile strength of sized AS4, AS7 and IM10 fibers was observed when compared to their respective un-sized fibers. However, the fiber surface modification by the use of heat treatment had an adverse effect on its tensile strength as a result of thermo-oxidative degradation effect with a reduction of about 35% when compared to other methods of surface modification such as the CNT and POSS grafting techniques. POSS and CNT grafted thermally treated T650-35 carbon fiber also showed improved tensile properties (8% - 13%) as compared to thermally treated fiber due to an effective reduction of stress flaws. The reliability of the fiber tensile strength obtained experimentally was modeled accurately by the use of two-parameter Weibull distribution function.

Some of the contributions made towards the improvement in the measurement of fiber-matrix interfacial performance are listed below:

- The uniqueness in the sample preparation approach for the fiber pullout test to characterize the fiber-matrix interfacial performance by the use of steel frame helped to reduce the meniscus cap thereby provided the means for accurate

measurement of the embedded length. The use of a laser-cut center-marked frame also allowed for proper alignment of the fiber under an optical microscope.

- Experimental investigation done to know the effect of sizing on the fiber-matrix interfacial performance showed that sizing contributed significantly to an improved interfacial shear stress (IFSS) for about 30% when compared to the un-sized type. The improvement in IFSS as seen in the AS4 sized fiber might be attributed to the increase in the surface energy, the fiber surface structure (roughness) and polarity match with the resin matrix as a result of sizing application.
- The surface modification of the fiber by either heat or POSS treatment also contributed to an improvement (~32%) in fiber-matrix interfacial strength.

5.2 Recommendation

The future works to be considered for this work should be:

- To develop a micro-mechanical model that can compute for the fiber-matrix interfacial strength. Various means of surface modification used for this work should also be considered to build this model.
- Deposition of CNTs on the fiber using alternative methods, such as the electro-phoresis deposition technique, should be considered for grafting CNTs on the fiber in order to eliminate fiber strength reduction due to the thermal degradation effect.

5.3 Limitations of the Research

Overview of the basic techniques used to carry out this work has shown that there are some limitations that are associated with the characterization of the single fiber tensile properties and the fiber-matrix interfacial properties. As a result, this section has been set apart to highlight these limitations.

Limitations on characterization of the single fiber tensile properties based on this work are listed below:

- The approach involved testing many samples (> 30) in order to improve the statistical accuracy. The success rate for the small gauge length samples (6.35mm) was ~ 40% due to the difficulty involved to access the small window size and the frame legs.
- Although all efforts was exercised to improve the random selection of the single fibers both from within and the bundle outer set there might still be a high tendency of selecting these fibers from the outer set.

Limitations on characterizing the fiber-matrix interfacial performance as related to this work could also be listed as follows:

- The height of the resin that was poured on the fiber embedded region could not be precisely controlled and maintained the same from sample to sample.
- Based on the point mentioned above the use of shear-lag model approach to find the interfacial shear stress (IFSS) was limited. There was over- or under-estimation of the IFSS due to the inaccuracy of the measurement of the effective radius of the fiber from the resin block surface.

- The number of filaments per strand used for the fiber-bundle pullout test could not be kept the same from sample to sample. All efforts were made to keep the same number of fibers for all the samples considered for this work and the effect of this could be found in the closest estimation of the debond force values.
- The success rate of ~ 30% was recorded for both single and bundle-fiber pullout tests.
- Quantification of the CNTs by thermogravimetric analysis was based on the residual mass evaluation. This quantitative approach could not precisely account for the total number of CNTs on each batch of treatment used in this work.

REFERENCES

[1] J.B. Donnet and R.C. Bansal, Carbon Black: Science and Technology, 2nd Edition, Marcel Dekker Inc., New York, 1-5, 1993

[2] K. Azami, S. Yamamoto, T. Yokono andY. Sanada, In-Situ Monitoring for Mesophase Formation Processes of Various Pitches by Means of High-Temperature ^{13}C-NMR*;* Carbon, 29, 943-947, 1991

[3] National Materials Advisory Board: Committee Report, High Performance Synthetic Fibers for Composites; National Academy Press, Washington DC, 52, 1992

[4] J.B. Donnet and R.C. Bansal, Carbon Fibers, 2nd Edition, Marcel Dekker Inc., New York, Pp. 55-63, 1990

[5] M. Ram and J.Riggs, Graphitization Process; U.S. Patent 3656904, 1972

[6] A. Takaku and J. Shimizu, Volume Contraction and Its Significance in Structural Formation during the Thermal Stabilization of Acrylic Fibers; Appl Polym Sci, 29,1319-1326, 1984

[7] J. Bromley, Carbon Fibers: Their Composites and Applications; Proc. International Carbon Fiber Conference, The Plastic Institute, London, 3, 1971

[8] J.N. Hay, Thermal Reactions of Polyacrylonitrile; Appl Polym Sci., A-1, 6, 2127-2135, 1968

[9] J.E. Bailey and A.J. Clarke, Oxidation of Acrylic Fibres for Carbon Fibre Formation; Nature, 234, 146-150, 1973

[10] V.I. Kasatochkin and V.A. Kargin, Chemical Coversion of Oriented Polyacrylonitrile; Dokl Phys Chem, 191, 1084-1087,1970

[11] P.J. Goodhew, A.J. Clarke and J.E. Bailey, A Review of the Fabrication and Properties of Carbon Fibres; Mater Sci Eng, 17, 3-30, 1975

[12] R. Seeberger, G. Kane, J. Hoffmann and G. Eggers, Accuracy Assessment for Navigated Maxillo-Facial Surgery Using an Electromagnetic Tracking Device; Cranio-Maxillofacial Surgery, 40, 156-161, 2012

[13] D. Mckee and N. Wadsworth, Surface Properties of Carbon Fibers; Chemistry and Physics of Carbon, Marcel Dekker, New York, 8, 151-241, 1973

[14] M. Druin, G. Ferment and V. Rad, Enhancement of the Surface Characteristics of Carbon Fibers; U.S.Pat., 3, 754, 957, Aug. 1973

[15] F. Molleyre and M. Bastick, High Temp-High Pressures, 9, 237, 1977

[13] T. Matsumoto, Mesophase Pitch and its Carbon Fibers; Pure and Applied Chemistry, 57, 1553-1562, 1985

[14] E. Fitzer and W. Frohs, The Influence of Carbonization and Post Heat Treatment Conditions on the Properties of PAN-Based Carbon Fibres; Carbon' 88 International Carbon Conference, 298-300, 1988

[15] I.C. Lewis, Process for Producing Carbon Fibers from Mesophase Pitch; U.S. Patent 4032430, 1977

[16] J. Goan, L. Joo and G. Sharpe, Surface Treatment for Graphite Fibers; 27thAnn Tech Conf Reinf Plast/Comp Inst, 27(21-E), 1-6, 1972

[17] E. Perakslis, S. Gardner and C. Pittman, Surface CompositionofCarbon Fibers Subjected to Oxidation in Nitric Acid Followed by Oxygen Plasma; Adh Sci Tech, 11 (4), 531-551, 1997

[18] R. Dauksys, Graphite Fiber Treatments which Affect Fiber Surface Morphology and Epoxy Bonding Characteristics; Adh, 5, 211-244, 1973

[19] J. Hoare, The Electrochemistry of Oxygen; Interscience, 13, 1968

[20] P. Ehrburger, J. Herque and J. Donnet, Electrochemical Treatment of Carbon and Graphite Fibers; Proc 4thInt Conf Carbon and Graphite Conf, Society of the Chemical Industry, London, 201, 1976

[21] J. Joiner and V. Findlay, Continuous Surface Treatment of Carbon Fiber; Brit. Pat. 1, 326, 736, Oct. 1969

[22] W. Wright, The Carbon Fiber/Epoxy Resin Interphase A Review; Polymers and Polym Comp, 3, 231-257, 1990

[23] A. Naveed, S. Man-Lung, Z. Ben, M. Arshad and K. Jang-Kyo, Tensile Strength of Glass Fibres with Carbon Nanotube–Epoxy Nanocomposite Coating; Comp, A-40, 1606-1614, 2009

[24] L. Drzal, Treatise on Adhesion and Adhesives; Marcel Dekker, New York, 6, 187-211, 1988

[25] L. Drzal, M. Rich, M. Koenig and P. Lloyd, Adhesion of Graphite Fibers to Epoxy Matrices. II. The Effect of Fiber Finish; Adh, 16, 133-152, 1983

[26] S. Yumitori, D. Wang and F. Jones, The Role of Sizing Resins in Carbon Fiber Reinforced Polyethersulfone (PES); Composites, 25, 698-705, 1994

[27] B. Harris, O. Braddell, C. Lefebvre and J. Verbist, The Surface Treatment of Carbon Fibers by Electropolymerization and Plasma Polymerization; Plastics Rubb and Comp Processing and Appl, 18, 221-240, 1992

[28] M. Endo, The Growth Mechanism of Vapor-Grown Carbon Fibers, Phd Thesis, University of Orleans, Orleans, France, 1975

[29] S. Iijima, Direct Observation of the Tetrahedral Bonding in Graphitized Carbon Black by High Resolution Electron Microscopy; Cryst Growth, 50, 675-683, 1980

[30] A. Oberlin, M. Endo and T. Koyama, Filamentous Growth of Carbon through Benzene Decomposition; Cryst Growth, 32, 335-349, 1976

[31] A. Oberlin, M. Endo and T. Koyama, High Resolution Electron Microscope Observations of Graphitized Carbon Fibers; Carbon, 14, 133-135, 1976

[32] S. Iijima, Helical Microtubules of Graphitic Carbon; Nature, 354, 56-58, 1991

[33] E.G. Galpern, I.V. Stankevich, A.L. Christyakov, and L.A. Chernozatonskii, Atomic and Electronic Structure of the Barrelenes B-Cm With M = 36+12n; JETP Lett, 55, 483- 486, 1992

[34] S. Iijima and T. Ichihashi, Single-Shell Carbon Nanotubes of 1-Nm Diameter; Nature, 363, 603-605, 1993

[35] D.S. Bethune, C.H. Kiang, M.S. De Vries, G. Gorman, R. Savoy, J. Vazquez, and R. Beyers, Cobalt-Catalysed Growth of Carbon Nanotubes with Single-Atomic-Layer Walls; Nature, 363, 605-607, 1993

[36] A. Thess, R. Lee, P. Nikolaev, H. Dai, P. Petit, J. Robert, C. Xu, Y.H. Lee, S.G. Kim, A.G. Rinzler, D.T. Colbert, G.E. Scseria, D. Tomanek, J.E. Fischer, and R.E. Smalley, Crystalline Ropes of Metallic Carbon Nanotubes; Science, 273, 483-487, 1996

[37] B. Yakobson and R. Smalley, Fullerene Nanotubes: $C_{1000000}$ and Beyond; American Scientist, 85, 324-337, 1997

[38] A.A. Puretzky, D.B. Geohegan, X. Fan, and S.J. Pennycook, Dynamics of Single-Wall Carbon Nanotube Synthesis by Laser Vaporization; Appl Phys A: Mater Sci and Proc., 70, 153-160, 2000

[39] T.N. Ebbesen, and P.M. Ajayan, Large-Scale Synthesis of Carbon Nanotubes; Nature, 358, 220-222, 1992

[40] X**.** Zhao**,** M. Wang, M. Ohkohchi and Y. Ando, Carbon Nanotubes Grown on the Surface of Cathode Deposit by Arc Discharge; Fullerene Science and Technology, 4, 1027-1039, 1996

[41] T. W. Ebbesen, P. M. Ajayan, H. Hiura and K. Tanigaki, Purification of Nanotubes; Nature, 367, 519

[42] D.S. Bethune, R.D. Johnson, J.R. Salem, M.S. De Vries and C.S. Yannoni, Atoms in Carbon Cages: The Structure and Properties of Endohedral Fullerenes**;** Nature, 366, 123-128, 1993

[43] Y. Ando, The Preparation of Carbon Nanotubes; Fullerene Science and Technology, 2, 173-180, 1994

[44] C. Journet, W. K. Maser, P. Bernier, A. Loiseau, M. Lamy De La Chapelle, S. Lefrant, P. Deniard, R. Lee and J. E. Fischer, Large-Scale Production of Single-Walled Carbon Nanotubes by the Electric-Arc Technique; Nature, 388, 756-758, 1997

[45] H. Dai, A.G. Rinzler, P. Nikolaev, A. Thess, D.T. Colbert and R.E. Smalley, Single-Wall Nanotubes Produced by Metal-Catalyzed Disproportionation of Carbon Monoxide; Chem Phys Lett, 260, 3-4, 1996

[46] H.M. Cheng, F. Li, X. Sun, S.D.M. Brown, M.A. Pimenta, A. Marucci, G. Dresselhaus and M.S. Dresselhaus, Bulk Morphology and Diameter Distribution of Single-Walled Carbon Nanotubes Synthesized by Catalytic Decomposition of Hydrocarbons; Chem Phys Lett, 289, 602-610, 1998

[47] J.H. Hafner, M.J. Bronikowski, B.R. Azamian, P. Nikolaev, A.G. Rinzler, D. T. Colbert, K.A. Smith and R.E. Smalley, Catalytic Growth of Single-Wall Carbon Nanotubes from Metal Particles; Chem Phys Lett, 296, 195-202, 1998

[48] E. Flahaut, A. Govindaraj, A. Peigney, Ch. Laurent, A. Rousset and C.N.R. Rao, Synthesis of Single-Walled Carbon Nanotubes Using Binary (Fe, Co, Ni) Alloy

Nanoparticles Prepared in Situ by the Reduction of Oxide Solid Solutions; Chem Phys Lett, 300, 236-242, 1999

[49] B.C. Satishkumar, A. Govindaraj, Rahul Sen and C.N.R. Rao, Single-Walled Nanotubes by the Pyrolysis of Acetylene-Organometallic Mixtures; Chem Phys Lett, 293, 47-52,1998

[50] B.C. Satishkumar, A. Govindaraj and C.N.R. Rao, Bundles of Aligned Carbon Nanotubes Obtained by the Pyrolysis of Ferrocene–Hydrocarbon Mixtures: Role of the Metal Nanoparticles Produced In Situ; Chem Phys Lett, 307, 158-162, 1999

[51] K. Hernadi, A. Fonseca, J.B. Nagy, D. Bernaerts and A.A. Lucas, Fe-Catalyzed Carbon Nanotube Formation; Carbon, 34, 1249-1257, 1996

[52] L. Tong, A. Mouritz and M. Bannister, 3D- Fiber Reinforced Polymer Composites, Elsevier Science, Oxford, pp. 1-12, 2002

[53] T. Chatterjee, A. Jackson and R. Krishnamoorti, Hierarchical Structure of Carbon Nanotube Networks, Am Chem Soc, 130, 6934-6935, 2008

[54] F.L. Mathews and R. Rawlings, Composite Materials Engineering and Science, CRC Press, Boca Raton, FL USA, pp. 29-77, 1999

[55] D.E. Resasco and J.E. Herrera, Encyclopedia of Nanoscience and Nanotechnology, 1, 23, 2003

[56] T. Guo, P. Nikolaev, A. Thess, D.T. Colbert and R.E. Smalley, Catalytic Growth of Single-Walled Manotubes by Laser Vaporization; Chem Phys Lett, 243, 49-54, 1995

[57] S. Reich, C. Thomsen and J. Maultzsch, Carbon Nanotubes: Basic Concepts and Physical Properties; 3, John Wiley &Sons- New York, 2008

[58] E. T Thostenson, Z. Ren and T. Chou, Advances in the Science and Technology of Carbon Nanotubes and Their Composites: A Review; Composites Science and Technology, 61, 1899-1912, 2001

[59] J.D. Bernal, The Structure of Graphite; Proc Roy Soc-A, 106, 749-773, 1924

[60] M.S. Dresselhaus, G. Dresselhaus, and R. Saito, Physics of CarbonNanotubes; Carbon, 33, 883-891, 1995

[61] D. E., Resasco, Carbon Nanotubes and Related Structures. In K.J, Klabunde, and R.M. Richards *Nanoscale Materials In Chemistry*, 2nd Edition. New York: NY, John Wiley, Wiley Interscience, 444-487, 2009

[62] Carbon Nanotubes- Wikipedia

[63] N. Mingo, D. A. Stewart, D. A. Broido, and D. Srivastava, Phonon Transmission through Defects in Carbon Nanotubes from First Principles; Phys. Rev. B 77, 033418, 2008

[64] A. Jorio, G. Dresselhaus and M. Dresselhaus, Carbon Nanotubes: Advanced Topics in the Synthesis, Structure, Properties and Applications, 1st Edition, Pg. 5, Springer, 2008

[65] E. Bekyarova, E. T. Thostenson, A. Yu, H. Kim, J. Gao, J. Tang, H. T. Hahn, T.-W. Chou, M. E. Itkis, and R. C. Haddon, Multiscale Carbon Nanotube-Carbon Fiber Reinforcement for Advanced Epoxy Composites; Langmuir, 23, 3970-3974, 2007

[66] K. Naito, J. Yang, Y. Tanaka, and Y. Kagawa, Tensile Properties of Carbon Nanotubes Grown on Ultrahigh Strength Polyacrylonitrile-Based and Ultrahigh Modulus Pitch-Based Carbon Fibers; Appl Phys Lett, 92, 231912, 2008

[67] S. Tzeng, K. Hung, and T. Ko, Growth of Carbon Nanofibers on Activated Carbon Fiber Fabrics; Carbon, 44, 859-865, 2005

[68] S. Yi, Z. Fan, C. Wu, and J. Chen, Catalytic Graphitization of Furan Resin Carbon by Yttrium; Carbon, 46, 378-380, 2008

[69] S. Zhu, C. Su, S.L. Lehoczky, I. Muntele, and D. Ila, Carbon Nanotube Growth on Carbon Fibers; Dia Rel Mater, 12, 1825-1828, 2003

[70] R. Sager, P. Klein, D. Lagoudas, Q. Zhang, J. Liu, L. Dai and J. Baur, Effect of Carbon Nanotubes on the Interfacial Shear Strength of T650 Carbon Fiber in an Epoxy Matrix; Compos Sci AndTech, 69, 898-904, 2009

[71] P. Eisenberg, R. Erra-Balsells, Y. Ishikawa, J. C. Lucas, A. N. Mauri, Y. Ishikawa, J. C. Lucas, H. Nonami and R. J. J. Williams, Macromolecules, 35, 1160 -1164, 2002

[72] POSS User's Guide-Version 2.06, Accessed 8/28/2012

[73] F. Zhao and Y. Huang, Grafting of POSS on a Carbon Fiber Surface: Novel Coupling Agents for Fiber/Polymer Matrix Composites; Mater Chem, 21, 3695-3703, 2011

[74] U. Zielke, K.J. Huttinger and W. Hoffman, Surface-Oxidized Carbon Fibers:I. Surface Structure and Chemistry; Carbon, 34, 983-998, 1996

[75] S. Park, J. Oh, J. Lee and K. Rhee, Influence of Oxygen Plasma Treatment on Impact Behavior of Carbon Fibers-Reinforced Composites; Solid State Phenomenon, 119, 159-162, 2007

[76] J. Schaefer, Effects of Electrophoretically Deposited Carbon Nanofibers on the Interface of Single Carbon Fibers Embedded in Epoxy Matrix; Carbon, 49, 2750-2759, 2011

[77] F. Zhao and Y. Huang, Improved Interfacial Properties of Carbon Fiber/Epoxy Composites Through Grafting Polyhedral Oligomeric Silsesquixane on Carbon Fiber Surface; Materials Letters, 64, 2742-2744, 2010

[78] P. Mahfuz and H. Granata, Treatment of Carbon Fibers with POSS and Enhancement in Mechanical Properties of Composites; SAMPE Conference Paper, 11, 2010

[79] H. Mahfuz, The Effects of POSS on the Interlaminar Shear Strength of Marine Composites under Various Environmental Conditions; Nanotech, 1, 115-118, 2010

[80] F. Zhao, Y. Huang, L. Liu, Y. Bai and L. Xu, Formation of a Carbon Fiber/POSS/Carbon Nanotube Hybrid Reinforcement and Its Effect on the Interfacial Properties of Carbon Fiber/Epoxy Composites; Carbon, 49, 2624-2632, 2011

[81] E. Bekyarova, E. Thostenson, A. Yu, H. Kim, J. Gao, J. Tang, T. Hahn, T. Chou, E. Itkis and C. Haddon, Multiscale Carbon Nanotube – Carbon Fiber Reinforcement for Advanced Epoxy Composites; Langmuir, 23, 3970-3974, 2007

[82] D. Bascom and M. Jensen, Stress Transfer in Single Fiber/Resin Tensile Tests, Adhesion, 19, 219-239, 1986

[83] Q. Zhang, J. Liu, R. Sager, L. Dai and J. Baur, Hierarchical Composites of Carbon Nanotubes on Carbon Fiber: Influence of Growth Condition on Fiber Tensile Properties, Composites Sc. and Tech., 69, 594-601, 2009

[84] M. Rich and T. Drzal, Interfacial Properties of Some High-Strain Carbon Fibers in an Epoxy Matrix, Reinforced Plastics and Composites, 7, 145-154, 1988

[85] J.Heil, M. Hall, D. Litzenberger, R. Clearfield, J. Cuomo, P. George and W. Carberry, A Comparison of Chemical, Morphological, and Mechanical Properties of Various Recycled Carbon Fibers, SAMPE Conference Proceedings, 54, 2009

[86] S. Feih, E. Boiocchi, E. Kandare, Z. Mathys, A. Gibsonand and A. Mourits, Strength Degradation of Glass and Carbon Fibers at High Temperature; Proc 17thInternat Comm Comp Mater, 2009

[87] D.P. Thibodeaux, J. Hebert, N.Abd. El-Gawad and J. Moraitis, Quality Measurements: Relating Bundle Strength to Single Fiber Strength Measurements, Cotton Sci., 2, 62-67, 1998

[88] J. Militky, D. Kremenakova, G. Krupincova and J. Ripka, Relations between Bundle and Single Fiber Strength, 2nd Internat Text, Cloth and Des Conf, Oct. 2004

[89] R. Nachane and K. Iyer, Prediction of Bundle Strength from Single-Fiber Test Data, Textile Research, 50, 639-641, 1980

[90] J. Yao and W. Yu, Tensile Strength and its Variation for PAN-Based Carbon Fibers. II. Calibration of the Variation from Testing; Appl. Polymer Sci., 104, 2625-2632, 2007

[91] J. Heil, M. Hall, D. Litzenberger, R. Clearfield, J. Cuomo, P. George and W. Carberry, A Comparison of Chemical, Morphological, and Mechanical Properties of Various Recycled Carbon Fibers; SAMPE Conference Proceedings, Pp. 54, 2009

[92] M.M. Stevanovic and D.R. Pesikan, Tensile Characteristics of Carbon Fibers; Mater. Sci. Forum, 352, 183-188, 2000

[93] M. Paiva, C. Bernardo and D. Edie, A Comparative Analysis of Alternative Models to Predict the Tensile Strength of Untreated and Surface Oxidized Carbon Fibers; Carbon, 39, 1091-1101, 2001

[94] S. Deng, L. Ye, Y.Mai and H. Liu, Evaluation of Fibre Tensile Strength and Fibre/Matrix Adhesion using Single Fibre Fragmentation Tests; Composites Part A, 29A, 423-434, 1998

[95] W.B. Downs and R.T.K Baker, Modification of the Surface Properties of Carbon Fibers; Mater Res, 10, 625-633, 1995

[96] D. Zhishuang, B. Zhang, F. Shi, M. Li and Z. Zuoguang, Effect of Sizing on Carbon Fiber Surface Properties and Fibers/Epoxy Interfacial Adhesion; App Surf Sci, 257, 6980-6985, 2011

[97] R. Allred, S. Wesson, L. Mccorkle, J. Sutter and D. Wheeler, Surface Characterization of Sized and Desized Toray M40J Carbon Fibers, 47thInter SAMPE Symposium, 1187-1196, 2002

[98] J.S. Lee and T.J. Kang, Changes in Physico-Chemical and Morphological Properties of Carbon Fiber by Surface Treatment, Carbon, 35, 209-216, 1997

[99] W. Yu and J. Yao, Tensile Strength and Its Variable of PAN-Based Carbon Fibers.I. Statistical Distribution and Volume Dependence; Appl Polym Sci, 101, 3175-3182, 2006

[100] D. Zhishuang, B. Zhang, F. Shi, M. Li , Z. Zuoguang and Y. Gu, Effect of Heat Treatment on Carbon Fiber Surface Properties and Fibers/Epoxy Interfacial Adhesion, App Surf Sci, 257, 8457-8461, 2011

[101] S. Wang, Z. Chen, W. Ma and Q. Ma, Influence of Heat Treatment on Physical-Chemical Properties of PAN-Based Carbon Fiber, Cer Internat, 32, 291-295, 2006

[102] L. Penn and E. Bowler, A New Approach to Surface Energy Characterization for Adhesive Performance Prediction; Surf Interfac Anal, 3, 161-164, 1981

[103] B. Miller, P. Muri and L. Rebenfeld, A Microbond Method for Determination of the Shear Strength of A Fiber-Resin Interface; Compos Sci Tech, 28, 17-32, 1987

[104] Y. Gorbatkina, Adhesive Strength of Fiber-Polymer Systems. New York: Ellis Horwood; 1992

[105] G. Tandon and N. Pagano, Micromechanical Analysis of the Fiber Push-Out and Re-Push Test; Compos Sci Technol, 58, 1709-1725, 1998

[106] R. Kerans and T. Parthasarathy, Theoretical Analysis of the Fiber Pullout and Pushout Tests; Am Ceram Soc, 74, 1585-1596, 1991

[107] A. Kelly and W. Tyson, Tensile Properties of Fiber-Reinforced Metals-Copper/Tungsten and Copper/Molybdenum; Mech Phys Solids, 13, 329-350, 1965

[108] L. Broutman, Measurement of Fiber-Polymer Matrix Interfacial Strength.In: Interfaces Compos STP-452. Philadelphia, PA: ASTM, P.27-41, 1969

[109] S. Zhandarov and E. Mader, Characterization of Fiber/Matrix Interface Strength: Applicability of Different Tests, Approaches and Parameters; Compos Sci Technol, 65, 149-160, 2005

[110] L. Drzal, M. Rich, M. Koenig and P. Lloyd, Adhesion of Graphite Fibers to Epoxy Matrices II. The Effect of Fiber Finish; Adh, 16, 133-152, 1983

[111] K. Hung, W. Kuo, T. Ko, S. Tzeng and C. Yan, Processing and Tensile Characterization of Composites Composed of Carbon Nanotube Grown Carbon Fiber; Composite-A, 40, 1299-1304, 2009

[112] P. Polacek and J. Jancar, Effect of Filler Content on the Adhesion Strength between UD Fiber Reinforced and Particulate Filled Composites; Compos Sci and Technol, 68, 251-259, 2008

[113] R.D. Mooney and F.J. Mcgarry, Resin-Glass Bond Study; 14thAnnual Tech Conf-Reinforced Plastic Composite Inst, 12E, 1965

[114] J.F. Mandell, J. Chen and F.J. Mcgarry, A Microdebonding Test for In-Situ Assessment of Fiber/Matrix Bond Strength in Composite Materials, Int. Journal of Adhesion and Adhesives, 1, 40-44, 1980

[115] M. Paiva, M. Nardin, C. Bernardo and J. Schultz, Influence of Thermal History on the Results of Fragmentation Tests on High-Modulus Carbon-Fibre/Polycarbonate Model Composites; Composites Sci and Tech, 57, 839-843, 1997

[116] J. Lim, J. Zhang, K. Masters and W. Chen, Effects of Gage Length, Loading Rates and Damage on the Strength of PPTA Fibers; Int Journal of Impact Eng, 38, 219-227, 2011

[117] M. Rich, and T. Drzal, Interfacial Properties of Some High-Strain Carbon Fibers in an Epoxy Matrix, Reinforced Plastics and Composites, 7, 145-154, 1988

[118] TA Instruments Dynamic Mechanical Analyzer Brochure- TA 284, 2010

[119] Hexcel Corporation: CarbonFiber Material Data Sheets (www.Hexcel.Com/Resources/Carbon-Fiber-Data-Sheets)

[120] Hexcel Corporation: Formal Conversation

[121] M. Gronli, M. Antal Jr. and G. Varhegyi, A Round-Robin Study of Cellulose Pyrolysis Kinetics by Thermogravimetry, Ind Eng Chem Res, 38, 2238-2244, 1999

[122] M. Hosokawa, K. Nogi, M. Naito and T. Yokoyama, Nanoparticle Technology Handbook; Elsevier Publisher, Oxford UK, Netherlands, 2007

[123] W. Jing, C. Ping, L. Hong, L. Wei, W. Baichen, Z. Chengshuang and N. Ren, Surface Characteristic of Poly(P-Phenylene Terephthalamide) Fibers with Oxygen Plasma Treatment; Surf. Interf Analysis, 40, 1299-1303, 2008

[124] L**.** Yunfeng, Z. Yan, D. Yuexin and D. Shanyi, Surface and Wettability Property Analysis of CCF300 Carbon Fibers with Different Sizing or Without Sizing; Mater. and Design, 32(2), 941-946, 2011

[125] K. Zukiene, V. Jankauskaite and S. Petraitiene, AFM Lateral Force Imagining of Modified Polychloroprene: A Study Based on Roughness Analysis, Appl Surf Sci, 253, 966-973, 2006

[126] J. Wang, P. Chen, H. Li, W. Li, B. Wang, C. Zhang and R. Ni, Surface Characteristic of Poly(**P**-Phenylene Terephthalamide) Fibers with Oxygen Plasma Treatment, Surf Interf Anal, 40, 1299-1303, 2008

[127] U. Cvelbar, S. Pejovnik, M. Mozetie and A. Zalar, Increased Surface Roughness by Oxygen Plasma Treatment of Graphite/Polymer Composite, Appl Surf Sci, 210, 255-261, 2003

[128] M.O.H. Cioffi, H.J.C. Voorwald, L.R.O. Hein, and L. Ambrosio, Effect of Cold Plasma Treatment on Mechanical Properties of PET/PMMA Composites, Composites Part A, 36, 615-623, 2005

[129] S. Yumitori, D. Wang and F. Jones, The Role of Sizing Resins in Carbon Fibre-Reinforced Polyethersulfone (PES); Composites, 25, 698-705, 1994

[130] J. Jones, J. Barr and R. Smith, Analysis of Flaws in High-Strength Carbon Fibers From Mesophase Pitch; Materials Science, 15, 2455-65, 1980

[131] M. Powell and G. Hosur, Treatment of Carbon Fibers with POSS and Enhancement in Mechanical Properties of Composites; SAMPE Conference Paper, 11, 2010

[132] D. Derek, Directional Vapor Depositionof Thermal Barrier Coatings; Chap 12-Pore Engineering, Phd Dissertation, Univ of Virginia, 2000

[133] A. Lima, A. Musumeci, H. Lu, E. Waclawik and G. Silva, Purity Evaluation and Influence of Carbon Nanotube on Carbon Nanotube/Graphite Thermal Stability; Therm Anal Calorim, 97, 257-263, 2009

[134] O. Dunnes, K. Mackenzie, and A. Harris, Synthesis of Multiwalled Carbon Nanotubes on Fly Ash Derived Catalysts; Environ Sci Tech, 43, 7889-7894, 2009

[135] J. Lehman, M. Terrones, E. Mansfield, K..Hurst, and V. Meunier, Evaluating the Characteristic of Multi-Walled Carbon Nanotubes; Carbon, 49, 2581-2602, 2011

[136] E. Mansfield, A. Kar and S. Hooker, Applications of TGA in Quality Control of SWCNTs; Anal Bional Chem, 396, 1071-1077, 2010

[137] F. Buffa, H. Hu and D. Resasco, Side-Wall Functionalizationof Single Walled Carbon Nanotubes With 4-Hydroxymethylaniline followed by Polymerization of ϵ-Caprolactone; Macromolecules, 38, 8258-8263, 2005

[138] C. Frein and A. Barron, Thermogravimetric Analysis of Single Walled Carbon Nanotubes; Connexions Module: M22972, Version 1.2, 2009

[139] I. Ismail and W. Hurley, Modelling Carbon Fibers Oxidationin Air at Constant Heating Rates; Carbon, 30, 419-427, 1992

[140] I. Ismail, On the Reactivity, Structure, and Porosity of Caron Fibers and Fabrics; Carbon, 29, 777-792, 1991

[141] I. Ismail and P. Walker, Detection of Low Temperature Carbon Gasification Using DSC and TGA; Carbon, 27, 549-559, 1989

[142] P. Hou, C. Liu, Y. Tong, S. Xu, M. Liu and H. Cheng, Purification of SWCNTs Synthesized by the Hydrogen Arc-Discharge Method; Mater Res, 16, 2526-2529, 2001

[143] F. Galasso and J. Pinto, Oxidation of Carbon and Metal Coated Carbon Fibers; Fiber Sci Tech, 2, 303-313, 1970

[144] M. Brown, P. Hayes and P. Prangnell, Characterization of Thin Silica Films Deposited on Carbon Fiber by an Atmospheric Pressure Non-Equilibrium Plasma (APNEP); Compos A, 33, 1403-1408, 2002

[145] I.M.K. Ismail, Structure and Active Surface Area of Carbon Fibers; Carbon, 25, 653-662, 1987

[146] S. Freiman, S. Hooker, K. Migler and S. Arepalli, Measurement Issues in Single Wall Carbon Nanotubes, NIST Recommended Practical Guide Special Publication, 96019, 4-18, 2008

[147] Y. Murakami, Y. Miyauchi, S. Chiashi and S. Maruyama, Characterization of Single-Walled Carbon Nanotubes Catalytically Synthesized from Alcohol; Chem Phys Lett, 374, 53-58, 2003

[148] M. J. Reis, A. M. Botelho Do Rego, J. D. Lopes Da Silva and M. N. Soares, An XPS Study of the Fibre-Matrix Interface Using Sized Carbon Fibres as a Model; Mater Sci., 30, 118-126, 1995

[149] P.E Mcmahon, Graphite Fiber Tensile Property Evaluation, ASTM Special Technical Publication STP-521 1973, 367-89

[150] M.D Petry, T. Mah., and R. Kerans, Validity of using Average Diameter for Determination of Tensile Strength and Weibull Modulus of Ceramic Filaments, Am. Ceram. Soc. 1997, 80, 2741-44

[151] K.L Pickering, and T.L Murray, Weak Link Scaling Analysis of High-Strength Carbon Fiber; Composites Part A, 30, 1017-1021, 1999

[152] W.A. Weibull, A Statistical Distribution Function of Wide Applicability; App. Mech., 18, 293-297, 1951

[153] B.J Bergman, On the Variability of the Fracture Stress of Brittle Materials; Mater Sci Lett, 4 (9), 1143- 1146, 1985

[154] B.J Bergman, On the Estimation of the Weibull Modulus; Mater Sci Lett, 3, 689-692, 1984

[155] K.Chen and R. Diefendorf, Residual Stress in High Modulus Carbon Fibers; Progress In Sci and Eng of Composites: Proceedings of the Fourth International Conference on Composite Materials ICCM-IV, 19, 97-105, 1982

[156] M. Guigon and A. Oberlin, Heat Treatment of High Tensile Strength PAN-Based Carbon Fibers: Microtexture, Structure and Mechanical Properties; Comp Sci And Tech, 27, 1-23, 1986

[157] A. Dibenedetto and P. Lex, Evaluation of Surface Treatments for Glass Fibers in Composite Materials; Polym Eng Sci., 29, 543-555, 1989

[158] P. Zinck, M. Pays, R. Rezakhanlou and J. Gerard, Mechanical Characterization of Glass Fibers as an Indirect Analysis of the Effect of Surface Treatment; Mater Sci., 34, 2121-2133, 1999

[159] C. Ahlstrom and J. Gerard, The Adhesion of Elastomer-Coated Glass Fibers to an Epoxy Matrix, Part 1: The Effect of the Surface Treatments on the Tensile Strength of the Glass Fibers; Polym Compos., 16, 305-312, 1995

[160] B. Larson, Toughness, NDT Education Resource Center (Http://www.Ndt-Ed.org), Iowa State University In Collaboration with National Science Foundation, 2001-2011

[161] C. Sauder, J. Lamon and R. Pailler, The Tensile Behavior of Carbon Fibers at High Temperatures up to 2400^{o}C, Carbon, 42, 715-725, 2004

[162] J. Yao, W. Yu and D. Pan, Tensile Strength and its Variation of PAN-Based Carbon Fibers. III. Weak-Link Analysis, Appl Polym Sci, 110, 3778-3784, 2008

[163] N. A. Siddiqui, M. Sham, B. Tang, A. Munir, and J. Kim, Tensile Strength of Glass Fibres with Carbon Nanotube–Epoxy Nanocomposite Coating, Composites Part A, 40, 1606-1614, 2009

[164] C. Yue and M. Quek, On Failure Phenomenon in Single-Fiber Pullout Tests; Mater Sci Lett, 14, 528-530, 1995

[165] M. Nishikawa, T. Okabe, K. Hemmi and N. Takeda, Micromechanical Modeling of the Microbond Test to Quantify the Interfacial Properties of Fiber-Reinforced Composites; Internat Journal Solids and Struct, 45, 4098-4113, 2008

[166] X. Gu, R. Young and R. Day, Deformation Micro-Mechanics in Model Carbon Fiber-Reinforced Composites; Mater Sci, 30, 1409-1419, 1995

[167] H.W. Rhee and J.P. Bell, Effects of Reactive and Non-Reactive Fiber Coatings upon Performance of Graphite/Epoxy Composites; Polym Compos, 12, 213-225, 1991

[168] P.C Varelidis, R.L Mccullough and C.D Papaspyrides, The Effect on the Mechanical Properties of Carbon/Epoxy Composites of Polyamide Coatings on the Fibers; Compos Sci Technol, 59, 1813-1823, 1999

[169] X. He, F. Zhang, R. Wang and W. Liu, Preparation of a Carbon Nanotube/Carbon Fiber Multi-Scale Reinforcement by Grafting Multiwalled Carbon Nanotubes on to the Fibers; Carbon, 45, 2559-2563, 2007

[170] P.S. Chua and M.R. Piggot, The Glass Fiber–Polymer Interface: I- Theoretical Consideration for Single Fiber Pullout Tests; Compos. Sci. Technol, 22,33-42, 1985